OF TECHNOLOGY
SEP 07 1988
LIBRARIES

The Prediction of Inlet Flow Stratification and Its Influence on the Performance of Air-Breathing Hypersonic Propulsion Systems

by

Mark Joel Lewis

S.B. Aeronautics and Astronautics, Massachusetts Institute of Technology, 1984
S.B. Earth and Planetary Science, Massachusetts Institute of Technology, 1984
S.M. Aeronautics and Astronautics, Massachusetts Institute of Technology, 1985

SUBMITTED TO THE DEPARTMENT OF
AERONAUTICS AND ASTRONAUTICS
IN PARTIAL FULFILLMENT OF THE
REQUIREMENTS FOR THE DEGREE OF
Doctor of Science
at the
Massachusetts Institute of Technology

June 1988

©1988, Mark J. Lewis
The author hereby grants to MIT and the Charles Stark Draper Laboratory, Inc.
permission to reproduce and distribute this document in whole or in part

Signature of Author _____
Department of Aeronautics and Astronautics
June 1988

Certified by _____
Professor Daniel E. Hastings
Thesis Supervisor
Associate Professor of Aeronautics and Astronautics

Certified by _____
Professor Alan H. Epstein
Associate Professor of Aeronautics and Astronautics

Certified by _____
Professor Edward M. Greitzer
H. Nelson Slater Professor of Aeronautics and Astronautics

Certified by _____
Professor Manuel Martinez-Sanchez
Associate Professor of Aeronautics and Astronautics

Accepted by _____
Professor Harold Y. Wachman
Chairman, Department Graduate Committee

Archives
OF TECHNOLOGY
SEP 7 '88
LIBRARIES

The Prediction of Inlet Flow Stratification and Its Influence on the Performance of Air-Breathing Hypersonic Propulsion Systems

by
Mark Joel Lewis

Submitted to the Department of
Aeronautics and Astronautics on June 20, 1988
in partial fulfillment of the
requirements for the degree of
Doctor of Science in Space Propulsion

A study is presented of the effects of inlet flowfield stratification on the performance of a supersonic combustion ramjet. Such engines are currently favored as the most practical means of providing airbreathing propulsion for transatmospheric flight to low earth orbit, in accordance with the goals of the National Aerospace Plane program. The primary source of inlet stratification presented in this study is the thick hypersonic boundary layer that is expected to form on the forebody of a typical transatmospheric vehicle.

The operating environment of a transatmospheric vehicle is described, based on some simple trajectory approximations using constraints on the airframe and combustor inlet conditions. It is shown that at high Mach numbers, the forebody boundary layer will be laminar, and the results of classical laminar hypersonic boundary layer theory are applied to estimate the inlet boundary layer thickness and properties at various points in a typical trajectory. The sensitivity of the boundary layer thickness to altitude, angle of attack, Mach number, and forebody shape are considered. The difficulties of matching the bow shock to the engine inlet lip are examined in light of the added effects of viscosity.

An analytical model is presented to study the propagation of the forebody boundary layer inside the engine channel based on a compound compressible streamtube method. The use of this model is justified by the well-known observation that supersonic streamtubes tend not to mix. The model is used to analytically investigate boundary layer effects inside a constant pressure combustor. The discrete streamtube model is expanded to handle a continuous profile with a no-slip condition at the wall. A means of conveniently relating the continuous model to the discrete solution is presented. This model is used to numerically study the effects of nonuniform flow inside an isentropic channel, and the performance of constant pressure and constant temperature combustors designed for uniform inlet conditions. The behavior of an inlet profile passing through a shock is also considered.

It is shown that even a small boundary layer can produce noticeable changes in free-stream properties inside the inlet. In the combustor models, it is seen that free-stream Mach number is generally increased, and so static pressure and temperature are decreased. These effects are related to estimates of the combustion reaction rate, and therefore to the total heat release and losses inside the engine. From this, engine performance, as measured by specific impulse, is correlated to the ingested boundary layer thickness. It is suggested that complete consideration of inlet efficiency must include losses induced in the combustor by the inlet flow field stratification, and that proper evaluation of inlet performance cannot be accomplished by area averaging flow properties.

Thesis Supervisor: Professor Daniel E. Hastings
Associate Professor of Aeronautics and Astronautics

Acknowledgements

It is traditional to begin the thesis acknowledgements by thanking one's advisor for his support and friendship. In this case, however, the sentiments are truly heartfelt. Prof. Daniel Hastings has been an outstanding advisor in every sense of the word, and his interest in this student's education, research, and career objectives has gone far beyond the call of duty. Working with Prof. Hastings has been one of the great pleasures of conducting this research; his incredible mathematical and physical insight, contagious enthusiasm, strong moral support, and friendly guidance will always be remembered and appreciated, and will be upheld as an example in the author's own future academic endeavors.

The author has also been blessed with the opportunity to work with the other outstanding professors on his committee, including of course Prof. Manuel Martinez-Sanchez, whose brilliance, concern, and zeal cannot help but be an inspiration. So many of the ideas in this work were suggested, clarified, and enhanced by Prof. Martinez-Sanchez that it would be more appropriate to list him as a joint author. Thanks are most sincerely extended to Prof. Alan Epstein, who remained a valued source of advice and encouragement, even though the subject of this doctoral thesis diverged somewhat from his own research interests. Sincere appreciation is also extended to Prof. Edward Greitzer for his helpful suggestions.

Many other individuals deserve thanks for their time and effort in providing guidance, suggestions, or corrections along the course of this research. Professor Jack Kerrebrock deserves particular praise for establishing and encouraging the hypersonic research effort at MIT, and for always being available for technical and personal consultations despite his busy schedule as Associate Dean of Engineering. Dr. Phil Hattis, the project contract monitor at the Charles Stark Draper Laboratory, has also offered extraordinary support and encouragement. Both of these individuals deserve additional appreciation for consenting to act as readers of this document. Prof. René Miller has had a guiding hand and has offered invaluable assistance in all aspects of this work. In addition, special thanks are extended to Prof. Frank Marble at the California Institute of Technology, for his wonderful insights and enthusiasm about the topic and conclusions contained in this work.

Many individuals in the Department of Aeronautics and Astronautics have contributed their time and experience to this work. Prof. Judson Baron and Prof. Jean Louis provided valuable consultations and educational background on many of the aspects of this thesis. Prof. Eugene Covert is also to be thanked for the interest he took in this work and his helpful suggestions on inlet design. Prof. Michael Giles and Prof. Mark Drela were kind enough to provide both software and expertise. Thanks also to Bob Haimes and Richard

Shapiro for providing various software products.

Another of the great pleasures of this project has been the opportunity to work with outstanding fellow students. Rodger Biasca has been a fine companion during the short dinners and long nights of writing, and was always willing to listen attentively and offer his own knowledgeable insights on scramjet design. He deserves a special thanks for having made available the results of his excellent work on modelling scramjet finite rate chemistry, which has been an invaluable resource. Officemates and coworkers Nicholaos Gatsonis, Alex Gioulekas, John Blandino, Jiong Wang, and Patrick Chang also provided wonderful company and valuable suggestions, and were polite enough to remain awake through (most of) the informal presentations on the subtopics of this work.

The support of this research effort by the Charles Stark Draper Laboratory is gratefully acknowledged. Appreciation is also extended to the Office of Naval Research, which provided support during a portion of this project.

This thesis is dedicated to the memory of my grandmother, Ruth Starace, who always wanted her grandson to be a doctor (albeit of a different kind), and in honor of her daughter Helen, who made it possible for her son to realize his grandmother's dream.

Contents

List of Figures

List of Tables

Chapter 1
Introduction

1.1 Renewed Interest in Hypersonic Flight

Within recent years, there has been a resurgence of enthusiasm for the use of hypersonic air-breathing engines as an efficient means of boosting vehicles into earth orbit, and for high-speed, long-distance travel on earth. Hypersonic research has been aimed principally at the development of supersonic combustion ramjets, or scramjets, ultimately capable of operating at Mach numbers beyond 24, into the range of orbital velocities. Such engines could offer advantages in boosting efficiency, since, unlike a conventional rocket, oxidizer will not be carried up in tankage, but rather obtained from the ambient medium.

The advantages of flying an air-breathing vehicle to orbit are apparent considering that oxidizer comprises a substantial portion of the gross lift-off weight of existing rocket-powered boosters. For instance, approximately 1/3 of the lift-off weight of the space shuttle is liquid oxygen, and that does not even include the oxidizer contained in the solid rocket booster propellant mixture. The Apollo Saturn V launch vehicle carried a total of 1,734,450 liters of liquid oxygen in its first three stages, which, with a weight of 2,081,000 kg, represented nearly 72% of the total lift-off weight of 2,913,000 kg [1]. Clearly, if this weight could be eliminated, enormous benefits would be realized in vehicle design. It seems almost foolhardy to carry oxidizer along to orbit through an oxidizing environment. A rocket carrying oxidizer through the atmosphere has been humorously compared to a fish swimming through the ocean with a canteen of drinking water on its back.

Because the reaction mass in an air-breathing engine consists mainly of gas ingested from the ambient reservoir, the specific impulse of such engines is much higher than that of rocket engines. It is usually assumed that specific impulses of about 2000 seconds are

achievable at Mach 10, dropping to about 1000 at Mach 20 [2]. This is compared to a characteristic specific impulse of 460 seconds that is currently the maximum obtainable with chemical rocket engines such as the space shuttle main engines.

Despite this promise of such savings, the advantages of air-breathing propulsion are not completely clear-cut. The reduction of weight associated with the removal of on-board oxidizer is partly offset by the increase in weight incurred by the use of an airbreathing engine. Rocket engines produce extremely high thrust for their own plant mass. For instance, the thrust-to-weight ratio of a space shuttle main engine (SSME) is 55. This is lower than many older engines, because much of the SSME's weight is concerned with reusability. An Apollo Saturn first stage F-1 engine had a thrust-to-weight ratio of 82; the MA-5 sustainer engine used by the Atlas booster has thrust-to-weight ratio of 120. By comparison, ramjets have a typical thrust-to-weight ratio of about 7. We can conclude that an air-breathing propulsion system will generally be much heavier than a traditional rocket engine for the same thrust level.

The oxidizer weight savings is also offset by the increase in airframe mass associated with building a vehicle for sustained atmospheric flight. In fact, as will be described in the next chapter, a transatmospheric vehicle will likely fly at dynamic pressures that exceed current flight vehicle experience. In addition, a hypersonic vehicle that exceeds Mach 12 or so will likely be actively cooled. The mass of such a cooling system will also subtract from the weight savings.

The design of a cooling system poses another weight problem; the vehicle surface will not only be cooled, but it has to be cooled recuperatively in order to supply sufficient enthalpy to the engine flow. Ablation would not be a viable option for a reusable vehicle. However, a stoichiometric volume of hydrogen probably has too small a heat capacity to cool the vehicle surface throughout the trajectory, so up to three or four times the stoichiometric volume of fuel will have to be carried to accomplish this cooling. This will produce a corresponding decrease in realizable specific impulse.

As with any vehicle, a hypersonic vehicle must fight drag in its flight through the atmo-

sphere, and the associated losses increase the total fuel required over that for a traditional rocket. This issue is trajectory dependent.

In addition to these mass issues, there are a multitude of research problems that are beyond the range of this present work. For instance, the design of a cryogenic fuel storage tank that will sit in close proximity to a very hot skin; the problem of maintaining static control on a vehicle which derives so much of its thrust on its forebody and aftbody; and the problem of mixing fuel and getting it to burn at high speeds.

This work will concentrate on the single issue of the generation of large-scale nonuniformities on the vehicle surface, and the effect these nonuniformities will have on the engine operation. Only those nonuniformities that are generated as a result of the steady-flow external vehicle fluid dynamics will be considered. Such problems as gusting, or unsteady pitching and yawing will *not* be examined. The goal will be to determine the importance of such non- uniformities to the combustion process and general engine design by comparing the performance of an actual engine with the expected characteristics of an engine designed for uniform inflow. Throughout, the issue of what would happen if a hypersonic engine were designed without taking the forebody flow profile into account will be considered.

As will be shown, the design constraints on a transatmospheric vehicle will be such that the engine will, under certain circumstances, ingest a thick boundary layer at extreme temperatures and very low density. Also, as will be argued, the ingested profile will not mix out, which is a general property of supersonic shear flows. This stratification must be dealt with in the engine design, and it will be of the utmost importance to determine how it influences engine operation. This work will not consider the details of any one specific engine design, so much as examine the overall influences of inlet stratification with as qualitative and fundamental an approach as possible.

1.1.1 Research Approach

In this work, existing classical laminar boundary layer solutions will be used to predict the boundary layer thickness entering a hypersonic engine along simple trajectory models.

The effect of these profiles on the forebody bow shock flow will first be examined. The proper conditions for shock matching will be derived, and the differences between the inviscid and boundary layer solutions will be highlighted.

The calculated forebody profiles will be used as inputs into a streamtube analysis of the flow inside a hypersonic engine. The behavior of multi-streamtubes will be explored with existing streamtube methods. In this document, the streamtube methods will be extended to a continuous profile with a no-slip condition at a wall and heat addition. This streamtube model will be coupled with an analytical boundary layer solution with which the behavior of the inlet flow will be explored. The continuous streamtube model will be used in a simple numerical procedure for following a profile through a combustor channel. The response of a profile to passage through an inlet shock will be derived here as well.

In deriving the continuous streamtube model, several simplifying assumptions will be made. It will be assumed that flow is either laminar or turbulent, and arguments will be presented for assuming completely laminar flow at high Mach numbers. The problem of separation and reattachment will not be covered, and it will generally be assumed that separation has little effect on the shape or thickness of a reattached boundary layer profile. Although the effect of a shock on the profile will be examined, it will generally be assumed that there are not strong shocks inside the engine channel. Where it is necessary to do so, vehicle geometries and trajectories will always be modelled with the simplest assumptions available.

1.2 Engine Selection and Design

1.2.1 The Scramjet Concept

It is obvious that, before the influence of nonuniformities inside hypersonic air-breathing engine can be analyzed, the general flow path of that engine must be clarified. There are presently several schemes for hypersonic propulsion which have received some attention. The most favored method, and the one that will be considered in this work, is the supersonic

combustion ramjet, or scramjet. A scramjet is similar to the more traditional ramjet in that the inlet flow is compressed not with turbomachinery, but from the ram effect of decelerating a high-speed stream. The airflow is then decelerated in a combustor, where fuel is added and combustion increases the flow enthalpy, to provide net thrust after expansion through a nozzle. The ramjet can be run up to moderately high Mach numbers, up to about Mach 6, because there are no rotating parts at the combustor exit, as there are in turbine-driven engines [2].

The upper limit in ramjet Mach number is set by the maximum temperature permitted in the combustor. Because the stream is decelerated to facilitate the combustion process, it reaches a static temperature that approaches the free-stream total temperature, which is given by the familiar isentropic relation

$$\frac{T_{\text{total}}}{T_{\text{static}}} = \left(1 + \frac{\gamma - 1}{2} M^2\right) \tag{1.1}$$

At $\gamma = 1.3$, this ratio is 1.15 at Mach 1, 2.35 at Mach 3, and 6.4 at Mach 6. Thus, as Mach number increases, the deceleration process eventually raises the combustor temperature to a value beyond the combustion temperature, so that fuel addition does not yield further enthalpy increase. At sufficiently high temperatures, added fuel will dissociate and so *remove* heat from the mean flow.

One solution to this Mach number limitation is to simply not decelerate the combustor flow. This is the concept behind the supersonic combustion engine which was first proposed about 30 years ago [3]. Incoming flow is kept at supersonic speeds throughout the combustor, so it never reaches the high stagnation temperatures associated with a low-speed combustor. In theory, such an engine could run at nearly any Mach number, so long as the combustor is capable of accomplishing the heat-addition process at the corresponding speed. This is why the scramjet is proposed for flying up to orbital velocities.

This present work will focus *exclusively* on the scramjet concept, because it is the only concept currently proposed which holds the promise of accelerating a hypersonic vehicle to orbital velocities. The scramjet is also about the simplest engine to analyze, since it essentially consists of a flow channel in which a hypersonic stream is decelerated to a lower (though supersonic) Mach number, heat is added, and the flow is accelerated out through a

nozzle. Analyzing scramjet flow is simply a problem in analyzing supersonic channel flow, and that is the approach that will be taken in this work.

The design of such an engine is made difficult by the requirement for accomplishing the combustion process at supersonic speeds. Because the combustion must proceed quickly in the high-speed flow if the combustor is to be of practical size, the selected fuel must be fast-burning, and this leads to the selection of hydrogen as the only practical candidate. It is not clear that the combustion process can be made to occur even with hydrogen, because at high-speed, shear layers tend not to mix as they do at low speed [4]. Thus, one of the critical designs issues being investigated in the field of hypersonic propulsion is a practical means to induce fuel mixing. Although this particular problem is beyond the scope of this work, the fact that streams do not mix in high speed flow is actually used here to simplify much of the analysis. It is a good assumption that profiles will not mix out, even over long path lengths, so that forebody velocity profiles can be assumed to retain their shape all the way into the engine channel.

Adding heat to a high Mach number flow results in a substantial total pressure penalty. Indeed, any heat addition increases the entropy of a flow and drives it towards unity Mach number, and so introduces losses [2]. For a given increment of heat to a flow, the logarithmic derivative of decreasing total pressure is a function of the flow Mach number, as can be seen from equation (10.10) in reference [2]:

$$\frac{1}{p_t}\frac{dp_t}{dx} = -\frac{\gamma M^2}{2\rho u C_p T_t}\frac{dQ}{dx} \tag{1.2}$$

where dQ/dx is the streamwise heat addition. This is equivalent to the more traditional expression for total pressure change as a function of total temperature, written in logarithmic derivative form:

$$\frac{dp_o}{p_o} = -\frac{\gamma M^2}{2}\frac{dT_o}{T_o} \tag{1.3}$$

Writing $u = M\sqrt{\gamma RT}$, $C_p = \gamma R/(\gamma - 1)$, and using the one-dimensional relationships for total temperature and density [5], the change in total pressure for a given change in heat is written as a function of the Mach number and total temperature:

$$\frac{dp_t}{dQ} = -\frac{(\gamma - 1)M(1 + \frac{\gamma-1}{2}M^2)^{\frac{\gamma+1}{2(\gamma-1)}}}{2\sqrt{\gamma RT_t}} \tag{1.4}$$

At low Mach numbers, the total pressure loss for a given heat increase is proportional to the Mach number:

$$\lim_{M\to 0} \frac{dp_t}{dQ} \simeq -\frac{(\gamma-1)M}{2\sqrt{\gamma RT_t}} \tag{1.5}$$

At high Mach numbers, losses are even more sensitive to Mach number:

$$\lim_{M\to \infty} \frac{dp_t}{dQ} \simeq -\left[\frac{\gamma-1}{2}\right]^{(3\gamma-1)/2(\gamma-1)} \frac{M^{2\gamma/(\gamma-1)}}{\sqrt{\gamma RT_t}} \tag{1.6}$$

Clearly, losses are much larger when heat is added to a given flow at higher Mach number. At $\gamma = 1.25$, characteristic of typical combustor conditions, the total pressure loss scales with M^{10}. As a result, the supersonic combustion ramjet suffers higher losses in its combustor in comparison to the traditional ramjet.

1.2.2 Nonuniformities and Scramjet Operation

From the results of classical hypersonic boundary layer theory, it is known that in certain cases a thick boundary layer will form on the surface of a hypersonic vehicle, and this will have the following effects:

- The vehicle skin will be surrounded by a high temperature layer which may represent a substantial fraction of the shock layer.
- The vehicle bow shock will be displaced outward and be sensitive to angle of attack.
- The flow entering the scramjet will be stratified in temperature, density, and mass flux
- The inlet flowfield profile thickness will scale inversely with the angle of attack at large angles.

The latter two effects are especially important in the scramjet because of the sensitivity of such an engine's performance to flow losses in the inlet, and the unacceptably high static thermodynamic conditions that may be encountered with small variations in Mach number. In comparison to a conventional ramjet, the scramjet suffers a high total pressure loss in the combustor because heat is added to the flow at supersonic speeds. This can be countered by

the fact that the inlet experiences relatively small losses because there need not be strong shocks present. Thus, good scramjet performance will depend in part on keeping inlet flow losses to a minimum.

The presence of flow nonuniformities in the scramjet will be important because even small changes in Mach number can produce large changes in thermodynamic properties. Also, a scramjet combustor which is designed to run near thermal choking at uniform inlet conditions may be driven to choke with a nonuniform inlet. These effects may not only be deleterious to engine performance, but generate temperatures and pressures which destroy the engine. A simple argument for this comes from the one dimensional compressible flow equations; a fractional change in Mach number produces a fractional change in the static pressure and temperature as:

$$\frac{\partial P}{P} = \frac{-\gamma M^2}{1 + \frac{\gamma-1}{2} M^2} \frac{\partial M}{M} \tag{1.7}$$

$$\frac{\partial T}{T} = \frac{-(\gamma-1) M^2}{1 + \frac{\gamma-1}{2} M^2} \frac{\partial M}{M} \tag{1.8}$$

In the small Mach number limit, $\partial P/P$ and $\partial T/T$ are insensitive to fractional changes in Mach number, but in the hypersonic limit,

$$\frac{\partial P}{P} \simeq \frac{-2\gamma}{(\gamma-1)} \frac{\partial M}{M} \tag{1.9}$$

$$\frac{\partial T}{T} \simeq -2 \frac{\partial M}{M} \tag{1.10}$$

so that slight changes in Mach number due to nonuniformities imply large real changes in pressure and temperature, possibly inhibiting combustion or destroying the engine. For $\gamma = 1.4$, $\partial P/P = 7 \ \partial M/M$. Real chemical effects, as typically encountered in hypersonic flows, can intensify the pressure variation by reducing γ. At $\gamma = 1.3$, $\partial P/P = 8\frac{2}{3} \ \partial M/M$; at $\gamma = 1.25$, $\partial P/P = 10 \ \partial M/M$.

1.2.3 Sensitivity of Combustion to Thermodynamic Conditions

One of the major issues in scramjet design is accomplishing combustion at high speeds in a combustor channel of reasonable length, assuming that fuel can be adequately mixed into the flow. Any process which delays or inhibits combustion will either reduce the amount of heat that is added in the engine, or require the design of a longer, heavier engine. Accordingly, the impact of the ingested boundary layer on the combustion process is an issue of central concern in this present work.

Figure 1.1 is a plot of the hydrogen-air system reaction time as a function of temperature and pressure [6]. These represent the time required to reach 95% completion, as measured by temperature. As would be expected, the reaction rate is a strong function of pressure at any given temperature. Note that for lower temperatures, there is a pressure at which reaction time is a minimum, and so combustor length is most reasonable. As pressure rises, secondary reactions within the hydrogen-air system become more important, and increase the time required for the reaction to go to completion. The addition of combustion enhancers such as silane or peroxide, as has been proposed to accelerate the combustion process [6], will alter this plot.

Ferri [7] has calculated the reaction time and has presented the following curve fit for the reaction time between 1000K and 2000K and .2 and 5 atm. This reaction time should not be confused with the combustion time presented in Figure 1.1, which is the sum of the reaction time plus the delay time leading up to the onset of ignition.

$$t_{\text{reaction}} = \frac{105}{p^{1.7}} \quad e^{-T/893} \tag{1.11}$$

with time in μsecs, pressure p in atm., and initial temperature T in degrees K. More recently, Rogers and Schexnayder [8] have presented an updated curve fit for the reaction time:

$$t_{\text{reaction}} = \frac{325}{p^{1.6}} \quad e^{-T/1250} \tag{1.12}$$

The differences between these fits are more in the absolute values of reaction time, rather than the sensitivity to thermodynamic conditions.

This equation neglects the effects of high pressure in limiting the combustion rate. For

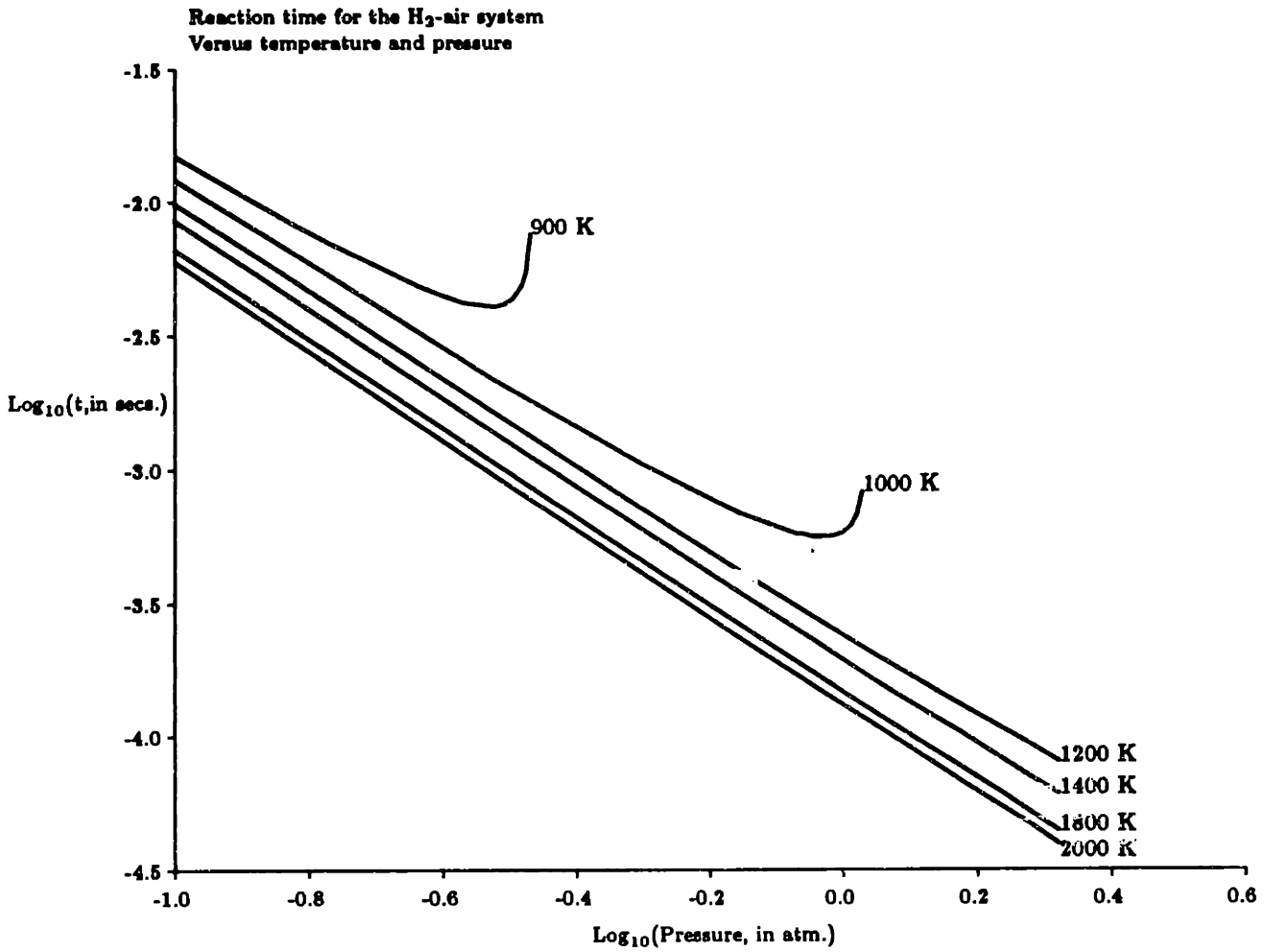

Figure 1.1: Time for completion of hydrogen combustion in air

instance, referring again to Figure 1.1, at 1000 K, combustion essentially ceases above one atmosphere due to the influence of secondary reactions. At 900 K, this limit is only about 1/3 of an atmosphere. In general, the cutoff pressure in atm. can be written as:

$$p_{\text{cutoff}} \simeq e^{.012\,T\,-12} \tag{1.13}$$

The reaction rate will also fall off at high temperature, and above about 3300 K at 1 atm, combustion will cease. Beyond this temperature, fuel addition will result in dissociation, and a net *loss* in total temperature. Figure 1.2 presents the equilibrium rise in temperature in the hydrogen-air system at 1 atmosphere, at various initial temperatures. This rise is linear, and can be approximated by

$$\Delta T = 2350\text{K} - .7315\ T_{\text{initial}} \tag{1.14}$$

in the vicinity of one atmosphere. The rate at which temperature is rising in the reaction can be approximated by dividing the equilibrium temperature rise in equation 1.14 by the reaction time of equation 1.12. The result is plotted in Figure 1.3. The heat addition rate is more sensitive to pressure than temperature.

It is therefore important that the pressure and temperature be kept within a rather narrow range once the combustor length, and thus the required reaction rate, is selected. This will be an important consideration in later chapters which will examine the influence of an inlet profile, and analyze the changes it produces in expected values of pressure and temperature in a combustor channel.

1.2.4 Other Propulsion Schemes

Although the low speed performance of a hypersonic vehicle will not be explored in this work, it is appropriate to comment briefly on the propulsion plant requirements for the initial phase of the transatmospheric trajectory. This will establish the appropriate operating range of the supersonic combustion engine.

Neither a scramjet, nor a ramjet can produce thrust at zero Mach number because they cannot compress without a ram effect. Therefore, a hypersonic vehicle must accelerate up to

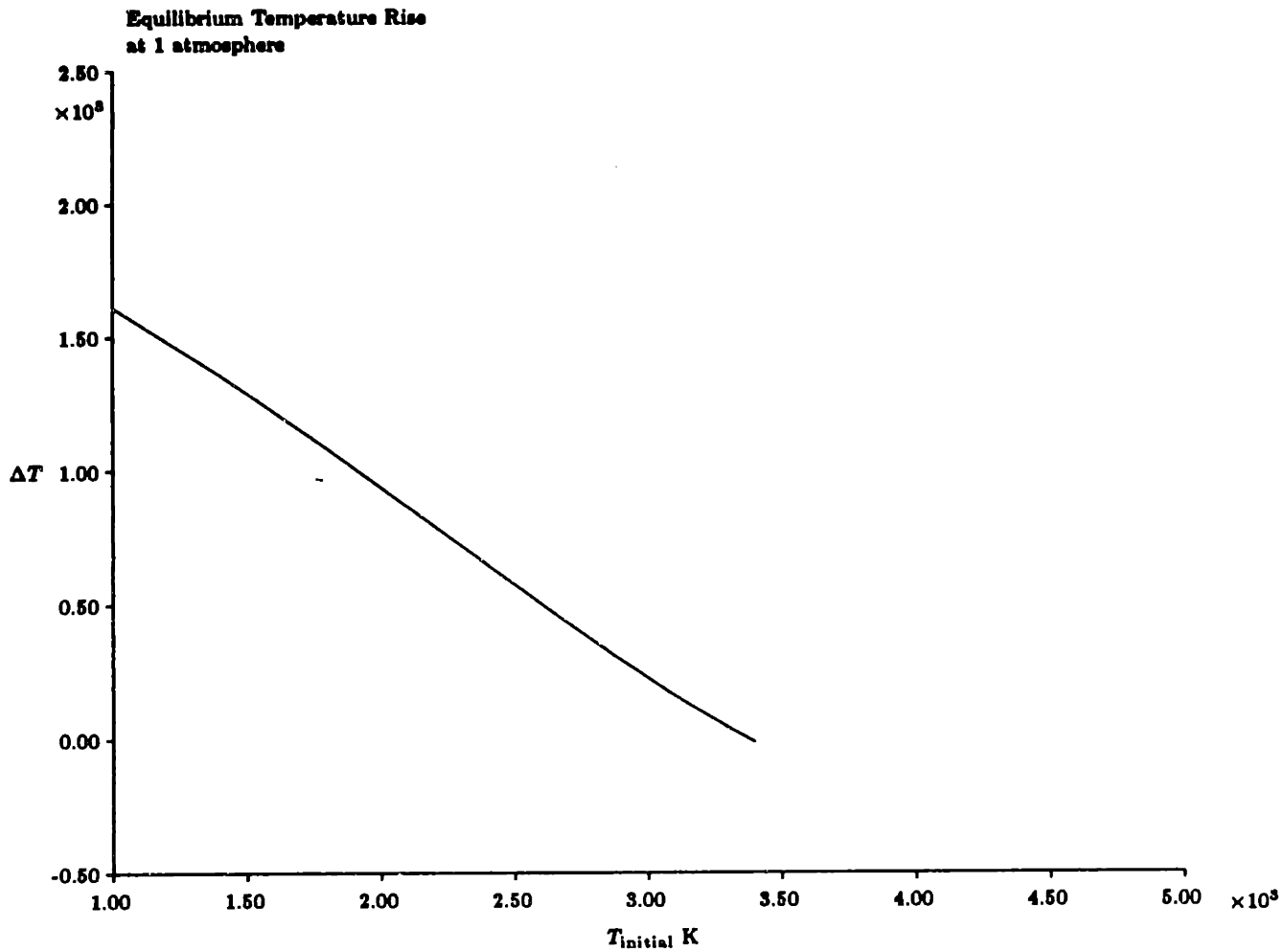

Figure 1.2: Equilibrium temperature rise versus initial temperature

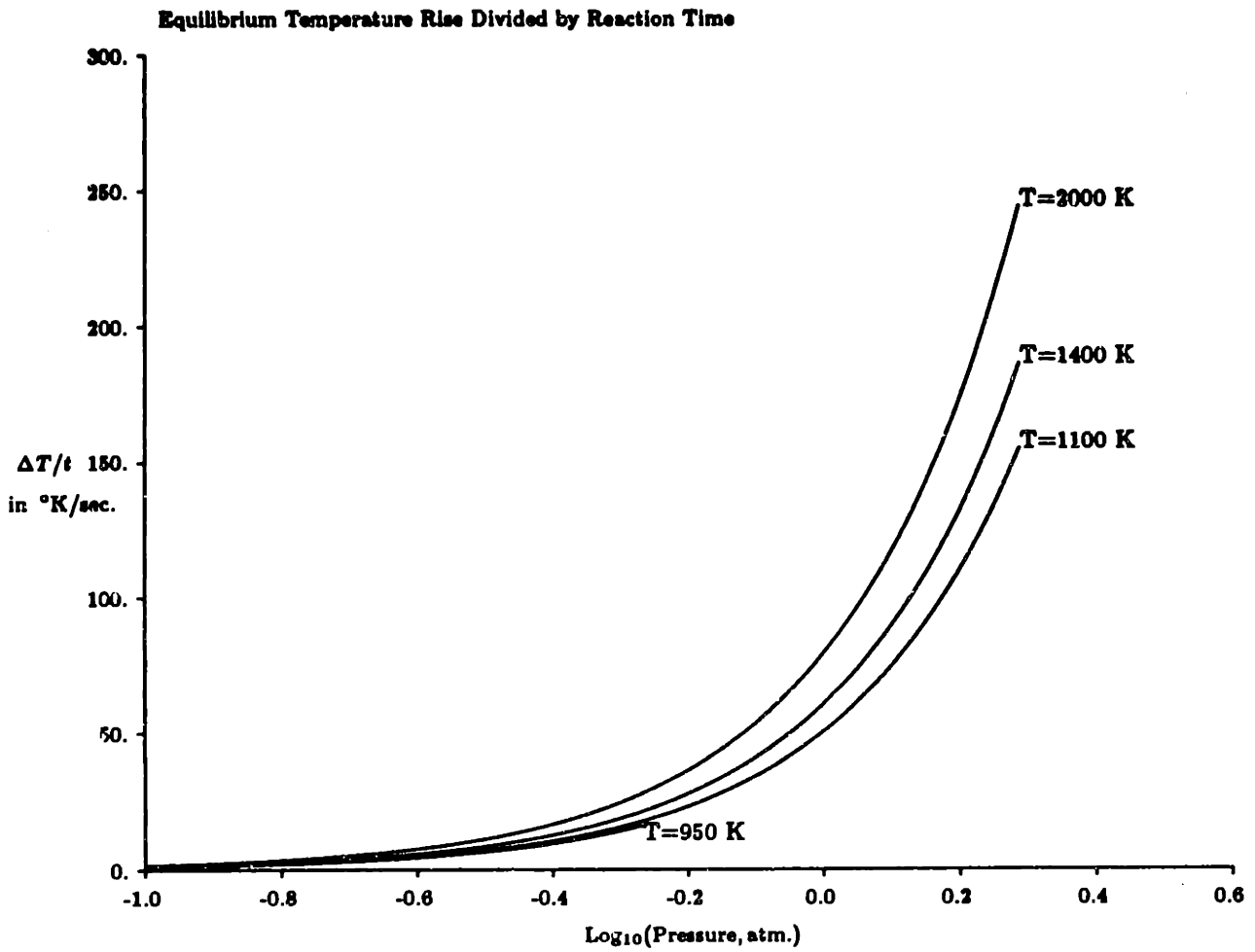

Figure 1.3: Rate of temperature rise at various initial temperatures, as a function of pressure

the speeds at which these engines could operate with some other means. Various proposals exist for engines that could carry a vehicle between Mach 0 and Mach 6, where scramjets are practical. These include rockets, traditional turbojet schemes, and assorted hybrids.

One difficulty in selecting appropriate engines is that each type of engine has its own particular operating range. For instance, traditional turbojets cannot exceed Mach 3, because the gas temperatures entering the combustor begin to approach the combustor exhaust temperature restriction imposed by the turbine material temperature limits. Scramjets do not operate well below Mach 6 because of the total pressure losses in the combustor, so it is suggested that, if turbine-powered engines are used for the initial acceleration, ramjets, or a ramjet mode of operation (i.e. with subsonic combustion) would have to be used to bridge the gap between Mach 3 and Mach 6.

A goal in hypersonic engine design is to encompass as much of the operating range of a transatmospheric vehicle without adding additional engine modules for each speed range. A means of doing this is to design engines which can operate over much wider ranges, or to extend the operating ranges of existing engines. An existing example of this concept is the Pratt and Whitney JT11D-20B bleed turbojet engines used on the SR-71, which have special flaps to bypass the compressor at high Mach number, so the afterburner can act like a ramjet.

A particularly novel hybrid concept is the air-turboramjet, which uses a compressor that is powered by a turbine run from a fuel-rich gas generator. The outflow of the turbine then mixes into the incoming stream, and combustion proceeds as in a ramjet or a scramjet. The advantage in this concept is that the turbine is not exposed to the incoming air, and so the only temperature limit is the compressor inlet temperature, which becomes restrictive in the vicinity of Mach 6 [9], where scramjets could take over.

It is not clear whether the performance of such an engine is really superior to that of a traditional after-burning turbojet. Such an engine could be run up to high Mach numbers by gradually reducing the fuel in the combustor to control the turbine inlet temperature. At high Mach number, the afterburner begins to work as a ramjet, and the compressor/turbine

path can eventually be bypassed, as is done on the SR-71.

As an aside, it is worth noting that the traditional air-breathing engines are not the only class of engines being proposed for hypersonic flight. One very different concept is the liquid air combustion engine, or LACE. Such an engine would use its store of cryogenic fuel (i.e. liquid hydrogen) to condense atmospheric air in some inlet/heat exchanger. The liquid oxygen in this condensed air could then be burned with the fuel in a conventional chemical rocket engine. The advantages of this concept are that it can be run from zero Mach number to hypersonic speeds, and the engine technology is well known. The primary disadvantage is the difficulty in designing an effective heat exchanger.

Another class of engines has been proposed that would use the propagation of expansion waves inside a channel to produce regions of cold air in the otherwise hot hypersonic flow, which could be used to power traditional turbomachinery [10]. However, the design of such engines is so impractical that they will not receive further attention in this work.

At the high Mach number range, it is questionable whether the scramjet will be sufficient to carry a hypersonic vehicle to orbit. It may be necessary to use rocket engines for the last phase of flight, for final orbital insertion, or to design a scramjet which could convert to a rocket mode, using a small reservoir of stored oxidizer. This work will not be concerned with this last phase of the trajectory.

1.3 Testing Difficulties and Verification

It has been suggested that the new generation of hypersonic vehicles will be designed entirely with computational techniques because of the difficulty in obtaining experimental data at the required conditions [11]. Unfortunately, without proper means of validating computational results, the reliability of such methods is suspect. Analytical methods can become hopelessly complicated when they are applied to anything beyond simple model problems.

The current hypersonic propulsion research environment can be divided into two classes

of hypersonic solutions. The first class consists of "simple" analytical models, generally one-dimensional, which attempt to determine fundamental physical principles, but which are difficult to apply to realistic engine and vehicle designs. In fact, the label "simple" is quite deceiving, for some of these models can become rather complex in their treatment of chemistry and losses.

A second class of solutions is the "complex" computational results. While these are more appropriate for determining the response of specific configurations, they are difficult to validate, and it is hard to extract meaningful physical insight from them. Also, many of the computational codes require massive run times, and so are inconvenient to use in a design process.

It is the goal of this research to bridge the gap between the "simple" analytical modelling and the "complex" computational solutions. It is hoped that certain fundamental physical principles important to the operation of scramjets can be made clear, while at the same time providing a meaningful basis for validating computational schemes. Simplifying assumptions have been sought which take advantage of the hypersonic conditions, so that analytically intractable problems can be reduced to tractable ones. Throughout, the rich body of hypersonic literature has been drawn upon, and applied as appropriate.

The lack of experimental data is a frustrating limitation in the development of analytical and computational solutions. The extreme Mach numbers at which scramjets are to operate exceed present experience with air-breathing engines. Current wind tunnel technology permits testing to about Mach 8, although actual air-breathing flight experience extends only somewhat above Mach 3. It is difficult to extrapolate these supersonic results to the hypersonic regime because of the increasing importance of real gas effects in the strong gradients and high temperatures encountered at very high Mach number. Thus, until hypersonic test vehicles can be flown, there will be a substantial gap between the knowledge required to successfully build and operate such a vehicle and existing hardware experience. Although it has been suggested that computational techniques will fill that gap, questions remain about proper and reliable code validation.

One area in particular which is inaccessible to current experimental techniques is the subject of this work, namely the study of inlet nonuniformities and their propagation through the scramjet. The procurement of pertinent experimental results is limited not only by the need for extreme Mach numbers at specific values of Reynolds number, but also by the coupling between the engine's internal flow and the external vehicle flow field. A proper simulation would therefore include not only the scramjet at high Mach number, but an appropriate vehicle forebody as well.

Chapter 2
Operating Environment and Vehicle Design Fundamentals

2.1 Designated Misions

In the current resurgence of hypersonic research, two vehicle mission profiles are proposed. The first concept is the so-called "Orient Express," designed to fly commercial traffic at hypersonic speeds across the globe. Such a vehicle would be a hypersonic cruiser, accelerating to some hypersonic Mach number ($\simeq$ 10) and then remaining at that speed until decelerating and landing. It is envisioned that an Orient Express could carry business passengers between New York and Tokyo in about two hours.

The second, and far more ambitious project receiving attention, is the notion of a hypersonic air-breathing space shuttle. In the simplest representation, such a vehicle would be a two-stage craft with a reusable air-breathing first stage, and a rocket-powered second stage, as is being studied in West Germany under the Sänger II program. The vehicle concept receiving the most attention in the United States is the single-stage-to-orbit, or SSTO vehicle. An SSTO would fly up to orbital speeds in the atmosphere, using air-breathing engines in a single reusable craft.

The design of a transatmospheric air-breathing vehicle is strongly dependent on the environment in which it will operate. Perhaps more than any vehicle yet designed, an aircraft such as that envisioned in the National Aerospace Plane program will be constrained to an extremely narrow operating envelope. The performance of the combustor, inlet, and nozzle will be so sensitive to changes in flow conditions that the vehicle will have to be designed with the trajectory and flight environment in mind.

Imbedded in the notion of a transatmospheric vehicles is the concept of vehicle/engine integration. The weight limits will be such that the outer surfaces of these vehicles will have to perform part of the propulsion plant function. For instance, the forebody will also serve as the engine inlet, and the aftbody will act as half of a plug nozzle. In a sense, the entire undersurface of the vehicle will be the engine, and what would normally be termed the propulsion plant will instead be merely a combustor. Thus, throughout this work, the reader should be careful of the distinction between the engine inlet, which actually refers to the external forebody compression surface, and the engine channel inlet, the opening leading into what is essentially just a combustor.

Because of the close coupling between the hypersonic vehicle design and its trajectory, it is difficult to define the trajectory independently of the vehicle configuration. This means that it is not meaningful to optimize a transatmospheric flight for a so-called "generic" transatmospheric aircraft, and no attempt will be made herein. However, it is possible to draw certain general conclusions about transatmospheric flight, and to use these as guidelines for trajectory selection and environment definition.

2.2 Environment Model and Trends

An air-breathing transatmospheric vehicle must fly through the relatively dense regions of the atmosphere on its way to orbital speeds. In strong contrast to trajectories for more traditional classes of rocket boosters, which aim to get above the atmosphere as quickly as possible to minimize drag, transatmospheric vehicle trajectories must remain low enough to provide sufficient reaction mass for the propulsion system. Thus, the selection of a transatmospheric trajectory is based strongly on the properties of the atmosphere, and on the aerodynamic performance of the aircraft and the propulsion system.

Before approximations are made of typical hypersonic transatmospheric trajectories, it is appropriate to describe the nature of the atmospheric profiles of temperature and density. Throughout this work, the atmosphere model that has been used is the *U.S. Standard Atmosphere, 1976* [12]. The reader is referred to that work for exact values of

the thermodynamic properties of the atmosphere in the range of interest here.

Throughout this work, a continuum fluids approach will be used to model the flow on the forebody and in the engine of a hypersonic vehicle. The validity of this approach is based on the fact that at the altitudes being considered, the atmospheric mean-free-path is very small. Mean-free-path is inversely proportional to the number density in the atmosphere, which decreases exponentially through the lower portion of the atmosphere. Thus, there is a considerable increase in mean-free-path as altitude increases. For instance, at sea level, the mean-free-path $\lambda_{mfp} = 6.6 \times 10^{-8}$ m, and at 50 km, $\lambda_{mfp} = 7.9 \times 10^{-5}$m. Compared to relevant vehicle dimensions, the flow can be treated as a continuum. Note that there may be local regions on the vehicle surface where mean-free-path is quite large, and the flow resembles rarefied, such as at a very sharp leading edge. These regions will not be here.

Some estimates can be made of the sorts of trajectories that would be characteristic of transatmospheric flight based on the limitation of thermodynamic and aerodynamic parameters. A more complete analysis of the trajectory would consider the equations of motion under assumptions of the vehicle's thrust/drag and lift/drag. However, it is assumed here that the thermodynamic considerations, such as combustor temperature and pressure, and structural limitations due to dynamic pressure will be the most difficult to avoid, while the thrust and lift can be tailored as required to meet these constraints.

2.3 Trajectory Selection

2.3.1 General Trends

Air-breathing vehicles must fly at relatively low altitudes in order to ingest sufficient air for engine operation, and to maintain acceptable thermodynamic conditions for combustion to proceed at a sufficient rate in the engine. so the combustion process is accomplished in a reasonably-sized combustor channel. An over-long combustion path length will increase required engine length, and thus mass, and so is undesirable.

There are two limits on the rate at which fuel can be added in the combustor. The first is the rate at which fuel will mix into the engine, and the second is the rate at which fuel will burn. The mixing problem is of paramount concern in hypersonic research, because at high-speeds streamtubes tend not to mix. There is a substantial research effort currently under way to determine if fuel mixing can be enhanced, or if it is even possible to realize.

A second limiting process is the reaction rate inside the engine. Hydrogen is usually indicated as the fuel of choice because it has such a fast combustion rate. If the combustion process is too slow, an engine which is designed for complete combustion heat release will be impractically long. If this reaction rate is slower than the mixing rate, the combustion must be sized based on the chemical kinetics inside the engine. In this work, the mixing problem will not be addressed; rather, the effect of varying thermodynamic conditions on the combustion rate will be explored, subject to the assumption that fuel mixing is possible and not rate-limiting. It is expected that the combustor will be reaction rate- limited at low pressure ($\simeq <$ 1/10 atm.) and mixing rate-limited at high pressure ($\simeq >$ 5 atm.) where combustion proceeds quickly.

Studies have shown that the combustor operation requires pressures in the range of about one atmosphere. As was shown in chapter 1, at low pressure, the combustion rate is slow because of the reduction in collision frequency. At higher pressures, three-body reactions tend to rob the combustion system of hydrogen, and so the reaction rate is reduced.

It is reasonable to assume that inlet air is delivered at temperatures near 1000 K. With typical stratosphere temperatures of about 220 K up to about 35 kilometers altitude, this implies a limit of five-fold increase in static temperature across the inlet shock system. For a three-shock inlet system in which each shock has the same temperature rise, the pressure rise associated with the total temperature increase would be a factor of approximately 80. In order to provide one atmosphere combustor pressure, the ambient pressure should therefore be about .013 atmospheres, which is found at 27 km altitude.

Because pressure falls off roughly exponentially with altitude, increased altitude results in dramatically decreased combustor pressure. For instance, at 45 kilometers, atmospheric

pressure is down to less than .002 atmospheres, while ambient temperature has risen to 310 K. In order to keep inlet temperatures at 1000 K, a three-shock inlet system would have an associated pressure ratio of 35, yielding a combustor inlet pressure of only .07 atmospheres, too low for effective combustion to occur.

The fundamental result of matching trajectory to combustor performance requirements is the conclusion that the engine operates best at relatively low altitudes. Conversely, constraints on the vehicle structure demand the opposite trend. Thermal limitations dictate trajectories that take the vehicle into higher altitudes where surface heating is reduced.

2.3.2 Constant Dynamic Pressure Trajectories

One indication of trajectory constraints is the dynamic pressure. In hypersonic flight, dynamic pressure correlates closely with engine inlet conditions, because dynamic pressure indicates the maximum pressure rise through the shock. The dynamic pressure limitation is generally less severe than that for the heating limit, especially at the high-speed portions of the trans- atmospheric trajectory. The dynamic pressure, $q_{\text{dynamic}} = \frac{1}{2}\,\rho(y)\,U^2$ is a function of both speed and local density. It is most convenient to plot the trajectory in terms of the Mach number, so that the known atmospheric temperature profile must be included in the trajectory:

$$M(y) = \sqrt{\frac{2\,q_{\text{dynamic}}}{\gamma R_{\text{air}} T(y) \rho(y)}} \tag{2.1}$$

$$= \sqrt{\frac{2\,q_{\text{dynamic}}}{\gamma p(y)}} \tag{2.2}$$

The trajectory is then solved by simply calculating M at each altitude, until the desired orbital velocity is achieved.

It is ultimately of interest to accelerate the transatmospheric vehicle to orbital speeds and beyond for SSTO flight. Orbital velocity in a low-earth orbit is 7.8 km/sec, so the final trajectory velocity must be at least that. Below 50 km, that translates to about Mach 26.

The air-breathing trajectory will likely bring a hypersonic shuttle to a final altitude

which is much lower than the desired orbital altitude. To get to orbital height, a hypersonic shuttle could fly beyond orbital speed, then pitch up and climb, losing velocity as it does so.

The required overspeed can be estimated by equating the excess kinetic energy to the required gain in potential energy for reaching the desired altitude. Thus, for such a maneuver, the final flight velocity would be:

$$U_{\text{final}} = 7.8 \text{ km/sec} + \sqrt{2\,g\,(h_{\text{orbital}} - h_{\text{final}})} \tag{2.3}$$

where h_{orbital} is the final desired orbital altitude, and h_{final} is the actual final altitude at the end of the constant dynamic pressure trajectory, before the pitch-up maneuver. In fact, for a typical value of $(h_{\text{orbital}} - h_{\text{final}}) \simeq 150$ km.,

$$\sqrt{2\,g\,(h_{\text{orbital}} - h_{\text{final}})} \simeq 1.7 \text{ km/sec} \tag{2.4}$$

The potential energy gain is only 22% of the kinetic energy. The final Mach number to orbit is shown in the trajectory plot of Figure 2.1. Note that losses due to drag during the pitch-up maneuver have been neglected. Figure 2.1 shows trajectories for dynamic pressures of 1/10, 1 and 10 atmospheres.

2.3.3 Constant Equilibrium Temperature Trajectories

At hypersonic speeds, the surface of the aircraft will become quite hot as the work done by drag on the air is converted to heat. The heating load to the vehicle surface must be limited or counteracted if the surface materials and the structure are to survive, especially if the vehicle is to be reusable.

Since the vehicle nose and leading edge sharp points will be the hottest points on the outer surface, the temperature limiting trajectory can be plotted by assuming some simple geometry, and then calculating the expected heat load. The heat load can be estimated from the Fay-Riddel heating law, based on a curve fit of numerical solutions to the compressible stagnation-point boundary layer equations [13]:

$$Q_{\text{stag.pt}} = \frac{.76}{Pr^{.6}}(\rho\mu)^{.1}_{\text{wall}}(\rho\mu)^{.4}_{\infty}\left[1 + (\text{Le}^{.52} - 1)\frac{h_D}{h_t}\right](h_t - h_{\text{wall}})\sqrt{\left.\frac{du}{dx}\right|_{x=0}} \tag{2.5}$$

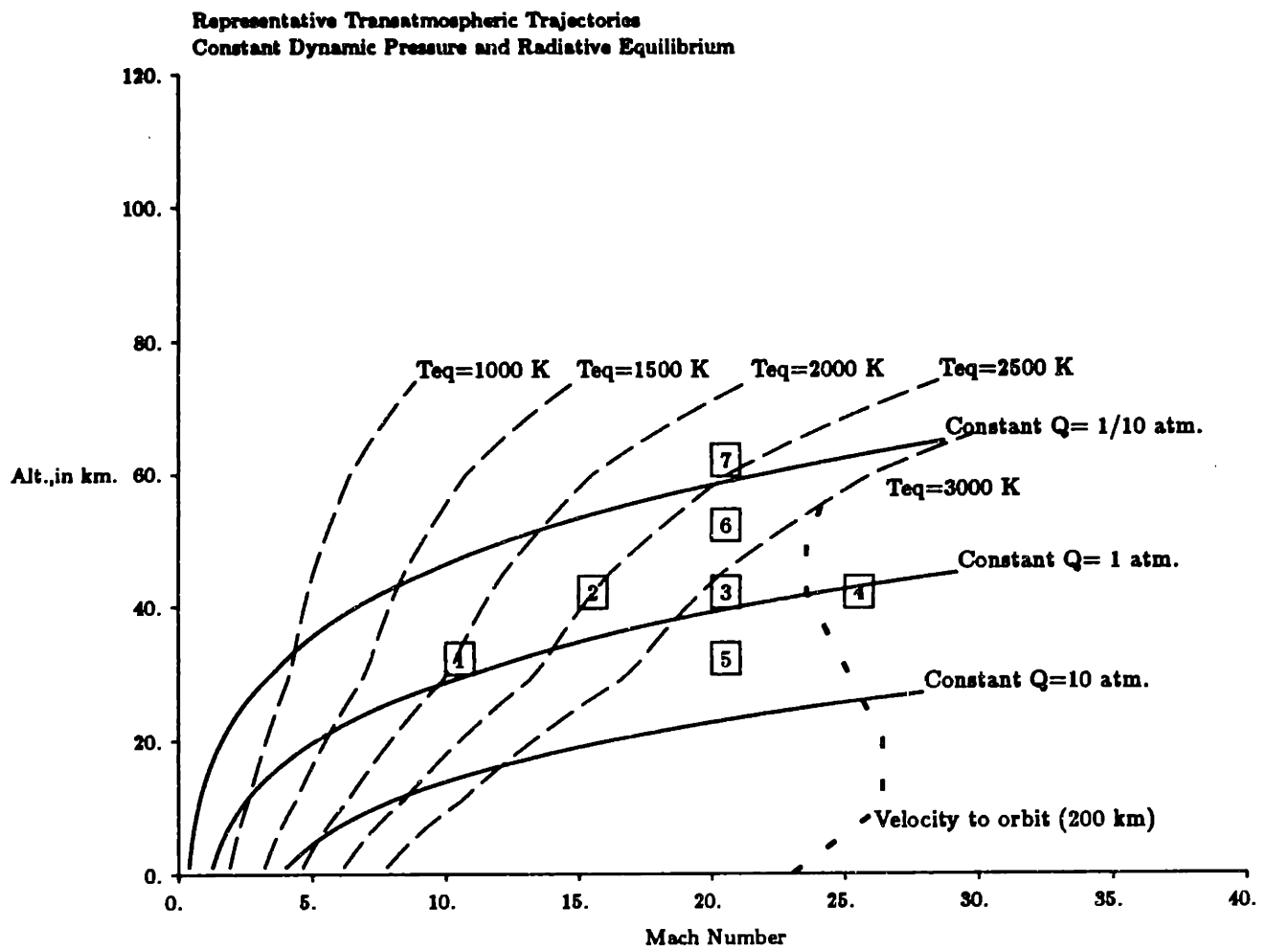

Figure 2.1: Constant dynamic pressure and constant radiative equilibrium temperature trajectories. Boxed numbers refer to points in the first column of Table 3.2.

where Le is the Lewis number, about 1.4 in the conditions of interest, h_D is the dissociation enthalpy, and $du/dx|_{z=0}$ is the streamwise gradient of velocity in the free-stream. This formula has been shown to match experimental data quite well by Rose and Stark [14].

From the Stefan-Boltzmann radiation law, the equilibrium surface temperature can be calculated by setting the radiated heat equal to the Fay-Riddel heating rate:

$$T_{\text{equilibrium}} = \left(\frac{Q_{\text{stag.pt.}}}{\epsilon \sigma} \right)^{1/4} \tag{2.6}$$

where ϵ is the assumed surface emissivity, about .8 for the most likely materials to be used [15].

The temperature limit on the nose of the space shuttle is 2500 K. It is assumed that materials capable of withstanding in excess of 2500 K for sustained periods will not be available. The constant radiative equilibrium trajectory required to keep a 1 meter diameter nose at 2500 K is plotted in Figure 2.1, along with trajectories for other nose temperatures. From the Fay-Riddel law, it is apparent that the stagnation point heating rate scales with the inverse square root of the stagnation point radius, so the radiative equilibrium temperature scales with the -1/8 power of nose radius. The 1 meter diameter nose quoted above is based on the space shuttle, and a hypersonic vehicle will likely have much sharper leading edges, corresponding to increased radiative equilibrium temperature. The 1000 K equilibrium contour for a 1 meter nose corresponds to 1800 K for a 1 cm nose; the 2500 K contour at 1 meter corresponds to 4500 K at 1 cm.

The trajectory plots in Figure 2.1 show that, below about Mach 10, surface heating is not a limiting factor, and the constant dynamic pressure trajectory will keep the hottest points on the vehicle within reasonable materials limits. However, above Mach 10 or so, the radiative equilibrium trajectory takes the vehicle to higher altitudes than the one atmosphere constant dynamic pressure plot. At Mach 18, the 2500 K heating limit requires an altitude that is higher than even the 1/10 atmosphere dynamic pressure trajectory.

2.3.4 Engine Inlet Constraints

The example given for flight at Mach 10 with 1 atmosphere inlet pressure and 1000 K inlet temperature suggested that, in general, combustion in a hypersonic airbreathing engine will operate proceed best at altitudes that are below those determined by airframe structure and heating constraints.

Figure 2.2 shows a set of trajectories plotted for the compression provided by a two shock inlet, each shock corresponding to a wedge at 5 degrees. Trajectories are shown for inlet pressures in the vicinity of one atmosphere, where a scramjet will have to operate. Also on the same plot are lines of constant inlet temperature for the 5 degree, two-shock inlet geometry. Note that in order to deliver between 1/2 and 1 atmosphere pressure, the vehicle will have to fly below 15 km at Mach 10, and below 25 km at Mach 25, corresponding to dynamic pressure of about 6 atmospheres. Inlet temperatures in this trajectory are reasonable, remaining below 1500 K throughout the flight.

In order to deliver higher inlet pressure, and thus fly at a higher altitude and lower dynamic pressure, the wedge angle can be increased, or ramps can be added to the inlet (the effect is the same). Figure 2.3 shows constant inlet pressure trajectories with a wedge angle of 10 degrees. Notice here that, in order to achieve between 1/2 and 1 atmosphere inlet pressure, the vehicle is now flying at 20 km at Mach 10, and 30 km. at Mach 25. This would result in dynamic pressures of about 3 atmospheres, which is still high, though more acceptable for the airframe than the 5 degree wedge solution.

Higher compression comes with a correspondingly higher inlet temperature. With the 10 degree wedge solution, the inlet temperature is 1000 K at Mach 10, and rises to 3000 K at Mach 25, as shown in Figure 2.3. This latter figure is too high for combustion to proceed, and is also too high for adding heat from a recuperator.

The requirement to match pressure and temperature along the trajectory suggests that it may be necessary to design a transatmospheric vehicle with a variable-geometry inlet, such that the inlet wedge angle can be modified. If the apparent inlet angle could be set to

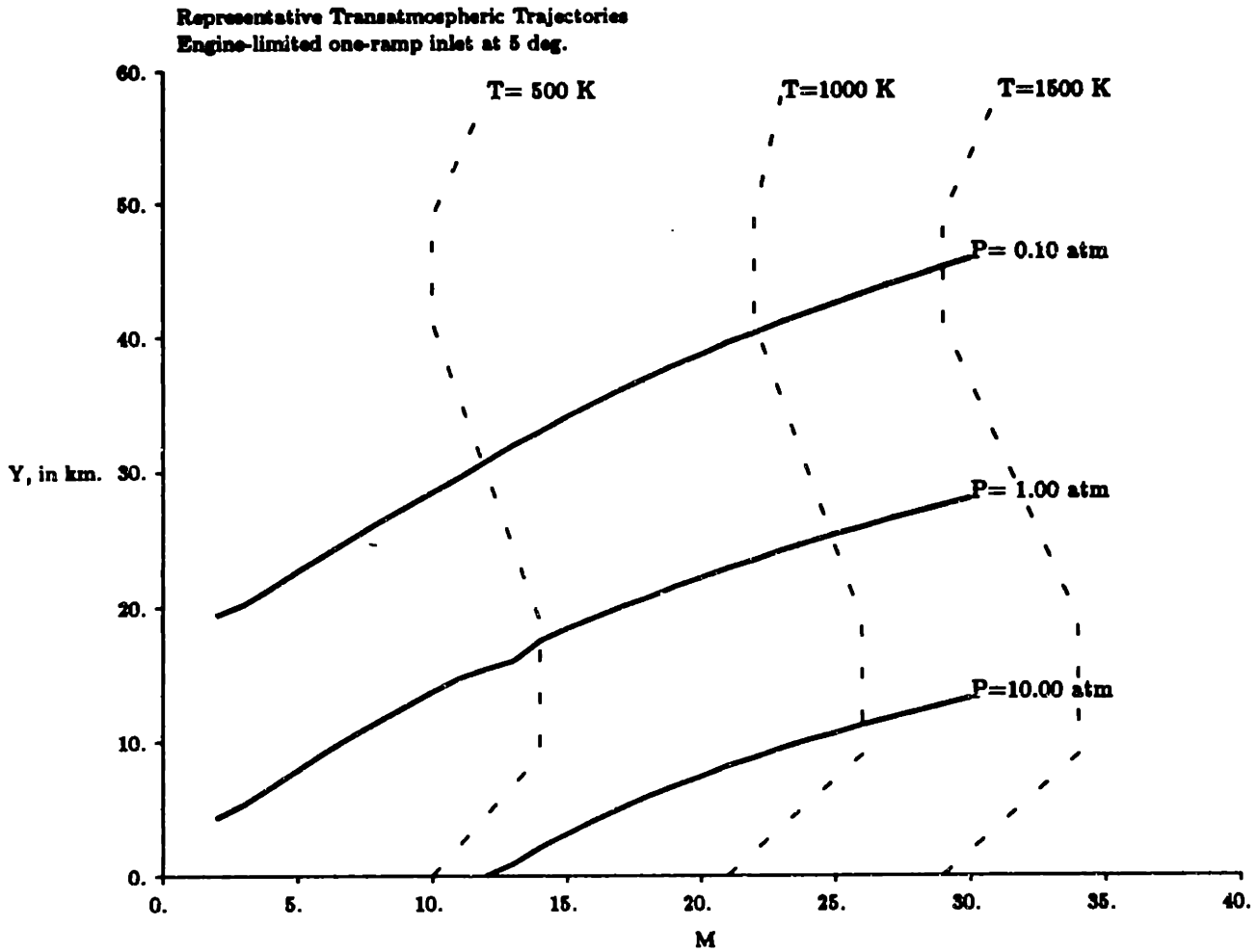

Figure 2.2: Constant inlet pressure and temperature for a two-shock inlet with 5 degree wedge angles

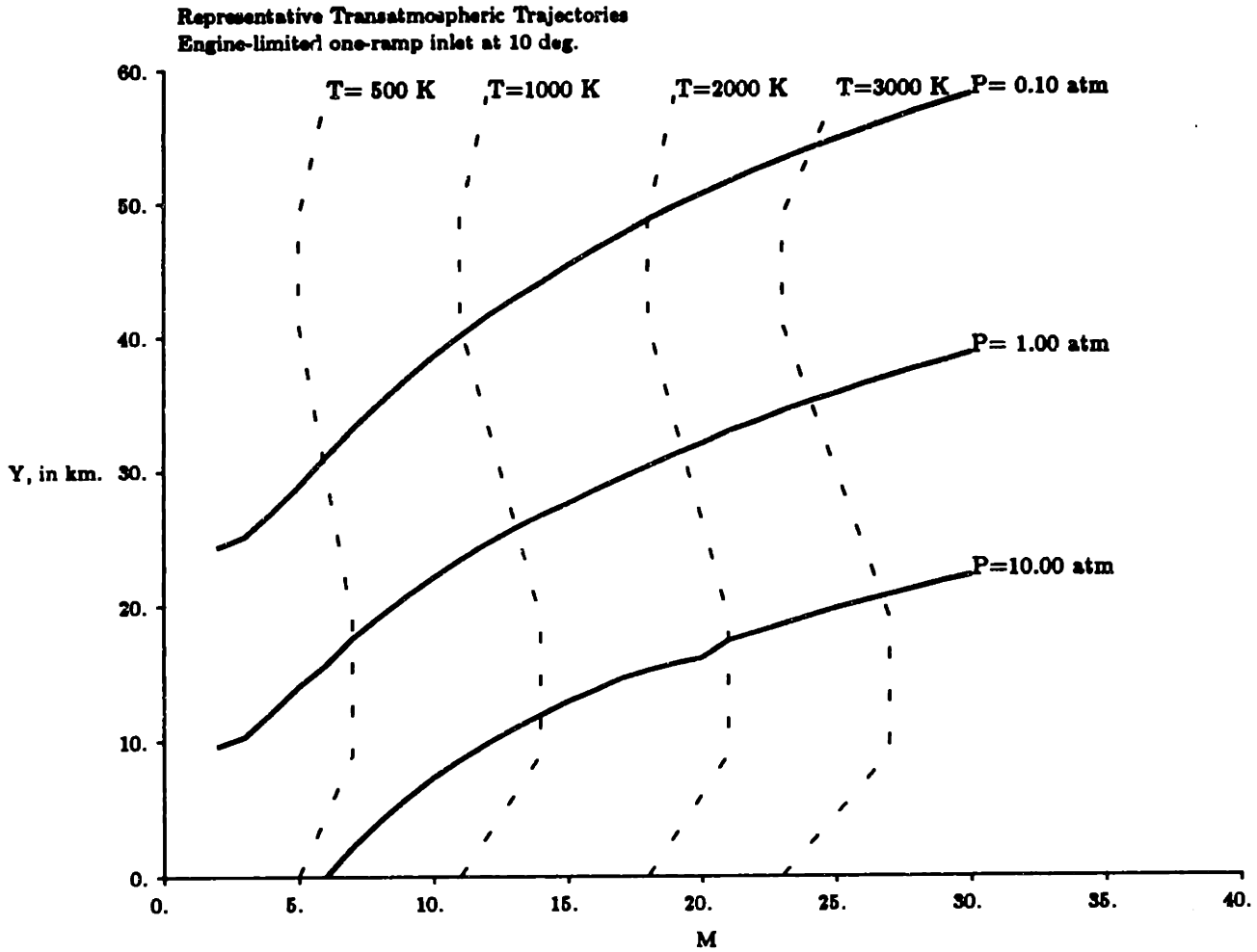

Figure 2.3: Constant inlet pressure and temperature for a two-shock inlet with 10 degree wedge angles

any desired value, a unique altitude would be determined for which the specified pressure and temperature would be delivered to the inlet at all supersonic flight Mach numbers.

The pressure- and temperature-matched altitude is determined by solving for the pressure ratio across an oblique shock as a function of the temperature ratio, without worrying about the wedge angle or shock angle explicitly. It will be assumed that the inlet will provide the necessary geometry to produce a shock of any appropriate angle. Starting with the Hugoniot relationship for the pressure ratio across a shock as a function of the density ratio [5]:

$$\frac{p_2}{p_1} = \frac{\left(\frac{\gamma+1}{\gamma-1}\right)\frac{\rho_2}{\rho_1} - 1}{\left(\frac{\gamma+1}{\gamma-1}\right) - \frac{\rho_2}{\rho_1}} \tag{2.7}$$

The simple equation of state is still valid in spite of dissociation and reactions as long as the individual species have minimal intermolecular forces. Introducing the temperature ratio from the equation of state

$$\frac{\rho_2}{\rho_1} = \frac{p_2}{p_1}\frac{T_1}{T_2} \tag{2.8}$$

we can write

$$\frac{p_2}{p_1} = \frac{\left(\frac{\gamma+1}{\gamma-1}\right)\frac{p_2}{p_1}\frac{T_1}{T_2} - 1}{\left(\frac{\gamma+1}{\gamma-1}\right) - \frac{p_2}{p_1}\frac{T_1}{T_2}} \tag{2.9}$$

Solving for the pressure ratio in terms of the temperature ratio:

$$\frac{p_2}{p_1} = \frac{\sqrt{(\gamma+1)^2\left(\frac{T_2}{T_1}^2+1\right) + 2(\gamma^2-6\gamma+1)\frac{T_2}{T_1}} + (\gamma+1)\left(\frac{T_2}{T_1}-1\right)}{2(\gamma-1)} \tag{2.10}$$

This is the pressure ratio across a single shock. For an inlet with n shocks, assuming there is equal temperature ratio across each shock and uniform γ, the overall pressure ratio in terms of the overall temperature ratio is:

$$\frac{p_2}{p_1} = \frac{\left(\sqrt{(\gamma+1)^2\left(\left[\frac{T_2}{T_1}\right]^{2/n}+1\right) + 2(\gamma^2-6\gamma+1)\left[\frac{T_2}{T_1}\right]^{1/n}} + (\gamma+1)\left(\left[\frac{T_2}{T_1}\right]^{1/n}-1\right)\right)^n}{2^n(\gamma-1)^n} \tag{2.11}$$

Thus, by specifying a temperature ratio, the pressure ratio is uniquely determined. Because there is no explicit dependence on Mach number in equation (2.11), there is a *fixed* altitude at which pressure and temperature are matched to the desired inlet conditions

regardless of speed. The variable inlet adjusts the shock angle so that, at any Mach number, the incident normal Mach number is fixed.

Figure 2.4 is a plot of the matching altitude versus the desired inlet pressure, for various inlet temperatures, on an inlet with two shocks. The results for inlets with higher numbers of shocks are about the same, as shown by Figure 2.5, which plots the matching altitude for a three shock inlet. From these figures, it is seen that, with a fully variable inlet, a transatmospheric vehicle would have to fly at 27 km altitude to keep its inlet at 1000 K and one atmosphere, which is consistent with earlier results. In general, for a given inlet pressure, lower inlet temperature requires lower flight altitude. For instance, to maintain the same one atmosphere pressure, the inlet temperature air would be 2000 K at 36 km., and have the unreasonable value of 3000 K at 40 km; to get 1/2 atmosphere at 1000 K, the matching altitude is about 30 km.

Figure 2.6 shows the wedge angle required to maintain 1000 K temperature at 1 atmosphere pressure. At Mach numbers greater than 15, this wedge angle does not change much with increasing Mach number. Also shown in Figure 2.6 is the difference between the shock angle and the wedge angle, which indicates how much the engine inlet would have to be moved in order to keep the shock attached to the engine lip, or how far off the shock would be on a fixed lip.

2.3.5 Engine-Airframe Trajectory Matching

The above results indicate that the engine will operate best with a low altitude trajectory. This is incompatible with the trend towards higher altitude which is required for practical airframe design. A constant radiative equilibrium trajectory takes the vehicle to unacceptably high altitudes at large Mach number. For proper engine operation, the temperature-limited flight profile is not acceptable. Rather, the vehicle will probably be flown on as low a trajectory as possible for the engine, operating at the highest acceptable constant dynamic pressure, and almost certainly taking a compromise in engine performance. A low trajectory means that the vehicle surface will be heated to intolerably high

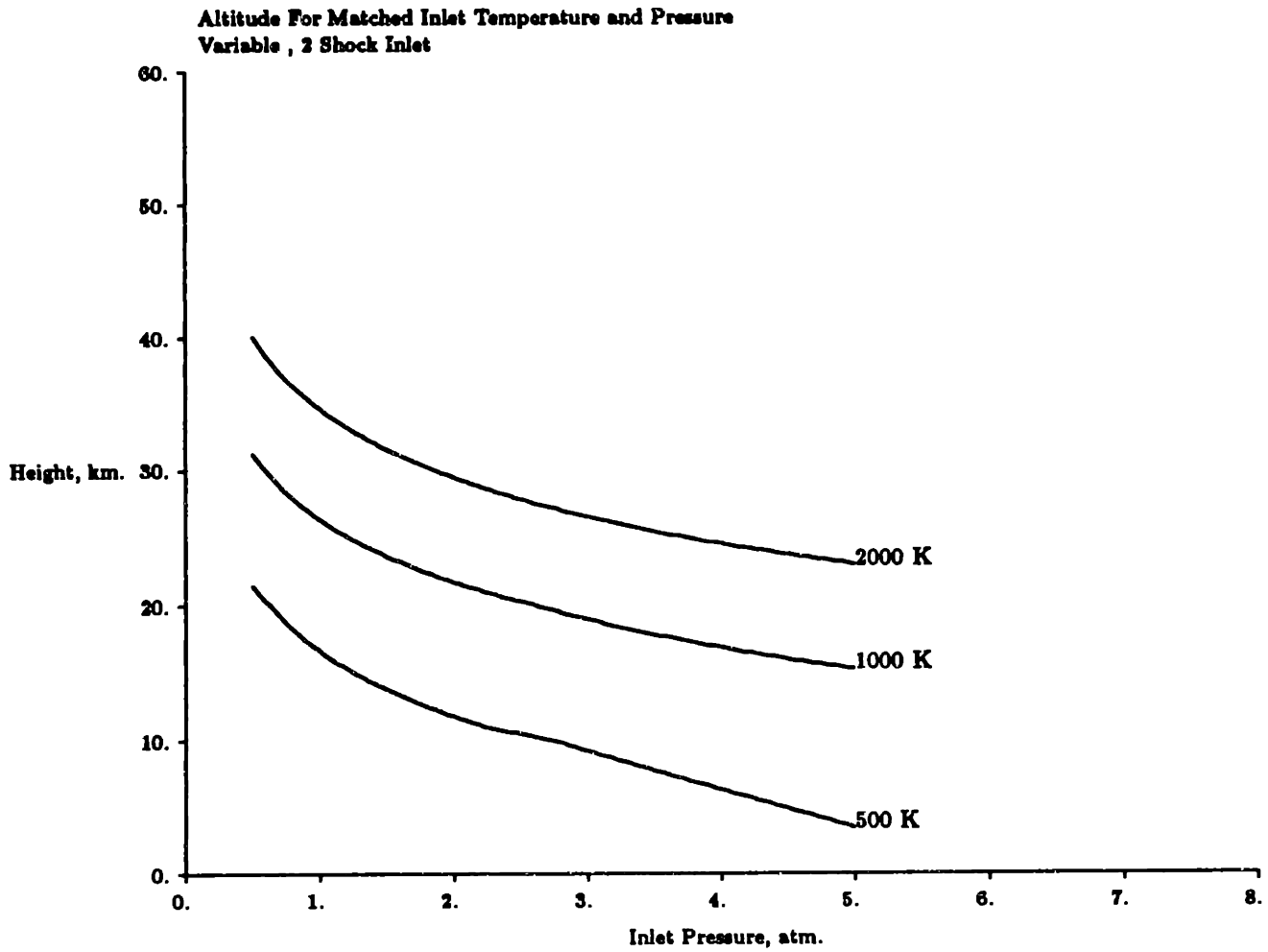

Figure 2.4: Altitude required to match temperature and pressure with a two-shock inlet

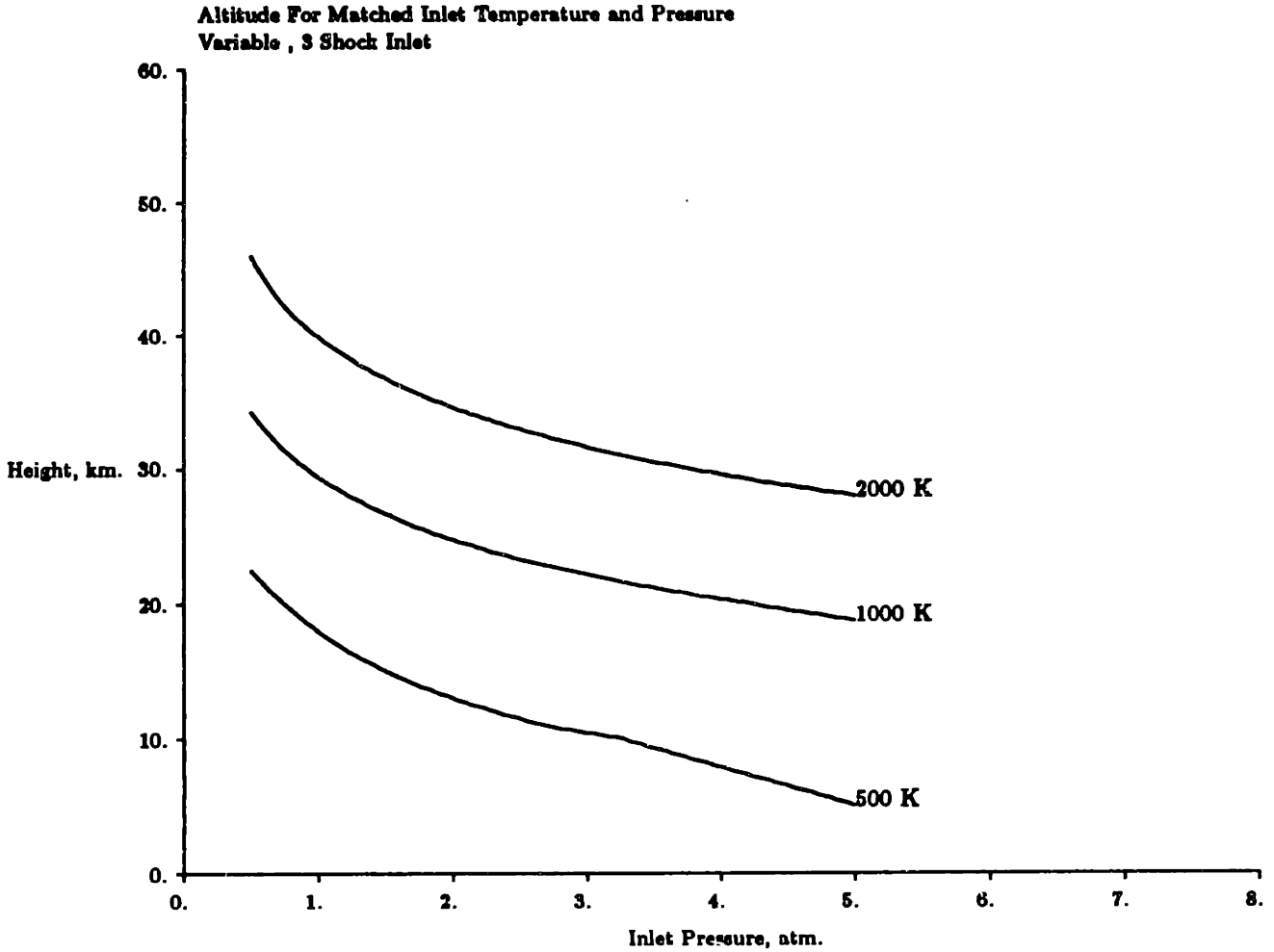

Figure 2.5: Altitude required to match temperature and pressure with a three-shock inlet

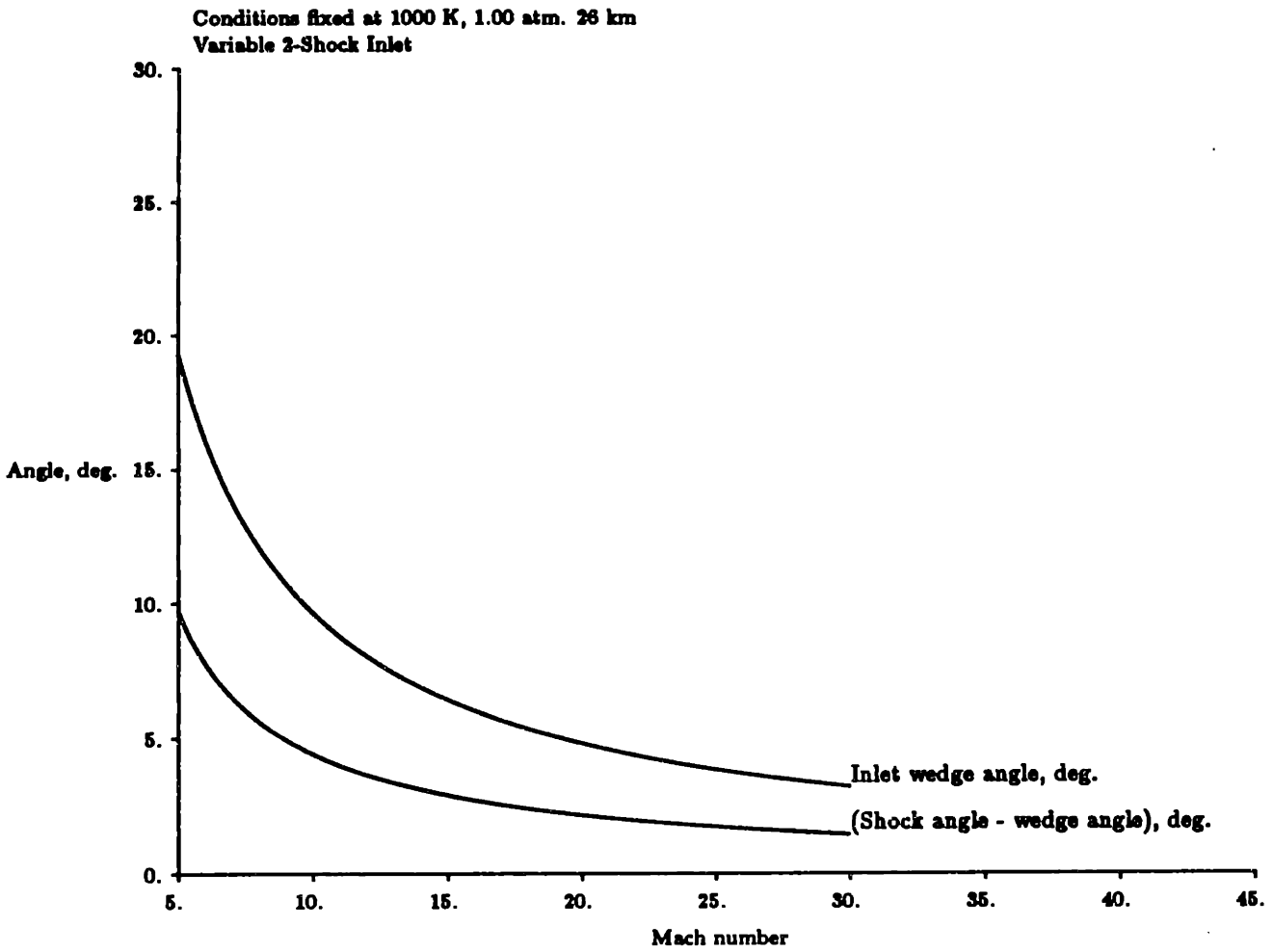

Figure 2.6: Inlet wedge angle and resulting difference between wedge and shock angles for 1000 K, 1 atm. variable inlet

values unless there is some active cooling.

A surface cooling scheme would presumably circulate the onboard cryogenic fuel through the aircraft skin in some manner, thereby heating the fuel before injecting it into the combustor. This recuperated heat may represent a substantial portion of the heat energy being delivered in the combustor at high Mach numbers. Indeed, at Mach numbers greater than 15, it is unlikely that combustion will proceed at all, and all the heat addition in the combustor will be derived from recuperated heat off the vehicle surface and the intrinsic fuel kinetic energy.

The problems in the design of such a cooling system are formidable. Not only must the system meet the mechanical requirements of reaching all portions of the surface with very little mass, but the required heat capacity of the cooling agent may increase the volume of cryogenic fuel that must be carried to several times the amount dictated by stoichiometry. These difficulties are beyond the scope of this present work.

By assuming the vehicle will have an active cooling system, the solution of the forebody flow field can be done with a constant, uniform wall temperature. In all of the following work, the cooling system will be assumed to deliver all of the heat removal required to maintain the wall at a preset temperature, and the details of the actual wall heat transfer process will not be explicitly considered. With a fixed wall temperature, the forebody laminar boundary layer can be solved with a similarity solution. This assumption is clearly a simplification.

Cooling will reduce the heat loss due to radiation. Because radiation scales with the fourth power of temperature, it is presumed that at the controlled wall temperatures provided by the cooling system, radiation is unimportant. This is shown using the Fay-Riddel solution. in Figure 2.7. The constant dynamic pressure trajectory is plotted against lines which indicate the fraction of the heat transferred to a 1 meter vehicle nose that is radiated away from a surface of constant 2000 K temperature, as provided by the cooling system. The 100% radiation contour thus corresponds to the radiative equilibrium trajectory for the surface temperature chosen, and at this point, no cooling would be necessary. As the

radiation represents a smaller fraction of the heating load, the cooling system must begin to work at removing heat from the surface. For smaller nose radius, the fraction of radiated heat would be smaller, since the equilibrium temperature would be higher. With a 1 cm nose radius, the contours shown for 1 meter radius would be reduced by a factor of 10.

It can be seen from Figure 2.7 that radiation is a relatively minor fraction of the convective heat transfer throughout most of a 1 atm. constant dynamic trajectory with surface cooling. This will be used to justify the neglect of radiation in solving for the forebody profile; the only heat transfer mechanisms that will be considered in the forebody flow will be collisional ones.

2.4 Vehicle Design Approximations

In order to calculate the stratification of flow properties at the inlet of a hypersonic vehicle, it will be necessary to make some approximations as to the general shape of the vehicle forebody. As of this writing, there are no finalized plans for the National Aerospace Plane, and the exact configuration of an air-breathing hypersonic transatmospheric vehicle is unknown. There are, however, certain design criteria that must be met by any of this class of vehicles, and so it is possible to describe a "generic" hypersonic aircraft. Such a vehicle is pictured in Figure 2.8.

As described above, one design goal is the construction of an integrated engine/airframe, in which the forebody undersurface acts as the inlet, providing compression of engine air, and the aftbody acts as a nozzle, so that the engine system consists of essentially the entire undersurface. In fact, this concept is not really new; for instance, the F-4 Phantom jet used the portion of its tail section fuselage behind the engines as a nozzle extension.

With the intention of using the forebody and aftbody as described, the combustor channel must sit somewhere in the middle of the vehicle undersurface, as shown in Figure 2.8. A strong requirement for the placement of this engine module is the matching of the aircraft bow shock to the channel lip. If the shock is swallowed inside the channel, reflecting

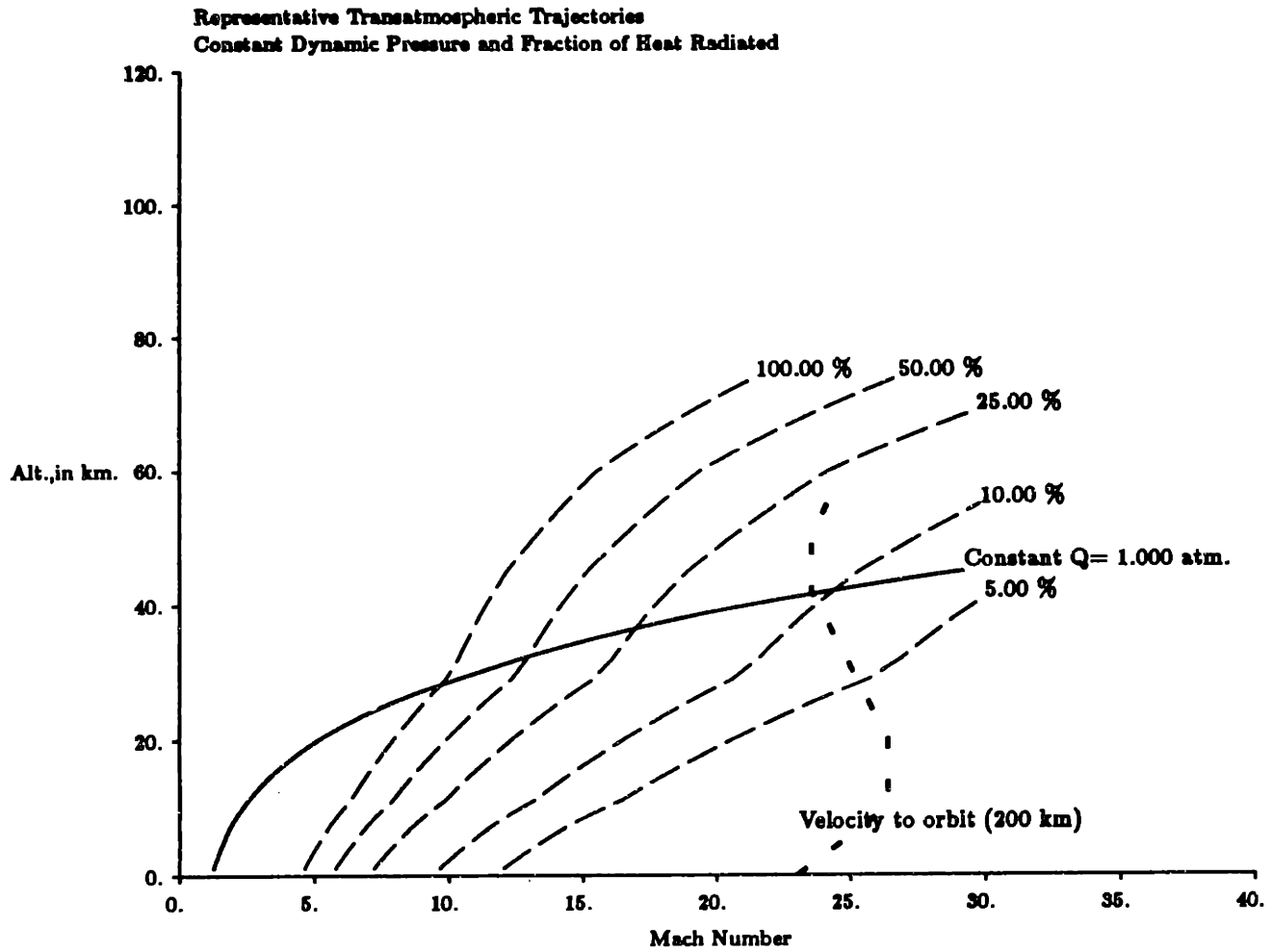

Figure 2.7: Constant dynamic pressure and percentage of heat reradiated with surface temperature of 2000 K on 1 meter radius nose.

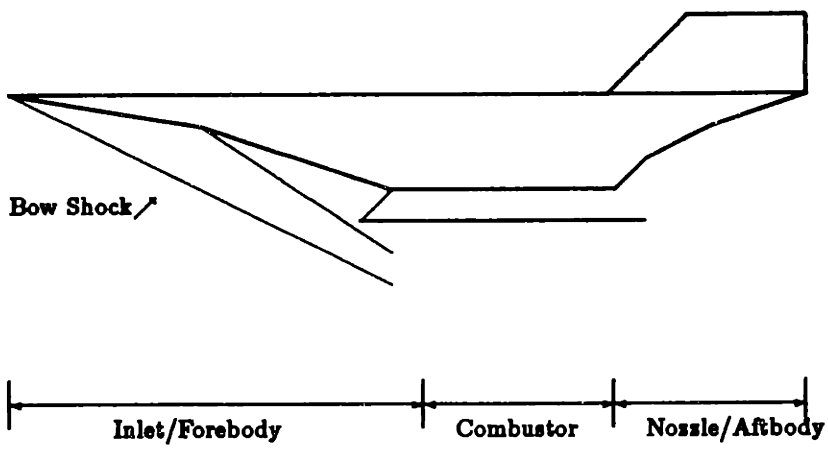

Figure 2.8: Generic hypersonic vehicle

shocks and enhanced heat transfer at the point of shock contact will be deleterious to engine operation. Recent work has shown that shock impingement on a leading edge can increase local heat transfer by 20 times the usual stagnation rate, which will burn through the most robust of materials [16]. On the other hand, if the bow shock falls below the engine cowl, the flow over the cowl will form another strong shock and introduce more wave drag on the vehicle. It is therefore assumed that the bow shock must approximately contact the engine cowl (without exactly contacting), a constraint that leads to many difficult control questions, some of which will be addressed later.

At hypersonic speeds, the bow shock will be pressed very close to the vehicle surface. Indeed, this is one of the defining characteristics of a hypersonic flow. The small angle between shock and surface means that the forebody must be very long in order for the engine to swallow sufficient mass, as shown in Figure 2.8. Because the flow is hypersonic, the vehicle must be thin to avoid strong shocks, a feature which is also shown in the picture. Note that the engine capture area is actually the streamwise-projected area from the bottom of the cowl to the tip of the nose, since all the flow under the shock is ingested in the engine when the shock is properly matched. The long forebody offsets the small wedge angle to provide sufficient capture area. It is assumed throughout this work that the forebody on a typical transatmospheric vehicle would be between 10 - 30 meters long.

It is this long forebody that has prompted the current investigation. Normally, it would be expected that flow over such a long surface would develop a thick boundary layer. In addition, hypersonic boundary layers tend to be thick in general because the high temperatures associated with decelerating high-speed flow produce very low densities and higher coefficients of viscosity. This effect is amplified at higher altitudes, where the lower ambient density yields even higher kinematic viscosity. It is also well established that shear profiles do not mix out in high-speed flow, so that once the boundary layer profile is formed it will tend not to mix out inside the engine [4].

It is unlikely that there is any way to avoid swallowing this boundary layer into the engine channel. The boundary layer is too hot to channel off, and the engine cannot be offset below the vehicle surface, as is commonly done in fighter aircraft, because of the

resulting blunt-body heating that would occur between the engine and the vehicle. Some researchers have nevertheless suggested that the boundary layer will be siphoned off before the flow enters the engine channel [11]. If this is true, the present study of nonuniformities must be treated as a worst-case scenario, and perhaps as a basis upon which the penalties and benefits of boundary layer bleeding can be evaluated.

In modelling the forebody flow, simple two-dimensional assumptions will be made for the vehicle geometry. It is rather uncertain at this point what the most desirable form of the forebody geometry is, although substantial research is being conducted in this area [17]. An actual hypersonic aircraft would have highly three-dimensional flow over its forebody, and thus entering its engine channel. Without knowing the details of a forebody geometry, it is difficult to speculate on the full three-dimensional nature of the flow. Therefore, in this work, the forebody flow has been modelled in only two dimensions. For instance, 2-d flat plate solutions have been used to model the forebody wall, and transition correlations have been made with axisymmetric cone data. In fact, the primary nonuniformities being examined here are essentially two-dimensional in nature, with three-dimensions adding an extra degree of complexity, but not necessarily more insight.

In specifying even a two-dimensional forebody geometry, there is still some basic uncertainty as to how the compression will be accomplished. For instance, we could picture a single-ramp undersurface, which is essentially a wedge at constant angle, or a forebody with one or more ramps of increasing wedge angle leading up to the engine inlet. As such, the forebody models to be used will handle ramps and their associated shocks. Examining the design advantages and disadvantages of a multi-ramp vehicle is beyond the scope of this work, but some effects of ramps will be demonstrated in the boundary layer solution.

Another issue in setting the basic geometry is the orientation of the engine channel with respect to the forebody. Traditionally, the engine unit is pictured as being parallel to the flow direction, so there is no strong shock below the cowl. This means that the flow must turn to enter the flow, which implies the formation of a shock at the engine inlet, unless the flow can be turned isentropically. With such an engine placement, the effect of this entrance shock on the engine profile must be considered. Another scheme would place the

engine cowl parallel to the forebody wall, and thus avoid the entrance shock. While this would reduce losses inside the engine, it will lead to the formation of strong shocks on the outside of the cowl, and thus increase vehicle drag. Both flow scenarios will be considered.

As described in chapter 1, only the scramjet propulsion concept will be studied in this work. This engine will be modelled as a two-dimensional channel, in which the inlet flow is decelerated to some combustor Mach number. For baseline comparisons, the combustor will be designed for constant pressure with unform inflow. Because this work attempts to deal with general trends in hypersonic flows, no specific engine geometries or flow conditions will be assumed, except where noted.

The nonuniformity flow path is thus a simple one. A profile will form on a flat plate at some angle of incidence, possibly with a ramp downstream. This flat plate flow will then enter a channel, where its effects on the channel properties will be noted in comparison to expected results for uniform inflow.

Chapter 3

Hypersonic Boundary Layer Displacement Thickness On the Vehicle Forebody

The first step in calculating the stratification entering a hypersonic airbreathing engine is estimating the boundary layer thickness and profile, for that will be the major source of inlet nonuniformities. In this work, the results of classical hypersonic boundary layer theory will be applied to the forebody of a hypersonic vehicle. An analytical approach will be retained throughout to describe the boundary layer properties.

3.1 Transition and the Laminar Model

It is difficult to determine whether the forebody will be laminar or turbulent because there is little data on hypersonic transition, and the ground test data that does exist conflicts with flight test data. Available data and trends at moderate hypersonic speeds will be extended to the range of Mach numbers typical in a transatmospheric trajectory.

Published steady-state wind tunnel transition data extends to Mach 8 [18], with transient test data to Mach 16 [19] [20]. From this data, certain trends are apparent. As Mack [18] has justified analytically, transition Reynolds number increases with increasing Mach number in the hypersonic range. Sheetz [20] found that transition Reynolds number is independent of wall temperature when plotted as a function of local Mach number.

Using the sharp cone data of Sheetz [20], a curve fit is found for transition Reynolds number:

$$Re_{\text{transition}} \simeq 6400\,(M_{\text{local}})^{3.66} \tag{3.1}$$

Table 3.1: Transition length from wind tunnel data

Mach Number	Altitude in km	Transition Point in m
6	30	2
25	30	100
6	50	20
25	50	900

Some representative transition points an flat plates are shown in Table 3.1. It is uncertain how closely this cone data represents transition on a flat plate.

The altitude at which transition occurs as a function of Mach number is plotted in Figure 3.1 against the constant dynamic pressure trajectories. On the one-atmosphere trajectory, a 30 meter forebody will be fully laminar above Mach 15, based on wind-tunnel correlations. Actual flight-test data have shown transition Reynolds numbers up to an order of magnitude greater than wind tunnel results, and studies such as that of Stetson [19] have also found hypersonic transition points can be pushed back by an order of magnitude due to leading edge bluntness. Shuttle reentry data has also shown laminar flow on that vehicle's underbelly [21]. Thus, we assume that at the top of the trajectory, the entire forebody flow will be laminar. It will be shown later that the laminar boundary layer produces the most dramatic results, so this assumption represents a worst case scenario.

3.2 Classical Laminar Boundary Layer Treatment

3.2.1 General Problem Considerations

It is appropriate to review laminar hypersonic boundary layer theory before applying some of the classical results to a transatmospheric vehicle. To model an aerospace plane forebody flow, we are considering the oft-solved problem of the formation of a boundary layer on a flat plate at angle of attack moving at high Mach number through a uniform flow.

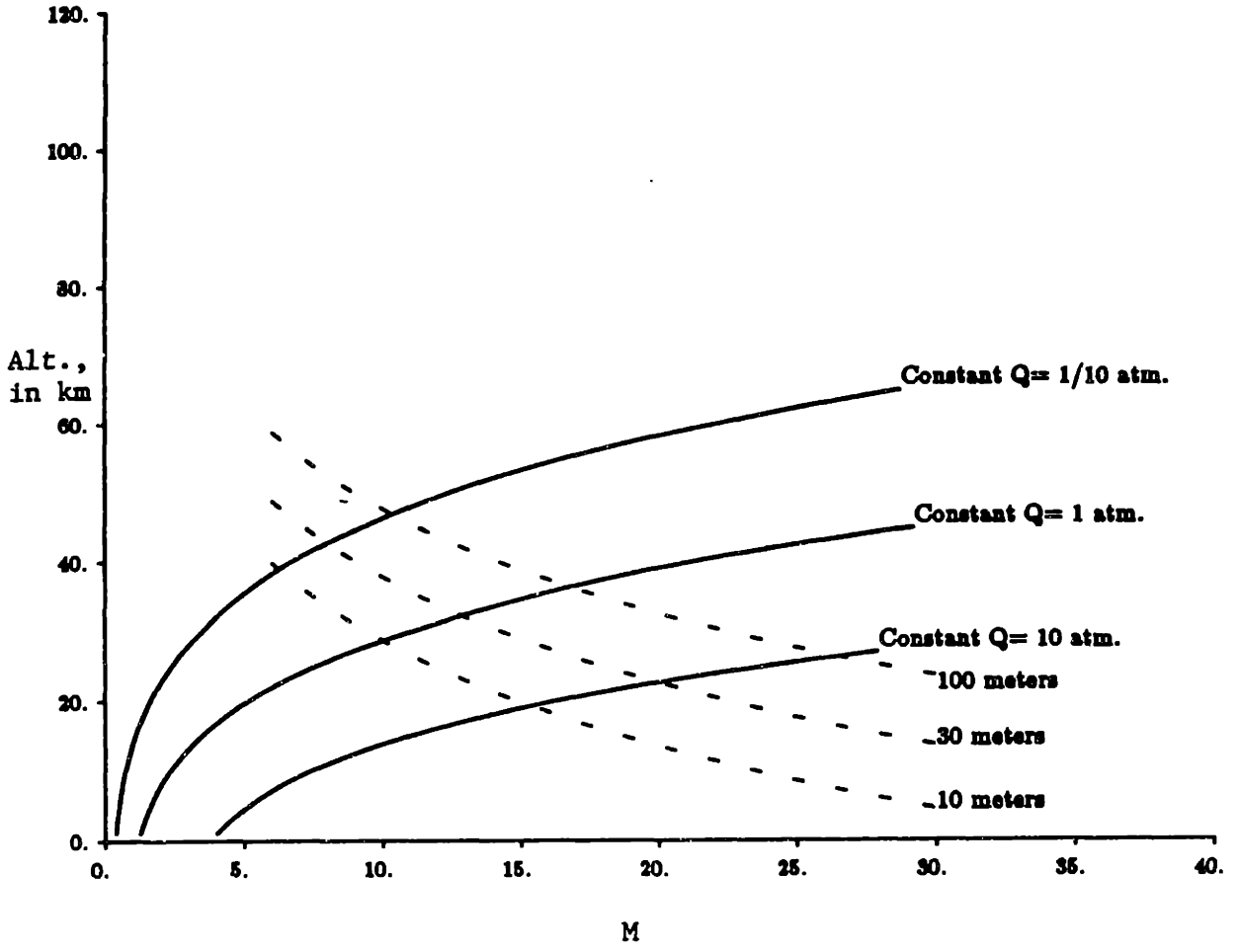

Figure 3.1: Estimated altitude for transition at 10 m, 30 m, and 100 m, along constant dynamic pressure trajectories

Table 3.2: Boundary Layer Thickness and Shock Height Above Surface

Point on Fig. 2.1	M	Alt., in km.	α	Cooled Wall?	at x =	Height, in m 5 m	10 m	30 m
[1]	10	30	0°	No	δ^*=	0.029	0.039	0.070
					y_{shock}=	0.491	0.992	2.895
[2]	15	40	0°	Yes	δ^*=	0.046	0.059	0.096
					y_{shock}=	0.370	0.720	2.077
[3]	20	40	0°	Yes	δ^*=	0.062	0.081	0.139
					y_{shock}=	0.304	0.598	1.649
[4]	25	40	0°	Yes	δ^*=	0.073	0.101	0.173
					y_{shock}=	0.261	0.480	1.336
[5]	20	30	0°	Yes	δ^*=	0.035	0.046	.077
					y_{shock}=	0.281	0.535	1.555
[6]	20	50	0°	Yes	δ^*=	0.119	0.162	0.291
					y_{shock}=	0.348	0.635	1.727
[7]	20	60	0°	Yes	δ^*=	0.211	0.298	0.564
					y_{shock}=	0.427	0.739	1.952
[3]	20	40	5°	Yes	δ^*=	0.024	0.030	0.055
					y_{shock}=	0.216	0.412	1.193
[3]	20	40	10°	Yes	δ^*=	0.014	0.015	0.023
					y_{shock}=	0.251	0.486	1.441
[3]	20	40	0°	No	δ^*=	0.094	0.124	0.218
					y_{shock}=	0.330	0.606	1.686

This problem is solved in two dimensions on a flat surface because the detailed geometry of a hypersonic forebody is not known, and because the two dimensional problem is the simplest. Undoubtedly, an actual vehicle forebody will experience three-dimensional effects, but the fundamental principles governing boundary layer thickness and profile will be outlined in a 2-d picture. A brief review of the classical solutions of this problem is presented in Appendix A.

The results of the laminar boundary layer model at a variety of conditions are shown in Table 3.2. The values presented in Table 3.2 are the height of the boundary layer and the bow shock measured from the surface, along a normal to the surface, at 5 meters, 10 meters, and 30 meters along the surface. The first column indicates location on the trajectory plot of Figure 2.1. These solutions all assumed a perfectly sharp plate, $Pr = .75$, and no angle of attack, unless otherwise noted. Cooled solutions assumed flat plate wall temperatures of

2000 K. Important observations from these results, which demonstrate the conclusions of classical hypersonic theory, are

- The boundary layer thickness increases dramatically with altitude (because kinematic viscosity ν increases nearly exponentially in the atmosphere).
- Large positive angles of attack drastically reduce the boundary layer thickness, an effect which is linear with angle of attack at large angle of attack.
- The bow shock is displaced from where it would be in an inviscid flow.
- Wall cooling and real-gas effects reduce the boundary layer size.

Figure 3.2 presents contours indicating the percentage of the inlet flow that is represented by the boundary layer 10 meters along the forebody. The boundary layer is referenced to the shock layer height H, which is the height of the shock above the surface and equals the sum of the boundary layer height, δ and the inviscid shock layer, Δ_s.These contours are calculated for vanishingly small forebody wedge angle, and assuming a straight forebody without compression ramps. As pointed out throughout this chapter, the boundary layer thickness is strongly dependent on vehicle geometry and attitude, so these contours should be taken as a rough indication of inlet conditions only. Note that since the boundary layer scales approximately with $\sqrt{x}$ and the shock layer height scales approximately with x at large x, the fractional thickness at distances other than 10 meters can be calculated by transforming the contours of Figure 3.2 into

$$\frac{\delta}{H}(x) = \frac{\sqrt{\frac{x}{10}}}{(\frac{1}{\delta/H|_{10}} - 1)\frac{x}{10} + \sqrt{\frac{x}{10}})} \tag{3.2}$$

where x is measured in meters. Thus, at 20 meters, what was the 20% contour at 10 meters becomes 15%, and the 50% contour becomes 41%. At 30 meters, the 20% contour at 10 meters represents the $12\frac{1}{2}$% contour, and the 50% contour at 10 meters becomes 37% at 30 meters.

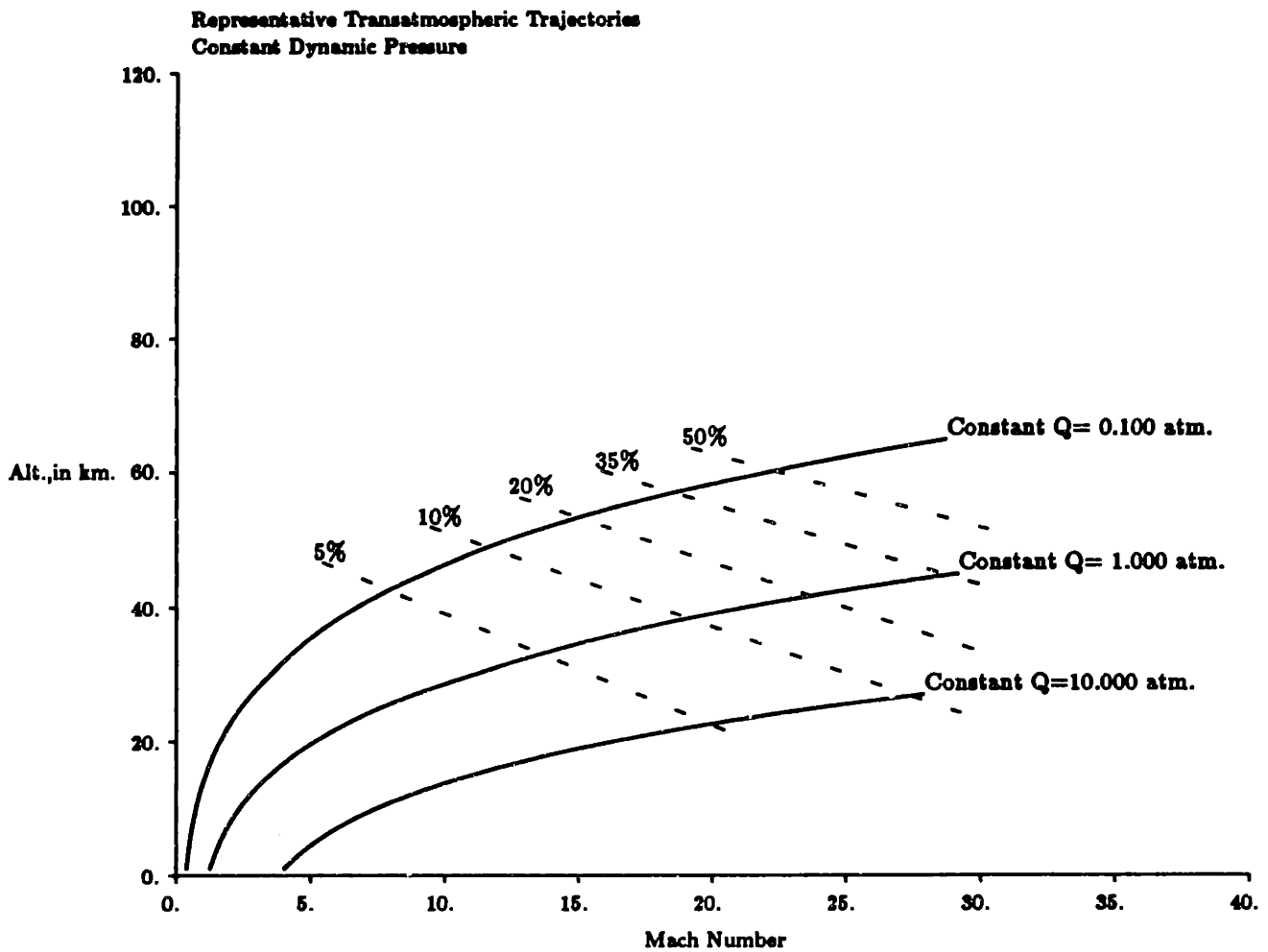

Figure 3.2: Percent of inlet flow occupied by boundary layer at 10 m, wall cooled to 2000 K with small wedge angles. At large wedge angles, thickness is reduced in inverse proportion to wedge angle.

3.2.2 Boundary Layers on Forebodies with Ramps

Some proposals for the design of a forebody/inlet surface on a transatmopsheric vehicle include the use of one or more compression ramps. The laminar boundary layer treatment described above has been adapted to account for these ramps as changes of wedge angle along the forebody surface. The shock that forms on such a ramp and penetrates the boundary layer produces a sudden increase in pressure, which in turn reduces the boundary layer thickness. Thus, a discontinuity in wedge angle produces a discontinuity in boundary layer thickness in this solution.

Above the ramp, the incident Mach number and thermodynamic conditions are no longer those of the uniform free stream, but rather the conditions present behind the bow shock. Because the ramp is typically located in the weak interaction range of the surface, the present code assumes those conditions are uniform and equal to the values in the weak interaction zone, although the bow shock will be actually be somewhat curved, and the incident properties on the ramp will be slightly nonuniform. These nonuniformities will be most pronounced at the leading edge of the ramp, but can be neglected given the far greater problem that the laminar boundary layer treatment cannot predict the separation that will occur in that region.

Based on reported experimental observations [22], it is assumed that the boundary layer separates and reattaches with little change in displacement thickness due to the separation itself (although increased pressure on the ramp will decrase the thickness). The primary effect of separation in this model is the formation of a bubble ahead of the ramp, which will have little effect on the properties or profile of the boundary layer itself, so the boundary layer heights before and after the ramp are smoothly connected.

Figure 3.3 is a typical boundary layer profile on a flat wall with a 5 degree ramp located 20 m. down the plate, flying at Mach 20 at 50 kilometers altitude. With the addition of a ramp, the position of the shock can no longer be simply estimated, so a computational solution has been applied. In this figure, the boundary layer displacement thickness has been calculated with the modified solution described above, then input as a wall boundary

to an inviscid Euler streamtube solver, which locates the shock [23]. Although it it is tempting to solve this flow field iteratively, that is, solving for the shock from the boundary layer solution, then obtaining the pressure distribution and recalculating the corresponding boundary layer thickness, and recalculating the shock position, such solutions tend not to converge, and so have not been attempted here [24]. More complicated algorithms exist for accomplishing an iterative solution, but were not pursued because of the excellent agreement between the non-iterative solution and approximate analytical methods.

As the ramp solution demonstrates, the increased angle of attack decreases the boundary layer height. From this point of view, the inlet ramp is desirable in reducing the level of nonuniformities entering the combustor, although the losses associated with the ramp shock may prohibit the adoption of such a forebody shape. It is suggested that there may be some optimum ramp angle which provides sufficient boundary layer compression while introducing a tolerable level of losses.

With an actual shock-boundary layer penetration, the boundary layer will depart from the similarity solution directly behind the point of shock penetration. It will approach the similarity solution downstream, at a distance which is characteristic of the time required for viscous effects to cross the boundary layer thickness. In fact, because the boundary layer is generally squeezed to very small thickness by the ramp shock, it has been assumed that the profile assumes the similarity immediately behind the shock. The inaccuracies introduced by this assumption are less significant than the neglect of separation.

3.3 Boundary Layer Profiles

3.3.1 Classical Compressible Boundary Layer Solutions

It is of interest for scramjet modelling to quantify the velocity, temperature, and mass flux profiles within the boundary layer, as an indication of the flow profile that will be intercepted by the inlet. In later chapters the forebody boundary layer profiles will be input to representative engine channels. These profiles will be calculated in accordance

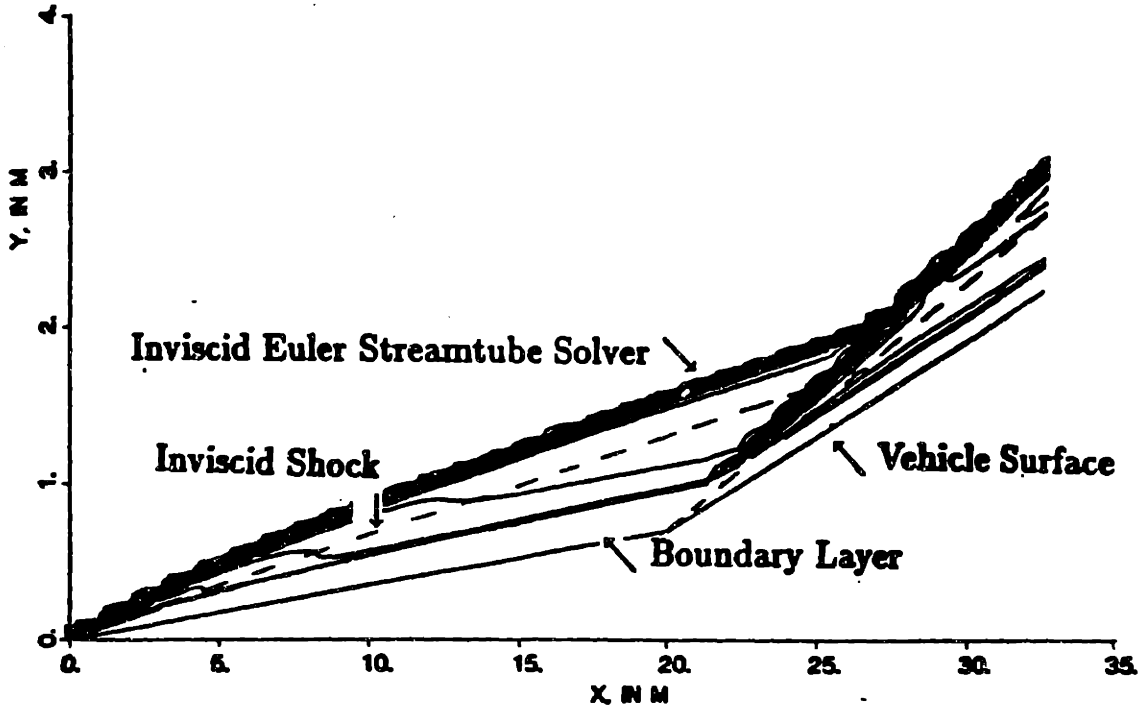

Figure 3.3: Cooled shock layer with ramp at Mach 20, 50 km

with the previously calculated displacement thicknesses.

Cohen and Reshotko [25] solved for the flat-plate laminar boundary layer temperature and velocity profiles using a Stewartson-Illingworth transformation from compressible to incompressible flow, for Prandtl number of 1. They have tabulated the behavior of a velocity function, $f' = \frac{U}{U_e}$ and an enthalpy function, $S = \frac{h_s}{h_o} - 1$. From their tabulated values, the required profiles can be calculated at Pr=1 in terms of a transformed spatial coordinate, η.

At a given value of η, velocity is determined directly from the velocity function:

$$U = U_e f'(\eta) \tag{3.3}$$

local static temperature is found in terms of f' and S:

$$\frac{T_{\text{static}}}{T_{\text{free-stream,total}}} = (1+S) - \left(\frac{\frac{\gamma-1}{2}M_e^2}{1+\frac{\gamma-1}{2}M_e^2}\right) f'^2 \tag{3.4}$$

and the real position is found by transforming from η coordinates:

$$y = \delta_{\text{b.l.}} \frac{\int_0^{\eta(y)} \frac{T}{T_o} d\eta}{\int_0^{\eta(\delta)} \frac{T}{T_o} d\eta} \tag{3.5}$$

where $\eta(\delta)$ is the value of η at the top of the boundary layer ($\simeq$ 3.4) and the actual boundary layer thickness is taken from the calculations of the previous section. Although the Cohen and Reshotko profiles were solved with the Chapman-Rubesin viscosity/temperature parameter equal to unity, normalizing to the calculated displacement thickness extends their validity to non-unity values, as per the transformation of Lees [26].

The integrals in equation (3.5) can be expressed in terms of S and f':

$$\int_0^\eta \frac{T}{T_o} d\eta = \eta + \int_0^\eta S\, d\eta - \frac{\frac{\gamma-1}{2}M^2}{1+\frac{\gamma-1}{2}M^2} \int_0^\eta f'^2\, d\eta \tag{3.6}$$

From the velocity and temperature, and taking pressure constant across the boundary layer, the density and mass flux can be calculated at each position.

Boundary layer profiles calculated with the above classical solution will be used to input the forebody flowfield conditions entering a scramjet inlet in chapter 6. We will see there appropriate boundary layer Mach number and temperature profiles characteristic of flight transatmospheric flight conditions.

3.3.2 Calculated Forebody Properties

With the above theory, we can examine some typical forebody profiles. Figure 3.4 is the calculated Mach number profile 10 meters down a flat plate with a wall temperature of 2000 K, calculated with the solution of Cohen and Reshotko. The velocity profile is shown in Figure 3.5. The corresponding temperature profile shows a high peak close to the wall, as indicated in Figure 3.6. Note that this figure is shown on a magnified scale. The temperature distribution shown has not included reaction and dissociation effects, and the peak temperature shown is much higher than would be realized with a more complete chemistry model.

From the temperature and velocity profiles, the mass flux can be calculated, and is presented in Figure 3.7. Note how little mass flux is carried in the boundary layer, leading to the hypersonic approximation of negligible boundary layer mass. Another property that will be of interest in this work is the inverse of the square of the Mach number, which will be shown to determine the relative influence of each streamtube in the flow. A plot of this function is shown in Figure 3.8. Note how quickly this value approaches infinity at the wall. This will be the subject of considerable development in later chapters.

In later chapters, characteristic profiles will be selected from different portions of the transatmospheric trajectory. When appropriate, these profiles will be presented.

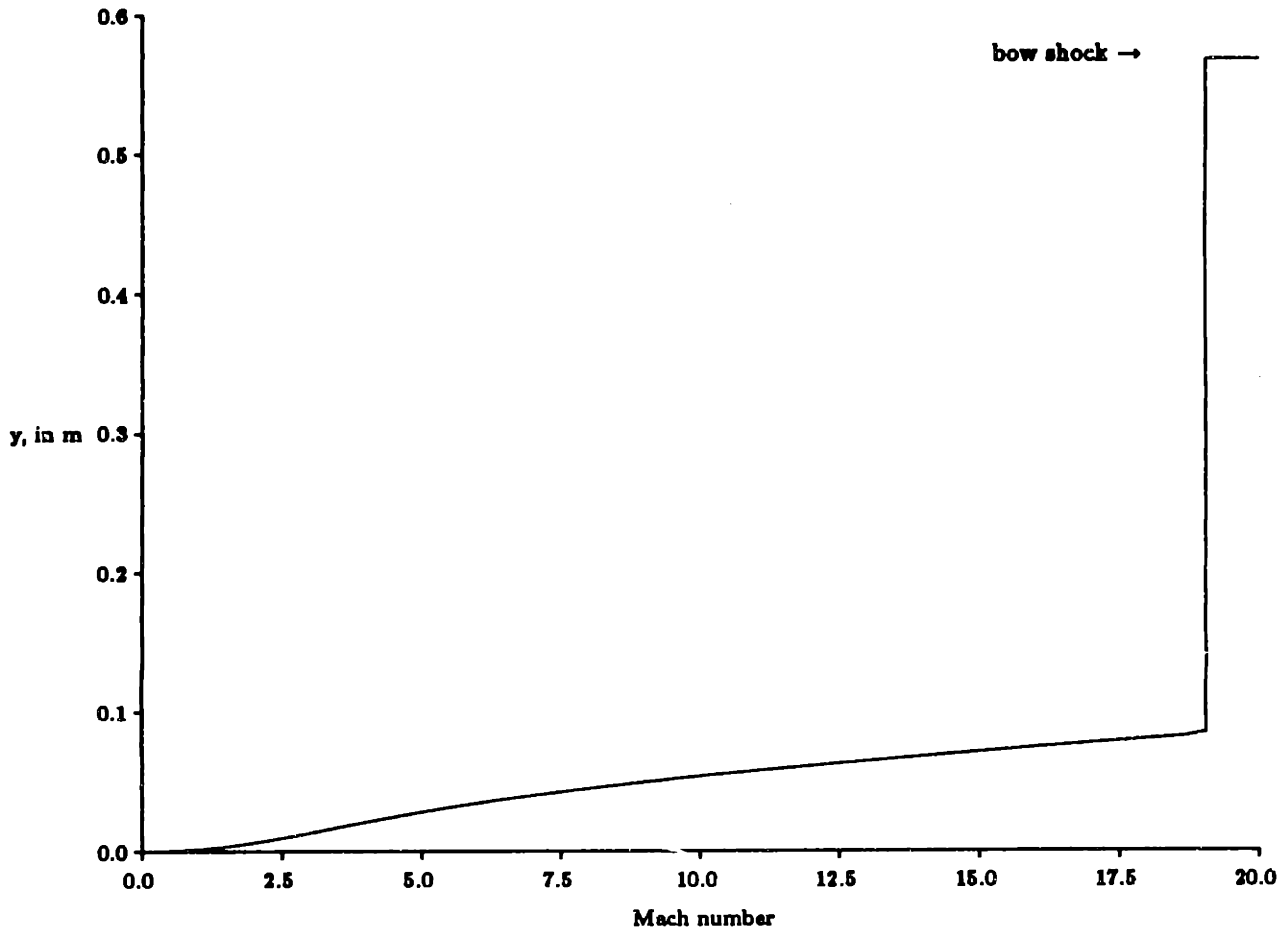

Figure 3.4: Mach number profile at Mach 20, 40 km

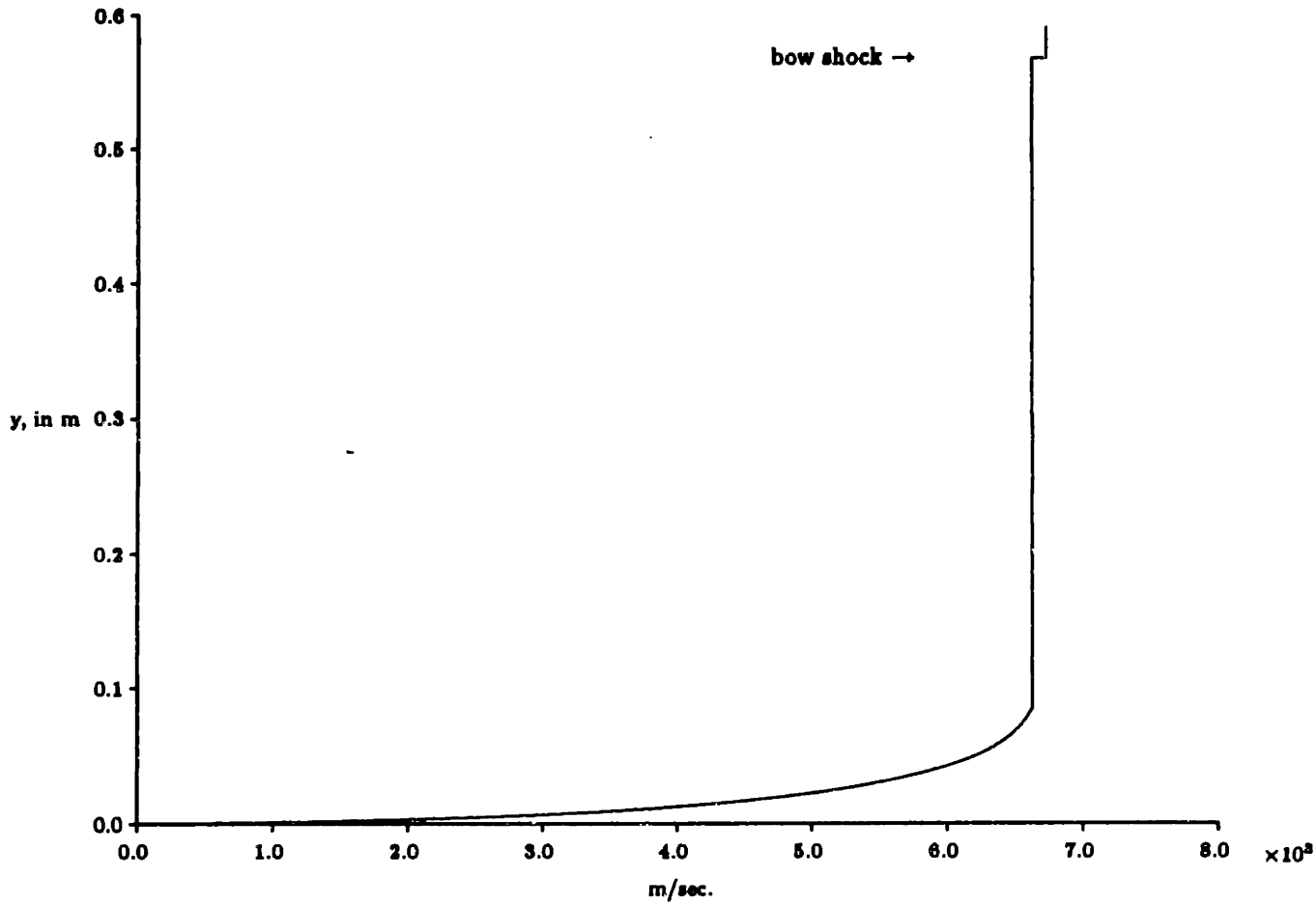

Figure 3.5: Velocity profile at Mach 20, 40 km

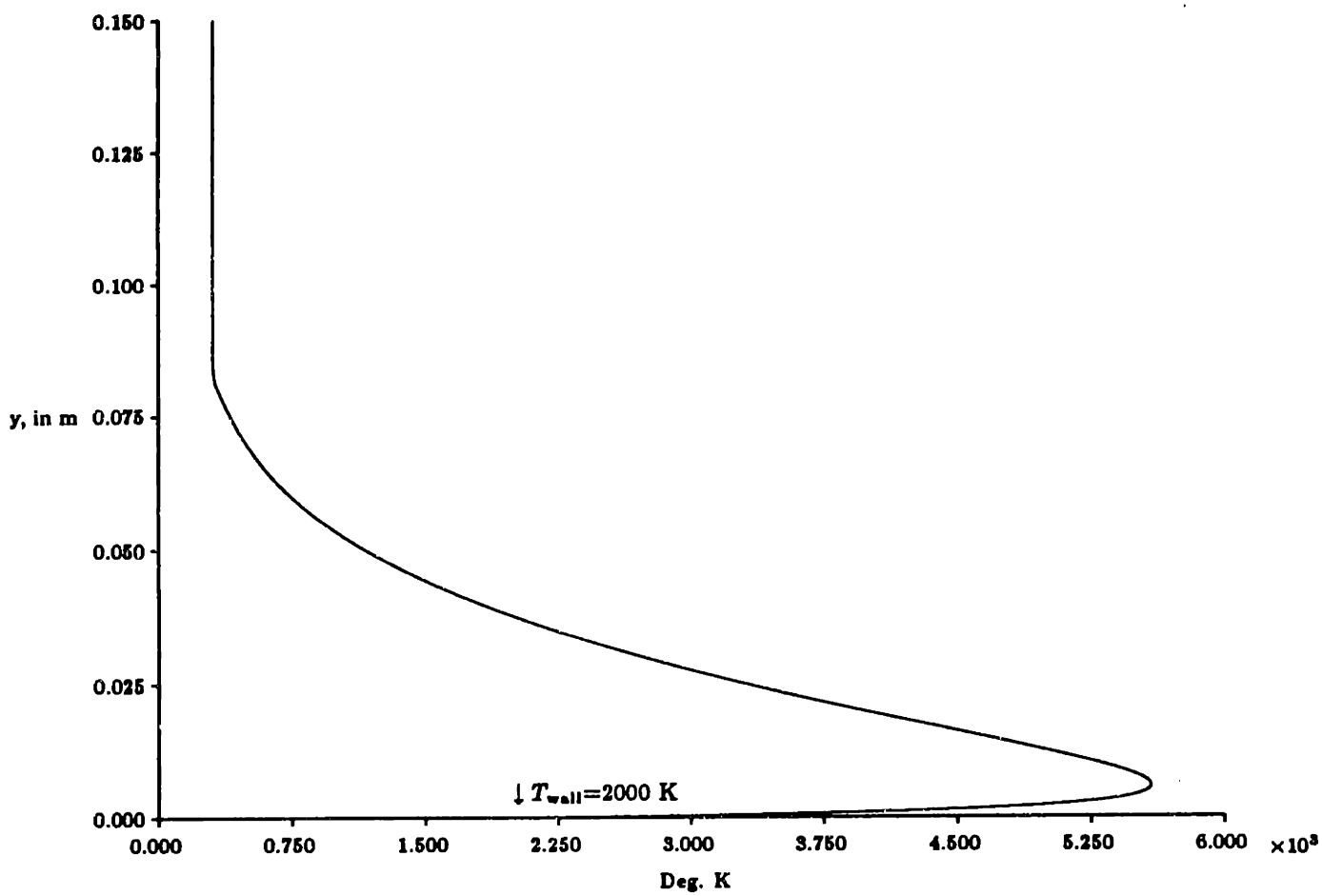

Figure 3.6: Static temperature profile at Mach 20, 40 km

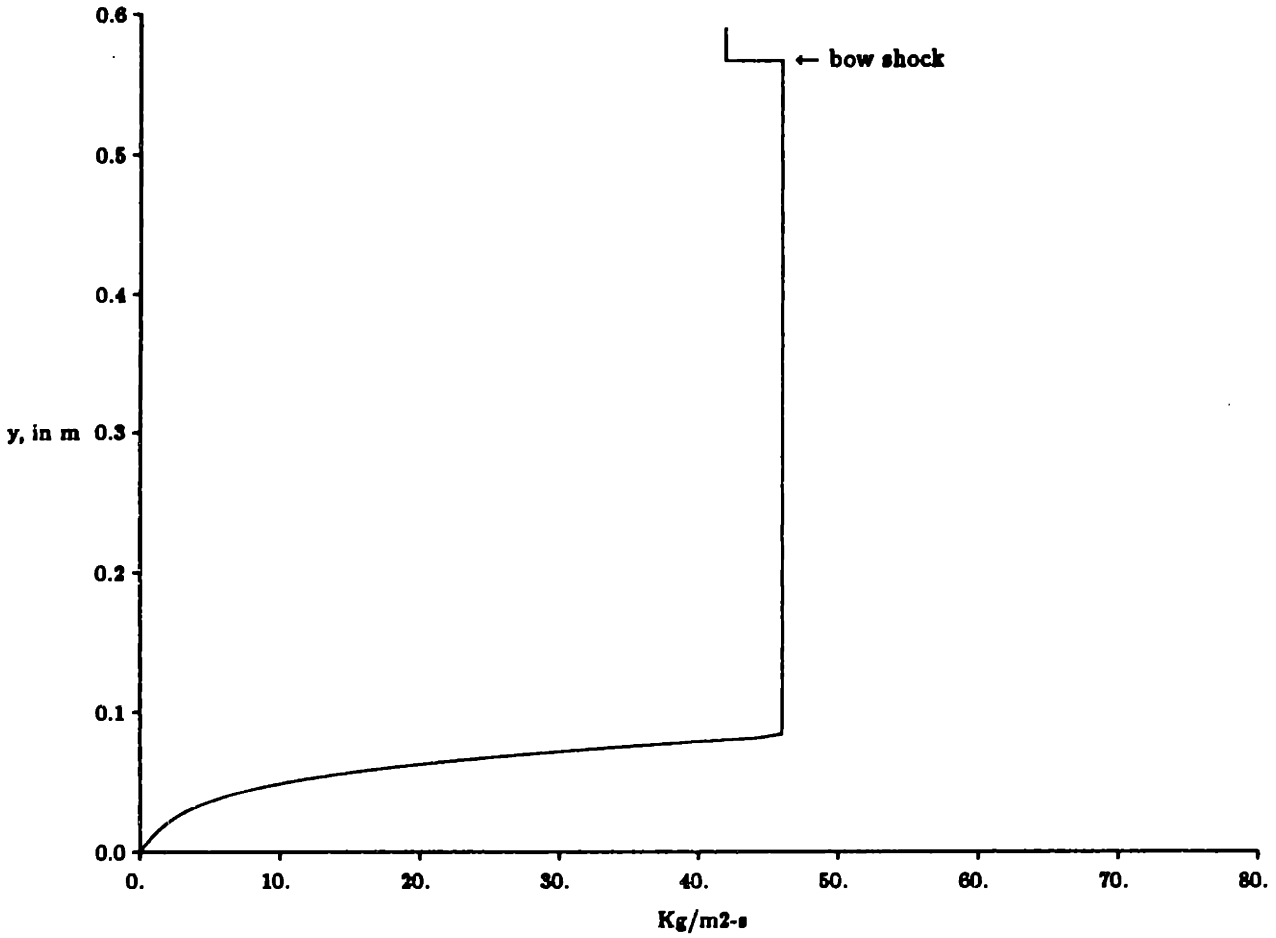

Figure 3.7: Mass flux profile at Mach 20, 40 km

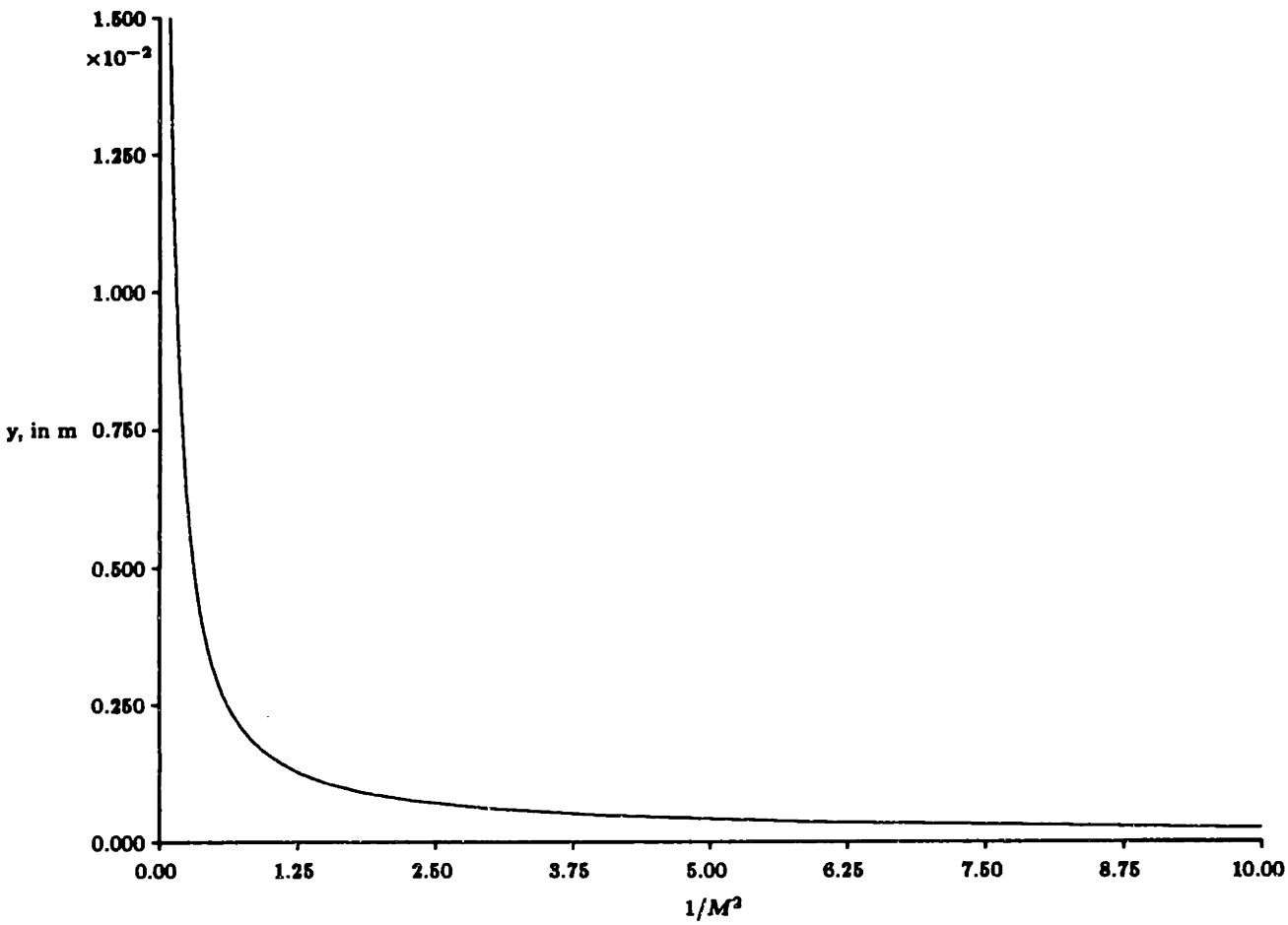

Figure 3.8: $1/M^2$ at Mach 20, 40 km

Chapter 4
Shock Position and Angle of Attack

In this chapter, the consequences of the boundary layer on the bow shock matching will be considered. Because the bow shock matching is important for proper engine operation, a change in the matching condition caused by the forebody nonuniformities will have an influence on engine design and vehicle performance.

The boundary layer adds to the effective thickness of the vehicle, and therefore displaces the bow shock. Without even worrying yet about the effect of the forebody boundary layer *inside* the engine, it is clear the the boundary layer will affect engine operation by complicating the bow shock/inlet lip matching. We will not be examing the consequences of a mismatch, so much as the conditions required for accomplishing the match, and how those conditions change when viscous effects are considered on the forebody.

In discussing the design of a hypersonic vehicle, it was mentioned that the bow shock should be located so that it nearly contacts the inlet lip. If the shock is below the lip, away from the vehicle, shocks will form outside the inlet and increase the drag of the vehicle. This is also an inefficient scenario for steady-state operation because it suggests that the scramjet is located too far back on the vehicle, and thus there is more skin friction on the vehicle surface than is necessary. If the shock is swallowed by the inlet, reflecting shocks will appear in the scramjet, thus leading to increased internal losses.

4.1 Steady-State Shock Matching Condition

4.1.1 Inviscid Shock Matching Solution

The presence of the boundary layer makes the shock position more sensitive to changes in angle of attack. In the inviscid case, the hypersonic shock is essentially fixed relative to the body, and is insensitive to small perturbations in wedge angle. Combining the vehicle geometric wedge angle with angle of attack, the relationship for total wedge angle versus shock angle, β, in a two-dimensional flow (which was already used in equation (A.14)) is:

$$(\alpha + \theta_{\text{wedge}}) = \beta - \Phi_{\text{relative}} \tag{4.1}$$

where

$$\tan(\Phi_{\text{relative}}) = \left[\frac{\gamma - 1}{\gamma + 1}\tan\beta + \frac{2}{(\gamma+1)M^2 \sin\beta\cos\beta}\right] \tag{4.2}$$

If the shock is stationary on the vehicle for small perturbations of wedge angle (i.e. angle of attack) then

$$\frac{\partial\beta}{\partial\alpha} = 1 \tag{4.3}$$

Taking the derivative of total apparent wedge angle with respect to the shock angle,

$$\frac{\partial\alpha}{\partial\beta} = 1 - \frac{\partial\Phi_{\text{relative}}}{\partial\beta} \tag{4.4}$$

where

$$\frac{\partial\Phi_{\text{relative}}}{\partial\beta} = \frac{\frac{\gamma-1}{\gamma+1}\frac{1}{\cos^2\beta} + \frac{2}{(\gamma+1)M^2}\left(\frac{1}{\cos^2\beta} - \frac{1}{\sin^2\beta}\right)}{1 + \left[\frac{\gamma-1}{\gamma+1}\tan\beta + \frac{2}{(\gamma+1)M^2\sin\beta\cos\beta}\right]^2} \tag{4.5}$$

A statically fixed shock (i.e. one with a position relative to the surface that is resistant to *low frequency* perturbations) will satisfy

$$\frac{\partial\Phi_{\text{relative}}}{\partial\beta} = 0 \tag{4.6}$$

which occurs when

$$\beta_{\text{fixed}} = \arctan\left[\left(1 + \frac{\gamma - 1}{2}M^2\right)^{-\frac{1}{2}}\right] \tag{4.7}$$

Table 4.1: Fixed Shock and Wedge Angles

Mach Number	Fixed Shock Angle	Fixed Wedge Angle	Normal Mach Number	Temperature Ratio
1.581	39.23°	0.00°	1.000	1.000
2	36.70°	7.50°	1.195	1.125
3.572	28.01°	14.12°	1.678	1.443
5	22.21°	12.94°	1.890	1.600
10	12.31°	7.94°	2.132	1.798
15	8.39°	5.51°	2.189	1.847
20	6.34°	4.19°	2.209	1.865
25	5.09°	3.38°	2.218	1.873
∞	0°	0°	2.236	1.889

so that at a given Mach number there is a particular shock angle (and thus, angle of attack) at which the shock is fixed relative to the vehicle. The normal Mach number across the shock is:

$$M_{\text{normal}} = M \sin(\beta_{\text{fixed}}) = M \left(2 + \frac{\gamma - 1}{2} M^2\right)^{-\frac{1}{2}} \tag{4.8}$$

Which approaches the limit $M_{\text{normal}} = \sqrt{2/(\gamma - 1)}$ at large M. For $\gamma = 1.4$ this limiting normal Mach number is 2.236.

Table 4.1 presents the fixed-shock wedge angles and shock angle at $\gamma = 1.4$ for several Mach numbers. There is no fixed-shock wedge angle for Mach numbers below 1.581 at this value of γ, and the maximum fixed-shock wedge angle is 14.12° at Mach 3.572. There are no fixed-shock wedge angles for the strong shock solutions. [1] The normal Mach number across the fixed shock is also shown.

The fixed-shock angle does represent a practical operating point because it provides reasonable temperatures inside the engine for typical ambient conditions. This can be seen from the value of the temperature ratio across the fixed shock, which is listed in the last column of Table 4.1. In the hypersonic limit, the temperature ratio across the fixed shock

[1] *strong shock* here refers to one in which absolute downstream Mach number is subsonic.

is 1.889 for $\gamma = 1.4$. On a two-shock inlet, that would raise an ambient temperature of 300 K to 1070 K, which is an acceptable value. With a three-shock inlet, the engine would see air coming in with static temperature of 2022 K for the same 300 K external temperature, which is still acceptable for combustion. Note that it would not be possible to fix the shocks of a multi-ramp inlet to the engine lip, so some compromise design would have to accepted for more complicated geometries.

4.1.2 Complications From the Viscous Solution

In viscous hypersonic flow, the shock position is no longer set by the shock angle alone, but also by the boundary layer thickness. The boundary layer thickness is sensitive to angle of attack, varying roughly in proportion to angle of attack at wedge angles in excess of a few degrees. Therefore, the boundary layer thickness must be considered in matching the shock to the inlet lip, and changes in that boundary layer thickness must be accounted for if the shock is to remain fixed. At large Mach number and small angle of attack, increasing angle of attack results in the shock *moving away* from the surface, but this effect will not in general be sufficient to cancel the effects of decreasing boundary layer thickness.

With the simplification that boundary layer thickness is inversely proportional to the wedge angle, the expression for the boundary layer height δ as a function of angle of attack α compared to some initial condition δ_i at apparent wedge angle $(\alpha_i + \theta_{\text{wedge}})$ is:

$$\delta(\alpha) = \delta_i \frac{\alpha_i + \theta_{\text{wedge}}}{\alpha + \theta_{\text{wedge}}} \tag{4.9}$$

The angular displacement between the top of the boundary layer and the surface, is defined here as ϕ, is:

$$\tan\phi = \frac{\delta_i}{x} \frac{\alpha_i + \theta_{\text{wedge}}}{\alpha + \theta_{\text{wedge}}} \tag{4.10}$$

where $\tan\phi \simeq \phi$ in the small angle approximation. The derivative of ϕ with respect to α is then:

$$\frac{\partial\phi}{\partial\alpha} = -\frac{\delta_i}{x} \frac{\alpha_i + \theta_{\text{wedge}}}{(\alpha + \theta_{\text{wedge}})^2} \tag{4.11}$$

This added angular displacement due to boundary layer thickness changes the apparent wedge angle, because the top of the boundary layer, not the vehicle surface, defines the downstream flow angle. Equation 4.1 is modified to include ϕ in the shock angle relation of

$$(\alpha + \theta_{\text{wedge}} + \phi) = \beta - \Phi_{\text{relative}} \tag{4.12}$$

where Φ_{relative} is now the angular displacement between the shock and the top of the boundary layer. The fixed shock solution will be one in which

$$\begin{aligned} \frac{\partial \alpha}{\partial \beta} &= 1 - \frac{\partial \Phi_{\text{relative}}}{\partial \beta} - \frac{\partial \phi}{\partial \beta} \\ &= 1 \end{aligned} \tag{4.13}$$

so that

$$\frac{\partial \Phi_{\text{relative}}}{\partial \beta} + \frac{\partial \phi}{\partial \beta} = 0 \tag{4.14}$$

which is the condition that changes in the angular displacement of the top of the boundary layer are identically cancelled by changes in the relative angular displacement between the boundary layer and the shock.

When this condition is satisfied, $\partial\alpha/\partial\beta = 1$, and we can write

$$\frac{\partial \phi}{\partial \beta} = -\frac{\delta_i}{x} \frac{\alpha_i + \theta_{\text{wedge}}}{(\alpha + \theta_{\text{wedge}})^2} \tag{4.15}$$

For small displacements, $\alpha + \theta_{\text{wedge}} = \beta - \Phi_{\text{relative}} - \delta_i/x$, and the derivative of the angular displacement of the boundary layer with respect to the shock angle is:

$$\frac{\partial \phi}{\partial \beta} = -\frac{\delta_i/x}{\beta - \Phi_{\text{relative}} - \delta_i/x} \tag{4.16}$$

For a given value of δ_i/x at Mach number M,the fixed shock has angle β which satisfies:

$$\frac{\frac{\gamma-1}{\gamma+1}\frac{1}{\cos^2\beta} + \frac{2}{(\gamma+1)M^2}\left(\frac{1}{\cos^2\beta} - \frac{1}{\sin^2\beta}\right)}{1 + \left[\frac{\gamma-1}{\gamma+1}\tan\beta + \frac{2}{(\gamma+1)M^2\sin\beta\cos\beta}\right]^2} - \frac{\delta_i/x}{\beta - \tan^{-1}\left[\frac{\gamma-1}{\gamma+1}\tan\beta + \frac{2}{(\gamma+1)M^2\sin\beta\cos\beta}\right] - \frac{\delta_i}{x}} = 0 \tag{4.17}$$

In fact, δ_i/H will vary all along the surface, so the fixed shock solution will also vary down the surface. Thus, even though the shock can be fixed against changes in α for the

conditions at the inlet lip, changes in wedge angle upstream of the lip will move the shock, and the fixed condition cannot be satisfied perfectly.

There is no closed-form solution for equation (4.17), but with a small angle approximation (shock angles must be small in the hypersonic regime to avoid unreasonable temperature and pressure rises), considerable simplification is possible:

$$\frac{\frac{\gamma-1}{\gamma+1} - \frac{2}{(\gamma+1)M^2\beta^2}}{1 + \left[\frac{\gamma-1}{\gamma+1}\beta + \frac{2}{(\gamma+1)M^2\beta}\right]^2} - \frac{\delta_i/x}{\beta - \left[\frac{\gamma-1}{\gamma+1}\beta + \frac{2}{(\gamma+1)M^2\beta}\right] - \frac{\delta_i}{x}} = 0 \qquad (4.18)$$

Equation (4.18) has been used to solve for the fixed-shock wedge angle and shock angle, and the results are presented in Figure 4.1. Fixed-shock conditions were determined as a function of Mach number at $\gamma = 1.4$, for a shock layer without a boundary layer (corresponding to Table 4.1), with 2% relative boundary layer thickness, and with 5% relative boundary layer thickness, referenced to the height of the shock. Above 5% boundary layer thickness, the required shock angle is too large for the small angle approximation to be valid. Above 20% thickness, no fixed shock solution can be found with even the full solution. That is because the inviscid shock motion is no longer of sufficient magnitude to cancel boundary layer motions, which scale with boundary layer thickness.

The boundary layer tends to raise the value of the fixed shock angle to unreasonable large values. For instance, with 2% relative boundary layer thickness, the fixed shock angle at Mach 20 has jumped from 6.34 degrees for the inviscid case to 9.99 degrees. This in turn will yield a normal Mach number of 3.470, with a temperature ratio across the shock of 3.274. This is unacceptable for typical ambient conditions; a two shock inlet would raise a 300 K ambient flow to 3216 K, which is too high for combustion to occur. It can be concluded that it is possible to cancel out the effect of angle of attack on boundary layer thickness on the shock motion by selecting an appropriate wedge angle, for relative boundary layer thicknesses of less than a few percent. The presence of a thick boundary layer, in excess of 5% of the shock layer, will mean that it is impossible to keep the shock fixed on the inlet lip without some active control or variable geometry.

The hypersonic boundary layer also increases the penalty of shock motion on scramjet

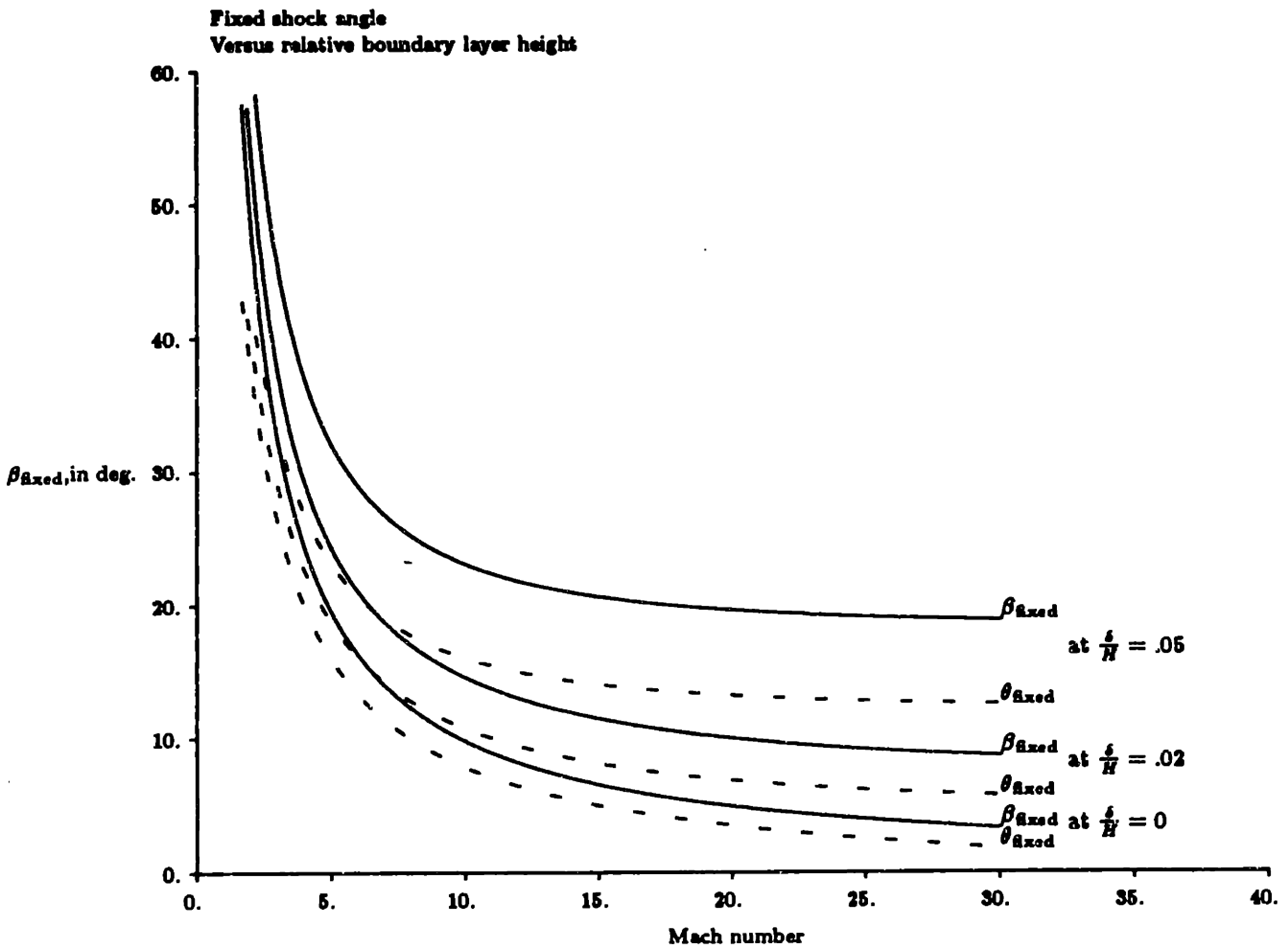

Figure 4.1: Fixed shock wedge angle and shock angle versus Mach number for various relative boundary layer thicknesses

performance because of density stratification. The boundary layer is essentially massless, so that variations in shock position can have large scale changes in the ingested mass flux by increasing the relative extent of the boundary layer through the shock region.

Having ascertained that the presence of a thick hypersonic boundary layer makes shock-inlet matching difficult at varying angle of attack for a fixed Mach number, the dynamic behavior of the boundary layer/shock system can be compared that with the purely inviscid solution. In fact, as is shown in Appendix B, even though the boundary layer can dramatically change the shock's response to gradual changes in angle of attack, it has very little effect on the dynamic behavior of the shock, subject to unsteady surface motions.

Chapter 5

Analytical Treatment of the Inlet Stratification with Discrete Streamtubes

5.1 Inlet Gradients and Multi-streamtube Modelling

5.1.1 General Development

To study the performance of a scramjet under various conditions, including inlet velocity, temperature, and mass flux gradients, a one-dimensional model has been constructed. The method of influence coefficients, outlined by Shapiro [27] is used to integrate Mach number and thermodynamic conditions in a channel of varying area under the influence of heat addition, mass addition, variable γ, and wall shear.

The 1-d logarithmic derivative of Mach number can be expressed in terms of the logarithmic derivatives of area (A), heat addition (Q), work (W), total enthalpy change (H), friction coefficient (f), drag (X), molecular weight ($\mathcal{W}$), added fuel mass (m), velocity (V), and γ, as:

$$\begin{aligned}\frac{dM^2}{M^2} = & \quad C_{MA}\frac{dA}{A} + C_{MQ}\frac{dQ - dW + dH}{CpT} \\ & + \; C_{MFr}\left(4f\frac{dx}{D} + \frac{dX}{\frac{1}{2}\gamma PAM^2} - 2\frac{V_{injected}}{V_{main}}\frac{dm}{m}\right) \\ & + \; C_{Mm}\frac{dm}{m} + C_{M\mathcal{W}}\frac{d\mathcal{W}}{\mathcal{W}} + C_{M\gamma}\frac{d\gamma}{\gamma}\end{aligned} \tag{5.1}$$

where the coefficients are all functions of local Mach number and γ only:

$$C_{MA} = -\frac{2\left(1 + \frac{\gamma-1}{2}M^2\right)}{1 - M^2} \tag{5.2}$$

$$C_{MQ} = \frac{1+\gamma M^2}{1-M^2} \tag{5.3}$$

$$C_{MFr} = \frac{\gamma M^2\left(1+\frac{\gamma-1}{2}M^2\right)}{1-M^2} \tag{5.4}$$

$$C_{Mm} = \frac{2(1+\gamma M^2)\left(1+\frac{\gamma-1}{2}M^2\right)}{1-M^2} \tag{5.5}$$

$$C_{MW} = -\frac{1+\gamma M^2}{1-M^2} \tag{5.6}$$

$$C_{M\gamma} = -1 \tag{5.7}$$

Similarly, the logarithmic derivatives of other properties such as static pressure can be expressed in terms of the independent variables :

$$\begin{aligned}\frac{dP}{P} = & \quad C_{PA}\frac{dA}{A} + C_{PQ}\frac{dQ-dW+dH}{CpT} \\ & + C_{PFr}\left(4f\frac{dx}{D} + \frac{dX}{\frac{1}{2}\gamma PAM^2} - 2\frac{V_{injected}}{V_{main}}\frac{dm}{m}\right) \\ & + C_{Pm}\frac{dm}{m} + C_{PW}\frac{dW}{W} + C_{P\gamma}\frac{d\gamma}{\gamma}\end{aligned} \tag{5.8}$$

with coefficients

$$C_{PA} = \frac{\gamma M^2}{1-M^2} \tag{5.9}$$

$$C_{PQ} = -\frac{\gamma M^2}{1-M^2} \tag{5.10}$$

$$C_{PFr} = -\frac{\gamma M^2\left(1+(\gamma-1)M^2\right)}{2(1-M^2)} \tag{5.11}$$

$$C_{Pm} = -\frac{2\gamma M^2\left(1+\frac{\gamma-1}{2}M^2\right)}{1-M^2} \tag{5.12}$$

$$C_{PW} = \frac{\gamma M^2}{1-M^2} \tag{5.13}$$

$$C_{P\gamma} = 0 \tag{5.14}$$

Except in special degenerate cases, there is no general closed form solution for these equations, and they must be solved numerically for a given pattern of channel area change, fuel mass addition, and heat addition, etc. With one dimension, this method cannot handle oblique shocks, and normal shocks must be fit, not captured. The influence coefficient method also has problems of numerical stability near M=1, where many of the coefficients become singular.

In this work, the one-dimensional solution of Hevenor, Bernstein, and Heiser [28] is extended to model nonuniform channel flow. A general expression for area change of a single streamtube in the presence of N tubes, as a function of the total area change, heat and fuel addition, friction, and mass addition is derived by equating the pressure variations of all streamtubes:

$$\left(\frac{dP}{P}\right)_i = \left(\frac{dP}{P}\right)_j + \mathcal{G}_{ij} \tag{5.15}$$

$\mathcal{G}$ can represent a pressure gradient, shock pressure discontinuity, or uniform pressure ($\mathcal{G} = 0$), and is defined as:

$$\mathcal{G}_{ij}(y_i, y_j) = \int_{y_i}^{y_j} \left\{\frac{d}{dy}\left(\frac{dP}{P}\right)\right\} dy \tag{5.16}$$

The heat and mass addition profiles are known, and friction can be determined from the relative velocities of the streamtubes. The total area change of the entire flow is also known, and we can solve for the individual area change in the *ith* streamtube from these given parameters by separating the area change from all other effects in the influence coefficient pressure expression:

$$\left(\frac{dP}{P}\right)_i = C_{PA}\left(\frac{dA}{A}\right)_i + \mathcal{H}_i \tag{5.17}$$

where the fractional changes in heat addition, friction, mass addition, γ and molecular weight, in the *ith* streamtube have been lumped into $\mathcal{H}_i$:

$$\mathcal{H}_i = \left\{C_{PH}\left(\frac{dT_o}{T_o}\right) + C_{Pw}\left(\frac{dw}{w}\right) + 4dx\left[C_{PH}\left(\frac{f}{D}\right)\right] + \ldots\right\} \tag{5.18}$$

Solving for area change,

$$\left(\frac{dA}{A}\right)_i = \frac{dA_{TOTAL} - (\mathcal{H})_i \sum_{j=1}^{N}\left(\frac{A}{C_{PA}}\right)_j + \sum_{j=1}^{N}\left(\frac{A}{C_{PA}}\right)_j [\mathcal{H}_j - \mathcal{G}_{ij}]}{C_{PA_i}\sum_{j=1}^{N}\left(\frac{A}{C_{PA}}\right)_j} \tag{5.19}$$

In the absence of friction, each streamtube is uncoupled from the other stream tubes once its own area change is known as a function of the total area change, and so it can be treated as a uniform one-dimensional flow. In the limit of infinitesimally small stream tubes, we can write equation (5.19) as a continuous function across the channel (with cross-section planar coordinates y and z):

$$\left(\frac{dA}{A}\right)(y,z) = \frac{dA_{TOTAL} - (\mathcal{H})_i \iint_{A_z} \frac{dA}{(C_{PA})_{y,z}} + \iint_{A_z}[(\mathcal{H})_{y,z} - (\mathcal{G})_{y,z}]\frac{dA}{(C_{PA})_{y,z}}}{C_{PA_{y,z}} \iint_{A_z} \frac{dA}{(C_{PA})_{y,z}}} \tag{5.20}$$

5.1.2 Two-Streamtube Analytical Model

The multi-streamtube model can be applied to any number of streamtubes. In chapter 6, the model will be extended to a continuous profile, in the limit of an infinite number of streamtubes, with corrections to allow for a no-slip condition at a wall. Before doing this, it will be of value to present some of the results of the simplest compound flow possible, with only two distinct streamtubes. The two-streamtube flow will contain all of the compound compressible flow behavior evident in more sophisticated models. Throughout the rest of this work, multiple streamtube behavior will be compared to analogous two-streamtube flows.

With two inviscid streamtubes, in a channel with area change but no heat addition, the individual area change of a stream tube is found by equating the logarithmic derivatives of static pressure across the channel. In terms of the total area change, the Mach number in both streams, and the ratio of the stream areas at each point in the channel, the area change of stream 2 (which will henceforth refer to a hypersonic flow) is:

$$\frac{dA_2}{A_2} = \left[\frac{1}{1 + \frac{M_2^2 (1-M_1^2)}{M_1^2 (1-M_2^2)} \mathcal{A}} \right] \frac{dA}{A_2} \tag{5.21}$$

where $\mathcal{A} \equiv \frac{A_1}{A_2}$ and $A = A_1 + A_2$, the total channel area.

If M_2 is hypersonic ($\lim_{M \to \infty}$), the area derivative becomes

$$dA_2 = \left[\frac{M_1^2}{M_1^2 - (1 - M_1^2)\mathcal{A}} \right] dA \tag{5.22}$$

For small values of M_1, the hypersonic stream does not experience much area change. Indeed, for values of $M_1^2 < \frac{\mathcal{A}}{\mathcal{A}-1}$ the hypersonic stream experiences an area change of the opposite sign to that of the channel. This is a result that was identified by Bernstein, et. al. [28] from wave analysis. With uniform γ, the influence of each stream is proportional to $A(\frac{1}{M^2} - 1)/\gamma$, so a low velocity stream can drive the behavior of the entire flow if it occupies a sufficiently large portion of the channel.

The low velocity stream experiences area change:

$$dA_1 = \left[\frac{-(1-M_1^2)\mathcal{A}}{M_1^2-(1-M_1^2)\mathcal{A}}\right] dA \tag{5.23}$$

so the presence of the boundary layer can either magnify or reduce the inlet deceleration and nozzle acceleration of the main flow, as found in our three-stream solutions.

A parameter is defined here to compare the behavior of Mach number in one of the double streams with a single stream in the same channel:

$$\mathcal{M} \equiv \frac{\left[\frac{dM^2}{M^2}\right]_{\text{double}}}{\left[\frac{dM^2}{M^2}\right]_{\text{single}}} \tag{5.24}$$

From the influence coefficient expression for Mach number in terms of area change, and the individual stream area change, the above parameter can be written for stream i in terms of stream j as:

$$\mathcal{M}_i = \left[\frac{(1-M_i^2)A_j + (1-M_i^2)A_i}{(\frac{M_i^2}{M_j^2}-M_i^2)A_j + (1-M_i^2)A_i}\right] \tag{5.25}$$

For stream 2, in the hypersonic limit,

$$\mathcal{M}_2 = \left[\frac{-1}{\frac{1}{M_1^2}\frac{A_1}{A}-1}\right] \tag{5.26}$$

If $\mathcal{A} > \frac{M_1^2}{1-M_1^2}$, the low velocity stream is most influential in characterizing the behavior of all the fluid in the channel. This dependence is an expression of the compound flow behavior outlined by Bernstein et.al., simplified in the hypersonic limit. If the low velocity stream is actually subsonic (as part of the boundary layer flow will be) the channel behavior can be summarized as follows:

- if $\mathcal{A} > \frac{M_1^2}{1-M_1^2}$, the entire flow behaves as if it were subsonic, even though part of the flow is supersonic.
- if $\mathcal{A} < \frac{M_1^2}{1-M_1^2}$, the entire flow behaves as if it were supersonic.

- if $A = \frac{M_1^2}{1-M_1^2}$, the entire flow is choked, even though neither of the individual stream tubes is sonic.

Because static pressures are coupled, both stream tubes must accelerate or decelerate together. This can be demonstrated rigorously :

$$\frac{M_1}{M_2} = \left[\frac{(M_1^2 - 1)}{M_1^2}\right] \tag{5.27}$$

so that $\frac{M_1}{M_2} < 0$ if $M_1 < 1$, and $\frac{M_1}{M_2} > 0$ if $M_1 > 1$.

In a converging channel,

$$\frac{dM_1^2}{d\left(\frac{A_1}{A}\right)} \propto \left(\frac{A_1}{A} - M_1^2\right) \tag{5.28}$$

so the two-stream flow in a converging channel will move towards compound choking. This is especially important in a scramjet, where a thick boundary layer may choke the entire flow in the inlet, even though the hypersonic region has not decelerated much.

5.1.3 Analytical Model With Heat Addition

The effect of heat addition can be added to the two-stream model most simply by assuming total temperature changes only in the high-speed stream. This is a reasonable approximation, because the high temperatures and low density of the boundary layer will preclude the addition of much heat in the combustor, as will be justified in chapter 11. At constant specific heat, the influence coefficient of total temperature on static pressure is

$$C_{PT_o} = -\frac{\gamma M^2 \left(1 + \frac{\gamma-1}{2} M^2\right)}{1 - M^2} \tag{5.29}$$

Introducing this into the static pressure equation for the hypersonic stream, and again equating static pressure in both streams, we find

$$dA_2 = \left[\frac{1}{1 + \frac{M_2^2}{M_1^2}\frac{(1-M_1^2)}{(1-M_2^2)} A}\right] dA$$

$$+ \left[\frac{1+\frac{\gamma-1}{2}M_2^2}{\frac{M_2^2}{M_1^2}\left(\frac{1-M_1^2}{1-M_2^2}\right)+A}\right]\frac{A_1 dT_o}{T_o} \tag{5.30}$$

In the hypersonic limit,

$$dA_2 = \left[\frac{M_1^2}{M_1^2-(1-M_1^2)A}\right]dA - \left[\frac{\frac{\gamma-1}{2}M_2^2(1-M_1^2)}{M_1^2-(1-M_1^2)A}\right]\frac{A_1 dT_o}{T_o} \tag{5.31}$$

Thus, even if the channel area is constant ($dA \rightarrow 0$) heat addition will change the relative areas of the streams. If M_1 is subsonic, heat addition increases A_2 and decreases A_1; if M_1 is supersonic, heat addition increases A_1 at the expense of A_2.

The influence of a boundary layer on the free-stream flow behavior is dependent on whether that boundary layer is best represented by a subsonic streamtube or a supersonic streamtube. The resolution of this issue depends on an extension of the multiple streamtube model to a continuous profile. Chapter 6 will detail an analytical investigation into the proper means of characterizing the boundary layer in terms that are analogous to this simple two-streamtube model. It will be seen in chapter 8 that the boundary layer is best typified by a *supersonic* streamtube in most of the flow situations relevant to a transatmospheric vehicle. Therefore, the entire channel flow will typically be compound supersonic when the channel flow is hypersonic.

5.2 Application to Constant Area Combustor

The two-stream model presented above is only instructive for identifying basic compound compressible flow trends. For realistic modelling, more streamtubes must be used, and that will be the subject of subsequent chapters. However, it is instructive to apply the results of the two-stream model to a simple combustor geometry, with the goal of identifying trends that will emerge later in more detailed numerical calculations.

The effect of a low-speed region in a channel flow with heat addition can be illustrated analytically with the example of a combustor designed for constant-pressure operation with

uniform inflow. In such a channel, the Mach number decreases in response to heat addition, but the area is selected such that static pressure and velocity remain constant. This same combustor design will be used in chapter 6 as a convenient baseline for comparing engine performance.

The uniform-flow constant-pressure area and heating profiles can be found easily from the influence coefficient expression for pressure:

$$\frac{dP}{P} = \left[\frac{\gamma M^2}{1-M^2}\right]\frac{dA}{A} - \left[\frac{\gamma M^2\left(1+\frac{\gamma-1}{2}M^2\right)}{1-M^2}\right]\frac{dT_o}{T_o} \tag{5.32}$$

where $dT = dT_o$ if velocity is constant. Constant pressure $dP/P = 0$ is satisfied by the condition:

$$\frac{dA}{dx} = \frac{\bar{A}}{\lambda_D}e^{x/\lambda_D} \tag{5.33}$$

$$\frac{dT}{dx} = \frac{\bar{T}}{\lambda_D}e^{x/\lambda_D} \tag{5.34}$$

Overlined values represent initial conditions, and λ_D is a design length scale that characterizes the rate at which heat is added to the flow. The corresponding Mach number and total temperature profiles will be

$$\frac{dM^2}{dx} = \frac{\bar{M}^2}{\lambda_D}e^{-x/\lambda_D} \tag{5.35}$$

$$\frac{dT_o}{dx} = \frac{\bar{T}_o}{\lambda_D}\left(1+\frac{\gamma-1}{2}M^2\right)^{-1}e^{x/\lambda_D} \tag{5.36}$$

The behavior of nonuniform flow with a low-speed streamtube is explored by inserting the above profiles for area and total temperature into the two-stream model of equation (5.30). For convenience, define:

$$\Upsilon = \frac{M_1^2(1-M_2^2)}{M_2^2(1-M_1^2)} \tag{5.37}$$

$$\Gamma = \frac{1+\frac{\gamma-1}{2}M_2^2}{1+\frac{\gamma-1}{2}M(x)^2} \tag{5.38}$$

Υ is another expression of the compound choking parameter, and Γ is the ratio of total temperature to the uniform flow value, at the same static temperature. In the particular

case of total area change being a small fraction of the initial area, the area change for the high-speed streamtube is then:

$$\frac{dA_2}{A_2} = \left\{\frac{1+\mathcal{A}(1+\Gamma/\Upsilon)}{1+\mathcal{A}\Upsilon}\right\}\frac{dx}{\lambda_D} \tag{5.39}$$

The pressure follows:

$$\frac{dP}{P} = \left[\frac{\gamma M_1^2}{1-M_1^2}\right]\left\{\frac{1+\mathcal{A}-\Gamma}{\mathcal{A}+\Upsilon}\right\}\frac{dx}{\lambda_D} \tag{5.40}$$

and the high-speed streamtube Mach number behaves as:

$$\frac{dM_2^2}{M_2^2} = \left[\frac{1}{1-M_2^2}\right]\left\{\left(1+\gamma M_2^2 - \frac{2(1+\frac{\gamma-1}{2}M_2^2)\mathcal{A}}{\mathcal{A}+\Upsilon}\right)\Gamma - \frac{2(1+\frac{\gamma-1}{2}M_2^2)\Upsilon(\mathcal{A}+1)}{\mathcal{A}+\Upsilon}\right\}\frac{dx}{\lambda_D} \tag{5.41}$$

The static temperature can be related to the total temperature and area profiles as well:

$$\frac{dT}{T} = \left[\frac{M_2^2}{1-M_2^2}\right]\left\{(\gamma-1)\left(\frac{1+\mathcal{A}(1+\Gamma/\Upsilon)}{1+\mathcal{A}/\Upsilon}\right) + \frac{(1-\gamma M_2^2)}{M_2^2}\Gamma\right\}\frac{dx}{\lambda_D} \tag{5.42}$$

The Mach number pressure, and temperature distributions can be written as

$$\frac{dM_2^2}{M_2^2} = \frac{dx}{\lambda_M} \tag{5.43}$$

$$\frac{dP}{P} = \frac{dx}{\lambda_P} \tag{5.44}$$

$$\frac{dT}{T} = \frac{dx}{\lambda_T} \tag{5.45}$$

where, for uniform inflow conditions, $\lambda_M = -\lambda_D$, $\lambda_T = \lambda_D$, and $\lambda_P = \infty$, corresponding to constant pressure. The values of λ as characterize the activity length of thermodynamic changes. For instance, a small λ_M means that the Mach number is behaving as if the channel were shortened, with flow properties changing quickly. Similarly, large λ_M corresponds to a flow with very gradual changes in Mach number. Negative λ_M means Mach number is decreasing, while positive values refer to increasing Mach number.

Because M_2 is a function of distance along the combustor channel, it is difficult to examine the behavior of the nonuniform flow at arbitrary x. However, at or near the

combustor entrance, $e^{-x/\lambda_D} \simeq 1$, and, assuming the high-speed stream Mach number equals the original design-value uniform-flow Mach number, $M_2 \simeq \bar{M}$, so $\Gamma \simeq 1$. The characteristic lengths, in terms of the original design length scale, are then:

$$\frac{\lambda_D}{\lambda_M} = \left[\frac{1}{1-M_2^2}\right]\left\{1+\gamma M_2^2 - \frac{2(1+\frac{\gamma-1}{2}M_2^2)(\mathcal{A}(1+\Upsilon)+\Upsilon)}{\mathcal{A}+\Upsilon}\right\} \tag{5.46}$$

$$\frac{\lambda_D}{\lambda_P} = \left[\frac{M_1^2}{1-M_1^2}\right]\left\{\frac{\gamma\mathcal{A}}{\mathcal{A}+\Upsilon}\right\} \tag{5.47}$$

$$\frac{\lambda_D}{\lambda_T} = \left[\frac{M_2^2}{1-M_2^2}\right]\left\{(\gamma-1)\left(\frac{1+\mathcal{A}(1+1/\Upsilon)}{1+\mathcal{A}/\Upsilon}\right)+\frac{(1-\gamma M_2^2)}{M_2^2}\right\} \tag{5.48}$$

In the hypersonic limit, these length scales are independent of the high-speed Mach number.

If the low-speed streamtube is subsonic, the compound compressible flow can experience either compound subsonic, compound choked, or compound supersonic behavior. On the other hand, if both streamtubes are supersonic, only compound supersonic behavior is possible. Although the properties of the flow with a subsonic streamtube will be considered in detail, it will be shown in chapters 8 and 11 that the proper representation of the boundary layer profile is with a *supersonic* streamtube for most cases.

Figure 5.1 shows the values of the characteristic pressure length and characteristic Mach number length as a function of low-speed to high-speed area ratio, with high-speed stream tube at $M_1 = 10$ and low-speed $M_2 = .5$. This channel can be compound supersonic, subsonic, or choked. In accordance with equation (5.47), the characteristic pressure length scale approaches ∞ as the area ratio goes to zero. This is the uniform flow limit, and experiences the consistent constant pressure behavior. The pressure scale $\lambda_P = 0$ when the low-speed stream tube has thickness such that $\mathcal{A} = -\Upsilon$. This corresponds to the compound choking condition found earlier. At a given low-speed Mach number, the characteristic pressure length scale is negative between the uniform flow and compound choking limits. The two-stream flow would therefore experience a favorable streamwise pressure gradient and corresponding acceleration. For low-speed streamtubes that are thicker than the choking criterion, the pressure gradient is finite and positive, acting against the direction of flow. As stated earlier, this behavior is insensitive to Mach number at high Mach number. In fact, for M_2 greater than about 4, this plot is essentially independent of M_2.

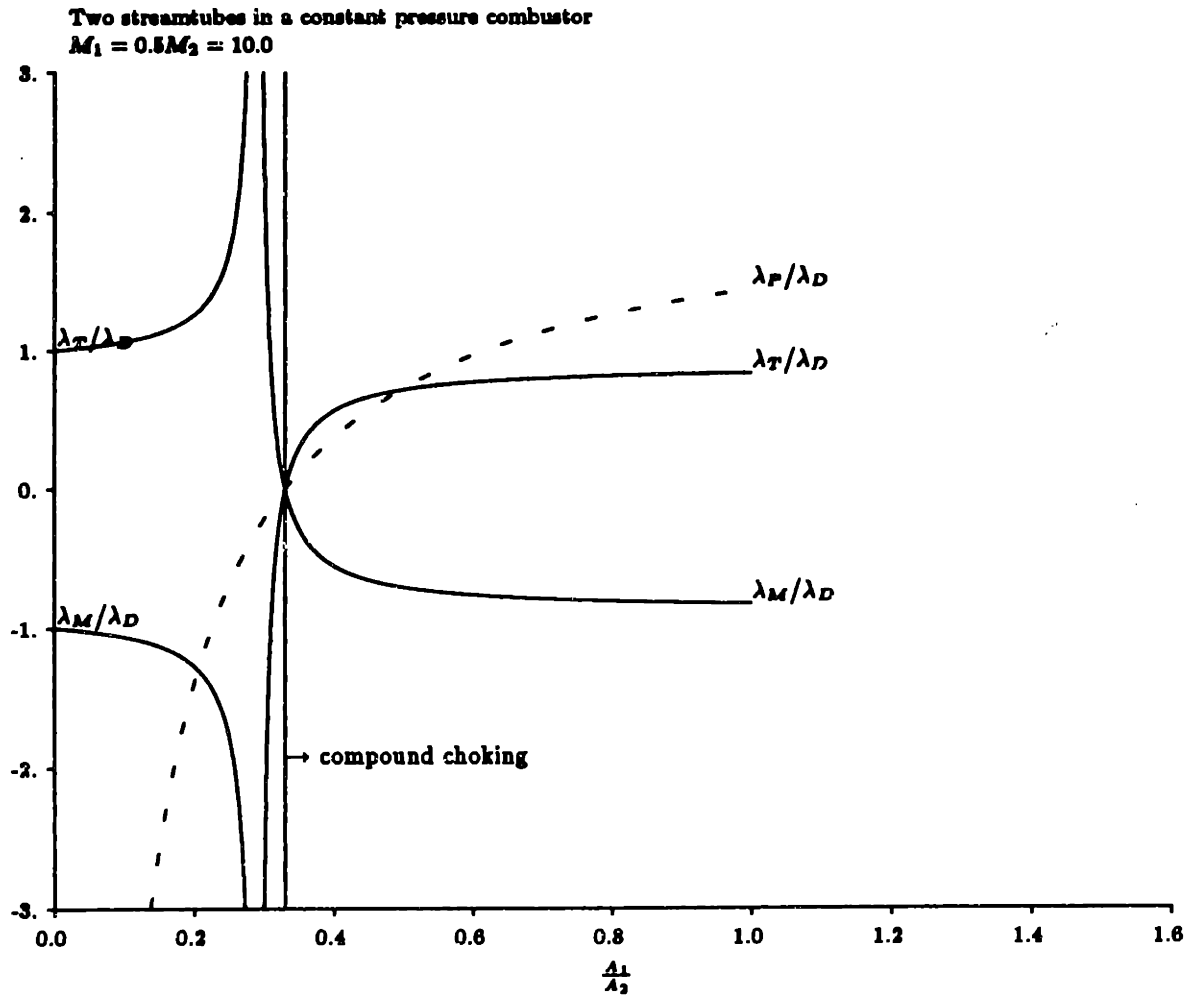

Figure 5.1: Characteristic Mach number, temperature, and pressure lengths in a constant pressure combustor with $M_1 = .5$, $M_2 = 10$

As shown in Figure 5.1, the characteristic Mach number length λ_M is also zero at the compound choking point. In the uniform limit, $\lambda_M/\lambda_D = -1$, as expected. However, between the uniform limit and the compound choking point, there is a region where $\lambda_M \rightarrow \infty$, corresponding to constant Mach number. From equation (5.46), this point corresponds to an area ratio:

$$\mathcal{A} = \frac{M_1^2(M_2^2 - 1)}{M_2^2[(\gamma - 2)M_1^2 + 1] + 2M_1^2} \tag{5.49}$$

With $M_1 = .5, M_2 = 10$, $\lambda_M \rightarrow \infty$ at $\mathcal{A} = .2897$. At this point, the nonuniform flow will tend to remain at its initial Mach number, rather than decreasing exponentially as did the uniform stream. Similarly, the area ratio at which $\lambda_T \rightarrow \infty$ is:

$$\mathcal{A} = \frac{M_1^2(M_2^2 - 1)}{M_2^2[(\gamma - 2)M_1^2 + 1]} \tag{5.50}$$

At the same conditions, $\lambda_T \rightarrow \infty$ at $\mathcal{A} = .2912$. The temperature behaves qualitatively like the Mach number, with the same choking point and a slightly different constant value area ratio.

The Mach number has three distinct types of behavior. Between the uniform limit of $\mathcal{A} = 0$ and the constant Mach number point, λ_M is negative and has greater magnitude than the design value, λ_D, and magnitude increases monotonically with area ratio. In this regime, Mach number is decreasing, and the rate of that decrease is falling with increasing area ratio. Between the constant Mach number point and compound choking, λ_M is positive, corresponding to an increasing Mach number. The rate of this increase grows with increasing $\mathcal{A}$, until it becomes singular at the choking point. For low speed streams that are thicker than the choking criterion, corresponding to compound subsonic flow, $\lambda_M < 0$, so Mach number is decreasing at a rate that decreases with increasing area ratio.

The area ratios at which compound choking and constant Mach number occur both depend on the magnitude of the low speed Mach number. However, the choking condition is more sensitive, so the spacing between these two points increases with increasing M_1. At small values of M_1 (*i.e.*, $M_1 < .2$), the choking and constant Mach number points coincide, so there is no area ratio at which Mach number is increasing down the channel.

Figure 5.2 is a plot of the two streamtube behavior when both streamtubes are super-

sonic, with $M_1 = 2$ and $M_2 = 10$. There is no compound compressible subsonic regime because there is no subsonic streamtube, but the low-speed streamtube does still have a noticeable influence on the net channel behavior.

Figure 5.3 presents the two-streamtube flow with low-speed Mach number $M_1 = .5$ and $M_2 = 20$. Comparing this with Figure 5.1, the channel behavior is quite insensitive to the magnitude of the hypersonic Mach number.

Finally, we can examine losses in the two-stream channel. As is well known, heat addition to a one-dimensional flow leads to a loss in total pressure, the magnitude of which increases with increasing Mach number. However, the total pressure is not influenced by changes in area, as indicated in equation (1.3), so in the nonuniform channel, with the same relative increase in total temperature, the logarithmic derivative of total pressure is proportional only to the local Mach number. The change in losses through the combustor channel with the addition of a low-speed streamtube depends solely on the changes in Mach number. When nonuniform effects keep Mach number higher than the design conditions, the total pressure drop will be increased; conversely, if Mach number is decreased, total pressure losses are decreased as well. These trends will be seen numerically in chapter 11, but it will also be shown that actual boundary layer profiles have less dramatic effects on the free-stream conditions than is indicated by the two-streamtube model, because the boundary layer tends to remain at a constant thickness.

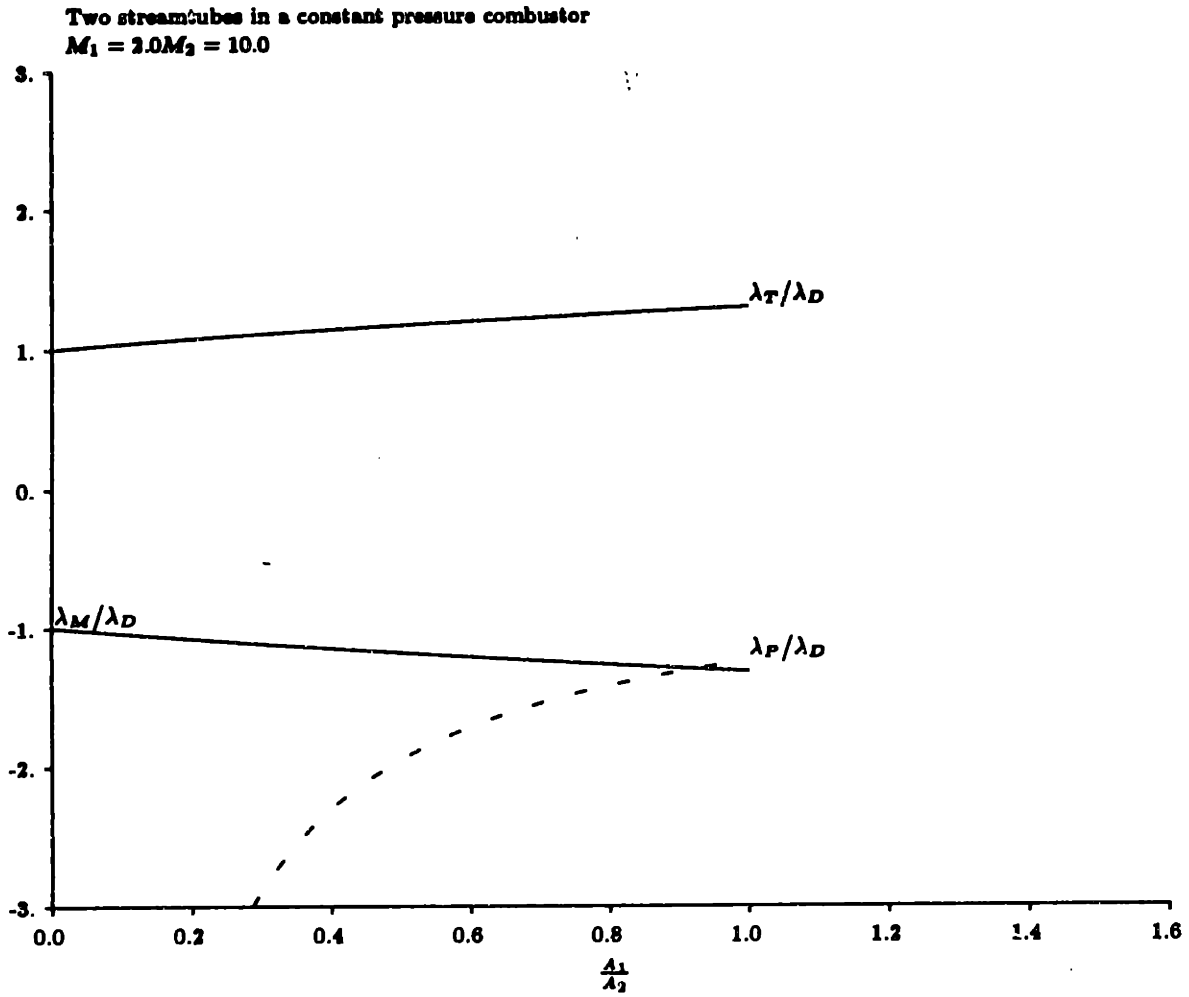

Figure 5.2: Characteristic Mach number, temperature, and pressure lengths in a constant pressure combustor with $M_1 = 2$, $M_2 = 10$

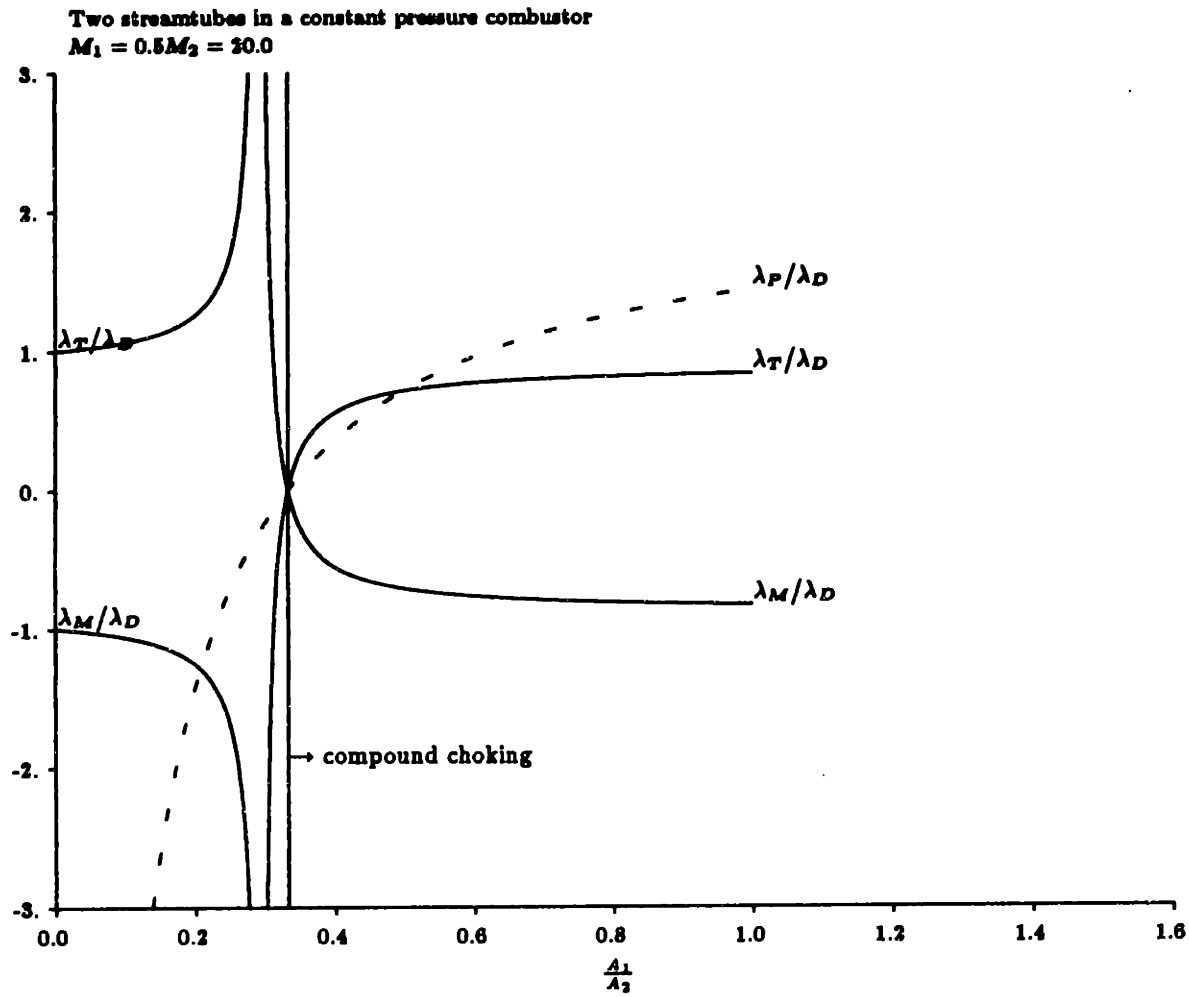

Figure 5.3: Characteristic Mach number, temperature, and pressure lengths in a constant pressure combustor with $M_1 = .5$, $M_2 = 20$

Chapter 6

Modelling Continuous Profiles with Compound Compressible Flow

6.1 Extension of the Compound Flow Model

6.1.1 Model Assumptions

The behavior of a two-streamtube channel flow has been examined under the influence of area change and heat addition. In solving for this behavior, it was assumed that the fluid flows in streamtubes of uniform local Mach number, and without a normal pressure gradient. In this chapter, the same approach will be taken for a flow consisting of many streamtubes, and will ultimately be extended to a continuous profile. The advantage of solving for a pressure-matched flow will be particularly apparent with multiple streamtubes because, once the matching condition is satisfied, all streamtubes can be treated independently from the rest of the channel flow.

It is tacitly assumed that viscous effects are unimportant inside the engine channel. Viscosity is required for generating the boundary layer profile on the forebody, but once that profile is formed, further viscous effects will be neglected. The validity of this assumption depends on the forebody being much longer than the channel length of the scramjet, so the residence time of flow inside the engine is much smaller than on the vehicle surface. Also in this model, formation and further growth of boundary layers inside the engine itself will be neglected.

This compound flow behavior is best characterized by the compound flow parameter,

β, which is defined in terms of the local static pressure, P, and channel height, H, as

$$\beta = \frac{dH}{dx} \Big/ \frac{d\ln P}{dx} \tag{6.1}$$

where x is the streamwise coordinate.

When β is positive, the channel is "compound subsonic" even though one or more of its streamtubes may be supersonic, meaning that the entire flow behaves as if it were subsonic, decelerating in an expanding channel and accelerating in a converging one. Conversely, when β is negatively valued, the entire flow is "compound supersonic," behaving as if it were supersonic, so that it accelerates in a diverging channel and decelerates in a converging one. At values of $\beta = 0$, the flow is "compound choked," and will not accept further reductions in channel area. This is the limit at which information will no longer propagate upstream, even though a part of the channel flow may be subsonic, because information propagation is limited by the pressure matching condition across the channel cross-section. This behavior was seen in the two-streamtube solution of the previous chapter.

Because the compound flow parameter depends on each individual streamtube's area and Mach number as

$$\beta = \sum_i \frac{A_i}{\gamma_i} \left(\frac{1}{M_i^2} - 1 \right) \tag{6.2}$$

a streamtube with very low Mach number, and thus a very large value of $1/M^2$, can dominate the behavior of the entire channel flow, even though its area is small. Similarly, at hypersonic conditions,

$$\left(\frac{1}{M^2} - 1 \right) \simeq -1 \tag{6.3}$$

so that at high Mach numbers, the compound flow parameter becomes independent of Mach number.

At this point, it is convenient to define another compound choking parameter, a uniform equivalent Mach number, which will be termed $\overline{M}$, and will be selected such that

$$\left(\frac{1}{\overline{M}^2} - 1 \right) \sum_i \frac{A_i}{\gamma_i} \equiv \sum_i \frac{A_i}{\gamma_i} \left(\frac{1}{M_i^2} - 1 \right) \tag{6.4}$$

or,

$$\overline{M} = \frac{1}{\sqrt{1 + \frac{\gamma_{average}\,\beta}{A_{total}}}} \tag{6.5}$$

In other words, a streamtube with equivalent uniform Mach number $\overline{M}$ will have the same response to channel area change as the non- uniform combination of streamtubes over the same area. A nonuniform channel flow could be replaced with a uniform flow at $\overline{M}$ and have the same β *at one station.*

Although the equivalent uniform streamtube concept is the most straightforward means of comparing the nonuniform flow to a uniform streamtube, the analogy cannot be carried beyond a single station in a channel. Changes in the value of $\overline{M}$ for a given change in channel area will not in general be equal to the change that would be observed in an actual uniform streamtube. Therefore, it would not be valid to calculate a channel flow by determining $\overline{M}$ at the inlet station, then replacing the entire flow by a uniform streamtube at that Mach number and following it as a 1-d streamtube.

From the definition of $\overline{M}$, it can be shown that the streamwise derivative of $\overline{M}$ for a multi-streamtube channel flow tends to be larger than the streamwise derivative of the Mach number for an actual uniform flow at that same Mach number. As an example, the streamwise derivative of $\overline{M}$ in a two-streamtube channel can be compared to a uniform streamtube by taking the derivative of equation (5.5) and using the area change relationship of equation (5.21):

$$\frac{\left(\frac{d\overline{M}}{dx}\right)_{2-\text{tubes}}}{\left(\frac{dM}{dx}\right)_{\text{uniform}}} = \frac{3(\mathcal{A}^2+\mathcal{A})\frac{1}{M_1^4}+\left(\frac{1}{\gamma}-3\right)(\mathcal{A}^2+\mathcal{A})\frac{1}{M_1^2}+(\mathcal{A}+1)^2}{3\mathcal{A}^2\frac{1}{M_1^4}+\left(\frac{1}{\gamma}-3\right)(\mathcal{A}^2+\mathcal{A})\frac{1}{M_1^2}+(\mathcal{A}+1)^2} \tag{6.6}$$

where the definitions of $\mathcal{A}$ and M_1 are the same as in chapter 5 and the Mach number of streamtube 2 is taken to be hypersonic ($M_2 \to \infty$). In the limit of small M_1, this reduces to

$$\frac{\left(\frac{d\overline{M}}{dx}\right)_{2-\text{tubes}}}{\left(\frac{dM}{dx}\right)_{\text{uniform}}} = \frac{(\mathcal{A}^2+\mathcal{A})}{\mathcal{A}^2} \tag{6.7}$$

so the $\overline{M}$ analogy fails in this respect.

6.1.2 Limitations on Discrete Streamtube Solutions

To treat an actual profile, the above streamtube model will be expanded to account for a continuous profile, such as that associated with a boundary layer. A primary difficulty of

approximating a continuous profile with discrete section can be demonstrated by examining successive approximations to a simple nonuniform profile. As an example, consider a linear Mach number profile, ranging from M=0 at y=0 to $M = M_e$ at y=A, with uniform γ. For one streamtube with uniform Mach number $M_e/2$:

$$\beta = \frac{A}{\gamma}\left(\frac{4}{M_e^2} - 1\right) \tag{6.8}$$

with 100 streamtubes, both area-averaged,

$$\beta = \frac{A}{\gamma}\left(\frac{492.4803}{M_e^2} - 1\right) \tag{6.9}$$

or, in general, for N streamtubes,

$$\beta = \frac{A}{\gamma}\left(\sum_{i=1}^{N}\left[\frac{N}{(i-\frac{1}{2})^2 M_e^2}\right] - 1\right) \tag{6.10}$$

In the limit of infinitely many streamtubes, $\beta \to \infty$.

The value of β depends on the number of discrete streamtubes selected. The discrete approximation is obviously a poor one, since any value of β can be obtained, depending on how small the streamtubes are taken. In this example, we have divided the profile into streamtubes of equal area; by varying the areas, the indeterminacy in β would have been even greater.

In the limit of infinitely small streamtubes, the β parameter can be expressed in integral form by converting A_i, the area of each streamtube at the specific streamwise station being examined, into a differential area, dA, over which the integration will be carried:

$$\beta(x) = \int_A \frac{dA}{\gamma}\left(\frac{1}{M(y,z)^2} - 1\right) \tag{6.11}$$

where x is the streamwise coordinate, and y and z are the planar coordinates at the given station. In two dimensions, this becomes:

$$\beta = \int_0^H \left(\frac{1}{M(y)^2} - 1\right)\frac{dy}{\gamma} \tag{6.12}$$

Considering the class of solutions for profiles such that

$$M(y) = M_e\left(\frac{y}{H}\right)^n \tag{6.13}$$

with constant γ,

$$\beta = \frac{H^{2n} y^{(1-2n)}}{\gamma(1-2n)M_e^2} - \frac{y}{\gamma}\Bigg|_{y=0}^{y=H} \tag{6.14}$$

For values of $n < 1/2$,

$$\beta = \frac{H}{\gamma}\left(\frac{1}{(1-2n)M_e^2} - 1\right) \tag{6.15}$$

For small values of n, (i.e. nearly uniform profiles) the β parameter is only slightly different from the uniform flow solution, and resembles a uniform flow with a slightly smaller free stream Mach number. Actual laminar boundary layer profiles are far from uniform, with nearly linear profiles that are best represented by values of $n \simeq 1$, especially near the wall. This greatly complicates the above formulation, because the integral diverges ($\beta \rightarrow \infty$) for values of $n \geq 1/2$. This implies that, no matter how small the boundary layer, the flow is always dominated by the wall.

This result is clearly non-physical, and it arises from the fact that the solution is attempting to satisfy a no-slip condition on the wall without viscosity. From the 1-d momentum equation,

$$\frac{du}{dx} = -\frac{1}{\rho u}\left(\frac{dp}{dx} - \frac{\partial \tau}{\partial y}\right) \tag{6.16}$$

accordingly, if there is no shear (i.e. inviscid flow), $du/dx \rightarrow \infty$ in the presence of a finite pressure gradient at zero velocity. This is an example of a well-known result of inviscid flow theory, that we cannot satisfy the no-slip condition without a second derivative viscous term.

6.1.3 Integral Form of the β parameter

In order to correctly account for the no-slip condition at a wall, while retaining the 1-d compound compressible flow model without averaging, the β parameter will be solved in integral form with the inclusion of viscous effects. Other less successful means of avoiding this problem are described in Appendix C. The development of Hevenor, Heiser, and Bernstein [28] will be modified with the addition of a shear gradient term which will exactly cancel the accelerating influence of a streamwise pressure gradient when the streamwise velocity equals zero.

The one-dimensional continuity, momentum, and energy equations in differential form are:

$$\text{Continuity} \quad : \quad \rho\, u\, A = \text{Constant} \tag{6.17}$$

$$\text{Momentum} \quad : \quad \rho u \frac{du}{dx} + \frac{dP}{dx} = \frac{\partial \tau}{\partial y} \tag{6.18}$$

$$\text{Energy} \quad : \quad C_P T + \frac{u^2}{2} = C_P T_o \tag{6.19}$$

$$\tag{6.20}$$

The continuity equation is written as:

$$\frac{d\rho}{\rho} + \frac{du}{u} + \frac{dA}{A} = 0 \tag{6.21}$$

From the equation of state, the logarithmic derivative of pressure is related to temperature in the energy equation, and density in the continuity equation:

$$\frac{dP}{P} = \frac{d\rho}{\rho} + \frac{dT}{T} \tag{6.22}$$

Dividing the momentum equation through by P,

$$\frac{dP}{P} = -\frac{\rho u}{P} du + \frac{\partial \tau}{\partial y}\frac{dx}{P} = \frac{d\rho}{\rho} + \frac{dT}{T} \tag{6.23}$$

and substituting for the pressure and temperature terms from equations (6.22) and (6.19),

$$-\frac{\rho u}{P} du + \frac{\partial \tau}{\partial y}\frac{dx}{P} = \left(\frac{d\rho}{\rho} + \frac{dA}{A}\right) + \left(\frac{dT_o}{T} - \frac{u\, du}{C_P T}\right) \tag{6.24}$$

Rearranging terms,

$$\frac{du}{u}\left(1 + \frac{u^2}{C_P T} - \frac{\rho u^2}{P}\right) + \frac{dA}{A} - \frac{dT_o}{T} + \frac{\partial \tau}{\partial y}\frac{dx}{P} = 0 \tag{6.25}$$

The seemingly complicated term in parentheses simplifies to

$$\left(1 + \frac{u^2}{C_P T} - \frac{\rho u^2}{P}\right) = 1 - M^2 \tag{6.26}$$

so that

$$du = -\frac{u}{1 - M^2}\left(\frac{da}{A} - \frac{dT_o}{T} + \frac{\partial \tau}{\partial y}\frac{dx}{P}\right) \tag{6.27}$$

This velocity term is then re-introduced in the original momentum equation (6.18), which is solved for the logarithmic derivative of pressure:

$$\frac{dP}{P} = \frac{\rho u^2}{P(1 - M^2)}\left(\frac{da}{A} - \frac{dT_o}{T}\frac{\partial \tau}{\partial y}\frac{dx}{P}\right) + \frac{\partial \tau}{\partial y}\frac{dx}{P} \tag{6.28}$$

The speed of sound is introduced again as $a^2 = \gamma P/\rho$, and the total temperature is related to local temperature at any point as $T_o = T(1 + \frac{\gamma-1}{2} M^2)$. The pressure expression can then be simplified as:

$$\frac{dP}{P} = \left[\frac{-\gamma M^2}{M^2-1}\right]\frac{dA}{A} + \left[\frac{\gamma M^2(1+\frac{\gamma-1}{2}M^2)}{M^2-1}\right]\frac{dT_o}{T_o} - \left[\frac{1+(\gamma-1)M^2}{M^2-1}\right]\frac{\partial \tau}{\partial y}\frac{dx}{P} \tag{6.29}$$

This last is nearly identical to Shapiro's influence coefficient expression for changes in pressure due to area change, heat addition, and friction, with the exception that the shear gradient has been retained in explicit form.

In order to solve for the pressure-matched streamtube model, we are interested in solving for the area of each 1-d tube, the above expression is written as:

$$\frac{dA}{A} = \left[\frac{1}{\gamma}\left(\frac{1}{M^2}-1\right)\right]\frac{dP}{P} + \left[1+\frac{\gamma-1}{2}M^2\right]\frac{dT_o}{T_o} - \left[\frac{1}{\gamma}\left(\frac{1}{M^2}-1\right)+1\right]\frac{\partial \tau}{\partial y}\frac{dx}{P} \tag{6.30}$$

With $dT_o = 0$,

$$\frac{dA}{A} = \frac{1}{\gamma}\left(\left[\frac{1}{M^2}-1\right]\frac{dP}{P} - \left[\frac{1}{M^2}-1+\gamma\right]\frac{\partial \tau}{\partial y}\frac{dx}{P}\right) \tag{6.31}$$

Thus,

$$\frac{dA}{dx} = \frac{A}{\gamma}\left[\frac{1}{M^2}-1\right]\left(\frac{d\ln P}{dx} - \frac{\partial \tau/\partial y}{P}\right) - A\frac{\partial \tau/\partial y}{P} \tag{6.32}$$

From the 1-d momentum equation (6.18), $u = 0$ at the wall, and the streamwise pressure gradient is exactly cancelled by the normal shear gradient:

$$\frac{dP}{dx} = \frac{\partial \tau}{\partial y} \tag{6.33}$$

For convenience, define:

$$\overline{\tau_w'} \equiv \frac{\partial \tau/\partial y}{dP/dx} \tag{6.34}$$

Then equation (6.32) can be written in simpler form:

$$\frac{dA}{dx} = \frac{A}{\gamma}\left[\frac{1}{M^2}-1\right]\left(1-\overline{\tau_w'}\right)\frac{d\ln P}{dx} - A\frac{\partial \tau/\partial y}{P} \tag{6.35}$$

Equation (6.35) reduces to the form used by Hevenor, Heiser, and Bernstein in the inviscid limit.

At the wall, $(1-\overline{\tau_w'}) = 0$, which cancels the $1/M^2$ singularity. Similarly, at some height above the wall, $(1-\overline{\tau_w'}) \simeq 1$, and viscous effects become unimportant. At that point, the

inviscid approximation is valid. In order to cancel the singularity, it is not sufficient to merely set $(1-\overline{\tau_w'}) = 0$ at the wall. Rather, $(1-\overline{\tau_w'}) \to 0$ as *fast* as $M^2 \to 0$ when $y \to 0$.

Following the method of solution applied to the inviscid case, the expression for the area change in one streamtube is related to the behavior in the entire channel by integrating equation (6.35) over all streamtubes. Again, the area of each streamtube, A_i, is taken to be the area of some infinitesimally small tube, and integrate over all tubes. In two dimensions, that means that A becomes a differential length element dy in the normal direction:

$$\frac{d(dy)}{dx} = \frac{dy}{\gamma}\left[\frac{1}{M^2}-1\right]\left(1-\overline{\tau_w'}\right)\frac{d\ln P}{dx} - dy\frac{\partial\tau/\partial y}{P} \tag{6.36}$$

The integral of the left hand side of the equation represents the streamwise change in the total channel area, H:

$$\begin{aligned}\int_0^H \frac{d(dy)}{dx} &= \frac{d}{dx}\left(\int_0^H dy\right) \\ &= \frac{dH}{dx}\end{aligned} \tag{6.37}$$

Thus, integrating both sides of equation (6.36):

$$\frac{dH}{dx} = \frac{d\ln P}{dx}\int_0^H \left[\frac{1}{M^2}-1\right]\left(1-\overline{\tau_w'}\right)\frac{dy}{\gamma} - \int_0^H \frac{\partial\tau/\partial y}{P}dy \tag{6.38}$$

where the uniform pressure assumption is used to pull the logarithmic derivative of pressure out of the integral. The last integral can be expressed simply in terms of the wall shear stress, as will be indicated below.

There are two integral components. The first integral is identical to the inviscid relationship between area change and logarithmic pressure gradient, with a correction for viscosity. The second derivative represents the total shear on the wall, and is entirely new in the viscous solution.

In the compound compressible flow solution, the flow properties were evaluated in terms of the pressure behavior for a given change in channel area. That worked for the inviscid case because there is a direct and unique relationship between channel area and flow properties For instance, for 1-d inviscid flow without heat addition, if the flow is choked, it must be choked at the minimum area point. The compound compressible choking point for multiple

inviscid streamtubes also occurs at the minimum area point, where $\beta = 0$. The compound flow is then characterized based on the response of the entire channel to changes in area. For instance, an expanding channel accelerates the compound supersonic flow, and decelerates a compound subsonic one.

With viscous flow, a direct comparison between area change and flow behavior is not possible. In 1-d flow, the presence of friction (and heat addition) will move the choking point ahead of the throat. Indeed, friction or heat addition can choke the flow in a constant area channel. It is no longer possible to describe the compound flow properties entirely on the basis of channel area. The more fundamental parameter for characterizing 1-d flow properties is $(1 - M^2)\, dM^2$. Shapiro [27] stated three rules of choking based on the value of this parameter:

- If $(1 - M^2)\, dM^2 > 0$ no changes are permitted in the flow parameters beyond M=1. The flow is then choked.
- If initially, $(1 - M^2)\, dM^2 > 0$, flow parameters can be changed beyond M=1 if $(1 - M^2)\, dM^2$ becomes < 0.
- If $(1 - M^2)\, dM^2 < 0$ no limiting effects are encountered in constructing the 1-d flow.

Shapiro solves for $(1 - M^2)\, dM^2$ from the influence coefficient expression for the logarithmic change in Mach number:

$$(1 - M^2)dM^2 = M^2 \left(1 + \frac{\gamma - 1}{2} M^2\right) \left[-2\frac{dA}{A} + (1 + \gamma M^2)\frac{dT_o}{T_o} + 2(2\gamma M^2 f)\frac{dx}{D}\right] \quad (6.39)$$

where f is the friction coefficient, defined so that

$$f \equiv \frac{\tau_{\text{wall}}}{\frac{1}{2}\rho V^2} \quad (6.40)$$

and D is the hydraulic diameter, defined as

$$D \equiv \frac{4dx}{dA_{\text{wall}}/A} \quad (6.41)$$

Since $\rho V^2 = \gamma P M^2$, we can see that, in Shapiro's formulation,

$$\frac{2\gamma M^2 f}{D} = 4\frac{\tau_{\text{wall}}}{DP} \quad (6.42)$$

In a 2-d channel, $A = H$ and $2\,dA_{\text{wall}} = dx$, so

$$\frac{2\gamma M^2 f}{D} = \frac{2\tau_{\text{wall}}}{P\,H} \tag{6.43}$$

Shapiro has placed all of the viscous shear at the wall; his flow is envisioned as being inviscid except at the interface between the fluid and the non-moving wall surface. This model is comparable to the explicit solution in this work because the wall shear is defined so that

$$\left(\frac{2\tau_{\text{wall}}}{P}\right)_{\text{Shapiro}} = -\int_0^H \frac{\partial \tau}{\partial y}\frac{dy}{P} \tag{6.44}$$

The bracketed portion of the right side of equation (6.39),

$$\left[-2\frac{dA}{A} + (1+\gamma M^2)\frac{dT_o}{T_o} + 2(2\gamma M^2 f)\frac{dx}{D}\right] \tag{6.45}$$

is, in the absence of heat addition,

$$\left[-2\frac{dH}{H} - 2\int_0^H \frac{\partial \tau}{\partial y}\frac{dy}{P}\right] \tag{6.46}$$

Thus, the parameter which will determine the nature of the compound flow is really

$$\frac{dH}{dx} + \frac{2\tau_{\text{wall}}}{P} = \int_0^H \left[\frac{1}{M^2} - 1\right]\left(1 - \overline{\tau_w'}\right)\frac{d\ln P}{dx}\frac{dy}{\gamma} \tag{6.47}$$

and the compound compressible flow for a continuous profile with shear is best characterized by a modified β parameter:

$$\beta = \int_0^H \left[\frac{1}{M^2} - 1\right]\left(1 - \overline{\tau_w'}\right)\frac{dy}{\gamma} \tag{6.48}$$

Note that with the introduction of the viscous term,

$$\beta \neq \frac{dH/dx}{d\ln P/dx} \tag{6.49}$$

as it is for the inviscid solution. The modified β parameter still has the same meaning as that of Hevenor, Heiser, and Bernstein:

- $\beta > 0$ flow is "compound subsonic"
- $\beta < 0$ flow is "compound supersonic"

- $\beta = 0$ flow is "compound choked"

The relationship between pressure change and area is written as:

$$\frac{d\ln P}{dx} = \frac{1}{\beta}\left(\frac{dH}{dx} + \frac{2\tau_{\text{wall}}}{P}\right) \tag{6.50}$$

Under the assumption of essentially inviscid flow in the engine, in which viscous effects are only important to retain the no-slip condition at the wall,

$$\beta \simeq \frac{dH/dx}{d\ln P/dx} \tag{6.51}$$

The solution can now be modified to include the effect of heat addition in the flow. When the one-dimensional area relationship was derived, the total temperature terms were originally included. Incorporating this into equation(6.35):

$$\frac{dA}{dx} = \frac{A}{\gamma}\left[\frac{1}{M^2} - 1\right]\left(1 - \overline{\tau_w'}\right)\frac{d\ln P}{dx} - A\frac{\partial\tau/\partial y}{P} + \left(1 + \frac{\gamma-1}{2}M^2\right)\frac{A}{T_o}\frac{dT_o}{dx} \tag{6.52}$$

which integrates to a modified version of equation (6.38):

$$\frac{dH}{dx} = \frac{d\ln P}{dx}\int_0^H \left[\frac{1}{M^2} - 1\right]\left(1 - \overline{\tau_w'}\right)\frac{dy}{\gamma} - \frac{2\tau_{\text{wall}}}{P} + \int_0^H \left(1 + \frac{\gamma-1}{2}M^2\right)\frac{1}{T_o}\frac{dT_o}{dx}dy \tag{6.53}$$

The temperature addition term serves a very different function in the one-dimensional area expression. Whereas the viscous term balanced the pressure term at the wall, and so was required to match the pressure gradient, no such requirement is placed on the heat addition.

With heat addition, the bracketted portion of the right side of equation (6.39) will read

$$\left[-2\frac{dH}{H} - 2\int_0^H \frac{\partial\tau}{\partial y}\frac{dy}{P} + \int_0^H \left(1 + \gamma M^2\right)\frac{dT_o}{T_o}\right] \tag{6.54}$$

So the value of β defined above is no longer the compound choking parameter, since it includes only pressure effects.

The streamwise pressure gradient is related to the channel area as:

$$\frac{d\ln P}{dx} = \frac{1}{\beta}\left(\frac{dH}{dx} + \frac{2\tau_{\text{wall}}}{P} - \int_0^H \left(1 + \frac{\gamma-1}{2}M^2\right)\frac{dT_o}{T_o}dy\right) \tag{6.55}$$

where, for most cases of interest here, viscosity can be neglected and

$$\frac{d\ln P}{dx} = \frac{1}{\beta}\left(\frac{dH}{dx} - \int_0^H \left(1 + \frac{\gamma-1}{2}M^2\right)\frac{dT_o}{T_o}dy\right) \tag{6.56}$$

The β parameter could be redefined to include the total temperature profile, but has not because that profile cannot be directly related to the one-dimensional flow, whereas the change in channel area is the same no matter what the profile.

6.2 Boundary Layer Profile in the Compound Compressible Flow

6.2.1 Laminar Profile Solution

With a formulation for compound compressible flow which will allow a solution for a profile without wall slip, the behavior of a stratified compressible flow entering a channel can be examined, such as the forebody flow on a hypersonic vehicle coming into a scramjet inlet. To do so, an assumption must be made as to the nature of the Mach number profile, and the viscous function in the wall region. The former will be input from the forebody boundary layer profile; the latter will be inferred from the expected properties of a viscous shear layer.

In Appendix A, the boundary layer profile on the forebody of a hypersonic vehicle is described using the classical solutions of the compressible laminar boundary layer. It was argued that the boundary layer will be laminar into the engine at high Mach number. The laminar profile, from the work of Cohen and Reshotko [25], will be used as an input profile to the compound compressible flow model.

The laminar boundary layer solution will be compared with the results obtained with a turbulent boundary layer profile. Because there is no simple method of handling the turbulent boundary layer growth on the forebody, boundary layer thicknesses were not calculated for the turbulent case. However, the channel flow model will be presented with a turbulent profile, corresponding to the effect of tripping the boundary layer as it enters the engine inlet.

Reviewing the work of Cohen and Reshotko outlined earlier, the boundary layer equa-

tions are solved in a transformed coordinate plane that converts the problem to an incompressible one. Solving for the Mach number in terms of the stream function, f, where $U = U_e f'(\eta)$ and the enthalpy function, S:

$$\begin{aligned} M &= \frac{U}{a} \\ &= \frac{U_e f'(\eta)}{\sqrt{\gamma RT}} \end{aligned} \tag{6.57}$$

with the similarity relationship for temperature:

$$T = T_o \left\{ (1 + S(\eta)) - \left(\frac{\frac{\gamma-1}{2} M_e^2}{1 + \frac{\gamma-1}{2} M_e^2} \right) f'^2(\eta) \right\} \tag{6.58}$$

and

$$M = \frac{U_e f'(\eta)}{\sqrt{\gamma RT_o \left\{ (1 + S(\eta)) - \left(\frac{\frac{\gamma-1}{2} M_e^2}{1 + \frac{\gamma-1}{2} M_e^2} \right) f'^2(\eta) \right\}}} \tag{6.59}$$

The free-stream Mach number is $M_e = U_e / \sqrt{\gamma RT_e}$, so equation (6.59) can be written as:

$$M = \frac{M_e f'(\eta) \sqrt{T_e / T_o}}{\sqrt{\left\{ (1 + S(\eta)) - \left(\frac{\frac{\gamma-1}{2} M_e^2}{1 + \frac{\gamma-1}{2} M_e^2} \right) f'^2(\eta) \right\}}} \tag{6.60}$$

The ratio of free stream static to total temperature, which appears in the numerator of equation (6.60) is the familiar isentropic relationship, $T_e/T_o = (1 + \frac{\gamma-1}{2} M_e^2)^{-1}$. The local Mach number at any position in the boundary layer is related to the free-stream Mach number and the functions f' and S, as

$$M = \frac{M_e f'(\eta) (1 + \frac{\gamma-1}{2} M_e^2)^{-1/2}}{\sqrt{\left\{ (1 + S(\eta)) - \left(\frac{\frac{\gamma-1}{2} M_e^2}{1 + \frac{\gamma-1}{2} M_e^2} \right) f'^2(\eta) \right\}}} \tag{6.61}$$

Inverting the square of both sides of equation (6.61):

$$\frac{1}{M^2} = \frac{(1 + \frac{\gamma-1}{2} M_e^2) \left\{ (1 + S(\eta)) - \left(\frac{\frac{\gamma-1}{2} M_e^2}{1 + \frac{\gamma-1}{2} M_e^2} \right) f'^2(\eta) \right\}}{M_e^2 f'(\eta)^2} \tag{6.62}$$

This function is integrated with respect to y in the streamtube coordinates. It will be most convenient to transform the y differential into η coordinates, and thus perform the integration in the transformed incompressible coordinate system:

$$\int_0^{y_{max}} \left(\frac{1}{M(y)^2} - 1 \right) \left\{ 1 - \overline{\tau_w'} \right\} \frac{dy}{\gamma} \rightarrow \int_0^{\eta_{max}} \left(\frac{1}{M(\eta)^2} - 1 \right) \left\{ 1 - \overline{\tau_w'} \right\} \frac{d\eta}{\gamma} \tag{6.63}$$

To transform $dy \rightarrow d\eta$:

$$\frac{\partial y}{\partial \eta} = \frac{\partial}{\partial \eta}\left(A(x)\int_0^{\eta}\frac{T(\eta)}{T_o}d\eta\right) \tag{6.64}$$

$$= A(x)\frac{T(\eta)}{T_o} \tag{6.65}$$

Normalizing to the known boundary layer thickness $\delta_{\text{b.l.}}$:

$$A(x) = \frac{\delta_{\text{b.l.}}}{\int_0^{\eta_\delta}\frac{T(\eta)}{T_o}d\eta} \tag{6.66}$$

where η_δ is the value of the transformed coordinate corresponding to the top of the boundary layer ($\simeq 3.4$ for the flat plate solution without pressure gradient). Then,

$$d\eta = \left(\frac{\int_0^{\eta_\delta}\frac{T}{T_o}d\eta}{\delta_{\text{b.l.}}\left\{(1+S(\eta)) - \left(\frac{\frac{\gamma-1}{2}M_e^2}{1+\frac{\gamma-1}{2}M_e^2}\right)f'^2(\eta)\right\}}\right)dy \tag{6.67}$$

Thus, the transformed integral expression for the inverse square of the Mach number is:

$$\int_0^H\left(\frac{1}{M^2}-1\right)\left\{1-\overline{\tau_w'}\right\}\frac{dy}{\gamma} =$$
$$\frac{1}{\gamma}\int_0^{\eta_\delta}\left(\left[\frac{(1+\frac{\gamma-1}{2}M_e^2)\left\{(1+S(\eta)) - \left(\frac{\frac{\gamma-1}{2}M_e^2}{1+\frac{\gamma-1}{2}M_e^2}\right)f'^2(\eta)\right\}}{M_e^2 f'(\eta)^2} - 1\right]\right. \tag{6.68}$$
$$\left.\times\ \frac{\delta_{\text{b.l.}}\left\{(1+S(\eta)) - \left(\frac{\frac{\gamma-1}{2}M_e^2}{1+\frac{\gamma-1}{2}M_e^2}\right)f'^2(\eta)\right\}}{\int_0^{\eta_\delta}\frac{T}{T_o}d\eta}\right)\left\{1-\overline{\tau_w'}\right\}d\eta$$

Substituting for the temperature profile in terms of f and S:

$$\int_0^H\left(\frac{1}{M^2}-1\right)\left\{1-\overline{\tau_w'}\right\}\frac{dy}{\gamma} =$$
$$\frac{1}{\gamma}\int_0^{\eta_\delta}\left(\left[\frac{(1+\frac{\gamma-1}{2}M_e^2)\left\{(1+S(\eta)) - \left(\frac{\frac{\gamma-1}{2}M_e^2}{1+\frac{\gamma-1}{2}M_e^2}\right)f'^2(\eta)\right\}}{M_e^2 f'(\eta)^2} - 1\right]\right. \tag{6.69}$$
$$\left.\times\ \frac{\delta_{\text{b.l.}}\left\{(1+S(\eta)) - \left(\frac{\frac{\gamma-1}{2}M_e^2}{1+\frac{\gamma-1}{2}M_e^2}\right)f'^2(\eta)\right\}}{\eta_\delta + \int_0^{\eta_\delta}S(\eta)d\eta - \left(\frac{\frac{\gamma-1}{2}M_e^2}{1+\frac{\gamma-1}{2}M_e^2}\right)\int_0^{\eta_\delta}f'^2(\eta)d\eta}\right)\left\{1-\overline{\tau_w'}\right\}d\eta$$

This value of β represents only the value of the boundary layer. The compound flow parameter for the free-stream flow will have to be added to this value to represent the

entire inlet flow field. This is the value of the compound flow parameter at one specific location, as the boundary layer begins to enter the channel. As the flow moves along the channel, the profile will change and new values for β must be derived.

For simplicity, the boundary layer compound flow parameter can be evaluated under the assumption that the free-stream Mach number is hypersonic ($M_e \rightarrow \infty$). Then equation (6.69) reduces to:

$$\int_0^H \left(\frac{1}{M^2} - 1\right)\left\{1 - \overline{\tau_w'}\right\}\frac{dy}{\gamma} = \frac{\delta_{\text{b.l.}}}{\gamma}\int_0^{\eta_\delta}\left(\left[\frac{\left(\frac{\gamma-1}{2}\right)\left\{(1+S(\eta)) - f'^2(\eta)\right\}}{f'(\eta)^2} - 1\right] \times \frac{\delta_{\text{b.l.}}\left\{(1+S(\eta)) - f'^2(\eta)\right\}}{\eta_\delta + \int_0^{\eta_\delta} S(\eta)d\eta - \int_0^{\eta_\delta} f'^2(\eta)d\eta}\right)\left\{1 - \overline{\tau_w'}\right\}d\eta \tag{6.70}$$

The transformed integral expression for $\beta_{\text{b.l.}}$ is independent of Mach number at high Mach number. This is at first surprising, because it would seem at cursory glance that the value of β would depend quite strongly on the free-stream Mach number. The boundary layer velocity is scaled with the free-stream velocity, so it might be suspected that an increase in free-stream Mach number would increase Mach number throughout the boundary layer by a fixed proportion, thereby decreasing the value of $1/M^2$ by the square of that proportion. However, there is another effect which must be considered. Because the boundary layer is compressible, density is sensitive to local temperature, which is in turn a function of the free-stream conditions and the local Mach number. Increasing the free-stream Mach number increases the temperature of the decelerated streamtubes with roughly the square of the Mach number, and thus decreases the density. This in turn effectively increases the area occupied by the low-speed streamtubes.

Near a hot wall, this density effect is approximately proportional to the square of the Mach number, so in the region where Mach number is small, and the inverse square of the Mach number dominates the value of the β parameter:

$$\frac{\partial\beta}{\partial y} = \left(\frac{1}{M^2} - 1\right) \simeq \frac{1}{\gamma M^2} \tag{6.71}$$

where y is the streamtube coordinate, proportional to M^2; the contribution to the value of β is therefore insensitive to Mach number.

Far from the wall, the flow density is quite insensitive to the free- stream Mach number because there is little deceleration, and thus little temperature rise over the free-stream value. Therefore, there is no density cancellation of the increasing Mach number in this region. However, the inverse of the square of the Mach number is a very small value when M is large, so that

$$\frac{\partial \beta}{\partial y} = \left(\frac{1}{M^2} - 1\right) \simeq \frac{-1}{\gamma} \tag{6.72}$$

and changes in Mach number have little effect on the value of β in this region as well. This is true in the free-stream as well. Thus, both high- and low-speed regions of the boundary layer are insensitive to Mach number at hypersonic free-stream conditions, as we found in the full analytical solution.

6.2.2 Turbulent Profile Solution

All of the above development has been for a laminar similarity profile, because that is the assumed form of the boundary layer on the forebody. It is possible, however, that the boundary layer will transition before entering the engine channel. This might occur at the base of a compression ramp, or it might be deliberately induced to enhance mixing. It is worth considering the difference between the laminar boundary layer and the turbulent one, especially for purposes of recommending the more desirable flow state.

In classical incompressible boundary layer theory, it is usually assumed that a turbulent boundary layer will be thicker than the corresponding laminar one formed under similar conditions. This generalization is no longer valid in the high-speed regime, where the laminar boundary layer thickness is greatly increased by the increasing viscosity at the characteristically high temperatures. The turbulent viscosity is not a molecular property, so much as a turbulent eddy mixing property, and can actually decrease with increasing temperature. Thus, the hypersonic turbulent boundary layer will generally be thinner than its corresponding laminar flow, especially at higher altitudes in a transatmospheric trajectory [9].

The influence of a laminar boundary layer on the compound compressible flow charac-

teristics of the entire channel flow will be much greater than a turbulent boundary layer of equal thickness because of the steeper velocity gradients in the turbulent profile. It is also known that a thicker boundary layer will have a more substantial impact on the compound compressible properties, which scale in proportion to streamtube area. Thus, if the turbulent profile is assumed to be thinner than the laminar one, an equal thickness comparison can be considered as a worst case scenario. If the turbulent boundary layer has a smaller effect than a laminar one of equal area, the actual turbulent boundary layer that would be formed under the appropriate flow conditions would have even less impact.

The calculation of the properties of a turbulent hypersonic boundary layer, like its low-speed counterpart, is made difficult by the lack of a complete theoretical understanding of this problem. There are means available for describing this boundary layer in semi-empirical form. Particularly noteworthy for their simplicity are attempts at using the known properties of turbulent incompressible boundary layers, and extrapolating to the compressible frame in exactly the same manner that the laminar boundary layer was considered, albeit without benefit of a self-consistent similarity solution.

Perry and East have presented some experimental data for flat plate turbulent boundary layer profiles at hypersonic conditions [29]. They took data in a range between Mach 8.87 and Mach 11.60, at momentum thickness Reynolds numbers between 6,630 and 16,700. Within this range, Perry and East found the turbulent boundary layer profile, normalized to the boundary layer 99 % velocity thickness, to be insensitive to Mach number and Reynolds number. They fit the boundary layer profiles to a modified law of the wall and law of the wake profile, and showed that it could be accurately described in transformed incompressible coordinates for normal distance $\overline{y}$ and velocity $\overline{u}$. Defining

$$\overline{y}^+ = \frac{\overline{y}\overline{u}_\tau}{\overline{\nu}} \tag{6.73}$$

where u_τ is the classical viscous reference velocity based on skin friction at the wall, τ_w:

$$u_\tau = \sqrt{\frac{\tau_w}{\rho}} \tag{6.74}$$

The law of the wall and law of the wake for the turbulent profile are then, following the

nomenclature of Perry and East [29]:

$$\overline{u}^+ = \overline{y}^+ \quad ;0 < \ln \overline{y}^+ < 10.64 \tag{6.75}$$

$$\overline{u}^+ = 2.43 \ln 7.5\overline{y}^+ \quad ;10.64 < \ln \overline{y}^+ \tag{6.76}$$

In transformed coordinates, the profile is approximately linear near the wall.

In fact, for the accuracy required in the calculations at hand, the distinction between transformed incompressible coordinates and real physical coordinates can be blurred in describing the profile. At the top of the boundary layer, the incompressible coordinates are nearly identical with the real coordinates because temperature is approximately the free-stream value.

Overall, the turbulent boundary layer profile can adequately be modelled in real space with a 1/7 power law above $y/\delta_{99\%} \simeq .1$, and a linear profile below that. Perry and East compared the real profile with 1/6 and 1/9 power laws, and suggested that a better fit would be the 1/6 law. The differences between a 1/6 law and a 1/7 law are not so significant in evaluating the β parameter, however.

The temperature profile is given by an empirical fit as recommended by Bertram, et al. [30]:

$$\frac{T_{\text{total}}(y) - T_{\text{wall}}}{T_{\text{total},\infty} - T_{\text{wall}}} = \left(\frac{u}{u_\infty}\right)^2 \tag{6.77}$$

where the values at ∞ are known free-stream conditions. Given the assumed form of the velocity profile, a Mach number profile can be calculated for given values of wall temperature ratio.

This turbulent profile can then be incorporated into the integral expression for the compound compressible flow parameter, as was done for the laminar boundary layer.

6.3 Incorporating the Boundary Layer with Inviscid Flow

6.3.1 Return to a Two-Streamtube Model

All of the above development has been for a boundary layer profile. In fact, the inlet flow is composed of the boundary layer region, and an inviscid region with essentially uniform properties. The influence of the inviscid region must be incorporated into the streamtube flow model, and can be done so with relative ease.

It will be convenient to include the inviscid streamtube with two goals in mind. First, it is most useful to parameterize the behavior of the entire flow by the ratio of boundary layer height to channel height. Thus, the entire channel will be considered in terms of the relative thicknesses of the boundary layer and the inviscid free-stream region. A second goal is to preserve the essential results of the simple two-stream models introduced in an earlier chapter. To this end, the boundary layer will be considered as a separate, "low-speed" streamtube [1], while the free-stream is considered as a uniform hypersonic layer. Thus, the boundary layer profile will be solved and incorporated into a single compound compressible flow representation, which will in turn be represented as a single streamtube interacting with the free-stream streamtube. The properties of the boundary layer will be summarized by comparison to a uniform streamtube. This will permit the complicated results of the laminar and turbulent profiles to be related to the fundamental behavior identified in the two- stream models presented in chapter 5.

In the compound compressible model, the effects of streamtubes on the net behavior of the entire channel flow can be added linearly, because the β parameter is a linear function of streamtube area. Thus, for the entire engine channel,

$$\beta_{\text{channel}} = \beta_{\text{boundary layer}} + \beta_{\text{free-stream}} \tag{6.78}$$

The β parameter has dimensions of area, but it is most convenient to work with a non-dimensionalized form of this parameter. If β is normalized to the entire channel height, H,

[1] "low-speed" meaning at a lower speed than the free-stream. The boundary layer may very well be mostly hypersonic

then, defining

$$\overline{\beta} = \frac{\beta}{A} \tag{6.79}$$

where β is calculated over a streamtube of area A, the normalized channel parameter is:

$$\overline{\beta}_{\text{channel}} = \frac{1}{H}\beta_{\text{boundary layer}} + \frac{1}{H}\beta_{\text{free-stream}} \tag{6.80}$$

With a boundary layer height of δ, $\overline{\beta}$ is used to write:

$$\beta_{\text{boundary layer}} = \delta\overline{\beta}_{\text{boundary layer}} \tag{6.81}$$

so that

$$\overline{\beta}_{\text{channel}} = \left(\frac{\delta}{H}\right)\overline{\beta}_{\text{boundary layer}} + \left(1 - \frac{\delta}{H}\right)\overline{\beta}_{\text{free-stream}} \tag{6.82}$$

The net channel flow can thus be parameterized in terms of the Mach number profile in the boundary layer, the free-stream uniform flow conditions, and the relative height of the boundary layer.

With a uniform free-stream,

$$\overline{\beta}_{\text{free-stream}} = \frac{1}{\gamma}\left(\frac{1}{M_e^2} - 1\right) \tag{6.83}$$

and the normalized boundary layer parameter is:

$$\overline{\beta}_{\text{boundary layer}} = \int_0^1 \left[\frac{1}{M^2} - 1\right]\left(1 - \overline{\tau_w'}\right)\frac{dy'}{\gamma} \tag{6.84}$$

where y' is the y coordinate normalized to boundary layer height.

The net Mach number, defined above in equation (6.4), provides a useful means of comparing the boundary layer profile with the two-stream model. Extending the definition to the integral form of the β parameter, $\overline{M}$ is once again defined so that

$$\frac{1}{\overline{\gamma}}\left(\frac{1}{\overline{M}^2} - 1\right) = \int_0^1 \left[\frac{1}{M^2} - 1\right]\left(1 - \overline{\tau_w'}\right)\frac{dy'}{\gamma} \tag{6.85}$$

As above, a uniform streamtube with Mach number $\overline{M}$ will have the same $\overline{\beta}$ as the nonuniform profile *at a given streamwise location*. The value of $\overline{\gamma}$ selected in defining the uniform Mach number $\overline{M}$ is an averaged representation of the variable γ through the boundary layer.

Once the value of β is known, it can be used to determine the streamwise change in free-stream Mach number, the streamwise change in the profile, and the streamwise variation in boundary layer thickness. These three factors will parameterize the entire channel flow problem, and provide direct comparison to the two-streamtube model. Solving for the streamwise change in boundary layer area:

$$\frac{d\delta}{dx} = \delta \int_0^1 \left[\frac{1}{M^2} - 1\right] \left(1 - \overline{\tau_w'}\right) \frac{d\ln P}{dx} \frac{dy'}{\gamma} \tag{6.86}$$

where the integral has been solved in a coordinate normalized to the boundary layer height. It is most convenient to use the relative thickness of boundary layer, δ/H, as the independent paramter:

$$\frac{d(\delta/H)}{dx} = \frac{1}{H}\frac{d\delta}{dx} - \frac{\delta/H}{H}\frac{dH}{dx} \tag{6.87}$$

The value of $d\ln P/dx$ in the boundary layer streamtubes is known from the β parameter across the entire channel. The explicit dependence of $d\delta/dx$ on the pressure derivative is removed by substituting with β under the inviscid approximation,

$$\frac{d(\delta/H)}{dx} = -\left[\left(\frac{\delta}{H}\right)\frac{1}{\overline{\beta}_{\text{channel}}}\int_0^1 \left[\frac{1}{M^2} - 1\right]\left(1 - \overline{\tau_w'}\right)\frac{dy'}{\gamma} - \frac{\delta}{H}\right]\frac{d\ln H}{dx} \tag{6.88}$$

$$= \left[\frac{1}{\overline{\gamma}}\left(\frac{\delta}{H}\right)\frac{1}{\overline{\beta}_{\text{channel}}}\left[\frac{1}{\overline{M}^2} - 1\right] - \frac{\delta}{H}\right]\frac{d\ln H}{dx} \tag{6.89}$$

This boundary layer parameter indicates how the relative thickness of the boundary layer changes with a change in channel area. For instance, if $\frac{d(\delta/H)}{d\ln H} = 0$, the relative thickness of the boundary layer does not change as the area of the channel changes. This is the case when the boundary layer profile is nearly uniform (i.e. $\overline{M} \simeq M_e$), and thus has little net effect on the behavior of the channel. On the other hand, when $\frac{d(\delta/H)}{d\ln H} = -\left(\frac{\delta}{H}\right)$, the boundary layer height is fixed. Regardless of the change in channel area, the boundary layer remains the same thickness; thus, all changes in the channel area are accomplished by the free-stream region. This situation is realized when $\overline{M} = 1$, so the boundary layer streamtube behaves as if it were a sonic flow. Following this trend, if $\overline{M} < 1$, the boundary layer will experience variations in thickness in the opposite sense of the changes in channel height.

It is also of interest to examine the response of Mach number for a given change in channel area, in both the free-stream and the boundary layer, as a function of the relative boundary layer thickness. The one-dimensional flow equations can be assembled in a

form that solves explicitly for Mach number. Noting that $2d\ln M/dx = d\ln M^2/dx$, the streamwise derivative of Mach number in the absence of heat addition is

$$(1-M^2)\frac{dM}{dx} = -M\left(1+\frac{\gamma-1}{2}M^2\right)\frac{d\ln A}{dx} \tag{6.90}$$

Substituting equation (6.35) for dA/A:

$$\frac{dM}{dx} = -\frac{\left(1+\frac{\gamma-1}{2}M^2\right)}{\gamma M}\frac{d\ln P}{dx} \tag{6.91}$$

Once again, the pressure derivative is related to the total channel area change through the β parameter in the inviscid approximation:

$$\frac{dM}{dx} = -\frac{\left(1+\frac{\gamma-1}{2}M^2\right)}{\gamma M}\frac{d\ln H/dx}{\overline{\beta}_{\text{channel}}} \tag{6.92}$$

This expression is valid for *any* inviscid streamtube in the channel. It is independent of the area of the specific streamtube being examined, and is related to the global properties of the channel geometry, and total channel β.

The streamwise change in free-stream Mach number due to channel area changes comes directly from equation (6.92):

$$\frac{dM_e}{dx} = -\frac{\left(1+\frac{\gamma-1}{2}M_e^2\right)}{\gamma M_e}\frac{d\ln H/dx}{\overline{\beta}_{\text{channel}}} \tag{6.93}$$

Since $\overline{\beta}_{\text{channel}}$ depends on the relative thickness of the boundary layer, as well as the boundary layer profile, dM_e/dx can in turn be parameterized in terms of the relative boundary layer thickness, δ/H. This is true no matter the form of the profile of the boundary layer, so that any profiles with the same $\overline{M}$ will produce the same acceleration or deceleration of the free-stream. Thus, the boundary layer profile will affect the free-stream in exactly the same manner as a uniform streamtube, once again demonstrating the analogy between the actual profile solution and the two-streamtube model.

6.3.2 Effects of Heat Addition

When $dT_o \neq 0$,

$$(1-M^2)\frac{dM}{dx} = -M\left(1+\frac{\gamma-1}{2}M^2\right)\left\{1-\overline{r'}\right\}\frac{dA}{dxA} + M\left(1+\frac{\gamma-1}{2}M^2\right)\left(\frac{1}{2}+\frac{\gamma}{2}M^2\right)\frac{dT_o}{dxT_o} \tag{6.94}$$

Substituting for dA/A and dT_o/T_o,

$$\frac{dM}{dx} = -\left(1+\frac{\gamma-1}{2}M^2\right)\left[\frac{\left\{1-\overline{\tau'}\right\}}{\gamma M}\frac{d\ln P}{dx}+\frac{M}{2}\frac{d\ln T_o}{dx}\right] \tag{6.95}$$

and the pressure term can be expressed as a function of the known channel area and assumed heat transfer profile:

$$\frac{d\ln P}{dx} = \frac{1}{\beta}\left(\frac{dH}{dx}-\int_0^H\left(1+\frac{\gamma-1}{2}M^2\right)\frac{d\ln T_o}{dx}dy\right) \tag{6.96}$$

assuming viscous effects are negligible. At each point, dM/dx depends on the local heat addition *and* the total heat addition.

Temperature is most easily related to the known quantity of heat addition, and the local Mach number, through the total temperature relationship:

$$T_{\text{total}}(y) = T_{\text{static}}\left(1+\frac{\gamma-1}{2}M(y)^2\right) \tag{6.97}$$

Thus, the local streamwise temperature change can be written as:

$$\frac{dT_{\text{static}}}{dx} = \left(\frac{dT_{\text{total}}}{dx}-T_{\text{static}}(\gamma-1)M(y)\frac{dM}{dx}\right)\frac{1}{\left(1+\frac{\gamma-1}{2}M(y)^2\right)} \tag{6.98}$$

Given the Mach number and total temperature streamwise variations, the streamwise static temperature variation at any point in the flow is uniquely determined. The streamwise change in the boundary layer profile Mach number requires that dM/dx be calculated at each position in the profile.

6.3.3 Deviations From Uniform Stream Model

For purposes of comparing the boundary layer inlet profile to a simple two-stream flow, a more useful parameter is the streamwise derivative of the net Mach number $\overline{M}$. This can be derived from the expression for streamwise derivative of Mach number *with* the viscous term included from the modified equation for dA/A:

$$\frac{dM}{dx} = -\frac{\left(1+\frac{\gamma-1}{2}M^2\right)}{\gamma M}\left\{1-\overline{\tau'}_w\right\}\frac{d\ln H/dx}{\overline{\beta}_{\text{channel}}} \tag{6.99}$$

From the definition of $\overline{M}$,

$$\overline{M} = \frac{1}{\sqrt{\int_0^1 \left(\frac{1}{M(y)^2} - 1\right)\left\{1 - \overline{\tau'}_w\right\} dy' + 1}} \tag{6.100}$$

where the effect of a gradient in γ has been ignored. Taking the x-derivative of $\overline{M}$:

$$\frac{d\overline{M}}{dx} = -\frac{\frac{d}{dx}\int_0^1 \left(\frac{1}{M(y)^2} - 1\right)\left\{1 - \overline{\tau'}_w\right\} dy'}{2\left(\int_0^1 \left(\frac{1}{M(y)^2} - 1\right)\left\{1 - \overline{\tau'}_w\right\} dy' + 1\right)^{3/2}} \tag{6.101}$$

The derivative of the integral in the numerator depends on the streamwise change in Mach number *and* the viscous function, $\overline{\tau'}_w$.

In order to retain an explicit dependence on Mach number, the viscous function in the above integral is written in terms of the Mach number, not the velocity. This naturally introduces errors in a nonuniform temperature environment, but it allows for the simplest solution of the derivative of the integral. With $\left\{1 - \overline{\tau'}_w\right\} \simeq M^2$ for $M < 1$ and $\left\{1 - \overline{\tau'}_w\right\} \simeq 1$ for $M \geq 1$:

$$\begin{aligned}
&\frac{d}{dx}\int_0^1 \left(\frac{1}{M(y)^2} - 1\right)\left\{1 - \overline{\tau'}_w\right\} dy' \\
&= \int_0^1 \left(\left\{1 - \overline{\tau'}_w\right\}\frac{d}{dx}\left(\frac{1}{M(y)^2}\right) - \left(\frac{1}{M(y)^2} - 1\right)\frac{d\overline{\tau'}_w}{dx}\right) dy' && (6.102)\\
&= -2\int_0^1 \left\{1 - \overline{\tau'}_w\right\}\frac{dM/dx}{M^3} - M\left(\frac{1}{M(y)^2} - 1\right)\frac{dM}{dx}\Big|^{M<1} dy' && (6.103)\\
&= -2\int_0^1 \left(\left\{1 - \overline{\tau'}_w\right\} - M^2\overline{\tau'}_w\right)\frac{dM/dx}{M^3} dy' && (6.104)\\
&= -2\int_0^1 \left\{1 - \overline{\tau'}_w\right\}^2 \frac{dM/dx}{M^3} dy' && (6.105)
\end{aligned}$$

The viscous function $\overline{\tau'}_w$ has not been replaced completely by the Mach number assumption because it goes to zero above $M = 1$.

Substituting equation (6.91)for dM/dx:

$$\frac{d}{dx}\int_0^1 \left(\frac{1}{M(y)^2} - 1\right)\left\{1 - \overline{\tau'}_w\right\} dy' = 2\int_0^1 \frac{\left(1 + \frac{\gamma-1}{2}M^2\right)}{\gamma M^4}\left\{1 - \overline{\tau'}_w\right\}^3 dy' \frac{d\ln P}{dx} \tag{6.106}$$

Thus, the streamwise derivative of the net Mach number is

$$\frac{d\overline{M}}{dx} \doteq -\frac{\int_0^1 \frac{(1+\frac{\gamma-1}{2}M^2)}{\gamma M^4}\left\{1-\overline{\tau'}_w\right\}^3 dy'}{\left(\int_0^1\left(\frac{1}{M(y)^2}-1\right)\left\{1-\overline{\tau'}_w\right\}dy'+1\right)^{3/2}}\frac{1}{\overline{\beta}_{\text{channel}}}\frac{d\ln H}{dx} \tag{6.107}$$

The streamwise derivative of the $\overline{M}$ will *not* in general be equal to the value obtained for a uniform stream.

The value of $d\overline{M}/dx$ scales with $1/M^4$ at small Mach number. This factor can drive the value of $d\overline{M}/dx$ to very different value than that for an actual uniform streamtube. As a profile encounters a pressure gradient, the low speed streamtubes an either accelerate or decelerate more readily than the high-speed ones. Since these streamtubes have a dominant influence on the uniform Mach number, especially when free-stream Mach number is not too large (i.e. $M < 5$), the effect of a pressure gradient on the uniform Mach number can be far more dramatic than for an actual constant-Mach number streamtube.

At larger Mach numbers, the derivative of the uniform Mach number is typically smaller than the value obtained for an idealized uniform stream. This is consistent with the observation that $\overline{M}$ tends to be independent of free-stream Mach number in hypersonic conditions, which was explained with the effect of increasing Mach number on the near-wall density profile.

Accordingly, in updating the boundary layer profile, the evolution of the streamtube positions must be traced. Each streamtube will experience a different area change in response to the change in channel area, and this will tend to distort the original inlet profile.

6.3.4 Following Streamtubes Through a Channel

The y coordinate used in the above formulations is the position of each streamtube that is being iterated over, and is not fixed in absolute coordinates. The streamtube coordinates are superposed over a fixed coordinate system, designated here by Y, in which $dY/dx = 0$, but $dy/dx \neq 0$.

The increase in height of each streamtube is equal to the change in area of the streamtube

extending from the the wall to the particular height being examined. From equation (6.35):

$$\frac{dy}{dx} = \int_0^Y \left(\left[\frac{1}{M^2} - 1 \right] \left(1 - \overline{\tau_w'} \right) \frac{d \ln P}{dx} \frac{1}{\gamma} - \overline{\tau_w'} \frac{d \ln P}{dx} \right) dy \tag{6.108}$$

in exactly the same manner as equation (C.11) was derived for inviscid flow. Substituting once more for $d \ln P/dx$,

$$\frac{dy}{dx} = \frac{1}{\overline{\beta}_{\text{channel}}} \frac{d \ln H}{dx} \int_0^Y \left(\left[\frac{1}{M^2} - 1 \right] \left(1 - \overline{\tau_w'} \right) \frac{1}{\gamma} - \overline{\tau_w'} \right) dy \tag{6.109}$$

From this equation, the profile can be properly advanced through the channel. At each y location, the new y coordinate for the streamtube being examined is calculated, so that at the next channel position, the profile can be mapped into its new configuration.

With expressions for β, $d(\delta/H)/dx$, dM_e/dx, and $d\overline{M}/dx$, the multistream model of hypersonic engine channel flow is complete. There is much information to be gained by simply applying these parameters at a given station in the channel, for instance at the channel inlet. However, for a complete picture of the channel flow, an iteration procedure can be used to follow the progress of the initial nonuniformity through the engine. The nearly one- dimensional approach, follows a methodology which is essentially identical to that developed for the two-streamtube system. The solution steps are:

1. Take an assumed engine profile (dH/dx), usually based on uniform flow conditions.
2. Start with inlet profile, free-stream conditions, and relative boundary layer height as inputs.
3. Determine $\overline{\beta}$ and $\overline{M}$ for the boundary layer from the assumed form of the boundary layer profile
4. Calculate $\overline{\beta}$ for the free-stream.
5. Calculate $\overline{\beta}$ for the entire channel from these component values.
6. The net Mach number, $\overline{M}$ can be computed to provide for a comparison with the two-stream flow model.
7. Calculate the change in position of each streamtube in the flow profile, dy/dx, and use this to update the boundary layer height at the next streamwise location.

8. Calculate the streamwise derivative of free-stream Mach number, dM_e/dx, and use this to update the Mach number at the next streamwise station. This also allows the updating of thermodynamic properties, which depend only on local Mach number, γ, and initial values.

9. Apply the same technique to calculate $dM(y)/dx$ at each point in the boundary layer profile, and update Mach number and thus thermodynamic properties at the next streamwise station.

10. With the new profile and free-stream conditions, begin the process again, iterating to the next streamwise location, beginning at step 3 above.

The relationship between channel area and streamwise pressure gradient can be modified to include changes in total temperature:

$$\frac{dy}{dx} = \frac{d\ln P}{dx}\int_0^Y \left(\left[\frac{1}{M^2}-1\right]\left(1-\overline{\tau_w'}\right)\frac{1}{\gamma}-\overline{\tau_w'}\right)dy + \int_0^Y \left(1+\frac{\gamma-1}{2}M^2\right)\frac{d\ln T_o}{dx}dy \quad (6.110)$$

The y coordinate of each streamtube is transformed from station 1 to station 2 as:

$$\frac{dy_2}{dy_1} = \frac{d\ln P}{dx}\left(\left[\frac{1}{M^2}-1\right]\left(1-\overline{\tau_w'}\right)\frac{1}{\gamma}-\overline{\tau_w'}\right) + \left(1+\frac{\gamma-1}{2}M^2\right)\frac{d\ln T_o}{dx} \quad (6.111)$$

where, as before, the channel pressure derivative is

$$\frac{d\ln P}{dx} = \frac{1}{\beta}\left(\frac{dH}{dx} - \int_0^H \left(1+\frac{\gamma-1}{2}M^2\right)\frac{d\ln T_o}{dx}dy\right) \quad (6.112)$$

At high Mach numbers, the total temperature is quite high, and heat addition in the channel will represent a small change in that value. For instance, at Mach 20 and static temperature of 300 K in the external flow, the total temperature of the flow inside the engine is 13,000 K, corrected for an average combustor $C_p \simeq 1600$ J/Kg K (C_p is so high due to dissociation [6]). The reaction of hydrogen with air generates approximately 10^8 J/kg. The stoichiometric ratio of hydrogen to air is $4/139 = .029$, taking into account that air is only 21 % oxygen. Thus, the hydrogen reaction is generating about 2.9×10^6 J/kg air. With an average heat capacity of 1600 J/kg-K [6], the increase in total temperature due to the hydrogen reaction is approximately 1800 K, or roughly $13\frac{1}{2}$ % of the total temperature over the entire engine channel length. Over a 5 meter long engine, if heat addition were uniform

(which it won't be), $d\ln T_o/dx \simeq .028$ per meter. One result of this is that the increment in exhaust velocity for a hypersonic engine over the inlet velocity is typically a small fraction of the flight velocity.

6.4 Selecting the Correct Boundary Layer Profile

6.4.1 Applicability of the Similarity Profiles in a Pressure Gradient

The forebody has been solved with a flat plate formulation, which assumes there are no streamwise pressure gradients. In fact, there will be some streamwise gradients due to shock curvature, but it can be shown that these have negligible effect on the boundary layer development [31]. However, once the profile enters the engine channel, it will be subject to pressure gradients. It is important to consider the impact of a pressure gradient on the boundary layer growth, and to examine how to correctly apply the zero-pressure gradient solution as an input to the engine channel flow.

The similarity solutions are defined in terms of an exponential velocity function, and characterized by the power of the exponent. This exponent is in turn used to establish the magnitude of the pressure gradient from the 1-d momentum equation applied to the free-stream region.

The velocity function is assumed to have the form:

$$U = U_e \xi^m \tag{6.113}$$

where ξ is the streamwise coordinate in transformed incompressible coordinates. In classical laminar boundary layer theory [32] the pressure gradient is defined by its effect on the free-stream velocity or Mach number with a value β (not to be confused with the compound compressible flow β) given by

$$\begin{aligned} \beta &= \frac{2m}{m+1} \\ &= \frac{2\xi}{M_e}\frac{dM_e}{d\xi} \end{aligned} \tag{6.114}$$

Once inside the engine channel, the flat plate boundary layer that was originally formed without a streamwise pressure gradient will experience a pressure gradient. The boundary layer will therefore behave in some range between that of the flat plate boundary layer, and an equilibrium solution for a boundary layer with given pressure gradient.

In solving for the behavior of a stagnation flow, Lees [26] assumed that the boundary layer at each point could be characterized by its local pressure gradient. His assumption was therefore that the boundary layer approached the equilibrium similarity solution at each station along the surface. However, in the stagnation flow solution, the boundary layer is always being examined at a position near its starting point. In the problem at hand, the boundary layer has formed over a very long path length, and then is subject to pressure variations over a comparatively small path inside the engine. It is most likely that the flow profile will retain its initial profile, and not approach the equilibrium similarity profile under the influence of the new pressure gradient.

The justification for this view of the profile's response to pressure changes is the time required for viscous effects to diffuse from the wall. This channel flow problem is similar to the classical starting problem of Rayleigh; a change in channel area perturbs the core velocity, which looks like an impulsive velocity increment at the wall. The no-slip condition is enforced at the wall, and the incremental vorticity generated at the wall diffuses into the flow at some characteristic diffusion rate. The wall-generated diffusion on the forebody crosses a distance equal to the boundary layer thickness, by definition. Thus, at the free-stream velocity of the forebody flow, it requires the entire path length of the forebody wall for viscous effects to diffuse into the flow one boundary layer thickness. Inside the engine, Mach number is reduced from the free-stream value, but most of that reduction is realized through an increase in temperature, not a decrease in velocity [6].

It is the engine channel length scale, in comparison to the forebody length, that determines the depth of penetration of viscous effects. A transatmospheric vehicle forebody will be between 20 and 30 meters in length; the characteristic length scale inside the combustor will be at most a few meters. It is therefore reasonable to assume that the boundary layer does not approach the equilibrium similarity solution, and the flat plate input conditions

can be used throughout, with a modification to allow for viscous cancellation of the streamwise pressure gradient at the wall. The flat plate boundary layer assumption makes the prediction of separation quite difficult.

6.4.2 Satisfying Shear Constraints at the Wall

The use of the flat plate boundary layer profile introduces a contradiction into the assumed multistream solution. The flat plate solution has no wall shear gradient to fight a pressure gradient, since there is no pressure gradient. However, that same profile must fight a pressure gradient inside the engine channel, and that means it must have shear at the wall. This means that the pressure changes experienced in the channel must change the form of the velocity profile, so the flat plate profile is no longer valid. However, if the viscous penetration depth into the flow is small, the profile remains valid with the addition of a shear component *at the wall.* The shear component is a second derivative of velocity, so the addition of this term will not appreciably alter the velocity profile itself, as long as this penetration region is close to the wall. This shear function is the $\overline{\tau'_w}$ term that was added to the compound compressible flow β parameter in order to retain the no-slip condition at the wall.

In the flat plate solution, velocity scales nearly linearly with the transformed incompressible coordinate η at the wall, so that

$$\left\{1 - \overline{\tau'_w}\right\} = \left(\frac{\eta}{\eta_{\text{penetration}}}\right)^2 \tag{6.115}$$

The exponential power should be 2 as a minimum, but it has been found that the value of the compound compressible parameter is insensitive to this power so long as it is sufficient to cancel the inverse square of the velocity. In chapter 3, it was shown that the value of $1/M^2$ is large only very close to the wall. As long as that region is adequately cancelled, the form of the function has relatively little consequence for the rest of the boundary layer profile.

It is most desirable, however, to determine a penetration height that is independent of the history of the flow, which can be evaluated at any given position along the channel

from the local conditions. Since pressure changes in the engine channel will be transmitted upstream only through the subsonic portion of the boundary layer, the *sonic line* of the local velocity profile will be selected as the viscous penetration height:

$$\left\{1 - \overline{\tau_w^i}\right\} = \left(\frac{\eta}{\eta_{sonic}}\right)^2 \tag{6.116}$$

This makes the formulation of the viscous compound compressible flow problem straightforward; the local profile is scanned, the sonic point is located, and from this, the viscous function is determined, and used in evaluating the compound compressible flow parameter. This confines viscous effects to a region very close to the wall in the hypersonic boundary layer, which corresponds to the assumption made above that the boundary layer flow is primarily inviscid inside the engine, except in the region very near the wall where pressure effects must be cancelled.

The viscous function can be defined in both real physical coordinates, or in the transformed incompressible coordinates used in solving the laminar boundary layer. The transformation between y and η coordinates is approximately linear for small values of y. As such, the distinction is not an important one, especially when referenced to the height of the sonic line, which is a physical condition independent of the coordinate frame.

The chosen form of the viscous function introduces two difficulties in solving the problem at hand. A practical problem mentioned above comes at free-stream Mach numbers close to unity, where the sonic point can be very high in the boundary layer profile and selection of the sonic point as a viscous penetration height implies that wall effects extend instantly across the boundary layer. For hypersonic free-stream conditions, it is most important that the wall pressure gradient be cancelled out. Once that is done, the net effect of the low speed region of the boundary layer profile is rather small, because that represents a very small portion of the total boundary layer. Thus, as long as the wall is handled satisfactorily, the exact form of the viscous function, and the assumed extent of viscous effects, are relatively unimportant.

A contradiction arises in the assumption of upstream information propagation through the subsonic portion of the boundary layer. In its simplest form, the multi-streamtube model

assumes constant pressure across the channel, which in turn constrains the propagation of information in subsonic regions when the flow is compound supersonic. This assumption leads to the condition of compound choking and compound supersonic flow, in which no information can propagate upstream. Even though the subsonic layers could transport information against the flow velocity, they are constrained from doing so by the supersonic streamtubes. In fact, on the small scale, there will be upstream information propagation through the subsonic layer, as in shock-boundary layer interactions [33], which cannot be accounted for correctly in this model.

In selecting a viscous penetration height based on sonic conditions, the assumption of pressure coupling is being violated. It is unreasonable to assume the channel flow will be completely coupled, as originally conceived. For instance, in the vicinity of a sudden pressure, such as at the combustor inlet, or across the shock, it is clear that the presence of the pressure gradient will be transmitted upstream through the boundary layer, as has been experimentally observed in shock-induced boundary layer separation [33]. The pressure matching condition must be taken as a generalization and a simplification which can be applied globally, but not locally.

The above formulation for the compound compressible β parameter is solved for each streamwise location. Once β is known, its value is used to evaluate the response of the profile to a known change in channel area, which allows for the calculation of a new profile. In general, it is most useful to translate the similarity solution into physical coordinates for purposes of such an iteration, especially if it is of interest to track the evolution of the initial profile. The similarity solution derived above is only useful at the inlet to the scramjet channel; once the profile is changed in the channel, it is most effective to operate in the physical coordinate domain. In subsequent chapters, the results of tracing such a profile through a model channel will be explored.

Chapter 7

Analysis of Profile Changes Through a Shock and Separation

7.1 Analytical Shock Solution with Profile

7.1.1 Inclusion of Inlet Shock

In the previous chapter, it was assumed that the forebody profile enters the engine channel unchanged, and then experiences changes due to channel contraction or expansion, and heat addition. This assumption will only be valid if the channel flow is entirely isentropic, or if the channel itself is mounted in parallel with the forebody surface. An isentropic channel may require too much turning to decelerate the flow to desired engine Mach numbers, and an angled engine will experience strong shocks, and thus drag, an its outer surface.

In many scramjet scenarios, the inlet flow will pass through a shock as it enters the scramjet channel, to turn it parallel to the direction of vehicle motion. In such a case, it can no longer be assumed that the inlet profile to the engine is the equilibrium boundary layer solution from the forebody. Rather, the profile will be the result of passing an equilibrium profile through a shock, and may acquire a strong normal pressure gradient. This is pictured in Figure 7.1.

To model the effect of shock passage on a profile, a streamtube approach is once again taken. For a given wedge angle, the shock angle in each supersonic streamtube can be calculated from oblique shock theory. Then, the Mach number in each streamtube is easily determined. Because the shock strength will vary through the profile, the pressure ratio will also vary. To preserve the one-dimensional model, the streamtube densities and Mach

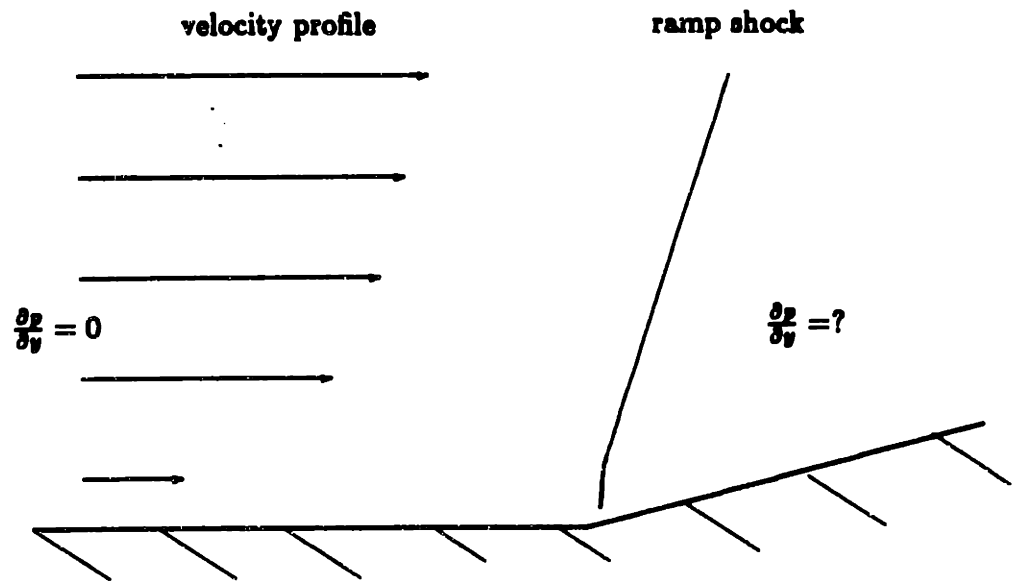

Figure 7.1: Velocity profile encountering a shock

numbers must be adjusted to re-equilibrate channel pressure, an assumption which will be valid some distance from the shock.

7.1.2 Application of Shock Relations to the Profile

One of the primary difficulties in solving for the effect of the shock on a profile is the lack of a closed form solution for the shock angle as a function of wedge angle. The well-known relationship between shock angle β_{shock} and wedge angle θ was used previously to calculate the "fixed shock" position, and is repeated below for convenience:

$$\tan\theta = 2\cot\beta_{\text{shock}}\left[\frac{M_1^2\sin^2\beta_{\text{shock}} - 1}{M_1^2(\gamma + \cos\beta_{\text{shock}}) + 2}\right] \tag{7.1}$$

This shock angle β_{shock} should not be confused with the compound compressible flow parameter or the boundary layer pressure gradient parameter.

In certain situations, this shock angle relation can be reduced to a closed form solution with simplifying assumptions. For instance, if both θ and β_{shock} are small, equation (7.1) can be solved in closed form. Unfortunately, we can make no such simplifying assumptions for this profile shock. The small angle assumption would be valid in the high-speed regions of the profile, where strong shocks must be avoided. However, at the low-speed regions

of the profile, such as the streamtubes close to the wall, the Mach number becomes low supersonic, approaching $M = 1$ at the sonic point. In the low speed flow, a small angle approximation for β_{shock} is no longer valid because small wedge angles produce shocks with large angles at small Mach numbers.

Without available simplifying assumptions, the shock angle relation must be solved for each Mach number with a root finder. Because of this, the behavior of the profile through the shock cannot be determined with an explicit closed form result for general profile shapes. Equation (7.1) is used to calculate the appropriate shock angle at each position in the profile.

Once the shock angle β_{shock} is calculated from the wedge angle θ at upstream Mach number M_1, the downstream Mach number M_2 is found simply from [5]:

$$M_2 = \frac{1}{\sin(\beta_{\text{shock}} - \theta)} \sqrt{\frac{M_1^2 \sin^2 \beta_{\text{shock}} + \left[\frac{2}{\gamma-1}\right]}{\left[\frac{2\gamma}{\gamma-1}\right] M_1^2 \sin^2 \beta_{\text{shock}} - 1}} \tag{7.2}$$

The ratio of downstream density ρ_2 to upstream density ρ_1 across the shock is also uniquely determined by the familiar shock relations:

$$\rho_2 = \rho_1 \left(\frac{[\gamma+1] M_1^2 \sin^2 \beta_{\text{shock}}}{[\gamma-1] M_1^2 \sin^2 \beta_{\text{shock}} + 2} \right) \tag{7.3}$$

The downstream pressure p_2 is related to the upstream pressure p_1:

$$p_2 = p_1 \left(1 + \frac{2\gamma}{\gamma+1} \left[M_1^2 \sin^2 \beta_{\text{shock}} - 1 \right] \right) \tag{7.4}$$

From the pressure and density, the temperature across the shock can be found with the equation of state.

It has thus far been assumed that the $\partial p/\partial y = 0$ across the channel. The shock will introduce a normal pressure gradient. Below Mach 1, there is no shock, so the downstream pressure equals the upstream pressure. On the other hand, if the free-stream Mach number is hypersonic, the shock angle will be very close to the wedge angle, so for a 5 degree wedge angle, at $\gamma = 1.3$, the upstream to downstream pressure ratio is $1 + .0086\ M_0^2$. At free-stream Mach number 10, this ratio is 1.86; for Mach number 20, the ratio is 4.44. Thus, the pressure behind the shock in the free-stream region may be up to 4 times greater than the

pressure at the base of the profile, clearly a substantial gradient that must be accounted for. Equation (7.4) demonstrates that, once the profile has passed through the shock, the pressure matching condition is no longer valid.

There are three ways of handling this pressure gradient. It can be neglected, assuming that the gradient will be small because the shock angle is small. Another option would be to carry the gradient through the channel by modifying the pressure matching relationship to include a pressure gradient. Finally, the pressure can be re-equilibrated downstream of the shock, adjusting the Mach numbers and thicknesses of the flow streamtubes until $\partial p/\partial y = 0$ and the pressure matching condition can once more be applied. The proper choice from among these options will depend on the strength of the gradient and the length scale over equilibration will occur. Appendix D will present a means of estimating the magnitude of the pressure gradient through a shock at small wedge angle.

7.2 Pressure Re-equilibration Behind the Shock

7.2.1 Estimating the Re-equilibration Length Scale

The one-dimensional model does not provide a mechanism by which the shock-induced gradient can re-equilibrate because it does not include the normal momentum flux across the channel. Further, there is no streamwise scale in the one-dimensional model. Because viscosity is included merely to cancel the pressure gradient at the wall to provide for a no-slip condition, there is no explicit appearance of pathlength-dependent terms. The only channel geometry that appears is the change in area, but, so long as that area change is referenced to some initial value, it does not matter how long the channel length is over which that change is occurring.

An external mechanism must be invoked to estimate the pressure equilibration length scale. The simplest view of the channel flow is to assume that the pressure gradient across the boundary layer will be removed through the action of a pressure wave travelling normal to the flow direction. It is reasonable to assume that, after a pass of such a compression

wave, and its associated reflected wave, the cross-wise pressure gradient will disappear. The streamwise length scale over which this will occur is therefore approximately equal to the distance travelled along the channel in the time it takes a compression wave to cross the boundary layer width δ at the sonic speed, $t_{cross} = \delta/a$:

$$x_{equilibration} \simeq u \; t_{cross} \tag{7.5}$$

so the ratio of the equilibration length scale to the boundary layer height is approximately equal to the Mach number inside the channel:

$$\frac{x_{equilibration}}{\delta} \simeq M \tag{7.6}$$

Thus, the equilibration length scale depends on both the channel Mach number, and the boundary layer width.

Estimates of the required channel width due to fuel injection [9] suggest that engine will be about two orders of magnitude longer than it is wide at the combustor. For moderate engine Mach numbers, the pressure gradient imposed by the shock will dissipate very rapidly through the channel. The shock/boundary layer interaction scenario associated with an oblique shock penetrating a boundary layer has been shown empirically to dissipate on a length scale that is on the order of the boundary layer thickness for lower Mach numbers (<3) [33].

Accordingly, it is assumed that the shock-induced pressure gradient dissipates very rapidly in the channel. The flow will therefore be modelled as an incoming profile crossing the shock, developing a pressure gradient, which then is removed by a re-equilibration process that adjusts the position of the streamtubes the Mach number, and the thermodynamic properties, in a constant area section without heat addition. The re-equilibrated profile will then be followed down the engine channel. The re-equilibration process will not return the flow profile to its pre-shock condition, because the shock crossing is an entropic process, while the re-equilibration is assumed to occur isentropically. Thus, the entire history of the flow between the upstream of the shock to the re-equilibrated station must be followed in order to account for the shock's effect on the profile.

7.2.2 Pressure Re-equilibration Mechanism

A primary effect of the boundary layer in the re-equilibration process will be to decreases the pressure in the free-stream region and the pressure in the boundary layer because the boundary layer is a compressible region which allows the free-stream to expand and assume a lower pressure. Since the boundary layer is being compressed, an inlet shock tends to reduce the importance of the boundary layer.

The pressure equilibration process is incorporated into the the one-dimensional flow equations by adjusting the pressure in each streamtube until all pressures are equal. This process must be solved iteratively, since it is not possible to calculate the final equilibrium pressure directly.

A result of one-dimensional analysis is that the stream area, referenced to some initial or sonic area, is a unique function of local Mach number and γ [34]. The streamtube pressure can be related to local Mach number and γ, so the area can be related to local pressure.

There is no mechanism to drive the one-dimensional solution to constant pressure on its own accord because the streamtubes do not interact viscously, except near the wall. The actual channel will depart from the one-dimensional behavior with a pressure gradient. Once a strong gradient is established, cross flow will become important, until the gradient is relieved. This flow can be modelled as a thickening or thinning of the one-dimensional streamtubes with reasonable accuracy. For instance, the flow in a high pressure streamtube will develop a cross-wise velocity component under the influence of the normal pressure gradient. This streamtube flow will therefore move away from the streamtube center, which will resemble the thickening of that streamtube. Similarly, a low-pressure streamtube, say near the wall, will see a net flow into towards its center, thus resembling a thinning. In order to force this behavior in the 1-d model, the uniform pressure condition must be imposed as a downstream condition. The process could alternately be modelled as mass exchange between fixed streamtubes, but that would be more difficult. Centrifugation due to streamtube turning is ignored.

The inviscid one-dimensional area relationship is [34]:

$$\frac{A}{A^*} = \frac{1}{M}\left[\frac{2}{\gamma+1}\left(1+\frac{\gamma-1}{2}M^2\right)\right]^{\frac{\gamma+1}{2(\gamma-1)}} \tag{7.7}$$

where the reference area, A^* is the area at sonic conditions, $M = 1$. From this expression, two stations in a streamtube are related in terms of their local Mach numbers, assuming γ is the same at both stations, by dividing the result of equation (7.7) at station 2, with area A_2 by the result at station 1, with area A_1, since A^* is the same at both stations:

$$\frac{A_2}{A_1} = \frac{M_1}{M_2}\left(\frac{1+\frac{\gamma-1}{2}M_2^2}{1+\frac{\gamma-1}{2}M_1^2}\right)^{\frac{\gamma+1}{2(\gamma-1)}} \tag{7.8}$$

Pressure is related to local Mach number via the familiar isentropic flow relationship for static pressure and total pressure, p_t, so the ratio of static pressure at station 2 to static pressure at station 1 is, with constant total pressure:

$$\frac{p_2}{p_1} = \left(\frac{1+\frac{\gamma-1}{2}M_1^2}{1+\frac{\gamma-1}{2}M_2^2}\right)^{\frac{\gamma}{\gamma-1}} \tag{7.9}$$

Therefore, the area relationship can be written in terms of pressure by rewriting this equation as

$$\left(\frac{1+\frac{\gamma-1}{2}M_1^2}{1+\frac{\gamma-1}{2}M_2^2}\right)^{\frac{\gamma+1}{2(\gamma-1)}} = \left(\frac{p_1}{p_2}\right)^{\frac{\gamma+1}{2\gamma}} \tag{7.10}$$

so that

$$\frac{A_2}{A_1} = \frac{M_1}{M_2}\left(\frac{p_1}{p_2}\right)^{\frac{\gamma+1}{2\gamma}} \tag{7.11}$$

The dependence on the downstream Mach number, M_2, can be removed, and the known profile of M_1 used in the solution. From equation (7.9):

$$1+\frac{\gamma-1}{2}M_1^2 = \left(\frac{p_2}{p_1}\right)^{\frac{\gamma-1}{\gamma}}\left(1+\frac{\gamma-1}{2}M_2^2\right) \tag{7.12}$$

Dividing through by M_1^2,

$$\frac{1}{M_1^2}+\frac{\gamma-1}{2} = \left(\frac{p_2}{p_1}\right)^{\frac{\gamma-1}{\gamma}}\left(\frac{1}{M_1^2}+\frac{\gamma-1}{2}\left[\frac{M_2}{M_1}\right]^2\right) \tag{7.13}$$

The area ratio depends on M_1/M_2; solving for this ratio in terms of pressure and initial Mach number:

$$\frac{M_1}{M_2} = \frac{1}{\sqrt{\left\{\left(\frac{p_1(y)}{p_2}\right)^{\frac{\gamma-1}{\gamma}}-1\right\}\frac{2}{(\gamma-1)M_1(y)^2}+\left(\frac{p_1(y)}{p_2}\right)^{\frac{\gamma-1}{\gamma}}}} \tag{7.14}$$

where p_1 has been written as a function of y to emphasize the fact that it is nonuniform, as opposed the the pressure at station 2, p_2, which is assumed to be uniform.

Inserting this relationship back into the area ratio expression,

$$\frac{A_2}{A_1} = \frac{\left(\frac{p_1(y)}{p_2}\right)^{\frac{\gamma+1}{2\gamma}}}{\sqrt{\left\{\left(\frac{p_1(y)}{p_2}\right)^{\frac{\gamma-1}{\gamma}} - 1\right\}\frac{2}{(\gamma-1)M_1(y)^2} + \left(\frac{p_1(y)}{p_2}\right)^{\frac{\gamma-1}{\gamma}}}} \tag{7.15}$$

In the following, station 1 will represent the profile directly behind the shock; station 2 will be the re-equilibrated region further downstream. The Mach number profile and pressure profile at station 1 are known from the calculated change in the initial profile across the shock. The only unknown in equation (7.15) is the final uniform pressure, p_2, which cannot be calculated directly.

The area ratio can be used to transform the profile geometry by converting the streamtube are to a differential element. If y_1 is the *streamtube* coordinate at station 1, and y_2 is the coordinate at the uniform station 2, the transformation law is, from equation (7.15):

$$\frac{dy_2}{dy_1} = \frac{\left(\frac{p_1(y)}{p_2}\right)^{\frac{\gamma+1}{2\gamma}}}{\sqrt{\left\{\left(\frac{p_1(y)}{p_2}\right)^{\frac{\gamma-1}{\gamma}} - 1\right\}\frac{2}{(\gamma-1)M_1(y)^2} + \left(\frac{p_1(y)}{p_2}\right)^{\frac{\gamma-1}{\gamma}}}} \tag{7.16}$$

The coordinate of the streamtube at station 2 which began at y_1, imbedded in fixed coordinate system Y, is then:

$$y_2(Y) = \int_0^{y_1} \frac{\left(\frac{p_1(y)}{p_2}\right)^{\frac{\gamma+1}{2\gamma}}}{\sqrt{\left\{\left(\frac{p_1(y)}{p_2}\right)^{\frac{\gamma-1}{\gamma}} - 1\right\}\frac{2}{(\gamma-1)M_1(y)^2} + \left(\frac{p_1(y)}{p_2}\right)^{\frac{\gamma-1}{\gamma}}}} dy \tag{7.17}$$

For simplicity of solution, the channel is assumed to have constant area between stations 1 and 2; the uniform pressure at station 2 is then the value which will satisfy the transformation:

$$H = \int_0^{H} \frac{\left(\frac{p_1(y)}{p_2}\right)^{\frac{\gamma+1}{2\gamma}}}{\sqrt{\left\{\left(\frac{p_1(y)}{p_2}\right)^{\frac{\gamma-1}{\gamma}} - 1\right\}\frac{2}{(\gamma-1)M_1(y)^2} + \left(\frac{p_1(y)}{p_2}\right)^{\frac{\gamma-1}{\gamma}}}} dy \tag{7.18}$$

In the hypersonic limit, the transformation expression becomes:

$$H = \int_0^H \left(\frac{p_1(y)}{p_2}\right)^{\frac{1}{\gamma}} dy \tag{7.19}$$

This is the familiar isentropic, adiabatic relationship between pressure and density, $P/\rho^\gamma =$ constant, and reflects that fact that, at high Mach number, changes in channel area tend to affect thermodynamic properties, but do not tend to change the flow velocity.

With the hypersonic assumption, the uniform pressure is:

$$p_2 \simeq \left(\frac{1}{H}\int_0^H p_1(y)^{1/\gamma} dy\right)^\gamma \tag{7.20}$$

which provides a reasonable first guess of the uniform pressure because the flow is predominantly hypersonic.

The low Mach number limit is incompatible with this inviscid assumption, however. In the $\lim_{M\to 0}$, the $1/M_1^2$ term in the pressure integral approaches ∞. This term multiples what will generally be a negative value under the square root of equation (7.18), and that in turn drives the entire expression under the square root to a negative value in the small Mach number limit. This is clearly a non-physical result, and it is once again due to the neglect of viscosity in the wall region.

In previous sections, viscosity was added with a functional dependence on height above the wall. In that case, however, the flow was pressure-equilibrated, and the viscous formulation could be added in the integral form with relative ease because pressure was constant across the channel. With a pressure gradient, the streamwise gradient cannot be removed from an integral formulation.

The simplest way to satisfy the wall condition is to use the *viscous*, constant area one-dimensional flow solution. In the absence of heat addition, and with no increase in area, the change in Mach number for a given change in pressure can be solved with viscous forces. It is assumed that the low-speed streamtubes do not change area much because viscous forces tend to counteract the area-changing effect of pressure gradient. This is a stronger requirement than that used in earlier sections, where viscosity varied throughout

the subsonic region, because now the entire subsonic region is viewed as being viscous-dominated.

7.2.3 Separation with Adverse Streamwise Pressure Gradient

In the inviscid flow, a streamtube can be accelerated to zero pressure, but there is a finite limit to the maximum pressure to which it can be decelerated. Not surprisingly, this maximum pressure is the local total pressure. It is quite likely the the so-called equilibrium pressure may be higher than the total pressure for a given streamtube, which means that the inviscid channel flow cannot reach that equilibrium pressure. The streamtubes with total pressure below the equilibrium value that the channel is moving towards cannot satisfy that equilibrium condition in the inviscid solution because the total pressure represents the maximum pressure that can be derived from an isentropic flow without doing work on it. This suggests that they can only reach the equilibrium pressure through some viscous interactions.

With the assumption of a lower inviscid limit, the problem is solved in closed form. With a separate, total pressure-deficient viscous layer, the lower limit of the integral in equation (7.18) should be the height of the viscous streamtube at the wall, $y_{viscous}$, not 0, since the area of the viscous stream does not change.

There are two limits of behavior for modelling the wall region, where total pressure is insufficient for reaching the equilibrium condition. In the first limit, viscous interactions between the low- and high-speed streamtubes would accelerate the low speed tubes, and increase the total pressure near the wall, while decreasing the total pressure of the inviscid flow. This is a convenient assumption, because it yields to relatively simple solution based on one-dimensional flow with friction.

For one-dimensional constant area flow, the pressure relationship is [5]:

$$\frac{p_2}{p_1} = \frac{M_1}{M_2}\sqrt{\frac{1+\frac{\gamma-1}{2}M_1^2}{1+\frac{\gamma-1}{2}M_2^2}} \qquad (7.21)$$

Unlike the inviscid one-dimensional equation, this cannot be solved explicitly for M_2 in terms of the pressure ratio and M_1. The final value of the equilibrated pressure is determined entirely by the inviscid region of the flow; with no area change, the viscous region has no direct effect on the transformation of free-stream properties between stations 1 and 2. Once the upstream pressure is determined from the inviscid solution, the Mach number at the wall region can be corrected.

The viscous shear solution derived above can only operate if viscous forces are of sufficient importance in the channel. One of the starting assumptions in the equilibration process was that the flow would reach uniform pressure rather quickly in the channel, within a few channel widths, and it is therefore questionable that frictional forces will have sufficient path length over which to act. This implies that equilibration in the low Mach number region must occur with an inviscid process.

It is postulated here that, for strong shocks, the equilibration will occur through a separation of the low-speed flow. For weak shocks, the imposed pressure gradient is quite small, and of little significance to the channel flow problem. Once that flow separates, it can be treated as a stagnant "bubble" of gas, which will compress until the desired equilibrium pressure is reached. This stagnant bubble will arise from the flow which has insufficient total pressure to rise to the desired uniform condition. Once the separation bubble forms, that flow is lost from the channel; beyond the bubble, the flow reattaches, and continues down the channel. As such, the new wall region is approximately the old streamline that corresponded to the total pressure limit.

Separation can be observed in any situation in the channel where pressure rises above the wall streamtubes' abilities to equilibrate. For instance, separation has been observed at the inlet of existing scramjet combustors, usually associated with the pressure increase brought on by the combustion process [11].

With the separation assumption, the uniform-pressure profile can be modelled as having been formed from all streamtubes capable of rising to the required equilibrium pressure. The lower limit on the integral of equation (7.18) is set to the point where total pressure is

just sufficient to permit the local streamtube to reach the desired static pressure. At that point, the problem of modelling a no-slip condition in inviscid flow reappears. For purposes of solution, it is assumed that the lower limit of the integration will be the *new* sonic point after pressure is equilibrated, allowing the area of the streamtubes below that to remain constant. From equation (7.12), the lower level of integration is set to the height at which:

$$M_1 = \sqrt{\left(\frac{p_2}{p_1}\right)^{\frac{\gamma-1}{\gamma}} \left(\frac{2}{\gamma-1}+1\right) - \frac{2}{\gamma-1}} \tag{7.22}$$

It is known from experiment that a separated hypersonic boundary layer reattaches. Indeed, Curle has demonstrated analytically, and confirmed experimental results, that the reattached hypersonic boundary layer has essentially the same profile as it had before separation [35]. Thus, it seems reasonable to ignore the separation as having little net effect on the shape of the profile downstream.

7.2.4 Calculation of Final Equilibrium Pressure

Returning to the inviscid solution, once the first adiabatic (hypersonic) approximation is used to estimate the final uniform pressure, the transformation can be calculated with equation (7.17). Then, this transform can be used to calculate a new downstream uniform pressure, p_2. The integration begins at the sonic line, below which the viscous flow solution is applied:

$$H = \int_{y_{viscous}}^{H} \frac{p_2^{1/\gamma} p_1(y)^{\frac{\gamma+1}{2\gamma}}}{\sqrt{\left\{p_1(y)^{\frac{\gamma-1}{\gamma}} - p_2^{\frac{\gamma-1}{\gamma}}\right\} \frac{2}{(\gamma-1)M_1(y)^2} + p_1(y)^{\frac{\gamma-1}{\gamma}}}} dy \tag{7.23}$$

Because p_2 is uniform across the channel (since it is, by definition, the equilibrated pressure), p_2 is extracted from under the integral:

$$p_2 = \left(\frac{1}{H} \int_{y_{viscous}}^{H} \frac{p_1(y)^{\frac{\gamma+1}{2\gamma}}}{\sqrt{\left\{p_1(y)^{\frac{\gamma-1}{\gamma}} - p_2^{\frac{\gamma-1}{\gamma}}\right\} \frac{2}{(\gamma-1)M_1(y)^2} + p_1(y)^{\frac{\gamma-1}{\gamma}}}} dy \right)^{\overline{\gamma}} \tag{7.24}$$

where $\overline{\gamma}$ is some average γ. Once p_2 is found iteratively, the transformation from the nonuniform profile to the uniform station is determined, and the new profile can be uniquely

determined based on the original profile generated by the shock. Mach number must also be corrected in each streamtube because of the area changes. With a known value of p_2, and the known profiles for M_1 and p_1, the new profile M_2 is uniquely determined.

Assembling the above treatment of the shock-generated profile, we can summarize the steps required to solve for the total effect of the shock on the initial inlet flow:

1. Start with the input profile from forebody calculations, at station 0 ahead of the shock.

2. Select the wedge angle which represents the flow turning into the engine channel. In general, the angle will be the same as the wedge angle due to vehicle forebody geometry.

3. From the wedge angle and known Mach number at each point, calculate the shock angle at each point along the profile. From the shock angle and upstream Mach number, the downstream Mach number and thermodynamic profiles are uniquely determined at station 1 behind the shock.

4. The nonuniform pressure profile at station 1 is transformed to a uniform profile at station 2 as outlined above. First, the uniform pressure is calculated with the iteration scheme of equation (7.24) in the supersonic regions, which is then used to calculate the new Mach number and thermodynamic conditions at each point. The iteration converges quickly.

5. Then, the position of each of the streamtubes is calculated at station 2 using the transformation from station 1, equation (7.17).

6. The Mach number below the subsonic profile is now corrected with a linear fit.

7. The profile at station 2 is the final result of passage through the shock, with uniform pressure, and can now be iterated through the known channel area changes and heat addition, using the methods outlined above.

Chapter 8

Numerical Study of Profile-Induced Variations at the Inlet

The developments of the previous chapters can be synthesized into a fundamental understanding of the propagation of forebody profiles through a scramjet channel, and its effect on the flow parameters. It is not necessary to follow a profile through a channel in order to examine the influence of the low speed regions. At any given station, the presence of a profile will affect the local conditions and streamwise derivatives of values such as the free-stream Mach number, and relative boundary layer thickness, as was derived in the previous chapter. The local influence of a forebody profile at the entrance to a combustor channel will be examined as a first indication of the importance of the boundary layer on the net flow behavior inside a supersonic combustion ramjet. Much information can be derived about the subsequent channel flow from response at the inlet station. In chapters 9 and 11, profiles will be followed through various channel shapes.

8.1 Streamwise Trends at the Inlet Station

8.1.1 Numerical Procedure

As described in chapter 6, the boundary layer model of Cohen and Reshotko can be included into the compound compressible model for laminar boundary layers, and a semi-empirical model can be used for the turbulent solution. In order to relate these results to the boundary layer thicknesses derived in chapter 3, the effect of the profile will be considered as a function of the relative thickness of the boundary layer. In each case, recall that the limit of zero boundary layer thickness will correspond to uniform flow.

8.1.2 Laminar Boundary Layer Profile

The influence of a laminar boundary layer is first considered at the engine inlet. Figure 8.1 shows the instantaneous value of the rate at which the relative boundary layer thickness will change with a given change in channel area. This figure is plotted for three values of the free-stream Mach number: 5, 10, and 20. For all cases, it was assumed that the free stream temperature is 1000 K, and the wall is cooled to 2000 K. This means that the ratio of wall temperature to adiabatic temperature is different for each line.

The behavior which was shown analytically is demonstrated in this plot. In the uniform limit, the boundary layer is always a fixed fraction of the channel height. This means that the derivative of the relative boundary layer height with respect to the logarithmic change in channel height is zero. The closer the boundary layer derivative is to zero, the more nearly uniform the net channel behavior is.

The zero-growth boundary layer solution is indicated on this plot by the "constant-height boundary layer" line. In this limit, the boundary layer height is fixed, so that any changes in the channel height are not accompanied by changes in the boundary layer thickness. In other words, if the channel area decreases, the constant-height boundary layer stays the same thickness and so the relative boundary layer height increases. Conversely, an increase in channel area results in a corresponding decrease in relative boundary layer thickness. In this limit, the boundary layer can be represented by a uniform Mach number, $\overline{M}$, of unity, because a sonic flow cannot change area in response to pressure changes.

Because all of the curves shown lie between the uniform flow solution and the constant-height line, the uniform Mach numbers in these cases are all supersonic. A subsonic uniform Mach number would have to fall on the other side of the constant-height boundary layer line. This means that, for the laminar boundary layer profile, and, as seen in Figure 8.2, for the turbulent boundary layer as well, the boundary layer can be represented as a uniform supersonic streamtube at the inlet station. This in turn means that the nonuniform channel flow is always *compound supersonic* entering the engine inlet.

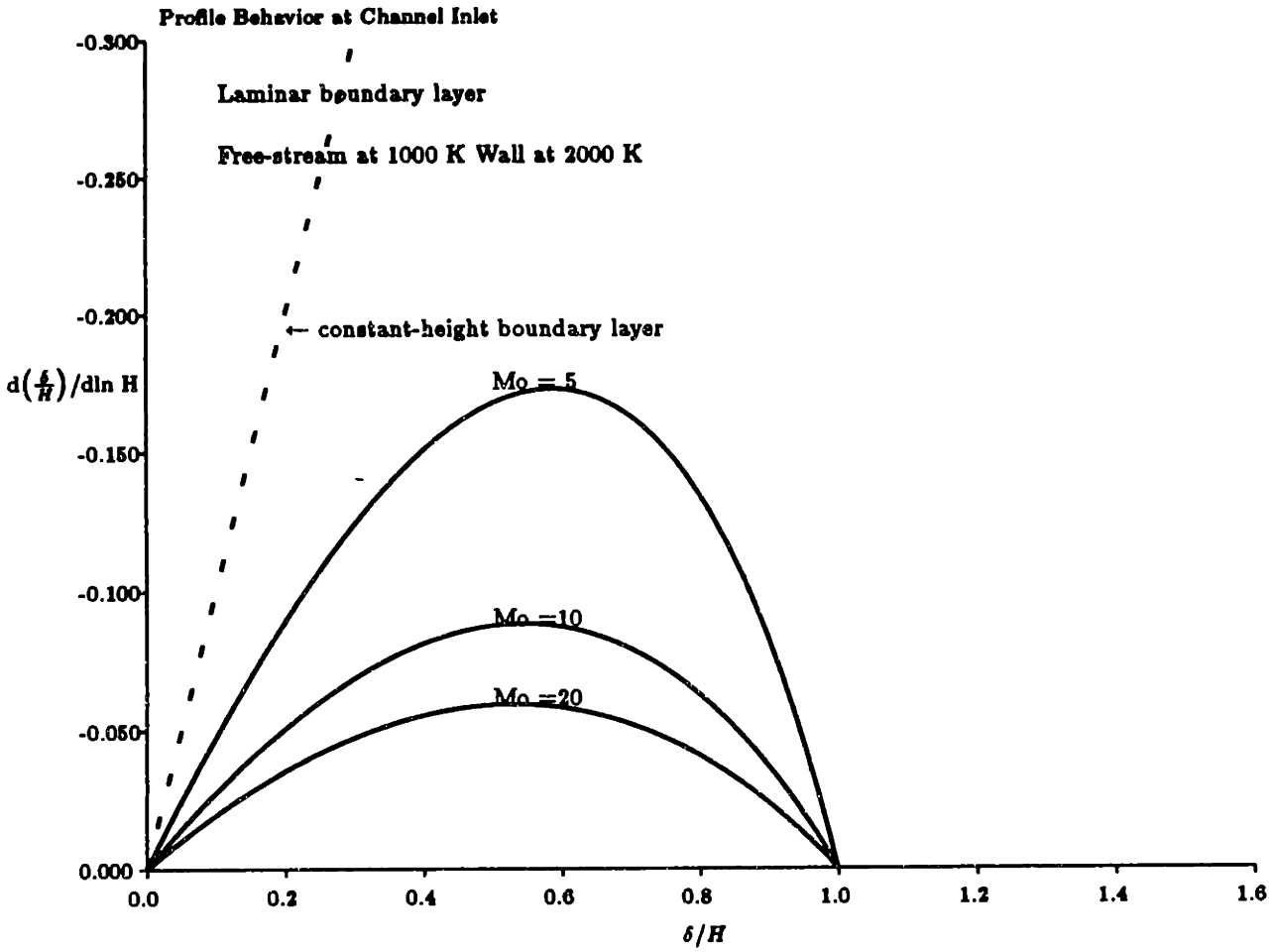

Figure 8.1: Relative laminar boundary layer thickness change with channel height

In Figure 8.1, the flow is uniform in the limit of zero boundary layer thickness. Similarly, when the relative boundary layer thickness is unity, the boundary layer fills the channel, so the derivative of relative boundary layer height with respect to he channel height is once again zero. Between these limits, the profile departs significantly from uniform behavior.

At Mach 5, the boundary layer is behaving almost exactly between the constant area and uniform limits. A change in channel area will result in a corresponding change in boundary layer height, but not as much as the free-stream area will change. Note that the vertical scale in Figure 8.1 is negative, so the relative boundary layer thickness varies in a negative sense to the channel height. If this profile flow is entering a converging channel, both the free-stream and the boundary layer will be getting smaller, but the free-stream will be getting smaller faster than the boundary layer, and therefore faster than a uniform flow would. Accordingly, a converging channel that is designed to reduce Mach number and increase temperature in a uniform flow will do so more dramatically in the nonuniform case

In Figure 8.1, the departure from uniform behavior is more pronounced at the lower Mach number than at the high, and at high Mach number, the difference in boundary layer behavior is less sensitive to Mach number. The curves for Mach 10 and Mach 20 lie close together, and if higher Mach numbers were shown, they would lie even closer still. This is an effect that was explained analytically, and it will be demonstrated again below.

8.1.3 Turbulent Boundary Layer Profile

In comparison to the laminar solution, the turbulent profile has relatively modest effect on the behavior at the channel inlet. Figure 8.2 is plotted for the same inlet and wall conditions as Figure 8.2. The vertical scale in Figure 8.2 is expanded by a factor of 150 over that of Figure 8.1. With a turbulent boundary layer, the channel flow behaves more nearly uniformly. Beyond Mach 10 or so, the boundary layer remains in perfect proportion to its original fractional height in the channel. This is not surprising, considering that the turbulent profile is much fuller, and so more nearly uniform, than the laminar boundary

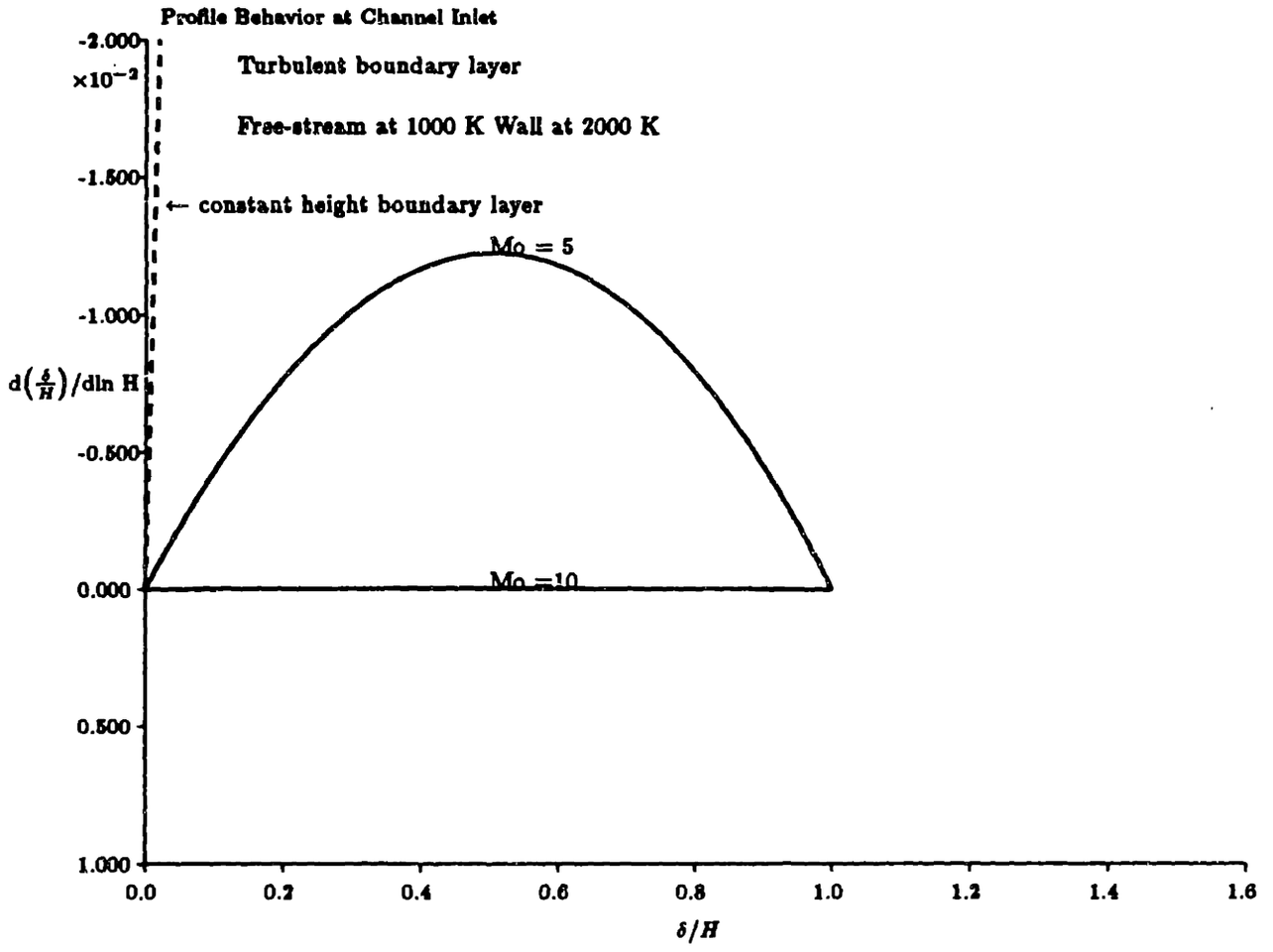

Figure 8.2: Relative turbulent boundary layer thickness change with channel height

layer.

8.1.4 Net Uniform Equivalent Mach Number

Another means of evaluating the influence of the inlet profile on the flow at the entrance station to the engine channel is by calculating the net uniform equivalent Mach number, $\overline{M}$, defined earlier, for the *entire* channel height. Figure 8.3 shows the net channel Mach number for various inlet Mach numbers, all with the same thermal conditions as before.

At $\delta/H = 0$, the flow is uniform and the net Mach number is the free-stream Mach number. At even moderate values of boundary layer fraction, there is a marked change in the net Mach number, particularly in the high Mach number profiles. As is shown, the Mach 20 free-stream profile has dropped by a factor of four when the boundary layer is only a fifth of the channel height. With the same boundary layer height, the Mach 10 profile has dropped to a uniform Mach number of 3. The Mach 5 inlet flow shows a much less dramatic change in Mach number.

With thicker boundary layers, the net channel Mach number quickly reaches an asymptotic limit, which is the uniform Mach number of the boundary layer alone. Recall that the importance of a streamtube's influence is proportional to its area, and inversely proportional to the square of its Mach number, minus one. Thus, with a larger boundary layer, its small uniform Mach number quickly begins to dominate the free-stream, and so the boundary layer determines the flow properties in the channel. The value of this asymptotic limit is quite similar over the range of Mach numbers shown. At free-stream Mach number 5, the uniform Mach number of the boundary layer is about 2; with free-stream Mach number 20, the boundary layer is represented by a uniform Mach number of 3. This is another expression of the result that the uniform Mach number for the boundary layer is insensitive to free-stream Mach number at hypersonic conditions. As Figure 8.1.4 demonstrates, the net Mach number with a turbulent boundary layer behaves as if the flow were nearly uniform, and the thermodynamic properties will therefore be similar to those of a uniform flow.

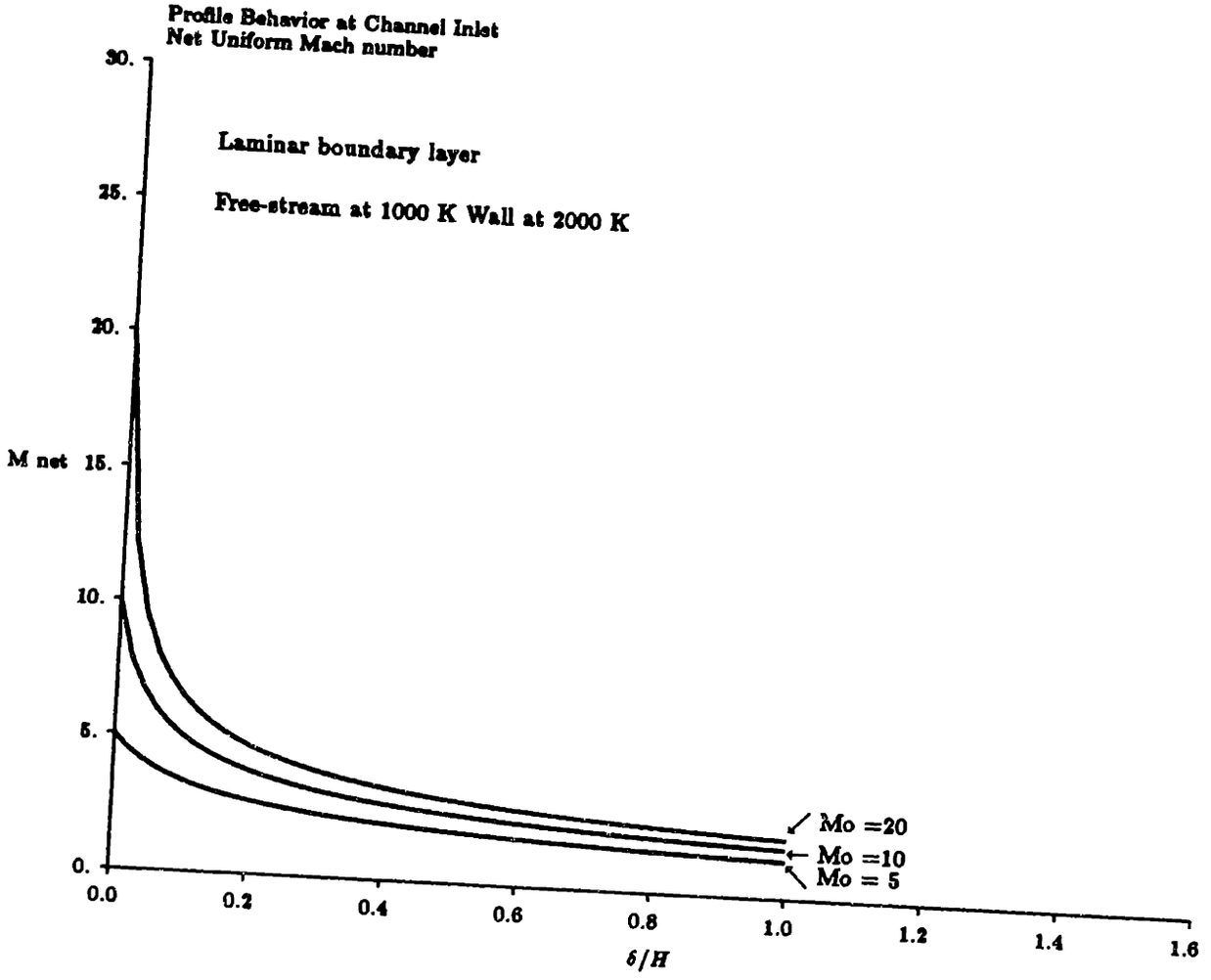

Figure 8.3: "Net" channel Mach number with laminar boundary layer

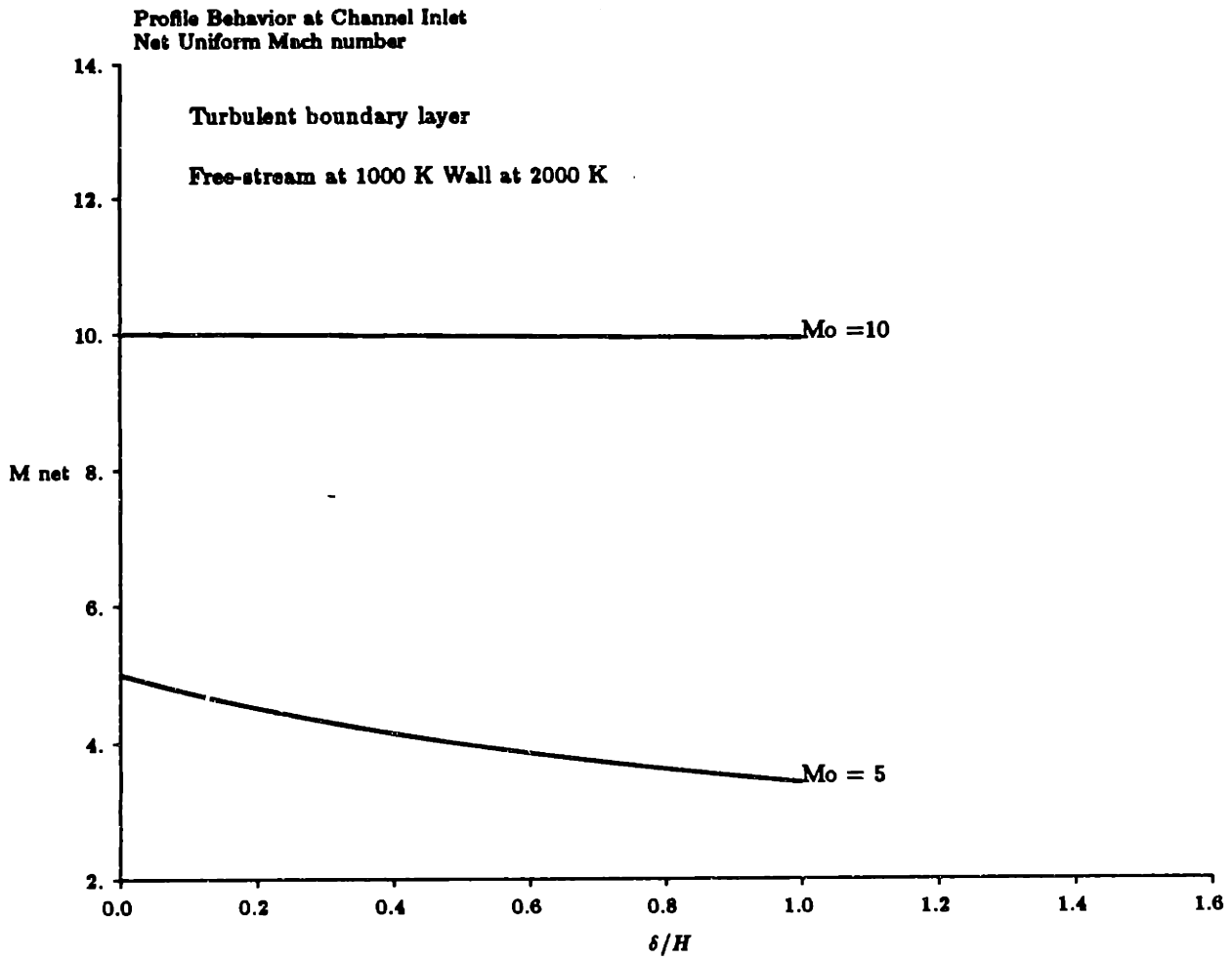

Figure 8.4: "Net" channel Mach number with turbulent boundary layer

8.1.5 Streamwise Derivative of Flow Properties

The ultimate question of interest in this analysis is how the boundary layer affects the thermodynamic conditions inside the engine, and this is best represented by the influence it has on the pressure and temperature in the combustor. At the inlet station to the engine channel, the effect that the boundary layer will have on properties farther downstream in the channel can be shown by examining the value of the streamwise derivative of the free-stream Mach number. If the streamwise derivative of Mach number is changed in comparison to the result for uniform flow, the derivative of thermodynamic conditions will be changed correspondingly. In turn, if the derivatives are affected at the inlet, the values downstream will be changed. The properties at the inlet can therefore provide much qualitative information about nonuniform behavior downstream.

Figure 8.5 is a plot of the derivative of the free-stream Mach number with respect to the logarithmic derivative of channel height, as a function of the boundary layer height relative to the channel height, for the same three Mach numbers. This derivative indicates how the free-stream Mach number will change when the channel area changes. At zero boundary layer height, the value of this derivative is that for a uniform inflow.

In Figure 8.5 the value of the streamwise derivative of free-stream Mach number is increasing as the boundary layer is increased in thickness. For instance, for free-stream Mach number of 5, the derivative is increased by about 50% over the uniform solution with a boundary layer filling half the channel. This means that the rate at which Mach number is decreasing in a converging channel is increased over that for a uniform flow. This effect is less dramatic at high Mach numbers because it takes more area change to alter Mach number in a high Mach number flow. However, the fact that this derivative is less sensitive to channel area change at high Mach number does not diminish the resulting change in thermodynamic conditions, because the logarithmic derivative of pressure is proportional to the logarithmic derivative of Mach number. In fact, as will be shown in a later chapter, the presence of the boundary layer profile will typically have only a small effect on the magnitude of the free-stream Mach number, but produce noticeable changes in static pressure and temperature, a general feature of hypersonic flows.

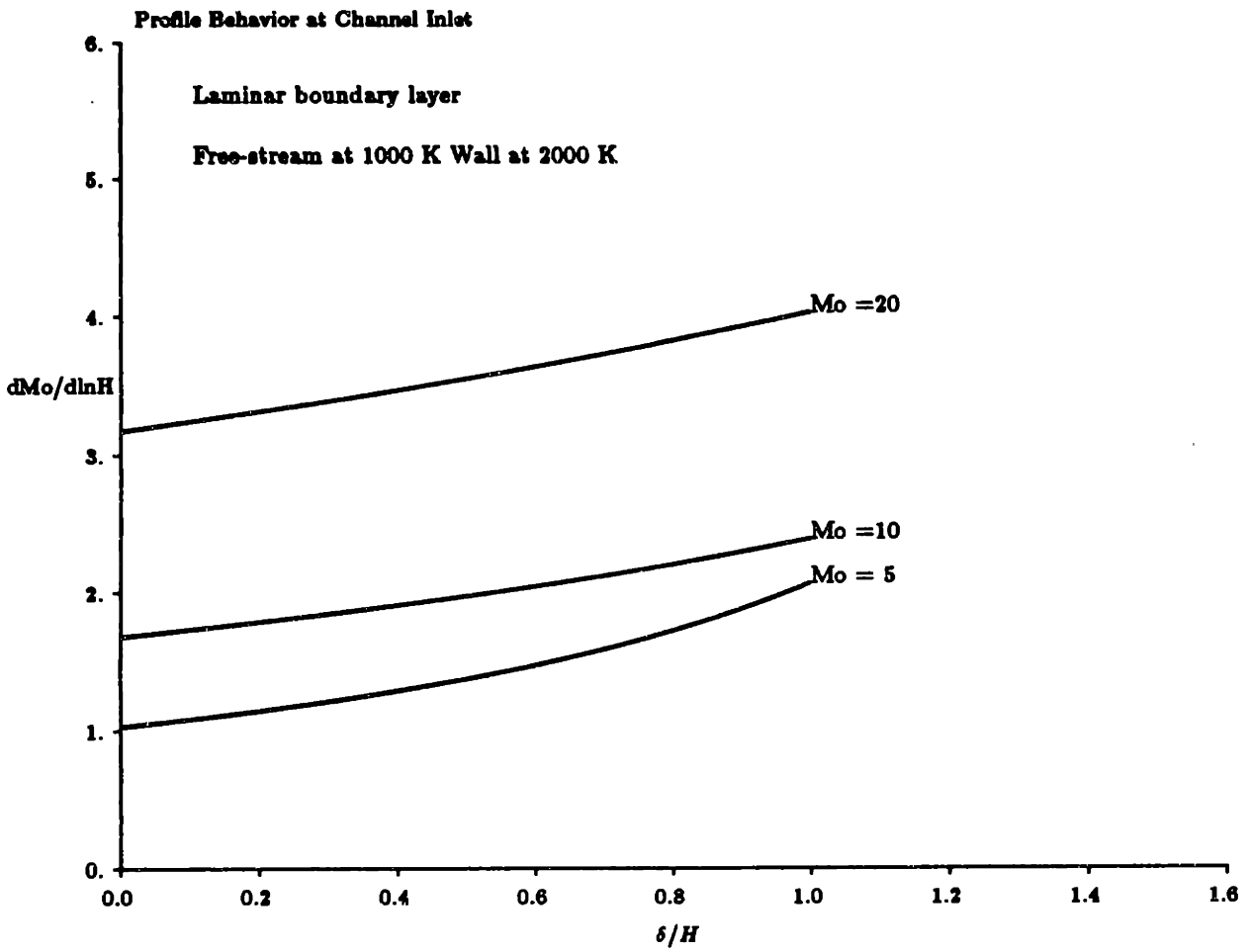

Figure 8.5: Streamwise derivative of free-stream Mach number with laminar boundary layer

This result can be understood in terms of the boundary layer growth trends demonstrated in Figure 8.1. With a laminar nonuniformity, the relative height of the boundary layer increases in a diverging channel, and increases in a converging channel. This means that the area change in the free-stream region is proportionately larger, which amplifies the effect of channel area change on the free-stream, produces larger gradients of Mach number.

In the turbulent case, the boundary layer remains in about the same proportion to the channel height at high Mach number. Figure 8.6 demonstrates that, for the turbulent boundary layer profile, there is essentially no change in the derivative of free-stream Mach number, as we would expect.

The only major difference between the uniform Mach number used to represent the boundary layer profile and the idealized uniform streamtube at that Mach number is the value of the streamwise derivative of that uniform Mach number. An analytical solution was presented for calculating the actual streamwise derivative of uniform Mach number. At the inlet, the value of this derivative is of little interest; only the trends and properties at that one station are important. It is of interest to examine the actual streamwise derivative of uniform Mach number, because that indicates how quickly the original boundary layer profile is steepening in response to an adverse gradient, or becoming more shallow in a favorable pressure field.

Figure 8.7 shows the derivative of uniform boundary layer Mach number with respect to the logarithmic derivative of channel height for inlet Mach numbers of 5, 10, and 20. These can be compared to the values presented in Figure 8.8 to see that the actual derivative is changing more slowly than would be calculated for an idealized uniform streamtube. This emphasizes the result that the uniform boundary layer Mach number is insensitive to free-stream Mach number, so that changing free-stream conditions have little effect on the uniform representation of the boundary layer. The smallest value of uniform Mach number derivative in the profile is found at the smallest free-stream Mach number (except at large relative profile thicknesses), while for the idealized streamtube, the smallest value is found with the largest free-stream Mach number.

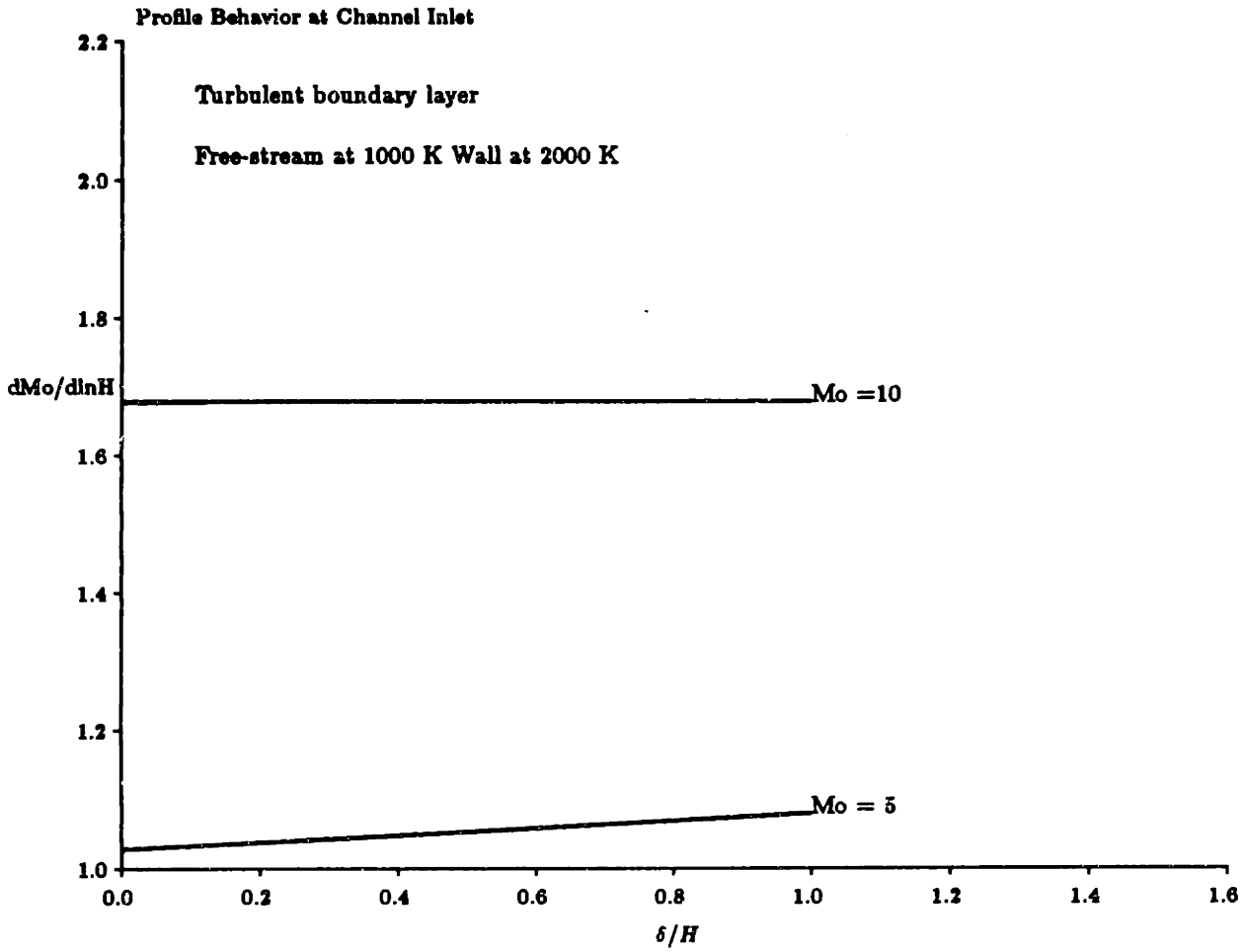

Figure 8.6: Streamwise derivative of free-stream Mach number with turbulent boundary layer

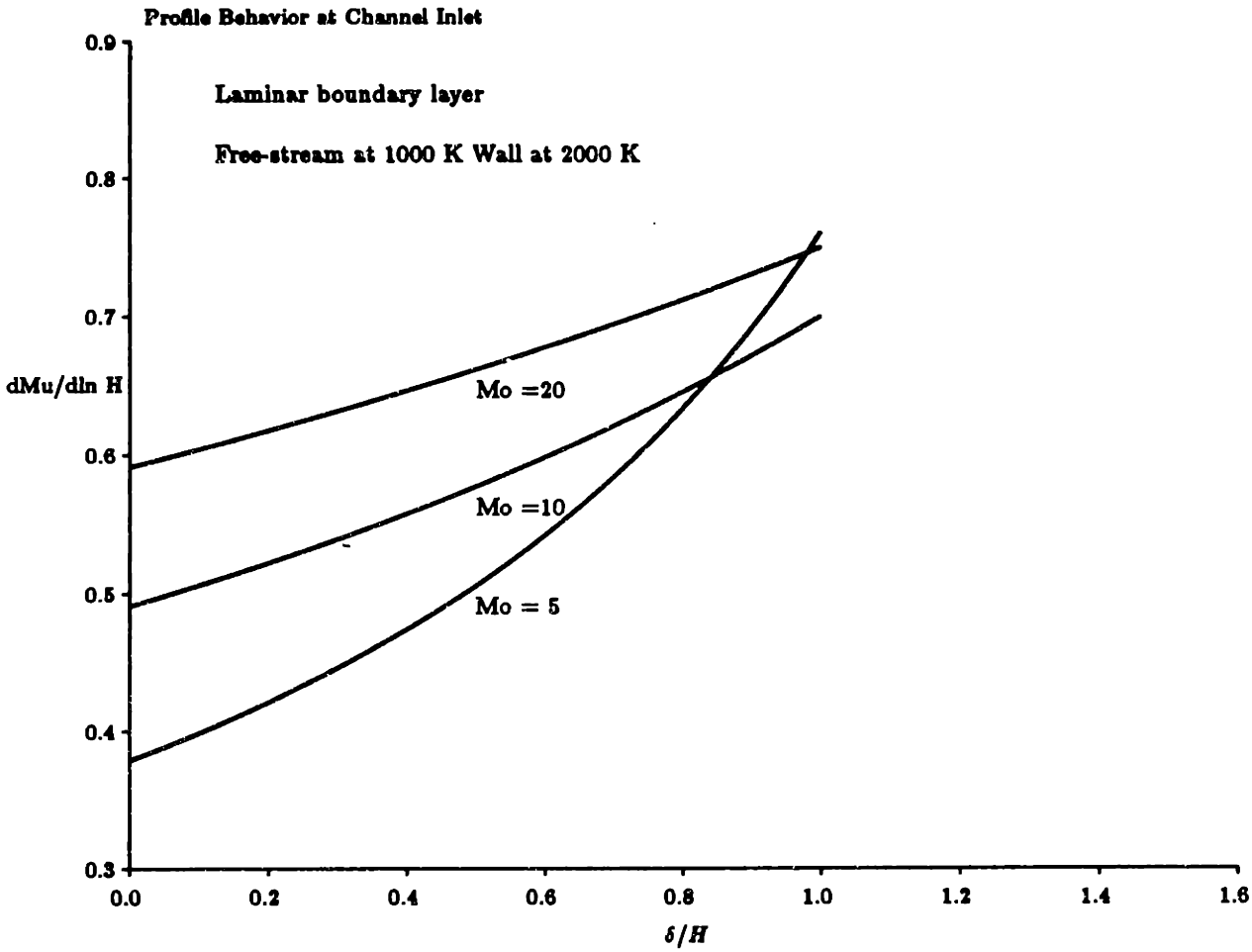

Figure 8.7: Streamwise derivative of uniform laminar boundary layer Mach number for the actual profile

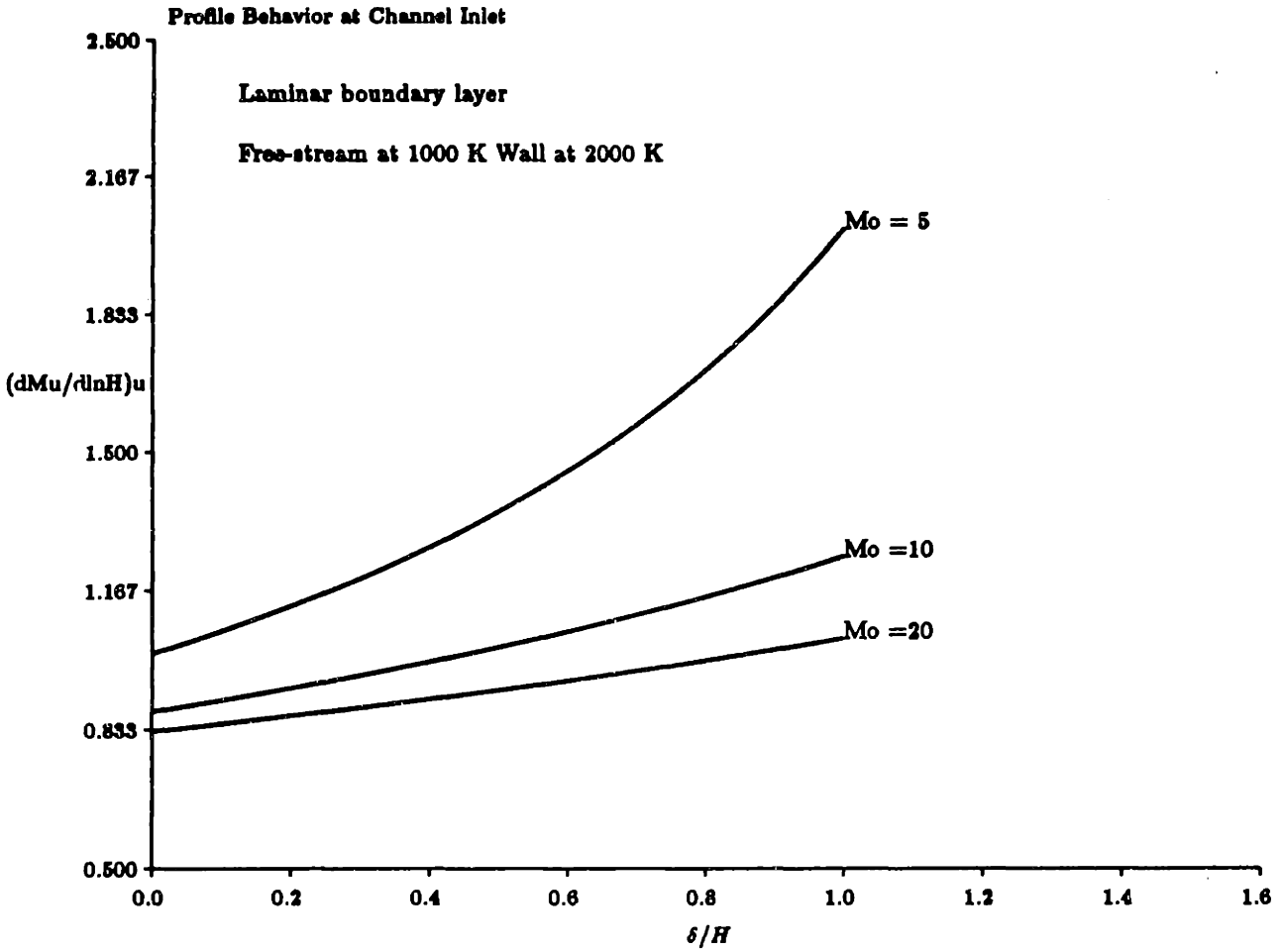

Figure 8.8: Streamwise derivative of uniform laminar boundary layer Mach number in an idealized uniform streamtube

In Figure 8.9, the actual value of the derivative of uniform Mach number is shown for the three Mach numbers divided by the value for an idealized uniform streamtube. The actual value is in every case smaller than the idealized value, and this effect is most pronounced at lower Mach number. The ratio of these two values is independent of the boundary layer fraction. This can be explained from the derivation of these derivatives in chapter 5; both the actual and idealized derivatives are functions of the profile, and proportional to the streamwise derivative of channel height and the inverse of the compound compressible flow parameter, $\overline{\beta}_{\text{channel}}$. Since these two are the same in both cases, the ratio is constant, independent of its relative thickness of the profile in the channel.

The turbulent boundary layer profile yields uniform Mach numbers which behave more closely to their idealized streamtube counterparts, which is once again a result of the full, nearly uniform nature of the turbulent profile. This is demonstrated in Figures 8.10 through 8.12.

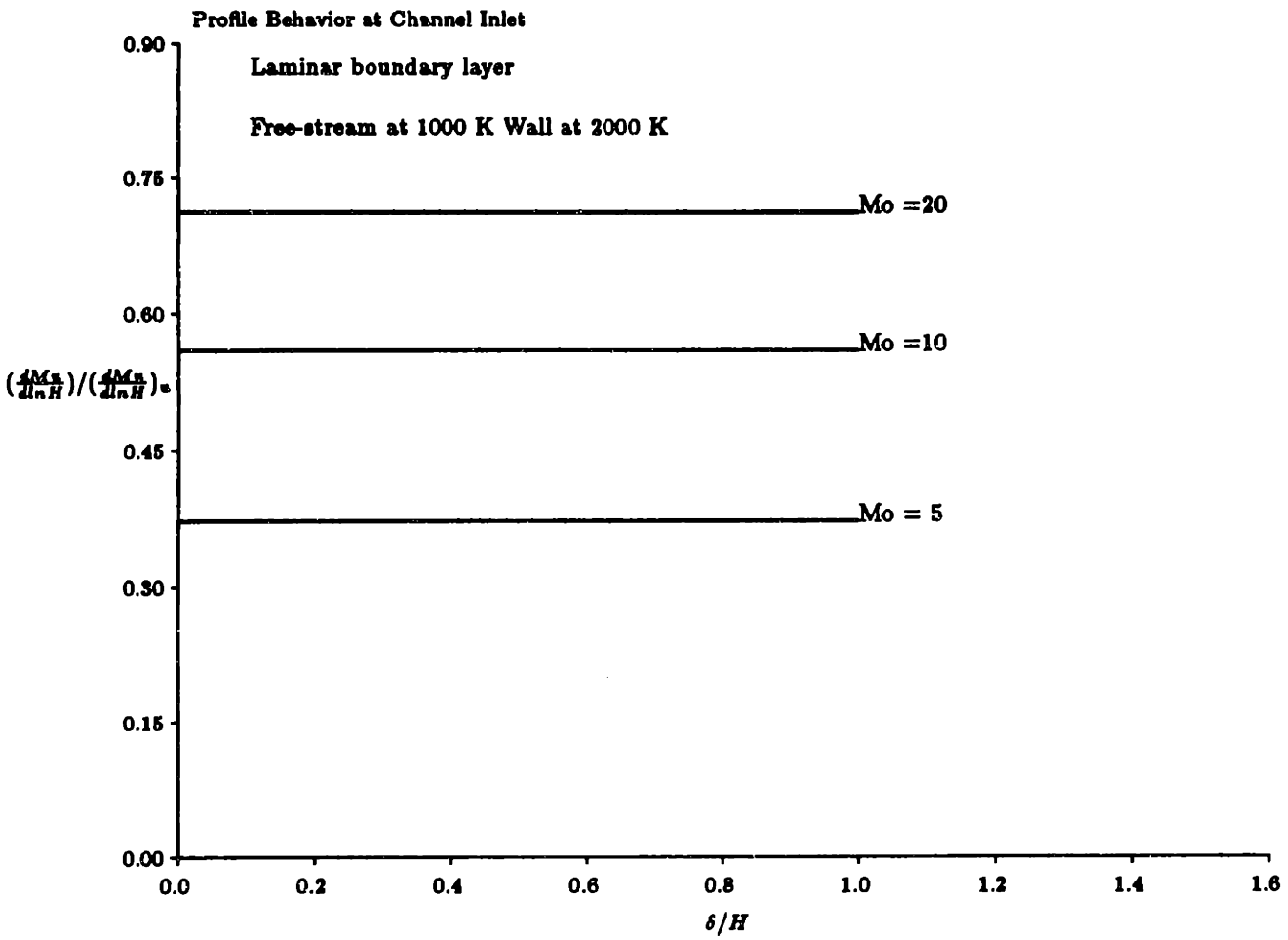

Figure 8.9: Streamwise derivative of uniform laminar boundary layer Mach number divided by result for an idealized uniform streamtube

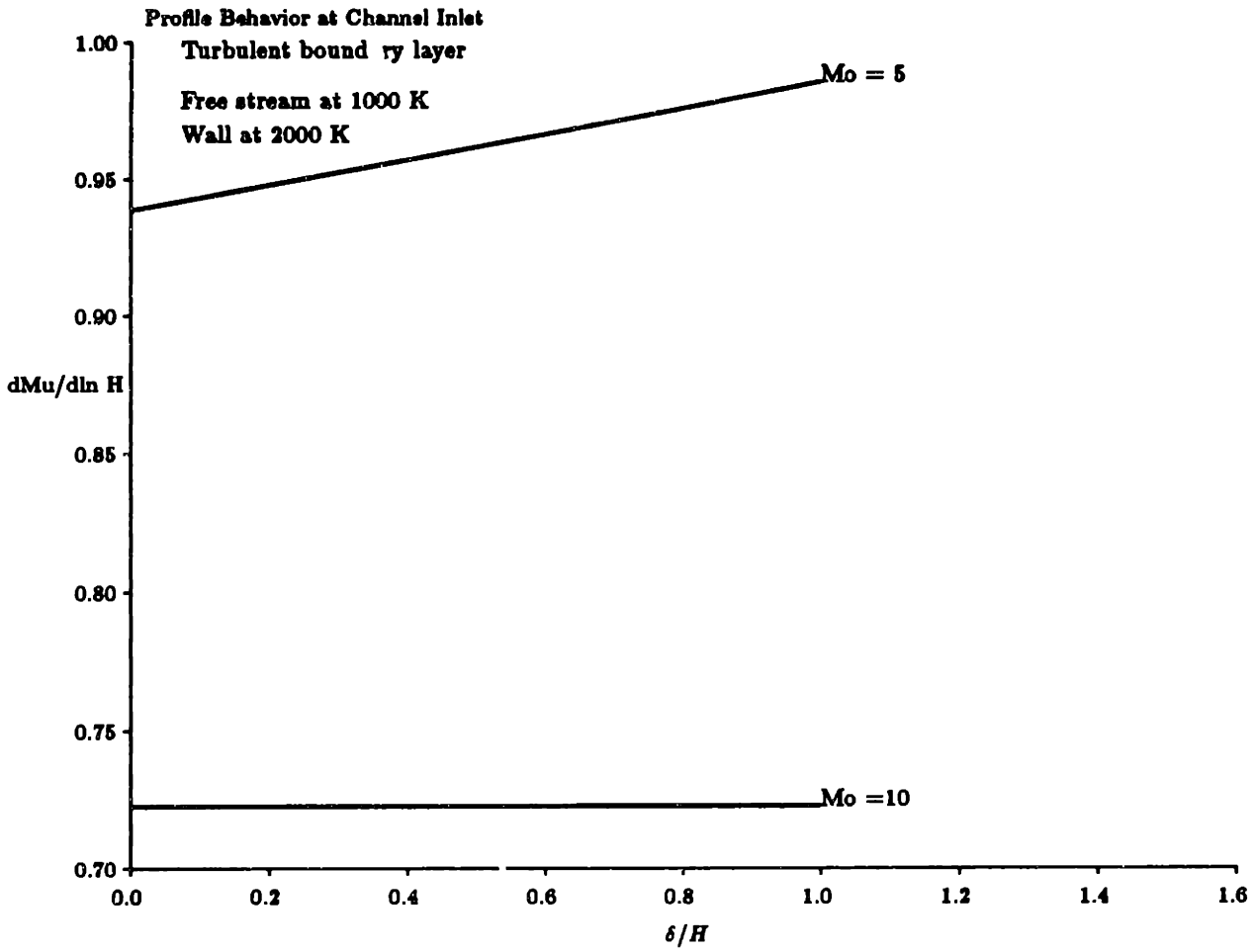

Figure 8.10: Streamwise derivative of uniform turbulent boundary layer Mach number for the actual profile

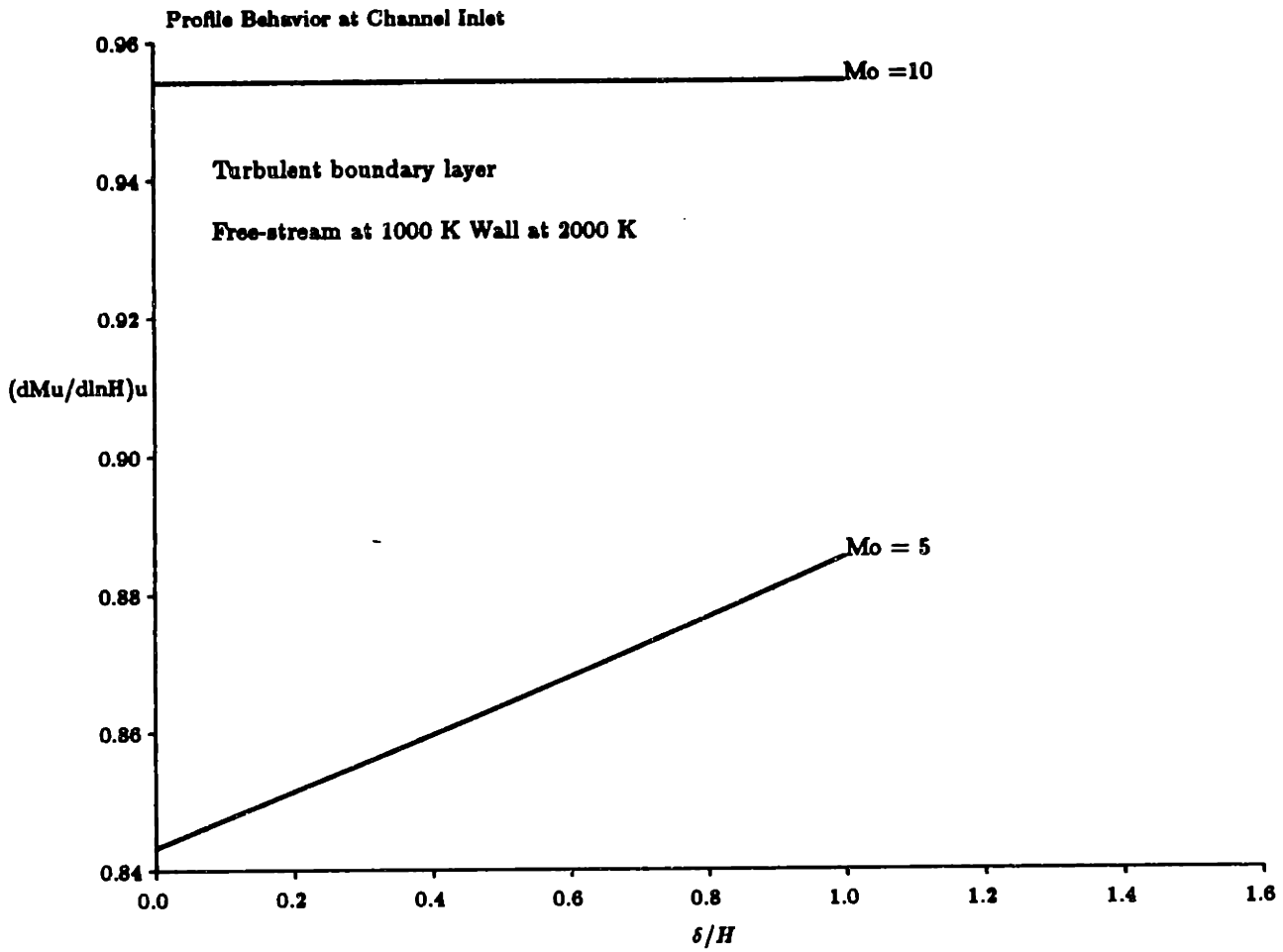

Figure 8.11: Streamwise derivative of uniform turbulent boundary layer Mach number in an idealized uniform streamtube

All of these examples have been shown for fixed wall temperatures and free-stream temperatures, independent of the selected Mach number. This is an idealized comparison, and it is of interest to examine the effect of changing the wall temperature or free-stream temperature. Since the laminar boundary layer solution depends only on the ratio of wall temperature to the adiabatic wall temperature, the influence of this parameter can be examined by varying either wall temperature or free-stream temperature.

In Figures 8.13 and 8.14, the values of net Mach number and the derivative of boundary layer thickness with respect to the logarithmic derivative of channel height are shown for inlet conditions at Mach 10, 1000 K, and wall temperatures of 1000 K, 2000 K, and 3000 K. As indicated, these correspond to wall temperature ratios of .0625, .1250, and .1875, respectively. Higher wall temperatures yield more substantial changes in the flow conditions at a given boundary layer thickness.

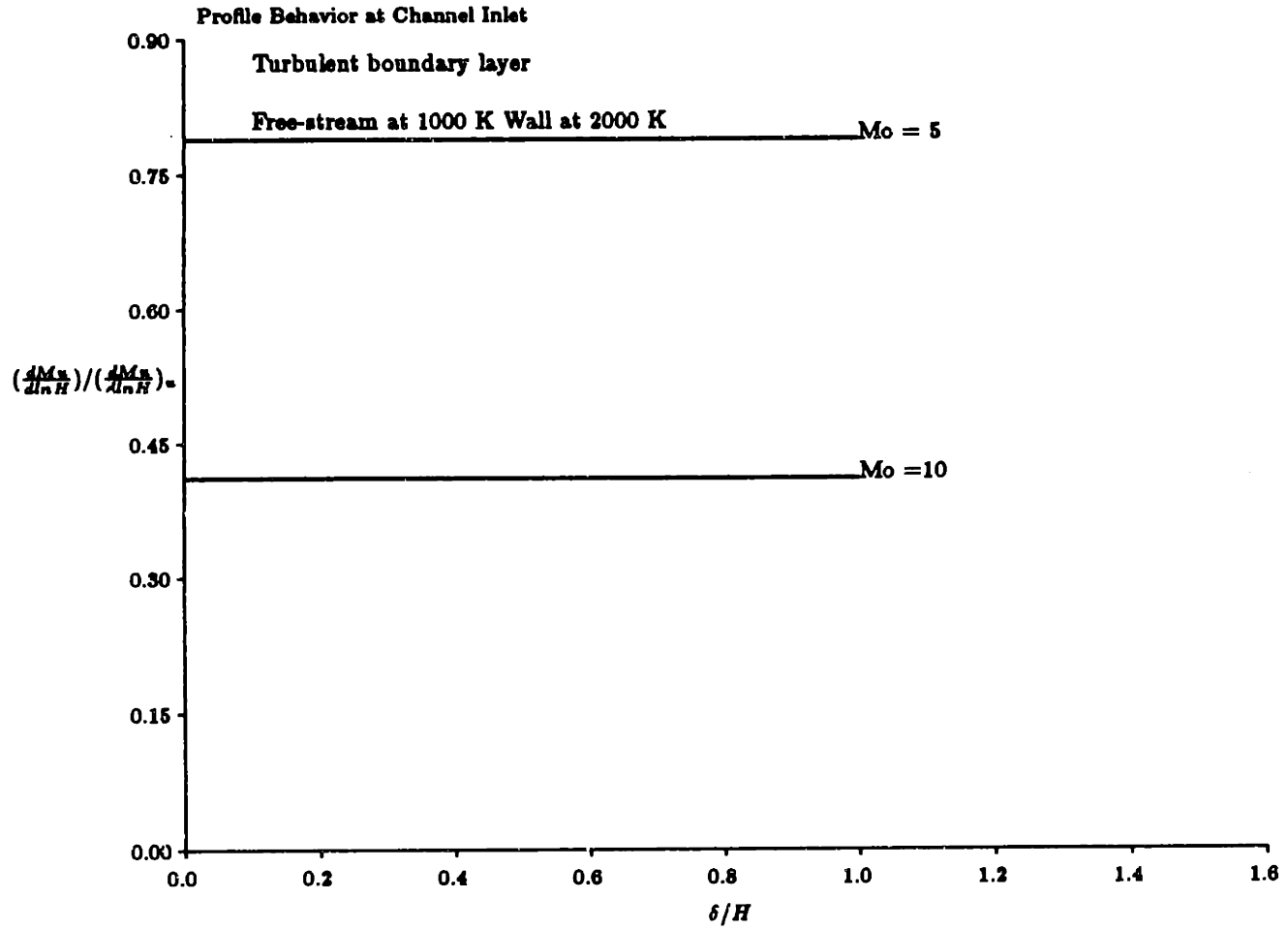

Figure 8.12: Streamwise derivative of uniform turbulent boundary layer Mach number divided by result for an idealized uniform streamtube

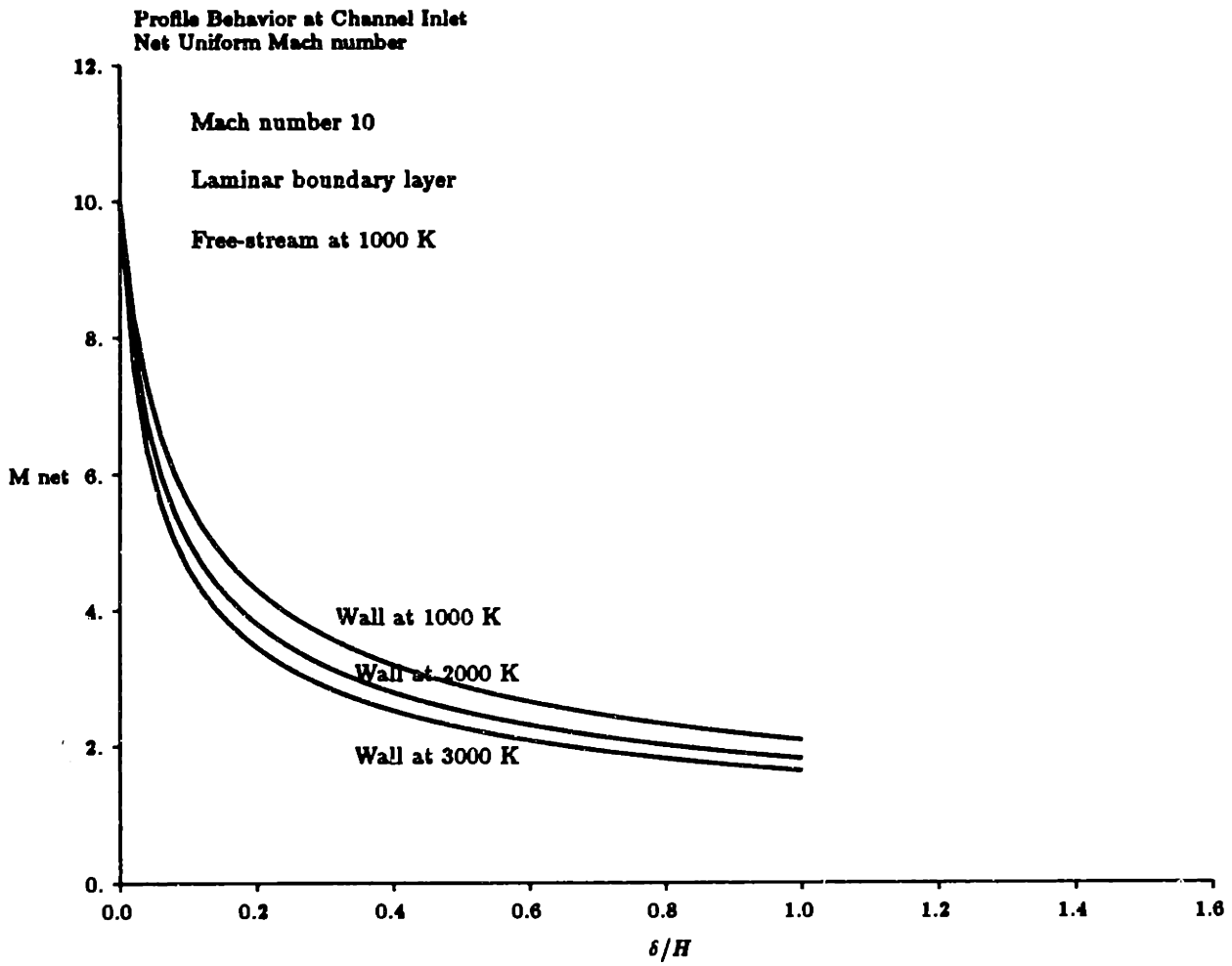

Figure 8.13: Net uniform Mach number with varying wall temperatures

8.2 Shock Effects on the Profile

The analytical solution of chapter 7 and Appendix D indicated that a uniform pressure profile will come through the shock with a pressure gradient that is of the order of the upstream pressure, divided by the boundary layer profile thickness. This gradient will equilibrate to a uniform pressure which is lower than the expected pressure for a uniform flow.

Figure 8.15 is a laminar boundary layer profile calculated for flight conditions at Mach 10, 30 km altitude, with a forebody wedge angle of 5 degrees, and a wall cooled to 2000 K. It was calculated using the method of Cohen and Reshotko, outlined in chapter 3. This profile will be used to start a numerical solution which solves for the profile directly behind a shock, an then determines the equilibrium pressure downstream, with the resulting profile.

In chapter 3, the laminar boundary layer thickness at Mach 10, 30 km altitude was calculated to be 4 % of the shock layer thickness 10 meters down the forebody, and 2.5% of the thickness 30 meters down the surface. Figure 8.16 shows the profile of Mach number at three stations: upstream of the shock (the equilibrium boundary layer), just behind the shock (with strong pressure gradient), and downstream of the shock, after the gradient has equilibrated. The presence of the boundary layer has had little effect on the magnitude of the free-stream Mach number, but there is a noticeable effect on the pressure downstream of the shock, as shown in Figure 8.17.

A more extreme example is for the flow corresponding to flight at Mach 20, 50 km. altitude, the profile for which is shown in Figure 8.18. The result of sending this profile through a shock on a five degree wedge is shown in Figure 8.19. As per calculations in chapter 3, it has been assumed that the boundary layer is 1/4 the total shock layer thickness under these flight conditions. The profile has been squeezed down in the equilibration process, which is what causes the reduced pressure in the free-stream. The pressure drop in the equilibration process is shown in Figure 8.20.

Passage through the shock also effects the temperature profile, as shown in Figure 8.21.

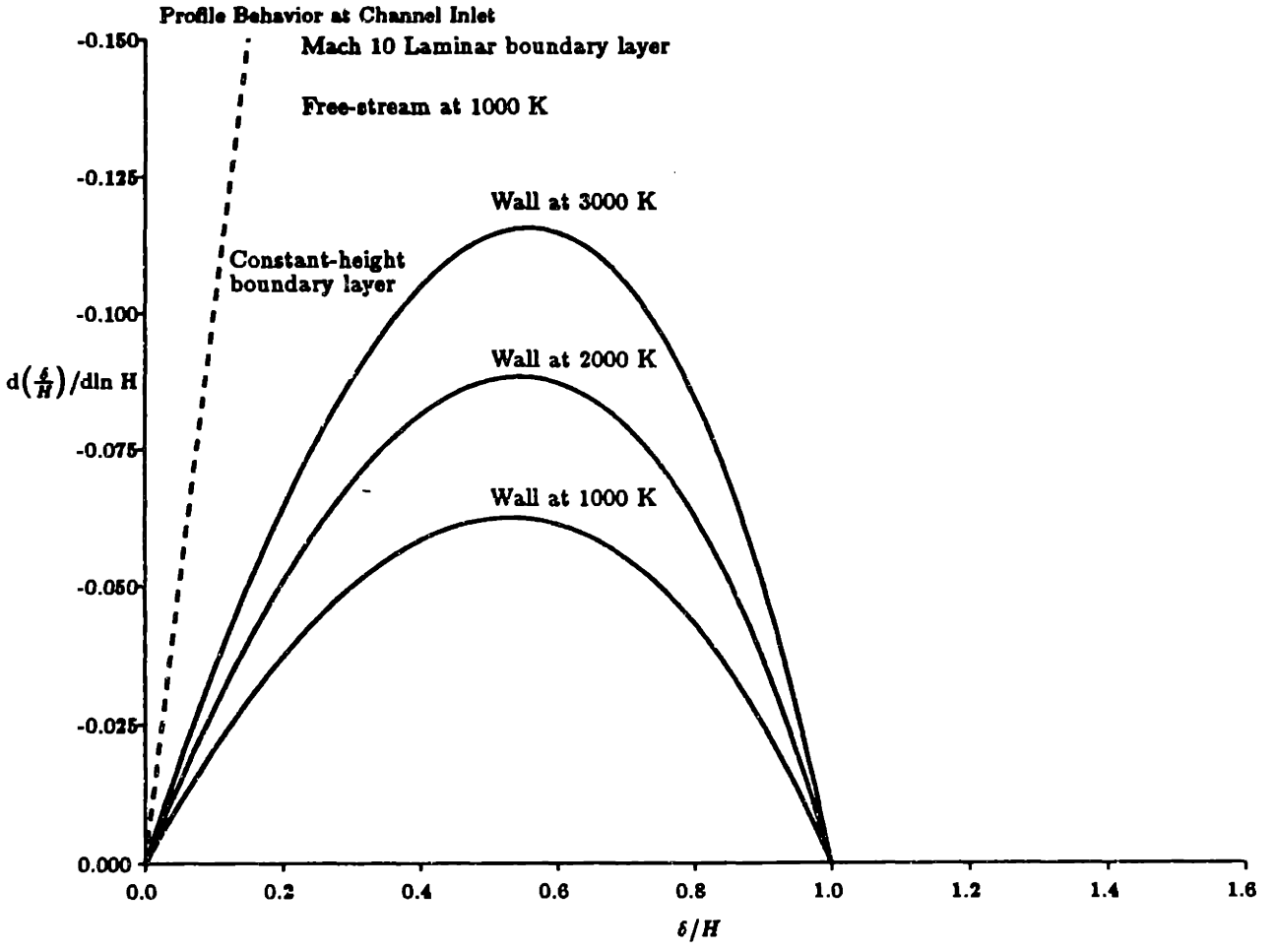

Figure 8.14: Derivative of relative boundary layer thickness for varying wall temperatures

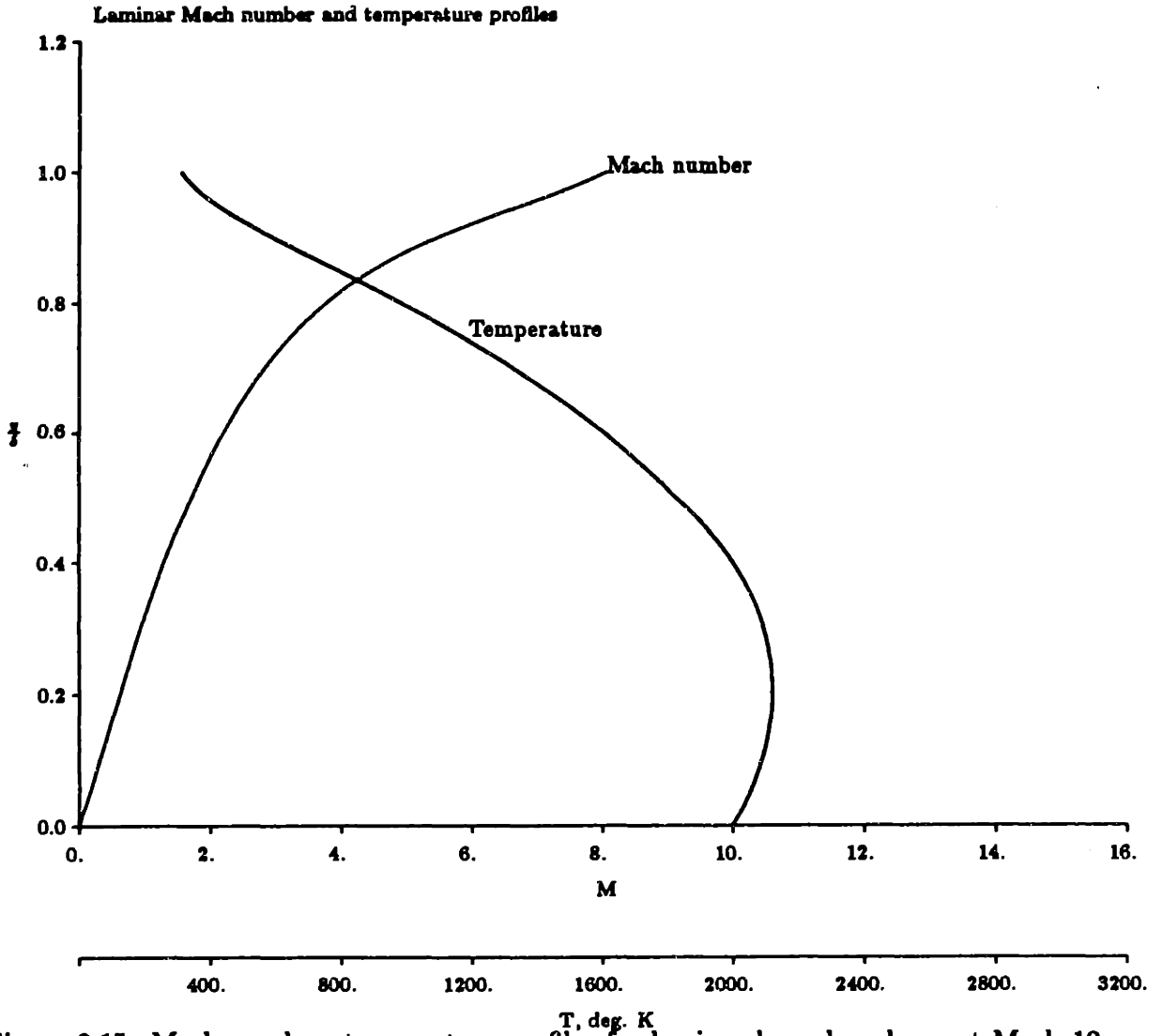

Figure 8.15: Mach number, temperature profiles for laminar boundary layer at Mach 10, 30 km altitude

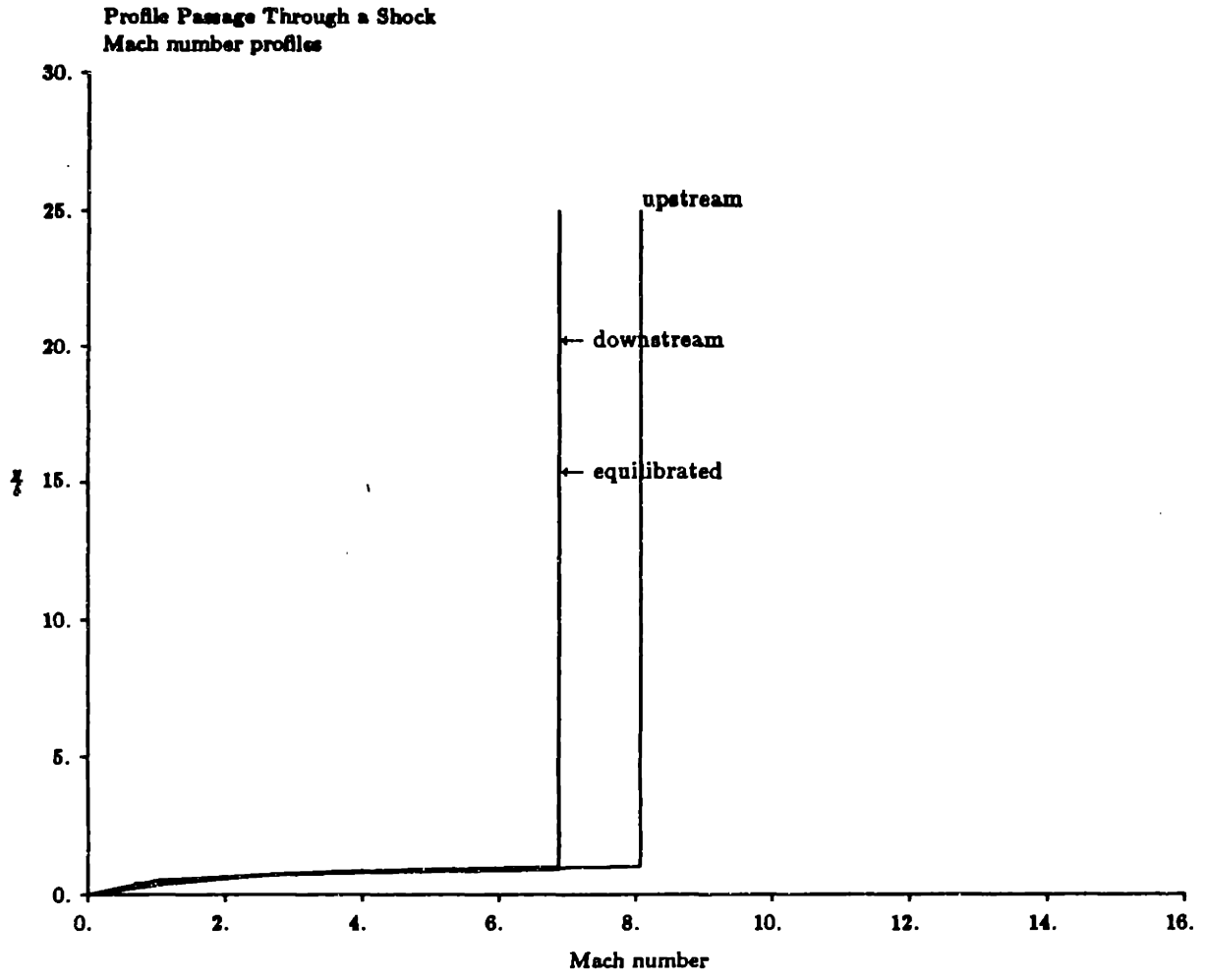

Figure 8.16: Mach number profile through a shock on a 5 degree wedge flight Mach number 10, altitude 30 km., 5 deg. wedge angle

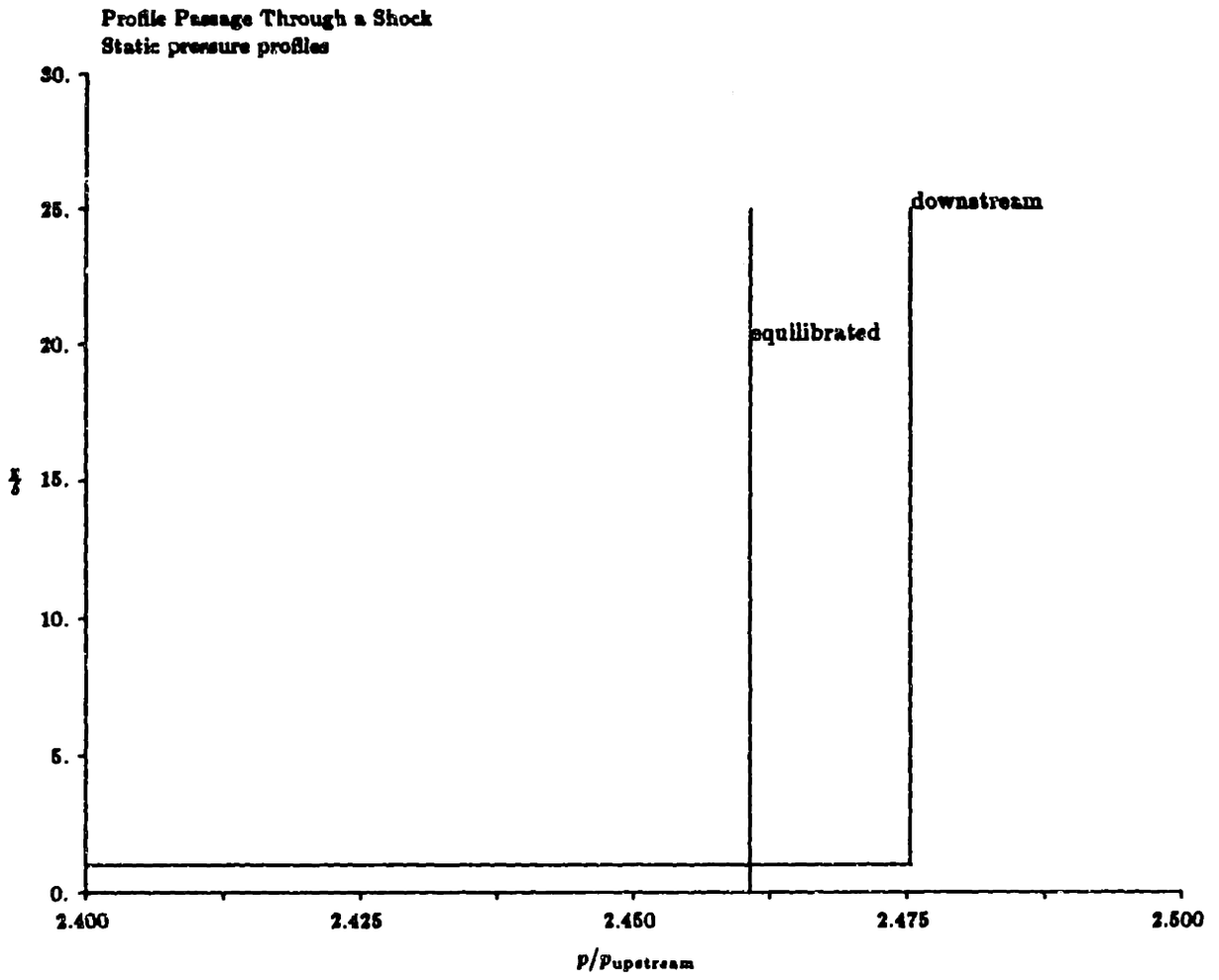

Figure 8.17: Pressure field directly downstream of the shock, and equilibrated normalized to upstream pressure, 5 degree wedge angle, Mach 10

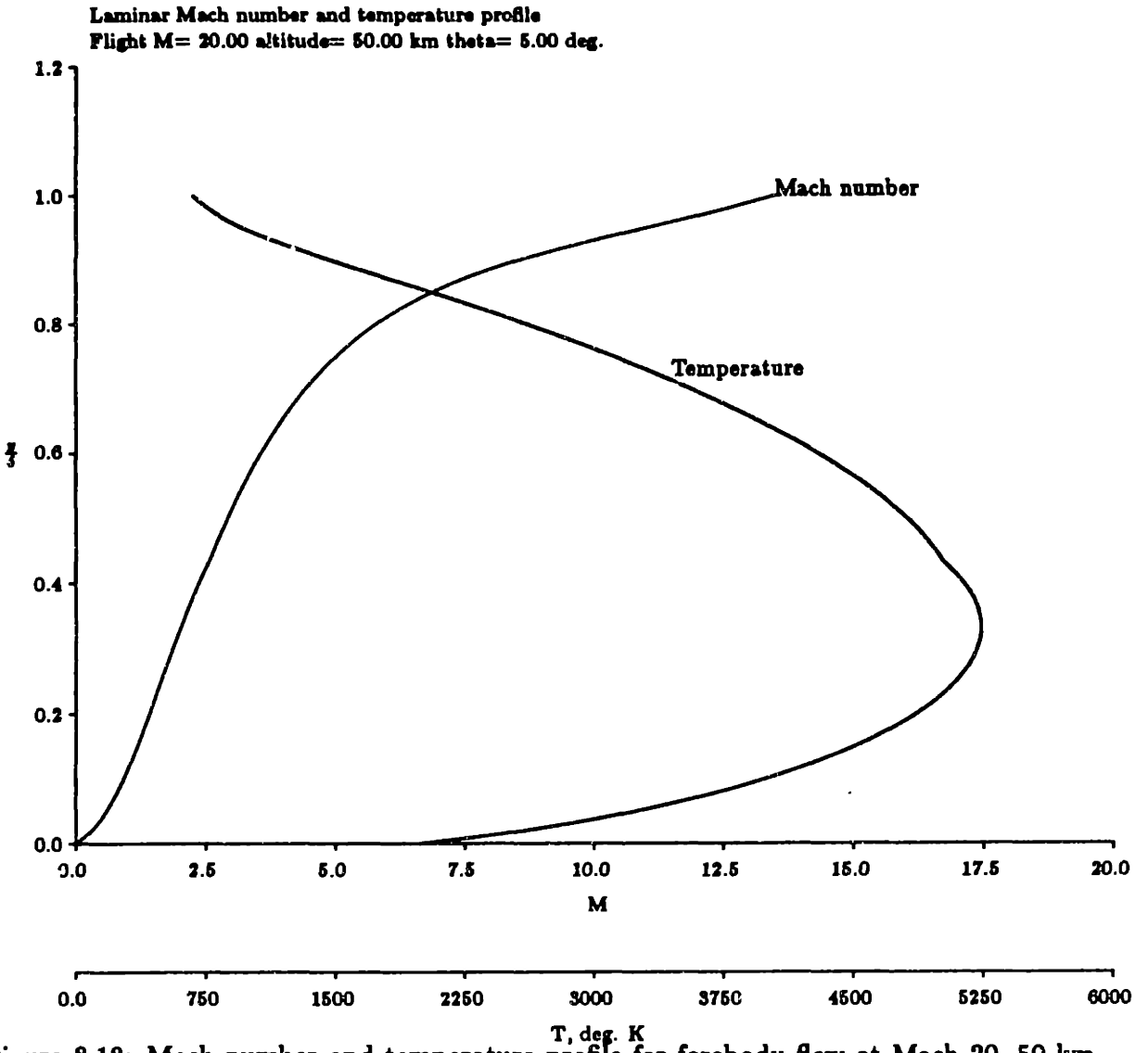

Figure 8.18: Mach number and temperature profile for forebody flow at Mach 20, 50 km altitude, with laminar boundary layer

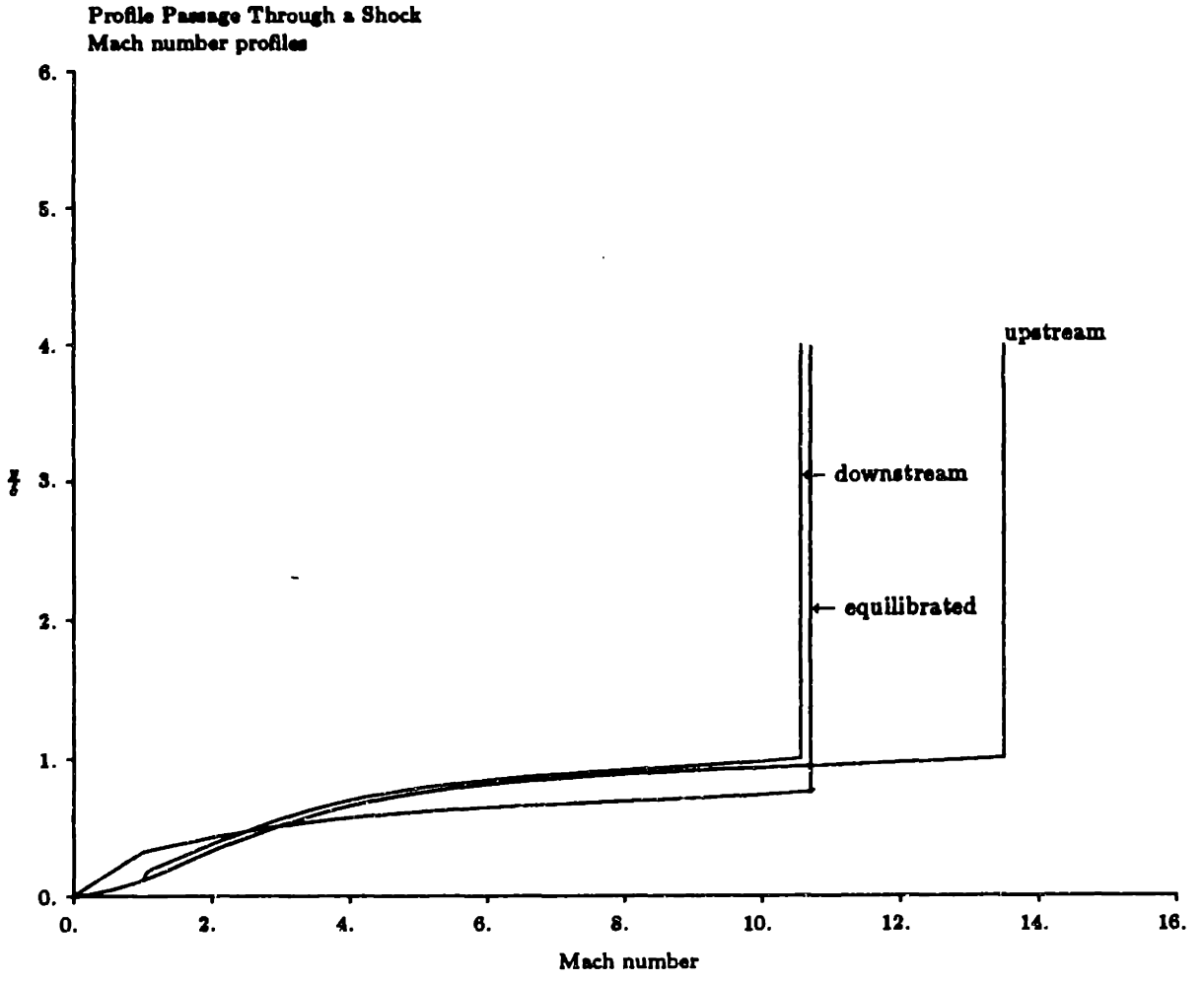

Figure 8.19: Mach number profiles upstream of a shock, immediately downstream, and equilibrated

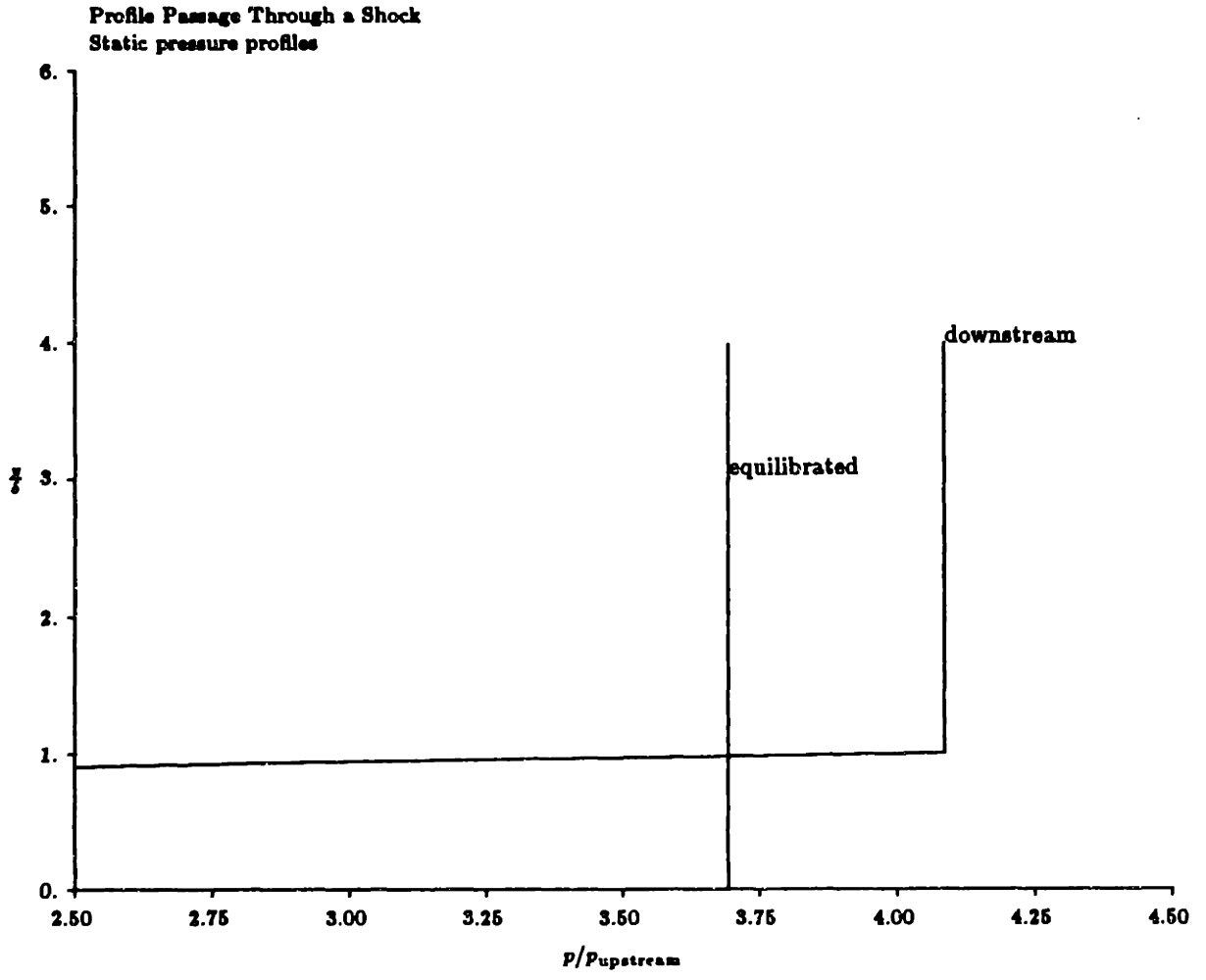

Figure 8.20: Pressure field directly downstream of the shock, and equilibrated normalized to upstream pressure, 5 degree wedge angle, Mach 20

Not surprisingly, the temperature rise across the shock produces an increase in temperature throughout the profile, except near the wall, where the flow is subsonic and there is no shock. The equilibration process raises the temperature in the boundary layer profile.

Figure 8.22 is presented as an example of the shape of the calculated shock through this profile. This was calculated by the method outlined in chapter 7, and is shown here as an indication of the curvature of this shock through the boundary layer profile. The shock does not touch the wall, because the wall region is subsonic. The effect of a shock on a turbulent boundary layer has not been presented because there is essentially no influence from the turbulent boundary layer.

Recall that in chapter 7, the shock problem had to account for the insufficient total pressure of the flow near the wall in the equilibration process, and it was postulated that this flow forms a separation bubble. Since none of the solutions presented here include the separation bubble, the actual flow field will be altered from that shown. This problem will be seen again when a profile is followed through a channel with adverse pressure gradient, and should be kept in mind.

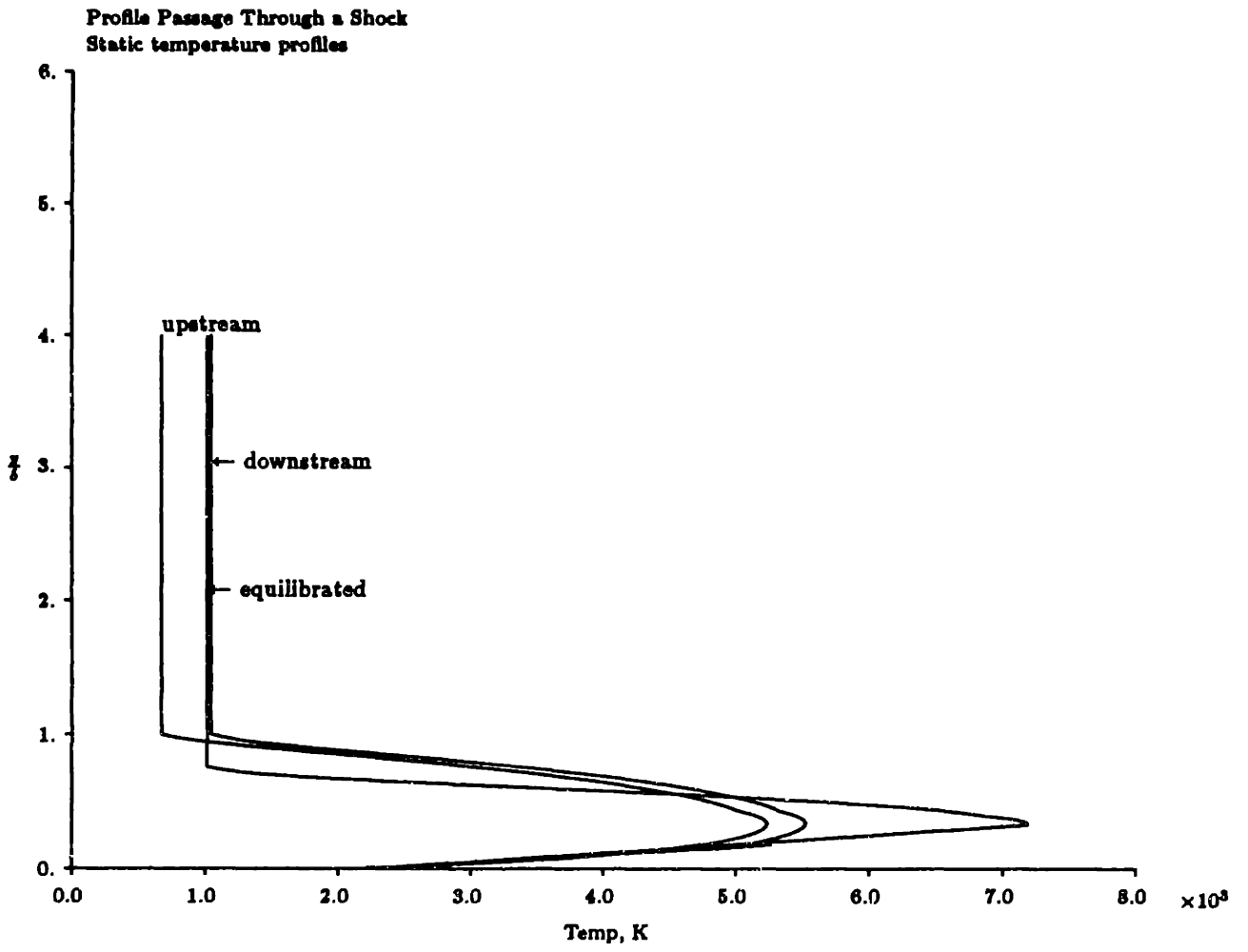

Figure 8.21: Temperature profiles upstream of a shock, immediately downstream, and equilibrated, Mach 20

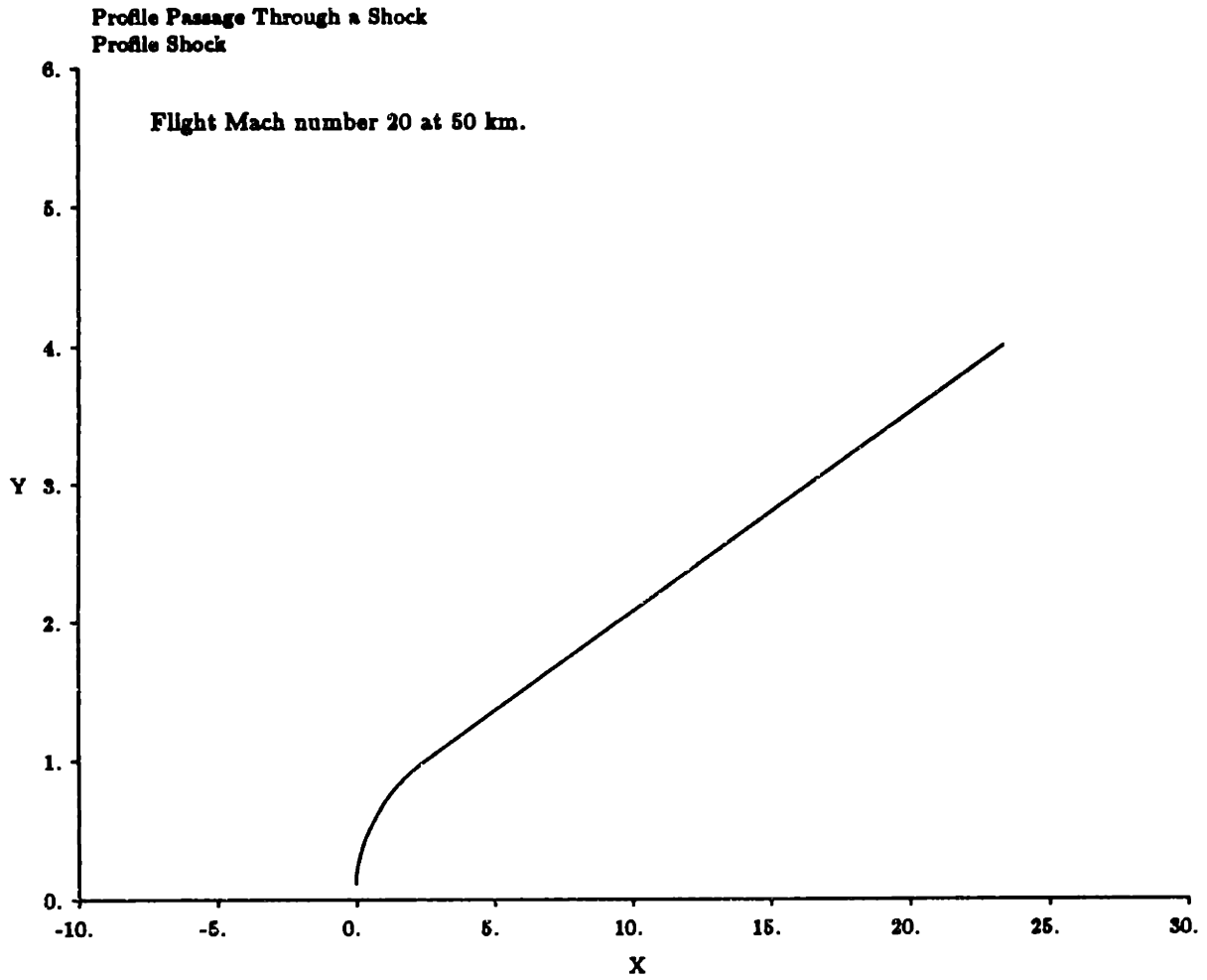

Figure 8.22: Shock through a forebody profile corresponding to Mach 20, 50 km, 5 degree wedge angle

Chapter 9
Profile Changes in a Converging/Diverging Channel

Having examined the effect of a nonuniformity at the inlet station, and used that to predict trends farther downstream, and having looked at how an inlet shock changes the profile, and how that profile affects the flow field, it remains to examine the propagation of such a profile through channels of given geometry and heat addition which model a supersonic combustor. Throughout, the calculated nonuniform behavior will be compared to the analytical solutions for uniform one-dimensional flow.

This study will focus on the middle of the transatmospheric trajectory, in the vicinity of Mach 15, because it is there that thermodynamic changes in the engine can have the most dramatic effects on combustion. At low Mach numbers, the boundary layer entering the engine will be thin enough to have little impact on net engine performance. At the highest Mach numbers, combustion will undoubtedly be impossible to achieve inside the combustor, and enthalpy increase will be derived entirely from the fuel enthalpy and kinetic energy.

9.1 Analytical Development

The simplest channel in which the evolution of a nonuniform profile can be followed is a convergent or divergent isentropic passage. In such a channel, there is no heat addition, so that flow properties change only through the action of the varying channel area. This might correspond to a converging section leading into the combustor region, or an expanding channel behind the combustor, leading into the nozzle.

Repeating the equation for area ratio between two stations, A_1 and A_2 at respective Mach numbers M_1 and M_2 in isentropic flow [34]:

$$\frac{A_2}{A_1} = \frac{M_1}{M_2}\left(\frac{1+\frac{\gamma-1}{2}M_2^2}{1+\frac{\gamma-1}{2}M_1^2}\right)^{\frac{\gamma+1}{2(\gamma-1)}} \tag{9.1}$$

It is not generally possible to solve for Mach number in terms of area in closed form. However, with some given initial conditions, the area can be determined as a function of Mach number. The area at any position x as a function of the initial conditions at station 1 is:

$$A(x) = A_1\frac{M_1}{M(x)}\left(\frac{1+\frac{\gamma-1}{2}M(x)^2}{1+\frac{\gamma-1}{2}M_1^2}\right)^{\frac{\gamma+1}{2(\gamma-1)}} \tag{9.2}$$

To study a profile propagating through the channel, dA/dx must be specified. This streamwise derivative of channel area is solved from an assumed Mach number profile. An exponential profile is convenient and will be used here. The same nomenclature that was introduced in chapter 5 and Appendix B will be used, though the characteristic length parameter is not related to heating in the present case, since there is no heat addition:

$$M(x) = M_1 e^{-x/2\lambda_D} \tag{9.3}$$

for positive λ_D, the Mach number is dropping, and the channel is divergent if supersonic. If λ_D is negative, Mach number is increasing and the channel is converging if supersonic. The distance required to reach a desired Mach number is:

$$\frac{x_{\text{final}}}{\lambda_D} = 2\ln\left(\frac{M_1}{M_{\text{final}}}\right) \tag{9.4}$$

The area profile is then a function of the streamwise coordinate:

$$A(x) = A_1 e^{x/2\lambda_D}\left(\frac{1+\frac{\gamma-1}{2}M_1^2 e^{-x/\lambda_D}}{1+\frac{\gamma-1}{2}M_1^2}\right)^{\frac{\gamma+1}{2(\gamma-1)}} \tag{9.5}$$

and the streamwise derivative of area is

$$\frac{dA_2}{dx} = \frac{A_2}{\lambda_D}\left[\frac{e^{x/\lambda_D} - M_1^2}{2e^{x/\lambda_D} + (\gamma-1)M_1^2}\right] \tag{9.6}$$

The throat is located at:

$$x_{throat} = 2\lambda_D \ln M_1 \tag{9.7}$$

Since total temperature is constant, the static temperature between station 1 and station 2 in the channel is simply:

$$\frac{T_2}{T_1} = \frac{1 + \frac{\gamma-1}{2} M_1^2}{1 + \frac{\gamma-1}{2} M_2^2} \tag{9.8}$$

so with the exponential profile, the temperature at any x position is

$$T(x) = T_1 \frac{1 + \frac{\gamma-1}{2} M_1^2}{1 + \frac{\gamma-1}{2} M_1^2 e^{-x/\lambda_D}} \tag{9.9}$$

and the pressure is

$$P(x) = P_1 \left(\frac{1 + \frac{\gamma-1}{2} M_1^2}{1 + \frac{\gamma-1}{2} M_1^2 e^{-x/\lambda_D}} \right)^{\gamma/(\gamma-1)} \tag{9.10}$$

It is more useful to limit temperature at the end of the channel. The non-dimensionalized length of the channel in terms of temperature is defined with equation (9.9):

$$\frac{x_{\text{final}}}{\lambda_D} = \ln \left(\frac{T_{\text{final}} \frac{\gamma-1}{2} M_1^2}{T_1 \left(1 + \frac{\gamma-1}{2} M_1^2 \right) - T_{\text{final}}} \right) \tag{9.11}$$

9.2 Numerical Results

The above description of Mach number and temperature can be used as a baseline for comparison to the behavior of the nonuniform flow. Channels will be designed for uniform inlet at the free-stream Mach number, then compared to the flow performance with profiles representative of forebody boundary layers at typical transatmospheric flight conditions.

The profile for Mach 20 flight at 50 km, shown in the previous chapter, has been input to a channel designed to take uniform flow for the initial static temperature of 673 K (on the forebody) to a precombustion temperature of 950 K. It was assumed that the boundary layer comprised 25 % of the inlet flow. With a wedge angle of 5 degrees at the forebody, the inlet Mach number is 13.3 under the assumed flight conditions.

The boundary layer height is plotted against the channel height in Figure 9.1. The resulting evolution of the Mach number profile is depicted in Figure 9.2, which shows the Mach number profile at five stations along the converging channel. Station coordinates are presented non-dimensionalized to the design length, λ_D. The profiles are shown in actual

non- dimensionalized height, referenced to the *initial* boundary layer height. The channel wall that continues the vehicle forebody is always at the zero position.

Figure 9.2 demonstrates that, in the adverse pressure gradient of a converging channel, the boundary layer profile tends to steepen, meaning that uniform Mach number, $\overline{M}$ through the boundary layer, gets smaller. This depends on the fact that the flow is still compound supersonic, because if it were compound subsonic, the pressure gradient would be favorable.

This steepening boundary layer once again raises the issue of separation, and it is appropriate to deal with that question here. When the flow through a shock was considered, it was shown that the boundary layer attempts to decelerate and rise to an equilibrated pressure, but since the total pressure near the wall is insufficient to accomplish this, it must separate. In fact, there is another scenario, which was ruled out because of the small time scales involved in reequilibration of the shock-induced pressure gradient in which the flow near the wall has its total pressure raised from work done on it by streamtubes farther out in the flow, acting through viscous transport.

In solving for the channel flow problem with the no-slip wall condition, a viscous function has been introduced to cancel the streamwise pressure gradient at the wall. This function assumes that viscous interactions between the wall streamtubes and those adjacent are always sufficient to fight an adverse pressure gradient. Thus, in making this assumption, it is tacitly assumed that there will be no separation, because every profile, no matter how steep, will be carried along by viscous interactions with the rest of the flow.

The calculations presented in this section experienced numerical integration instabilities that are related to the actual physics of separation. In carrying a profile through the channel, the analytical code used to generate these figures applies a very simple Euler forward method to update each streamtube Mach number by its local derivative. If the spacing between stations is too large, the Mach number derivative in an adverse gradient can become larger than the local Mach number, so at the next station, Mach number is negative. When the station spacing is small enough, the viscous assumption is sufficient to always match the requirement of fighting the adverse gradient, so this instability is not seen.

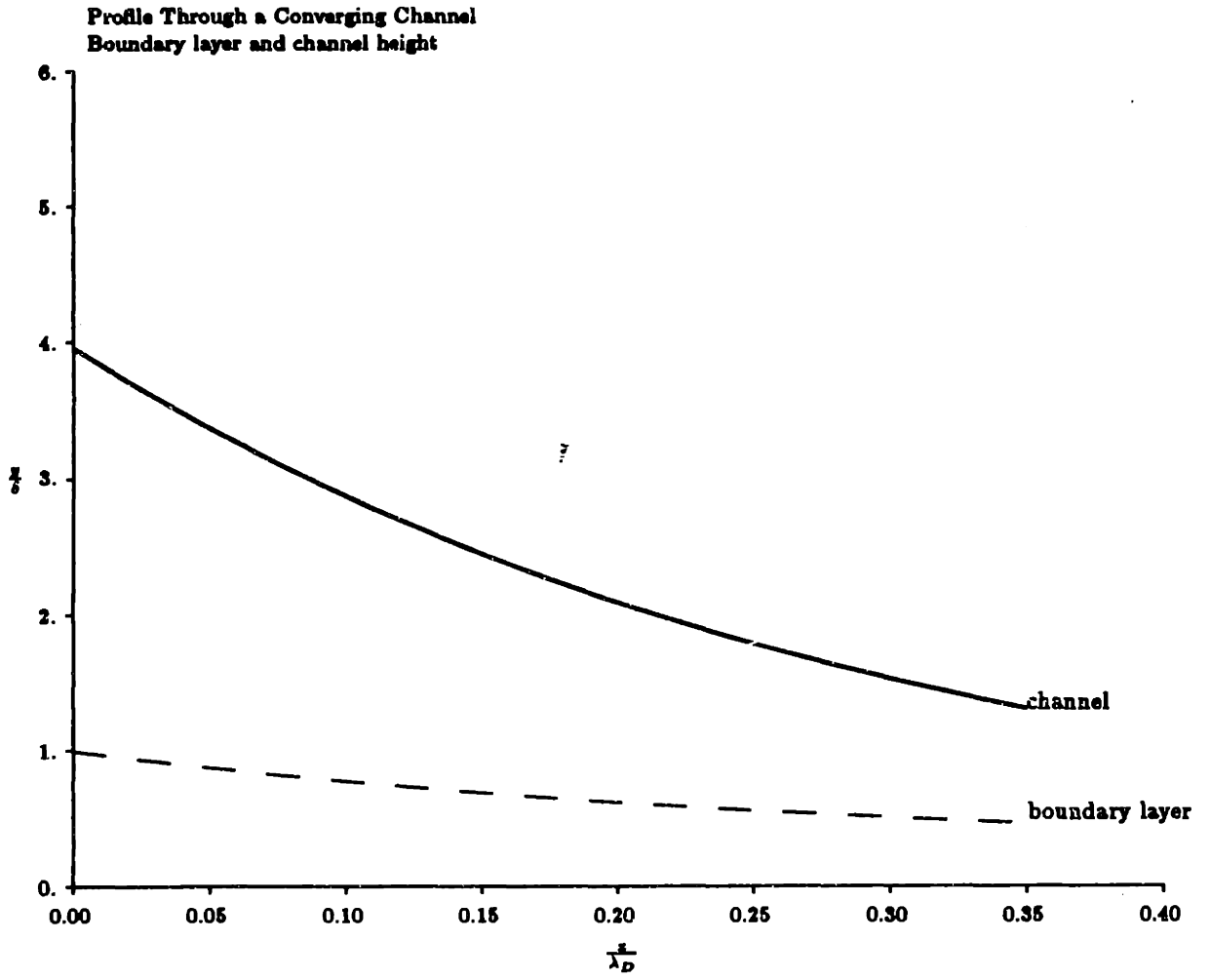

Figure 9.1: Boundary layer height and channel height for a converging channel for Mach 20 flight at 50 km.

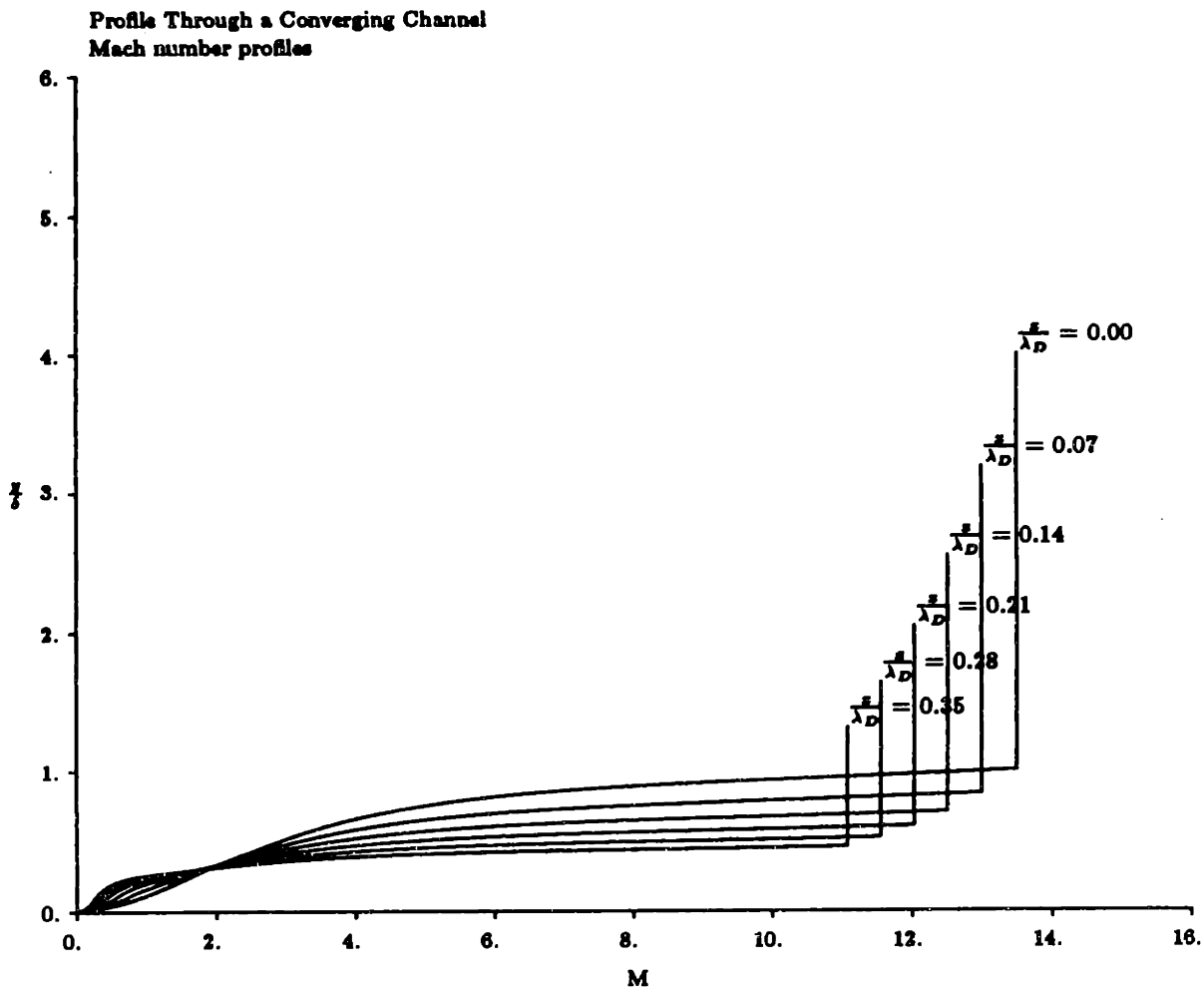

Figure 9.2: Mach number profile at various stations in a converging channel, for Mach 20 flight at 50 km.

This numerical phenomenon is modelling the separation effect; if the profile steepening happens gradually enough that there is enough time for work to be done on the near-wall streamtubes through viscous interactions, the flow will not separate. However, if the pressure gradient is so large that pressure changes occur faster than viscous interactions can counteract them, we can expect separation. This is why it was assumed that the flow behind the shock will separate, but that the flow in an engine channel may not if the channel area changes gradually enough. It also suggests that a sudden rise in pressure inside the combustor will have more likelihood of inducing separation, a phenomenon which will be approached later in this chapter.

The Mach number plots in Figure 9.2 show the growth of the boundary layer *relative* to the channel. The boundary layer height changes very little over the entire channel length, so almost all of the channel area change is accommodated by the free-stream, not the boundary layer, and this effectively increases dA/A in the free-stream. This effect was predicted from the studies of flow at the inlet station, from the derivative of relative boundary layer height with respect to channel height.

In accordance with this nearly constant boundary layer height, the uniform Mach number in the boundary layer is rather constant, as shown by the bottom line in Figure 9.3. This is not surprising since it was found analytically in chapter 8, and numerically at the inlet station, that the boundary layer net Mach number for an actual profile tends to change more slowly than that for a uniform streamtube. This is in spite of the obvious steepening of the Mach number profile, because the contribution of the very lowest velocity regions to the uniform Mach number are cancelled by the no-slip viscous assumption.

Also shown in Figure 9.3 are the actual free-stream Mach number, the predicted uniform Mach number for this channel design, and the net Mach number that characterizes the entire channel, boundary layer and free-stream combined. The effect of the boundary layer has been to reduce the free-stream Mach number only slightly below that of the predicted uniform value in this case. This slight effect is important to the thermodynamic conditions, which are very sensitive functions of Mach number at high Mach number, as was pointed out in section 1.2. The relative insensitivity of free-stream Mach number to the effect of

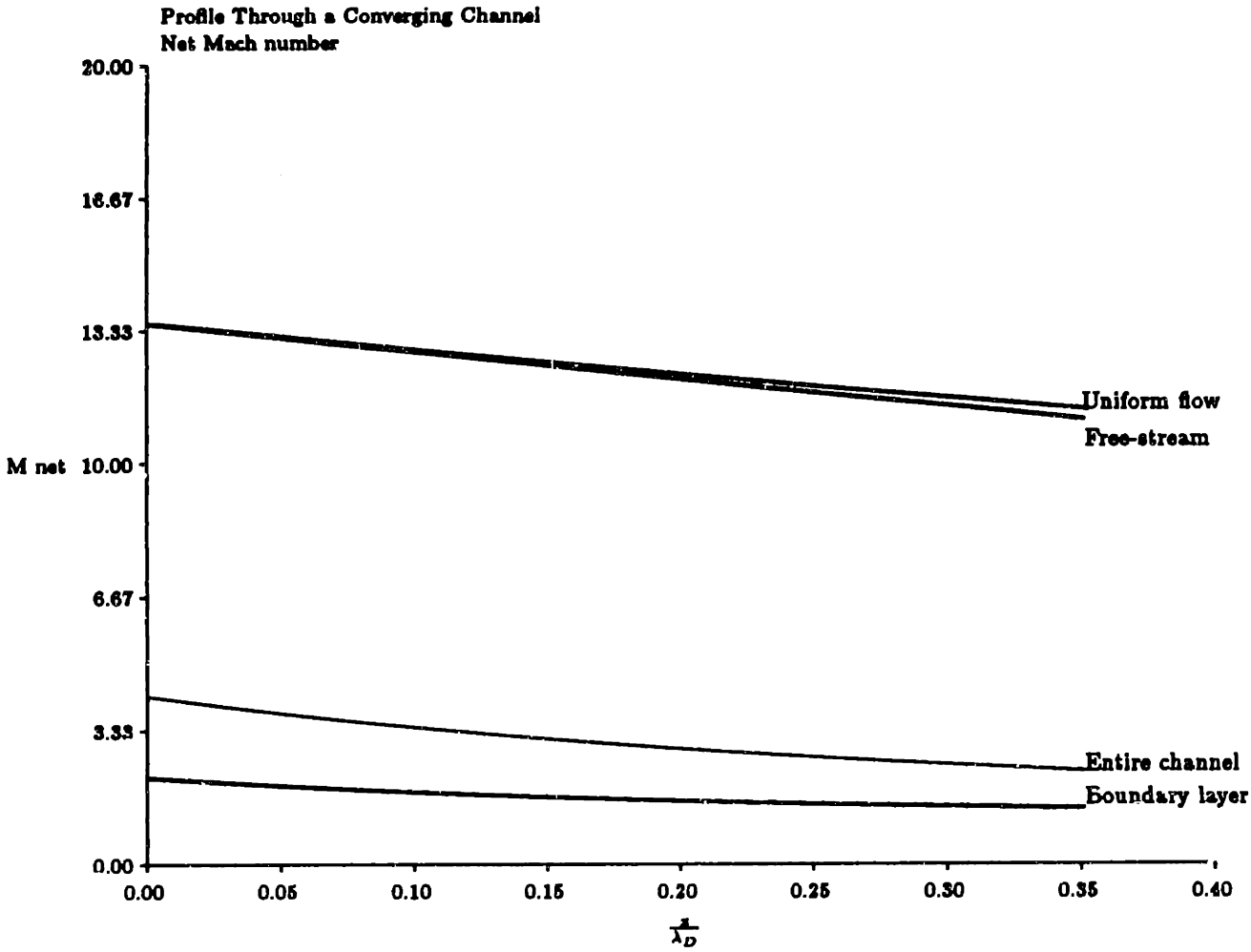

Figure 9.3: Uniform Mach numbers for entire channel and boundary layer compared to free-stream Mach number and expected uniform inlet Mach number for Mach 20 flight at 50 km.

the boundary layer is easily seen from the influence coefficient expression for the change in Mach number for a given change in channel area:

$$\frac{dM}{M} = -\frac{1 + \frac{\gamma-1}{2}M^2}{1 - M^2}\frac{dA}{A} \tag{9.12}$$

which, in the hypersonic limit, yields:

$$\frac{dM}{M} \simeq \frac{\gamma - 1}{2}\frac{dA}{A} \tag{9.13}$$

The most dramatic effect of a slight drop in Mach number is a 20 % rise in static pressure, as shown in Figure 9.4. Also in the figure are the static pressure profiles in the same channel for uniform flow at Mach 3 and Mach 4 at the inlet. These Mach numbers were chosen because the uniform Mach number for the entire channel is in the vicinity of Mach 4, but as seen in the plot, assuming that the flow thermodynamics is that of a Mach 4 flow does not yield the correct result. Indeed, the Mach 3 solution is closer to the profile solution, suggesting that the net channel behavior is that of an even lower velocity flow than the prediction of the uniform Mach number at the inlet. The initial area-averaged Mach number at is 11.4, so that gives a poor indication of the flow behavior. Once again, it is worth noting that averaging of flow properties is unjustified.

Figure 9.5 presents the static temperature in the free-stream with the profile, and for uniform flow at the initial free- stream Mach number in the same channel. The small drop in free-stream Mach number has produced a noticeable change in temperature, though not nearly as dramatic as that in temperature, as would be expected from the simple analysis of chapter 2.

Figure 9.6 shows the static temperature profiles at the same non-dimensionalized streamwise stations as the Mach number profiles of Figure 9.2. The temperature profile of this channel flow steepens, and the peak temperature rises substantially, with the compression process. This model does not account for dissociation effects, and the high temperatures shown are likely to be diminished by dissociation reactions, but the trend towards higher temperatures, a steeper profile, and thus more heat transfer in the decelerating profile are worth noting.

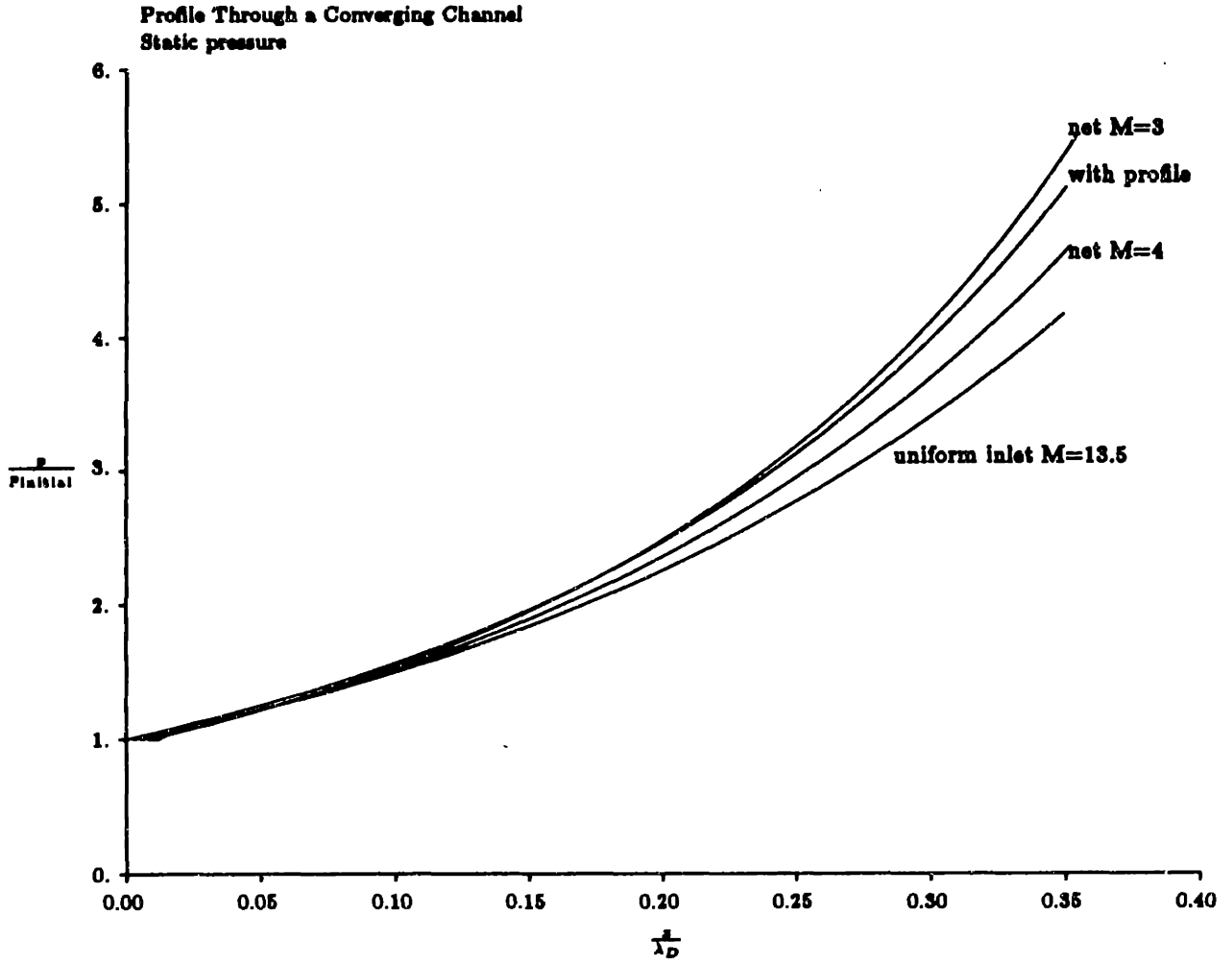

Figure 9.4: Static pressure with Mach 20, 50 km. profile and uniform flow

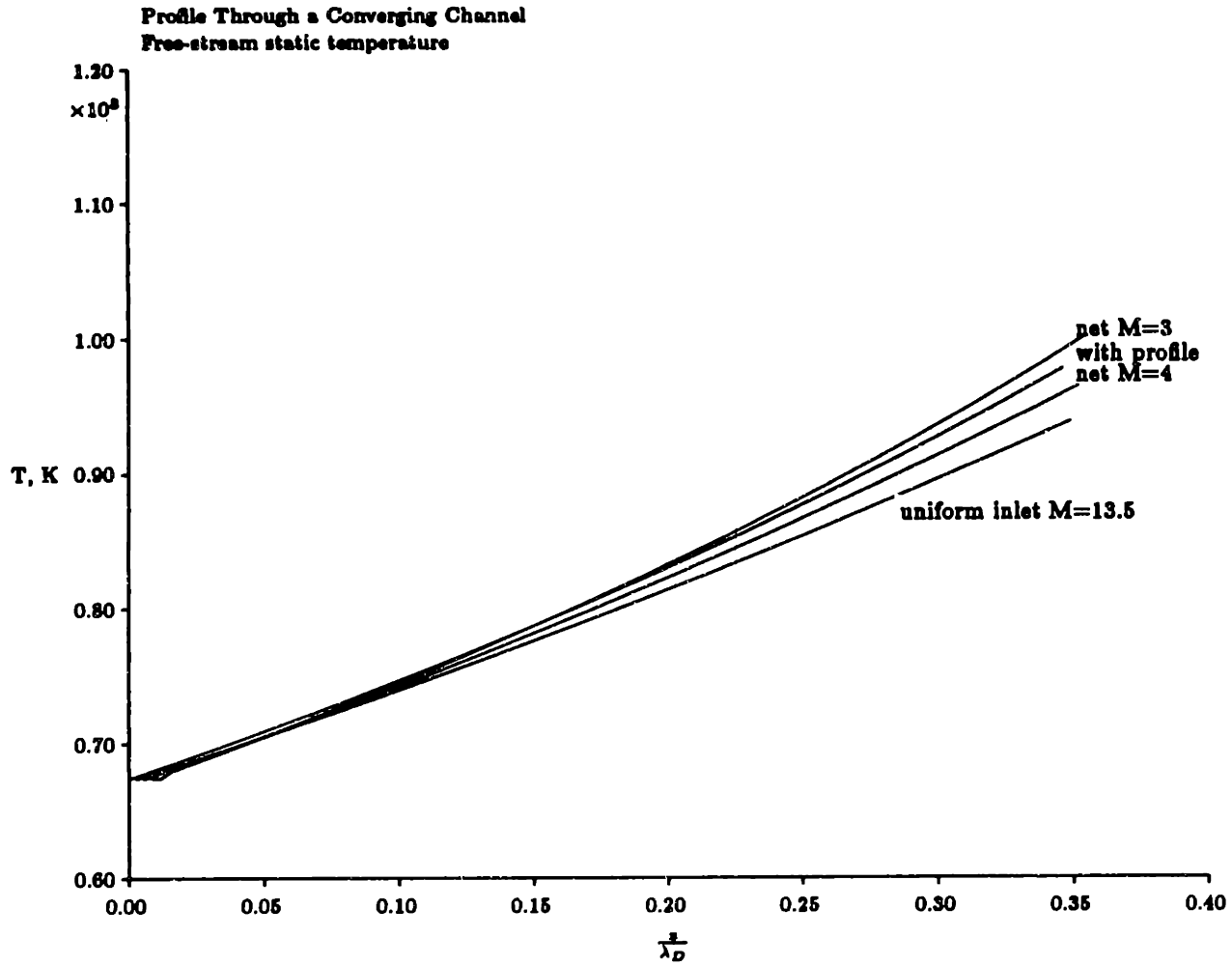

Figure 9.5: Static temperature with Mach 20, 50 km. profile and uniform flow

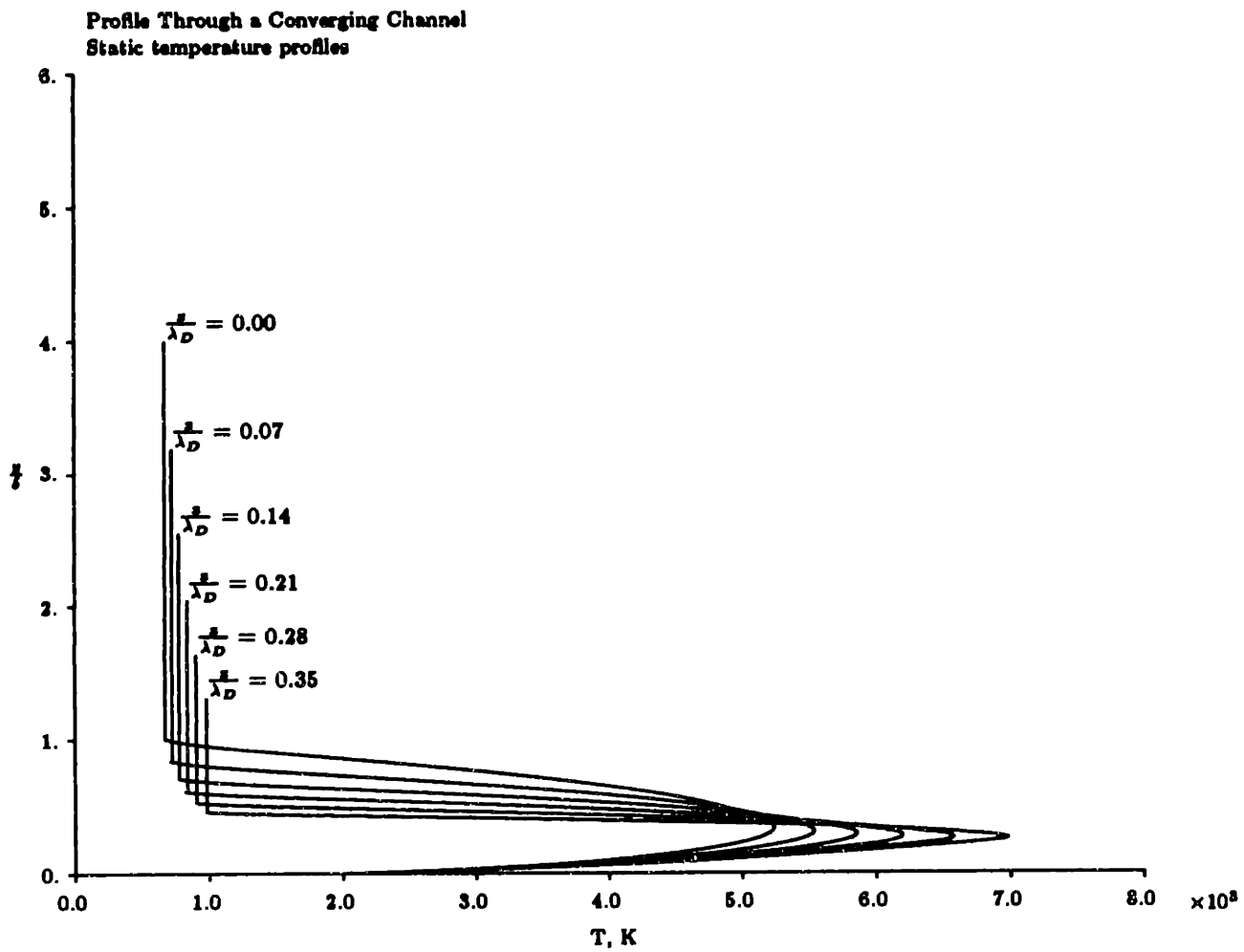

Figure 9.6: Temperature profile at various stations in a converging channel, for Mach 20 flight at 50 km.

For the same flight conditions with turbulent boundary layer, the profile has much less dramatic results if the boundary layer is turbulent. Figure 9.7 shows the Mach number and temperature profiles corresponding to flight at Mach 20, 50 km altitude, with a 5 degree wedge angle.

Sending this profile into the same channel as that used with a laminar boundary layer, and assuming the same boundary layer thickness, little change is seen in channel properties over those expected for uniform inflow. In fact, turbulent boundary layers will tend to be thinner than their laminar counterparts because turbulent eddy viscosity does not rise with temperature, so that assumption is a worst-case scenario. Figures 9.8 and 9.9 present the static pressure and temperature down the channel, which compare very closely to the expected values for uniform flow. Figure 9.10 presents the Mach number profiles at various stations along the channel.

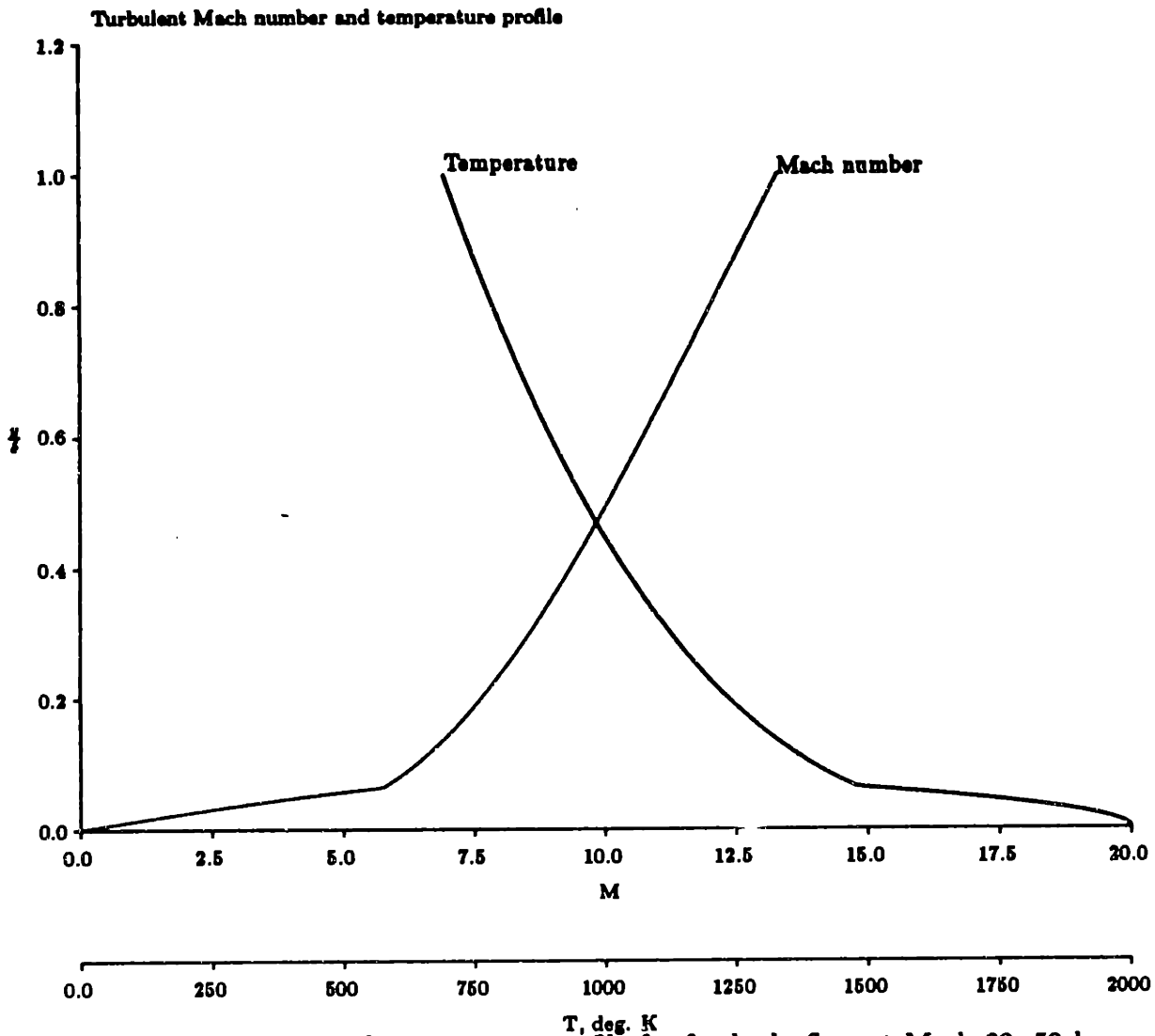

Figure 9.7: Mach number and temperature profile for forebody flow at Mach 20, 50 km altitude, with turbulent boundary layer

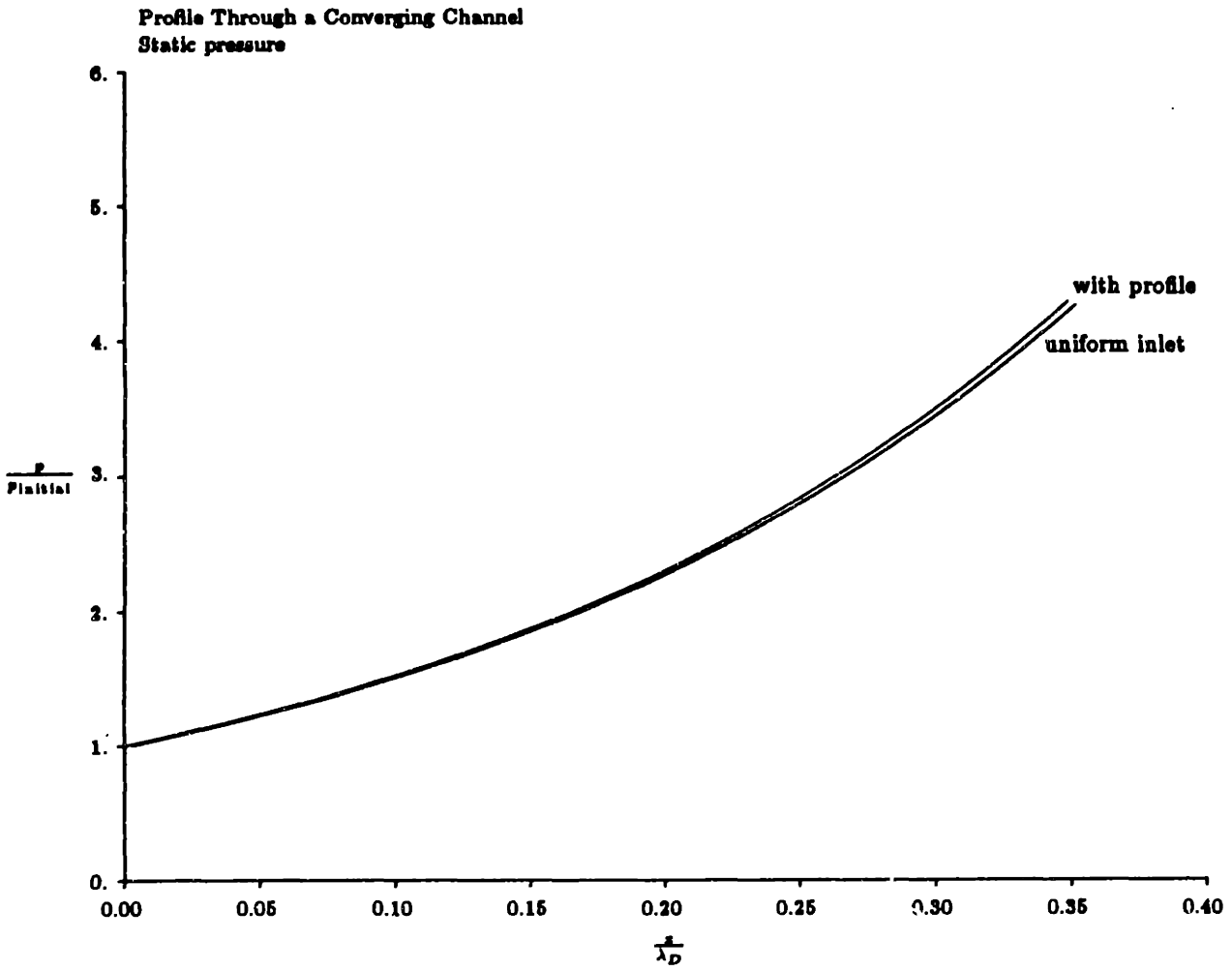

Figure 9.8: Static pressure with Mach 20, 50 km. profile and uniform flow for turbulent boundary layer

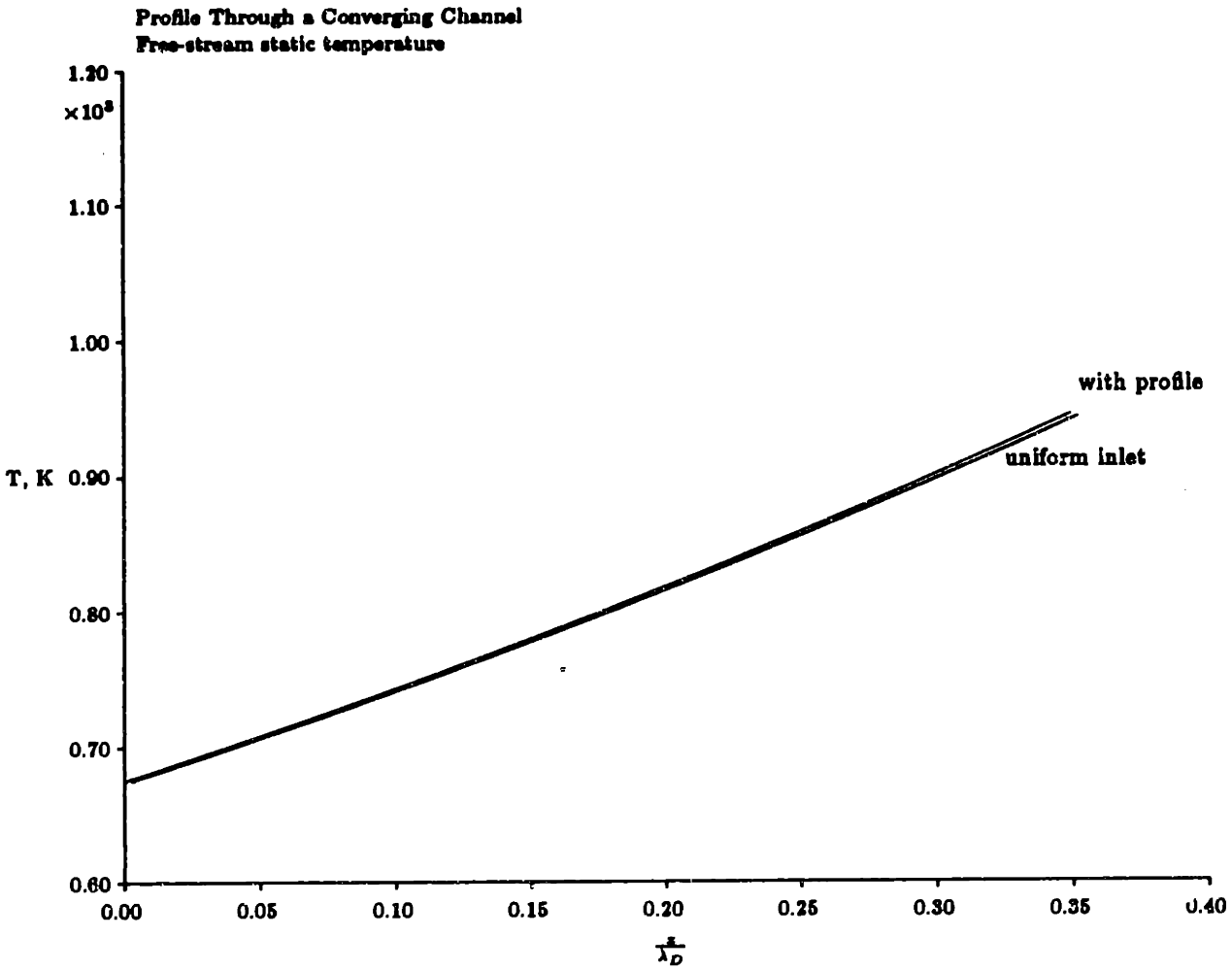

Figure 9.9: Static temperature with Mach 20, 50 km. profile and uniform flow with turbulent boundary layer

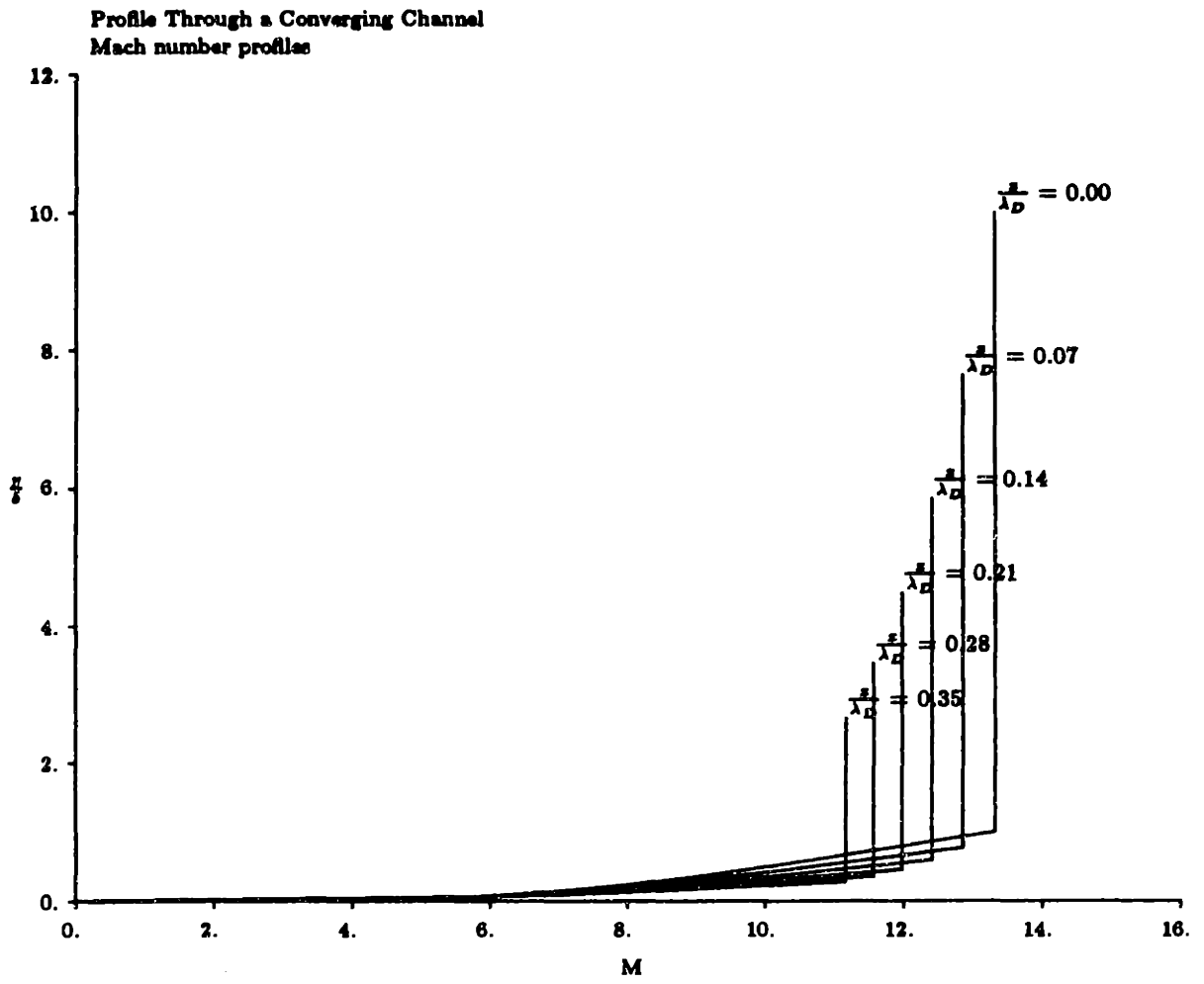

Figure 9.10: Mach number profile at various stations in a converging channel, for Mach 20 flight at 50 km., turbulent boundary layer

Not surprisingly, the fuller turbulent profile produces much less dramatic changes in the thermodynamic properties because it is nearly uniform, which is exactly as was predicted by examining the inlet station at the beginning of this chapter. Figure 9.12 presents the uniform Mach number for the boundary layer, the entire channel, and the free-stream Mach number. The expected Mach number for a uniform channel is not shown on this plot because it is so close to the actual free-stream value. As expected, the net Mach number for the boundary layer is quite high (much higher than in the laminar case) so the net Mach number of the entire channel is close to the uniform value. As shown in Figure 9.11, the turbulent boundary layer remains in almost the same proportion to channel area that it starts with, so the value of the logarithmic derivative of area in the free-stream, dA/A, is nearly identical to that for the entire channel.

As a further example of flow in a converging channel, the behavior of a profile that is typical of lower Mach number flight is considered. The profile for Mach 10 flight at 30 km altitude and laminar boundary layer profile is input to a channel designed to raise it from the initial 312 K to 950 K, and ignoring the consequences of the extremely high pressure rise associated with this process. It is assumed that the profile begins as 4% of the shock layer thickness.

As shown in Figure 9.13, the boundary layer thickness remains nearly constant. Figure 9.14 shows the Mach number contours for this flow. In order to accomplish this temperature rise, a substantial decrease in area is required. The consequences of this are that the boundary layer uniform Mach number, which is quite low, quickly dominates the entire flow, as is apparent in Figure 9.15. The resulting extra compression of the free-stream results in a final static pressure that is about twice the value obtained with the uniform flow design conditions, as shown in Figure 9.16, and a static temperature that is about 20% higher than for uniform inflow, presented in Figure 9.17.

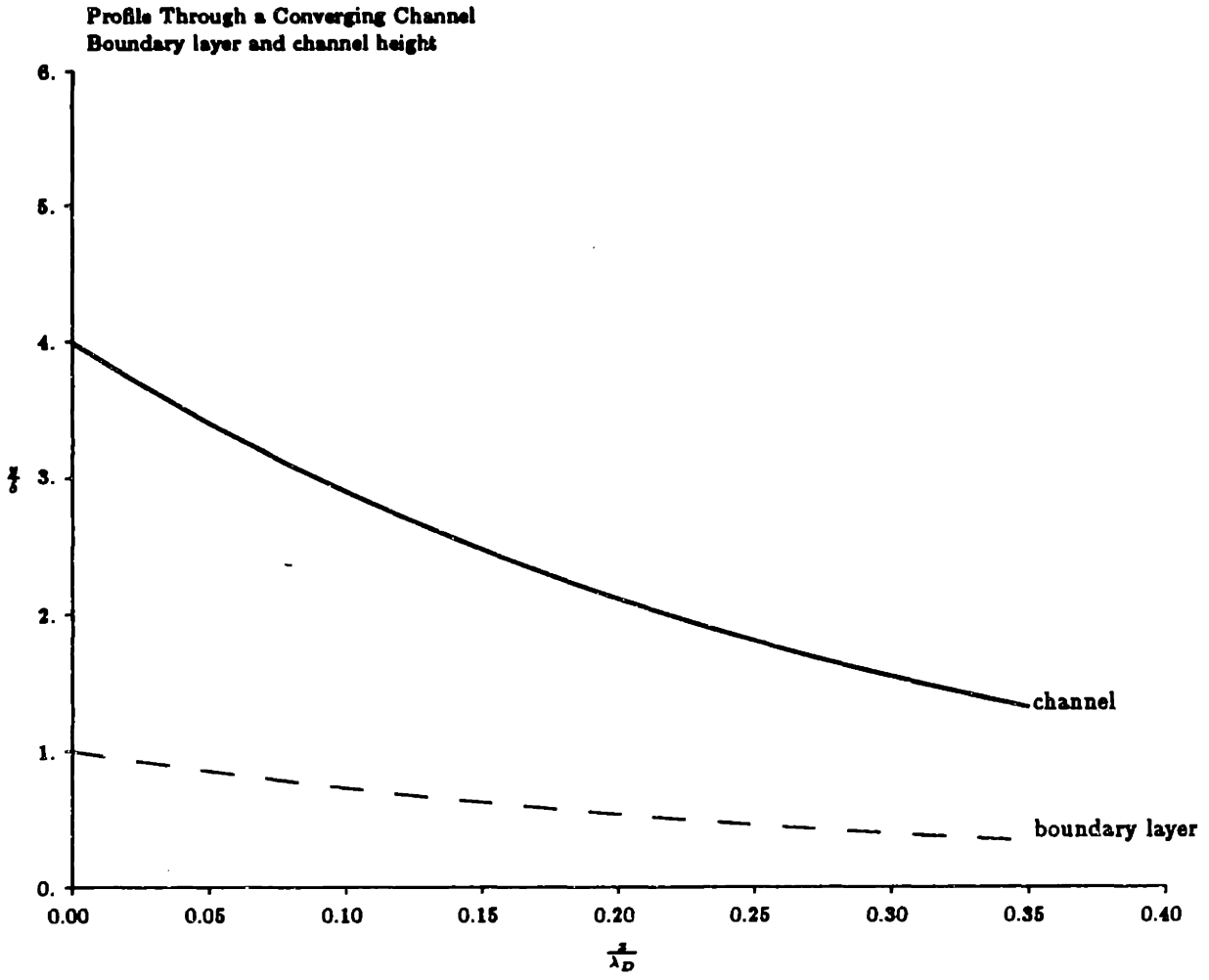

Figure 9.11: Boundary layer height and channel height for a converging channel for Mach 20 flight at 50 km., turbulent boundary layer

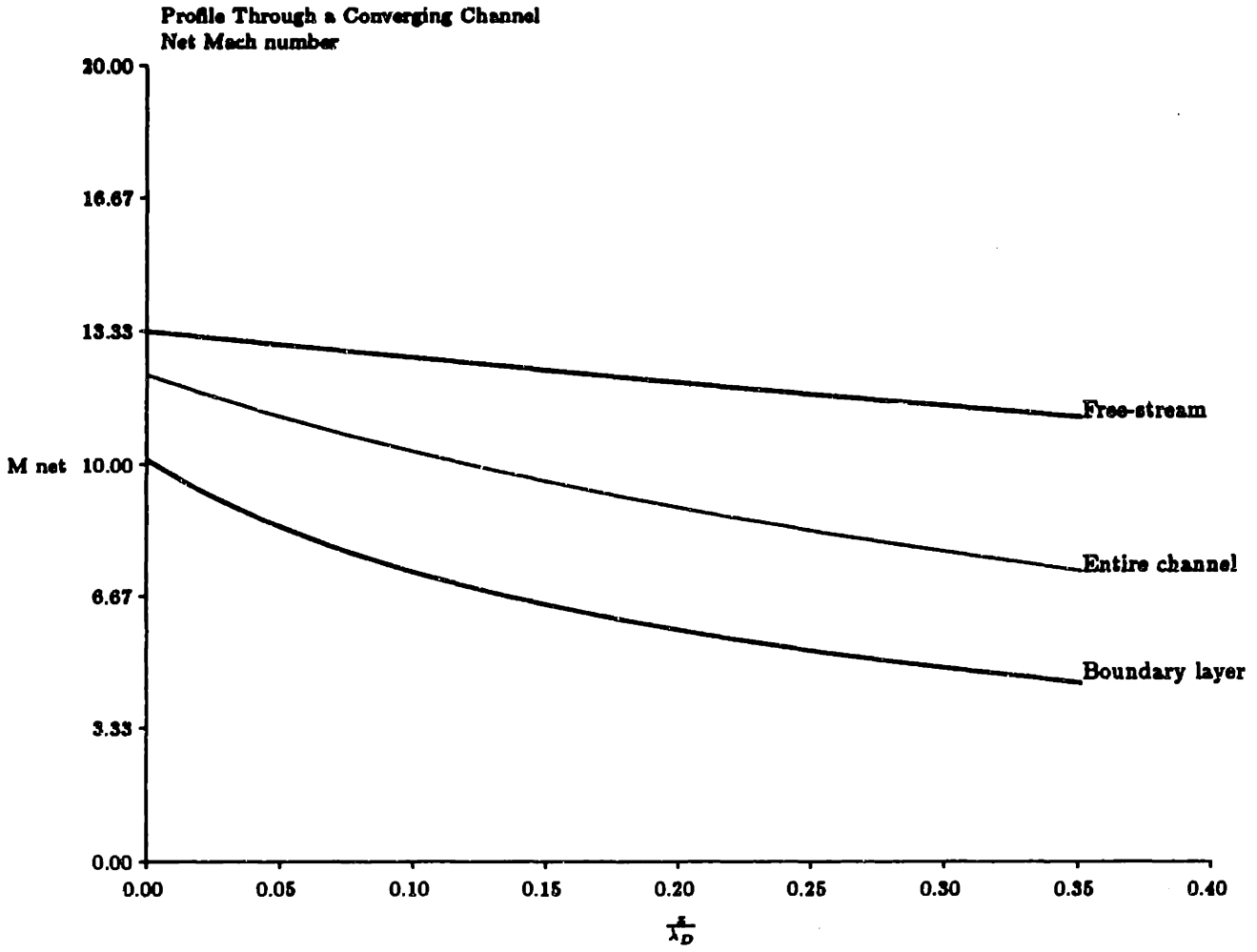

Figure 9.12: Uniform Mach numbers for entire channel and boundary layer compared to free-stream Mach number for Mach 20 flight at 50 km., turbulent boundary layer

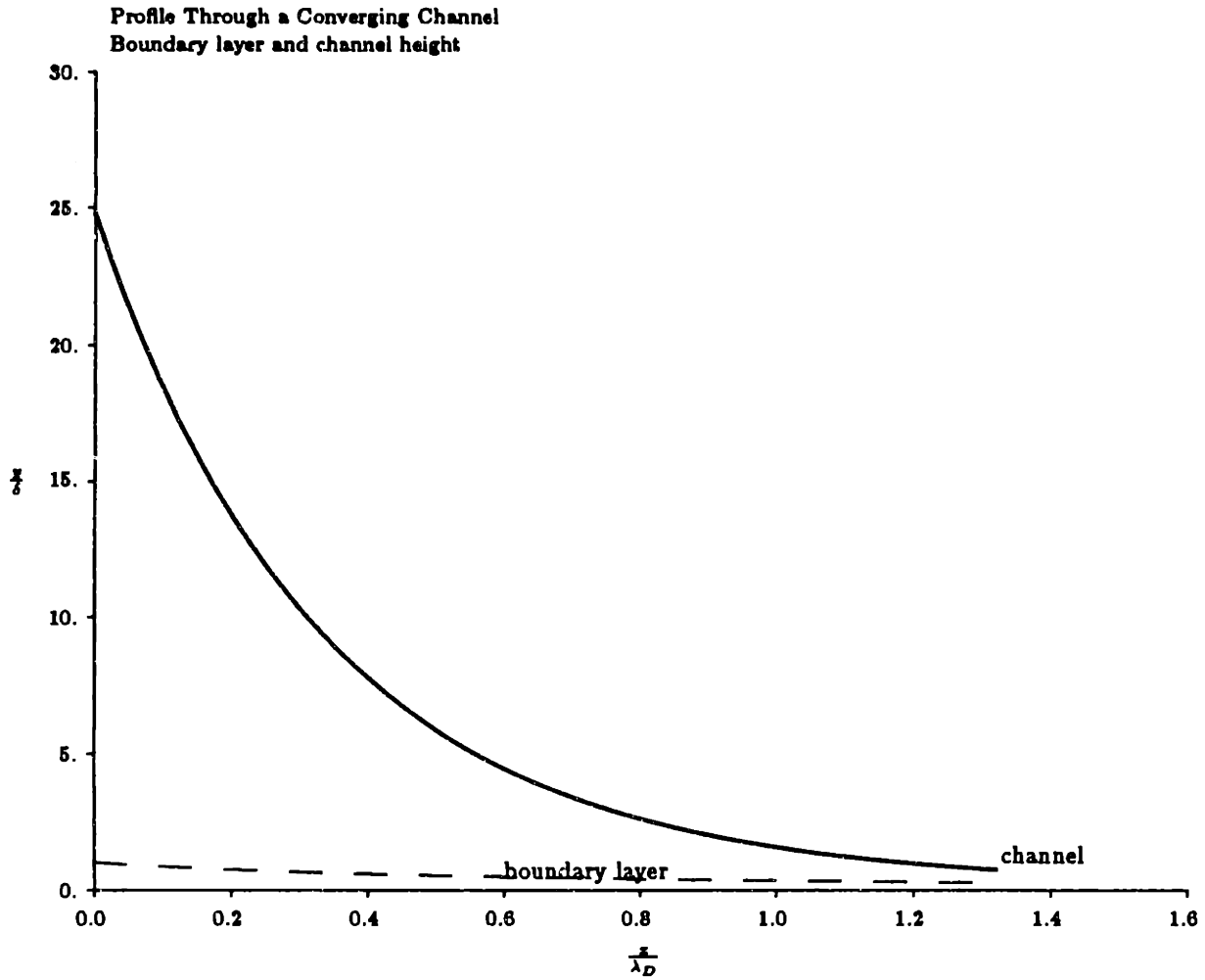

Figure 9.13: Boundary layer height and channel height for a converging channel for Mach 10 flight at 30 km., laminar boundary layer

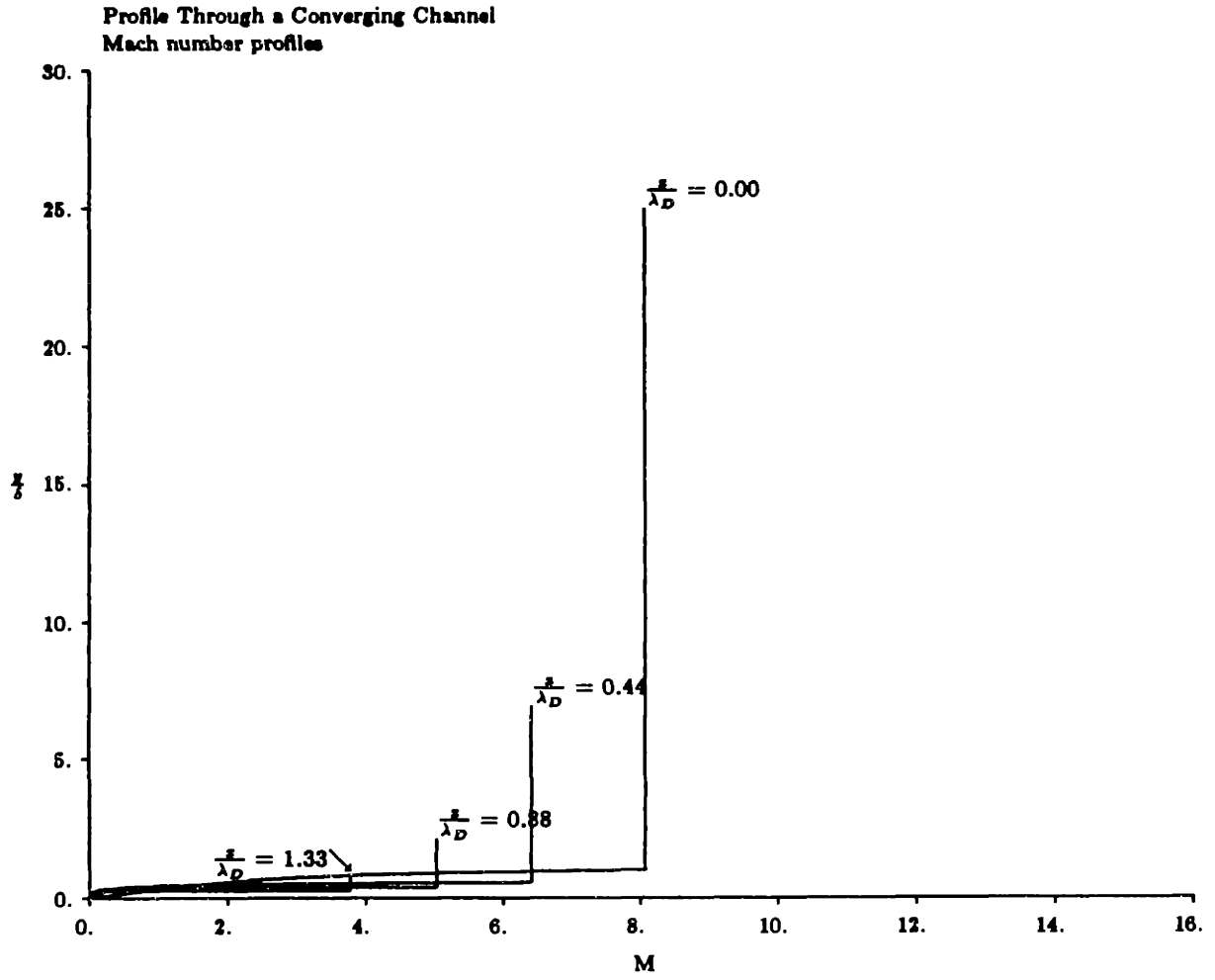

Figure 9.14: Mach number profile at various stations in a converging channel, for Mach 10 flight at 30 km., laminar boundary layer

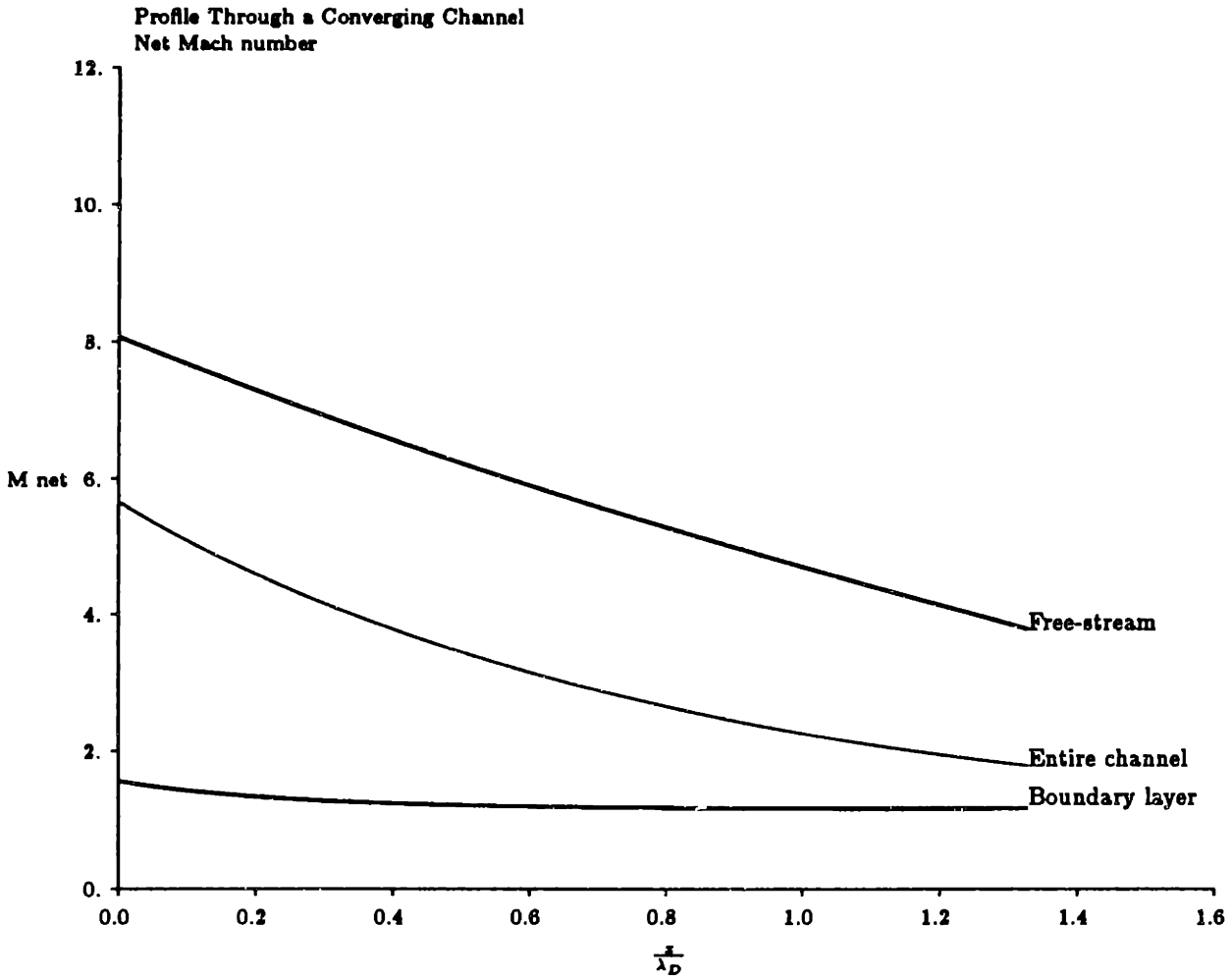

Figure 9.15: Uniform Mach numbers for entire channel and boundary layer compared to free-stream Mach number for Mach 10 flight at 30 km., laminar boundary layer

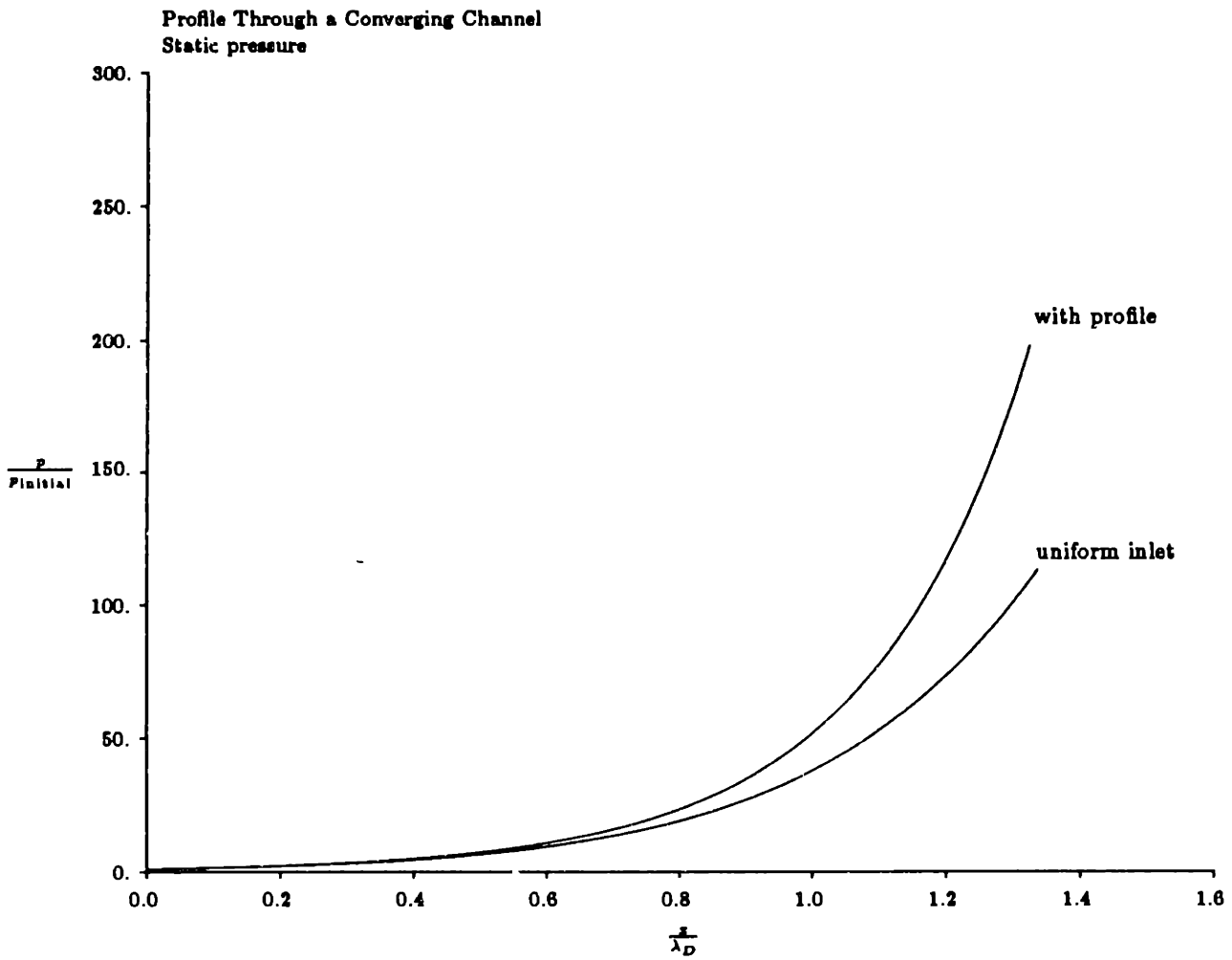

Figure 9.16: Static pressure with Mach 10, 30 km. profile and uniform flow for laminar boundary layer

As an extreme example of the boundary layer influence in an isentropic channel, the behavior of flow with a profile in a converging channel that has been designed to bring the uniform fre-stream Mach number from 4.2 to 1.3 is examined. This would be characteristic of a channel designed to raise the static temperature to 1000 K for flight at Mach 6, 20 km. Figure 9.18 shows the free-stream Mach number of the flow with a 5% boundary layer compared to a uniform inlet. The presence of the boundary layer drops the free-stream Mach number to unity, choking the flow even though the uniform flow is not choked.

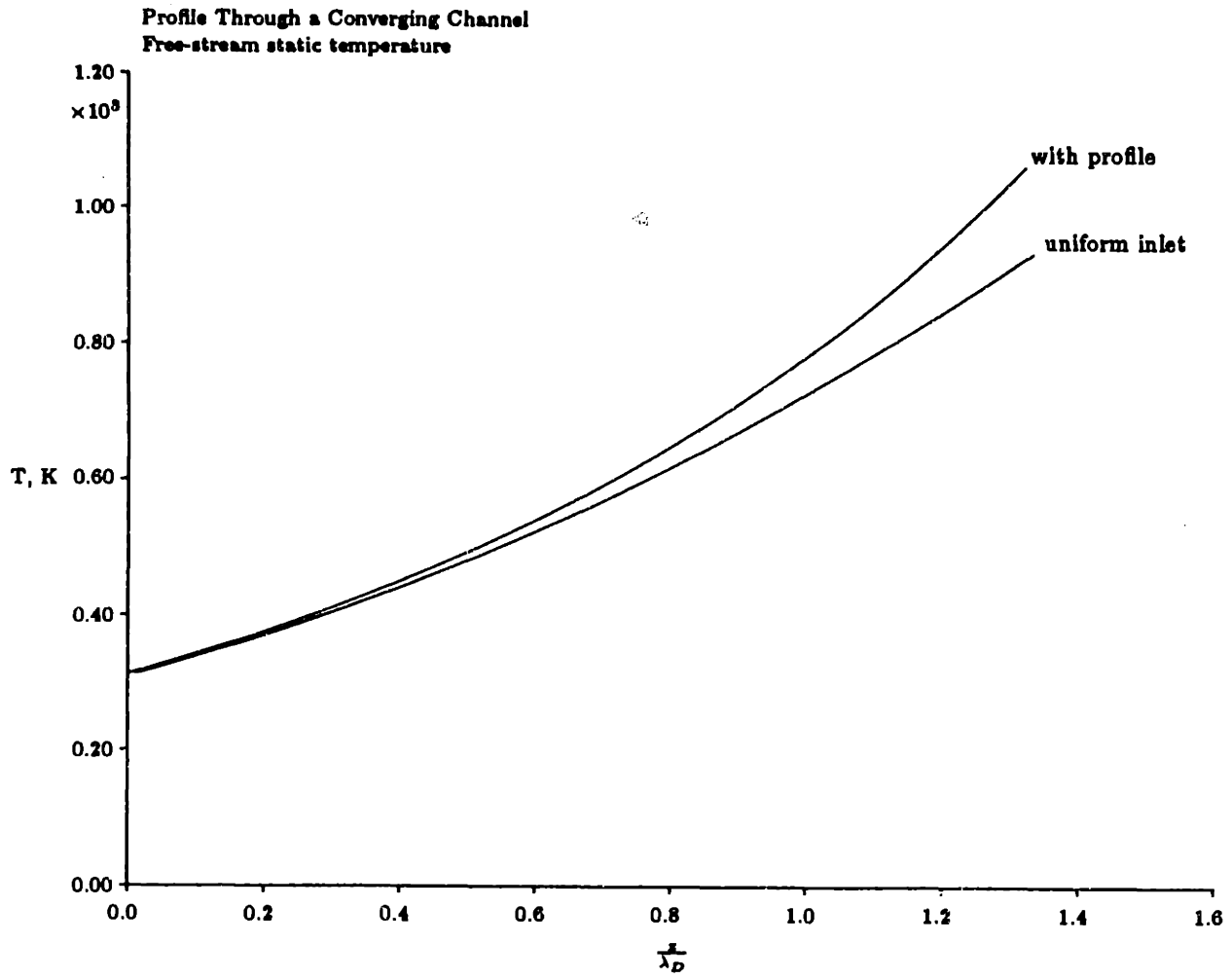

Figure 9.17: Static temperature with Mach 10, 30 km. profile and uniform flow with laminar boundary layer

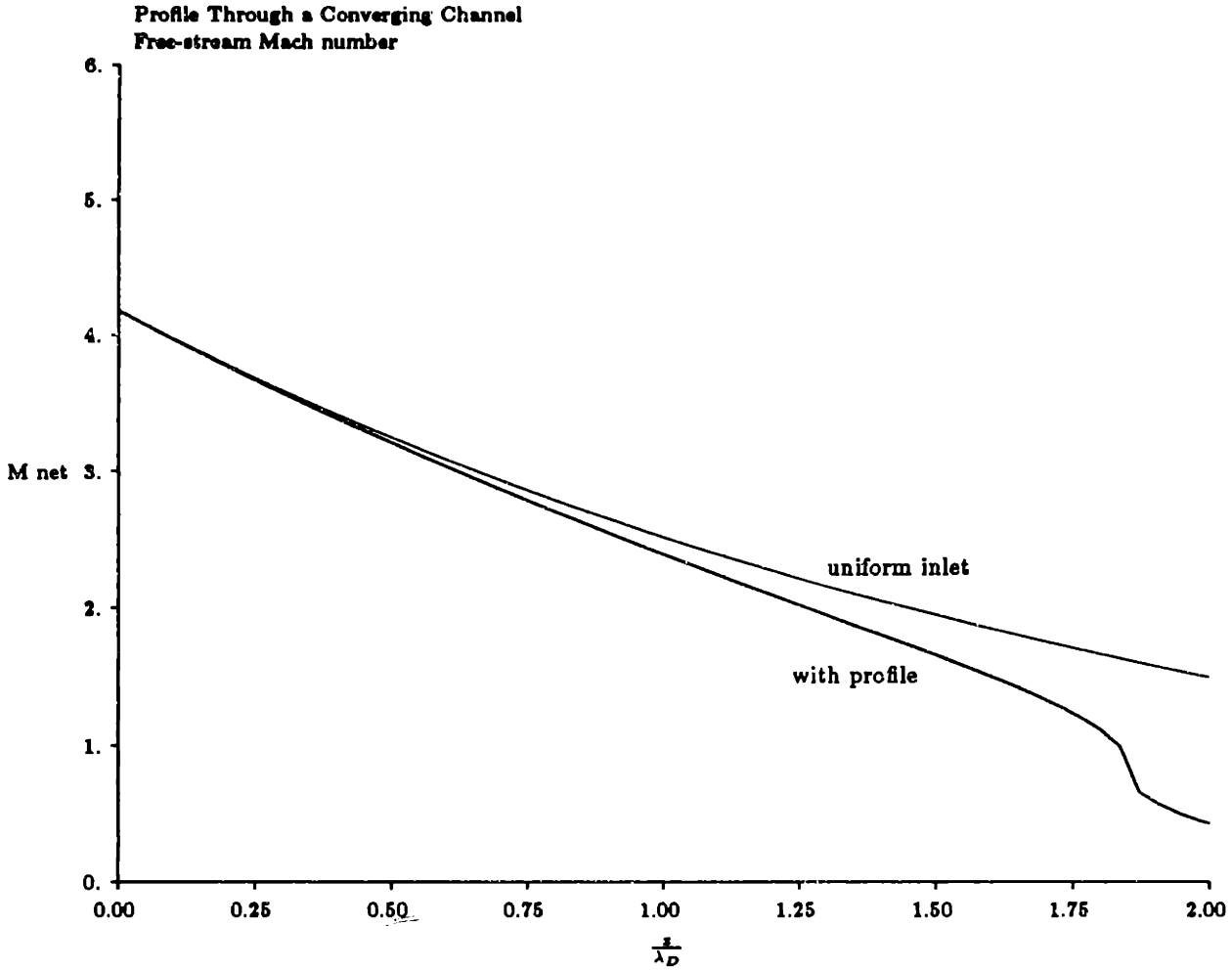

Figure 9.18: Convergent channel flow choked by the boundary layer influence

Chapter 10
Analytical Models of Combustor Performance with Uniform Flow

The culmination of this work will be the study of a profile through a combustor channel, and the resulting effect on thermodynamic properties and the combustion process. Before this is presented, analytical models of combustor performance for *uniform* inlet conditions will be compared. These will serve as a basis of comparison to calculated behavior with the inlet profile. In addition, the analytical designs will be used to set the basic geometry and heating profiles of the combustor channels to be used in the numerical solutions

10.1 General Modelling Considerations

The actual design of a high-speed combustor is, as discussed in chapter 1, a difficult, if not impossible task. Perhaps the most important question in combustor design is whether a scheme can be found for adequately mixing the injected fuel into the atmospheric flow. The issue of fuel injection and mixing will not be explored here, except to say that all of the combustion processes and heat addition mechanisms discussed here will be dependent on finding some means of accomplishing complete mixing. It is clearly of little use discussing a combustive heat addition process if the fuel cannot be mixed into the flow.

As indicated in chapter 1, the rate at which the supersonic combustion process will proceed will be extremely sensitive to local thermodynamic conditions. A prediction of the combustion kinetics is beyond the scope of this work. However, it will be pointed out where inlet nonuniformities lead to variations in the expected thermodynamic properties, which will undoubtedly affect combustor design. Some simple combustion rate modelling will be

incorporated using the results of reference [6].

The combustion process will be modelled as a simple increase in total enthalpy in the flow. No attempt will be made to include the drag effects of fuel addition, or to include changes in flow mass flux or average molecular weight into the solutions, except as they figure into changes in the specific heat. In addition, it will be assumed that mixing can be accomplished uniformly, and that the heating profile can be tailored as desired.

There are two fundamental limits of combustor operation. The first is designed to accomplish combustion at constant static pressure, and therefore constant velocity. The other limit of operation is a constant temperature combustor, in which heat addition translates directly into increased velocity. In order to study nonuniformities in an engine, the performance of combustors designed to operate in these two limits will be explored for uniform flow, as a basis of comparison for numerical solutions of flow with an inlet profile. Appendix E presents analytical solutions for one-dimensional combustors.

10.2 Comparison of Constant Pressure and Constant Temperature Combustor Designs

Since the constant pressure and constant temperature designs described above represent extreme limits of operation, it is worth comparing their performance for an inlet flow of some given properties. It will be found that the constant temperature design must be modified to make it more practical, so the constant pressure combustor will actually be compared to several different types of designs based on the original constant temperature concept.

For purposes of practical engine design, it is not possible to achieve constant temperature operation throughout the combustor. This can be seen simply from the fact that the area ratio of the channel is an exponential function of the inlet Mach number. It is therefore necessary to reduce the inlet Mach number, and thus raise the static temperature, in order to keep the expansion ratio to a reasonable limit. This will be discussed below, when two hybrid constant temperature schemes are introduced. As a comparison, a simple combustor will

be considered with constant temperature throughout. Altogether, four combustor schemes will be considered here for baseline definition: complete constant temperature, constant temperature after isentropic compression, constant temperature after rapid heat addition, and constant pressure.

For all of these combustors, it will be assumed that inlet flow is delivered at Mach 6, 1000 K static temperature. This corresponds to a flight Mach number of about 14 at 30 km, at 4150 m/sec., near the midpoint of a transatmospheric trajectory. This is just at the limit of transition for a 30 meter forebody. As stated above, it will be most convenient to work with an average value of C_p in the combustor, so the total temperature entering the combustor must be corrected accordingly. With $C_p = 1600$ J/Kg-K, $\gamma \simeq 1.25$, the total temperature of the gas entering the combustor is 5500 K. At the average value of combustor C_p, it will be raised 1800 K from the available chemical energy of the hydrogen reaction, as calculated in the previous chapter.

Combustor 1: Constant Temperature Throughout

Following the behavior derived above for a constant temperature combustor, the final Mach number in a channel that is kept at the inlet temperature 1000 K with equation(E.21) is 7.1, which corresponds to an expansion ratio of 6850. That is a completely unreasonable figure, for it suggests that an engine with an initial channel height of 1 meter would have to expand to about 7 kilometers in order to keep the flow temperature down to 1000 K! This design defeats the original intention of a constant temperature scheme, that of adding heat at the highest temperature possible. It is clear that some means must be found to raise the flow temperature before the constant temperature process begins. Two such options will be persued below.

Continuing with the analysis of this obviously impractical design, the efficiency can be determined by calculating the total pressure at the exit. The constant temperature combustor operating at inlet conditions of 1000 K static temperature, inlet Mach number 6, had an exit flow with Mach number 7.10, and total temperature of 7300 K. The pressure ratio across the combustor is then given by equation (E.31) as $p_2/p_1 = 1.23 \times 10^{-4}$. It

is questionable whether it is realistic to expect combustion to continue down to such low pressures. The total pressure at the combustor exit is given by the isentropic formula:

$$p_{\text{total}} = p\left(1 + \frac{\gamma - 1}{2} M^2\right)^{\gamma/(\gamma-1)} \tag{10.1}$$

and equals 2.55 atm at the exit, compared to 5.03×10^3 at the inlet; this is a sizable loss, and a not very surprising one, considering that all the heat was added at such a high Mach number.

The exhaust velocity is calculated from the equation of enthalpy conservation:

$$u_{\text{exit}} = \sqrt{2\left(C_{p,\,\text{engine}} T_o - C_{p,\,\text{exit}} T_{\text{exit}}\right)} \tag{10.2}$$

where, for a perfectly expanded nozzle,

$$T_{\text{exit}} = T_o \left(\frac{p_{\text{exit}}}{p_o}\right)^{(\gamma-1)/\gamma} \tag{10.3}$$

With varying γ, this can only be used as an estimate with some average value of γ.

The total temperature has risen 1800 K from combustion. There is an additional contribution due to the incoming enthalpy of the hydrogen fuel, relative to the engine air stream. If hydrogen is used to cool the vehicle surface, it will be entering the engine with an initially high enthalpy. The fuel is also entering with the kinetic energy corresponding to the vehicle's velocity, and this is also released as heat when it enters the engine air, which is at a nearly fixed velocity relative to the ambient environment. These two contributions can be included in the increase in total temperature in the engine:

$$\dot{m}_{H_2}\left(C_p(T_{\text{injected}} - T_{\text{engine}}) + \frac{U^2_{\text{relative}}}{2}\right)_{H_2} = \dot{m}_{\text{air}+H_2} C_{p,\,\text{combustor}} T_o \tag{10.4}$$

With an average engine $C_p \simeq 1600$ J/Kg-K, this added heat raises a stoichiometric mixture 500 K (and lowers total pressure somewhat, which will be ignored here). In fact, a practical transatmospheric vehicle may require much more fuel for cooling than would be required by stoichiometry, and the resulting heat addition from this added fuel would be proportionately higher. Adding the heat from a stoichiometric mixture to the release from combustion, for perfect expansion at 30 km. altitude, ambient pressure of .0116 atm.,

and a typical exhaust $C_p \simeq 1330$ J/kg-K [6], the exhaust velocity is 4216 m/sec. This engine would have a specific impulse of 230 seconds, although the geometry is completely unrealistic.

Combustor 2: Constant Temperature after Isentropic Compression

If that same inlet flow is decelerated isentropically to a static temperature of 2800 K before the combustion process begins, the initial Mach number would then be 2.78 at constant $\gamma = 1.25$. The channel contraction would be a factor of 1/47 in order to accomplish this compression. The final Mach number would then be 3.59 with an expansion ratio of 19.48. This is certainly more reasonable, but still quite large. However, since the flow was originally decelerated through a channel which contracted 47 times, the final combustor exit area is actually .41, or about 2/5 of the original inlet area. In essence, the expansion ratio through the combustor is so large because it is working like a "pre-nozzle" in keeping the kinetic energy of the flow so high [36]. A nozzle typically converts flow thermal energy into kinetic energy, but this combustor keeps the energy in directed motion. With such changes in channel area, the one- dimensional approximations made throughout this work would be questionable.

In this second constant temperature combustor, the flow is decelerated isentropically to the constant temperature region. There, it drops from Mach 6 to Mach 2.78. There is no total pressure loss in the isentropic portion of the channel; the static pressure rises 172 times. Such a large rise in pressure would probably lead to boundary layer separation and associated problems. In the constant temperature region, the pressure drops by a factor of 3.95×10^{-2} for an overall ratio of 6.79. The total pressure would be 8.24×10^2 atm., a sizable gain over the first constant temperature design. The exhaust velocity is correspondingly higher at 4800 m/sec, with a specific impulse of 2280 seconds.

Combustor 3: Constant Temperature After Rapid Heating

This above example indicates that the constant temperature combustor is only a practical device when it is operating at a very high temperature and low initial Mach number. The flow temperature does not have to be raised with an isentropic converging channel,

however. It might just as well be raised with a rapid combustion process, followed by the constant temperature region, such as heat addition in a constant area duct. From the well-known solution of heat addition in a constant area channel, the final Mach number in the constant area duct can be calculated from the given initial conditions.

The temperature ratio between stations 1 and 2 in a constant area duct with heat addition is a function of the corresponding Mach numbers [5]:

$$\frac{T_2}{T_1} = \left(\frac{1+\gamma M_1^2}{1+\gamma M_2^2}\right)^2 \left(\frac{M_2}{M_1}\right)^2 \tag{10.5}$$

With a given inlet temperature, and an assumed value for final outlet temperature, the outlet Mach number of the constant area duct is found by rearranging the above equation to solve for M_2 :

$$M_2 = \frac{1+\gamma M_1^2}{2\gamma M_1}\sqrt{\frac{T_1}{T_2}} + \sqrt{\frac{(1+\gamma M_1^2)^2}{4(\gamma M_1)^2}\frac{T_1}{T_2} - \frac{1}{\gamma}} \tag{10.6}$$

where the lower-valued root of the quadratic has been neglected on physical grounds.

The total temperature ratio between two stations in the constant area duct is defined in terms of the Mach numbers and static temperature from the definition of the total temperature:

$$\frac{T_{\text{total 2}}}{T_{\text{total 1}}} = \left(\frac{1+\gamma M_1^2}{1+\gamma M_2^2}\right)^2 \left(\frac{M_2}{M_1}\right)^2 \left(\frac{1+\frac{\gamma-1}{2}M_2^2}{1+\frac{\gamma-1}{2}M_1^2}\right) \tag{10.7}$$

As an aside, it can be seen that, given an assumed functional form for the Mach number, the total temperature profile is determined. For instance, if the Mach number is assumed to be an exponential function, as usual, then

$$M(x) = M_{\text{initial}}\, e^{-x/2\lambda_C} \tag{10.8}$$

so the total temperature at any point is

$$T_{\text{total}}(x) = T_{\text{total 1}} \left(\frac{1+\gamma M_1^2}{1+\gamma M_1^2 e^{-x/\lambda_C}}\right)^2 \left(\frac{1+\frac{\gamma-1}{2}M_1^2 e^{-x/\lambda_C}}{1+\frac{\gamma-1}{2}M_1^2}\right) e^{-x/\lambda_C} \tag{10.9}$$

and taking the streamwise derivative, the required heating rate is:

$$\frac{dT_{\text{total}}}{dx} = \frac{T_{\text{total}}}{\lambda_C} \frac{(M_1^2 - e^{x/\lambda_C})e^{x/\lambda_C}}{(e^{x/\lambda_C}+\gamma M_1^2)(e^{x/\lambda_C}+\frac{\gamma-1}{2}M_1^2)} \tag{10.10}$$

where λ_C is a scale length, as before, and the total length of this constant area duct is, as per equation (E.10):

$$\begin{aligned} \frac{x_{\text{final}}}{\lambda_C} &= 2\ln\left(\frac{M_1}{M_{\text{final}}}\right) \\ &= -2\ln\left(\frac{1+\gamma M_1^2}{2\gamma M_1^2}\sqrt{\frac{T_1}{T_2}} + \frac{1}{M_1}\sqrt{\frac{(1+\gamma M_1^2)^2}{4(\gamma M_1)^2}\frac{T_1}{T_2} - \frac{1}{\gamma}}\right) \end{aligned} \tag{10.11}$$

Chemical calculations have shown this zone of rapid heating will typically be a fraction of the constant temperature region to follow, say on the order of 20% [6], even though most of the heat release will occur here.

Returning to the problem at hand, to take the inlet flow from 1000 K at Mach 6 to 2800 K with constant area heat addition, the final flow Mach number is 3.43 at $\gamma = 1.25$. This means that the total temperature was raised by a factor of 1.26. With an inlet total temperature of 5500 K, the initial added heat has increased total temperature by 1418 degrees before the flow reaches 2800 K static temperature. If the completed combustion process adds 1800 K to the total temperature, the constant temperature region adds 382 K.

With an inlet Mach number to the constant temperature region of 3.43 the final Mach number would still be 3.59 because the total temperature is the same, and the static temperature is also the same. The corresponding expansion ratio is 1.92. This is even more reasonable, and suggests that the proper means of operating a constant temperature combustor is indeed to first use a rapid combustion process to bring the flow up to the maximum permitted temperature.

In this constant temperature combustor, the Mach number at the start of the constant temperature region is 3.43. Using the well-known formula for pressure change in a constant area duct with heat addition [5]:

$$\frac{p_2}{p_1} = \frac{1+\gamma M_1^2}{1+\gamma M_2^2} \tag{10.12}$$

the static pressure ratio is 2.93, then it drops by a factor of .5 in the constant temperature region. At Mach 3.59, this corresponds to a total pressure of 1.53×10^2 atmospheres, not quite as good as the design with an isentropic inlet channel. Note that the adverse pressure gradient at the entrance to the combustor rise is somewhat more reasonable in this design,

if still high. The exhaust velocity is then slightly lower than above, 4710 m/sec, and specific impulse is 1950 secs.

Combustor 4: Constant Pressure

Recall that the supposed advantage of the constant temperature combustor is to provide increased efficiency by keeping the flow temperature as high as possible. The performance of this type of combustor can be compared to that of the constant pressure combustor derived earlier. First, the non-dimensional length of the constant pressure combustor is calculated for the same heat addition, using equation (E.10), and it is found to equal 1.03, referenced to the exponential heat addition length scale.

With an inlet temperature of 1000 K, the exit temperature is 2800 K, the same value selected for the exit temperature of the constant temperature combustor. The Mach number has dropped from the inlet value of 6 to 3.59, the same exit Mach number as in the constant temperature combustor with the same exhaust static temperature. At this Mach number, and with the constant static pressure of 1 atm., the exit total pressure is 1.21×10^2 atm. The corresponding exhaust velocity is 4690 m/sec, and specific impulse is 1900 secs.

As suspected, the constant pressure combustor takes a higher loss than the constant temperature design when the constant temperature is very high. However, if the constant temperature is low, the losses in that design can be higher than in the constant pressure design. The practical constant temperature designs have adverse pressure gradients, so it may be desirable to accept the higher losses of the constant pressure design and avoid flow problems. Since the design with rapid heat addition, then constant temperature did not have such a large adverse pressure gradient as the one with isentropic compression, it is probably the most practical constant temperature concept even though its losses were slightly higher.

From the above examples, it seems clear that the two most reasonable combustor schemes are:

- Constant pressure throughout. At Mach 6, $I_{sp} \simeq 1900$ sec.

- **Rapid heat addition to high temperature, then constant temperature. At Mach 6, $I_{sp} \simeq 1950$ sec.**

These will be used for numerical analysis in chapter 11.

Chapter 11
Numerical Solutions of Profiles Through Combustor Channels

Numerical solutions will be presented for nonuniform inlet flow into the constant pressure and constant temperature combustor geometries derived in the last chapter. In each case presented, the combustor will be designed to operate at the Mach number, pressure, and temperature of the inlet *free-stream*. Deviations observed due to the presence of the ingested boundary layer can therefore be compared directly to the analytical solutions calculated above. Once again, it should be noted that the combustor designs presented here have been selected because they represent opposite limits of operation. In actuality, achieving either constant pressure or constant temperature operation will depend on the mixing rate and details of fuel injection and combustion that have not been included in this model.

In the following examples, only the results of laminar boundary layer profiles at the inlet have been shown. In each case a turbulent boundary layer produces minimal changes in the combustor performance, as compared to the laminar solution at the same flight conditions and relative boundary layer thicknesses.

11.1 Constant Pressure Combustor

11.1.1 Without Changes to the Heating Rate

The calculated behavior of the profile in a combustor designed for constant pressure can be compared to the analytical solution presented above. The inlet conditions specified for the above examples, Mach 6 at 1000 degrees, are approximately those encountered in Mach

16 flight at 30 km altitude, with a 12 degree forebody wedge angle, assuming no inlet shock at the scramjet entrance. The resulting profile with laminar boundary layer is pictured in Figure 11.1. At these conditions, the boundary layer will will typically fill 10% of the inlet area.

This profile can be input to the channel flow model developed in chapter 6. First, it will be assumed that the local thermodynamic conditions have no effect on the pattern of heat release inside the engine. It will be seen that the resulting engine behavior is quite similar to the expected uniform inlet performance. Then, the profile will be run in the channel with suitable approximations to the change in heating rate caused by variations in the local thermodynamic properties. It will be found that, when heating changes are accounted for, the profile has a dramatic effect on the combustor performance, as measured in the final total temperature and total pressure in the free-stream.

Figure 11.2 shows the Mach number profiles at five stations located along a constant pressure combustor. The combustor has been designed to take a uniform flow from Mach 6 to Mach 3.59, and even with the profile, this is accomplished. The static pressure also follows the rise from 1000 K to 2800 K that was expected with a uniform profile, as shown in Figure 11.3.

The corresponding boundary layer profile through the channel, and uniform Mach number are presented in Figures 11.4 and 11.6, respectively. Note that the boundary layer grows slightly, as shown in the magnified Figure 11.5, but not in proportion to the channel area. This means that the relative change in area for the free-stream tube is greater than that for the entire channel, and the pressure drop is therefore greater than in a uniform flow. The uniform Mach number that would be used to characterize the boundary layer at each point is a nearly constant 1.7, which drops the effective Mach number for the entire channel to somewhat over 4 at the inlet, versus 6 for the free-stream. A good approximation for the boundary layer would be a constant area streamtube at some constant Mach number.

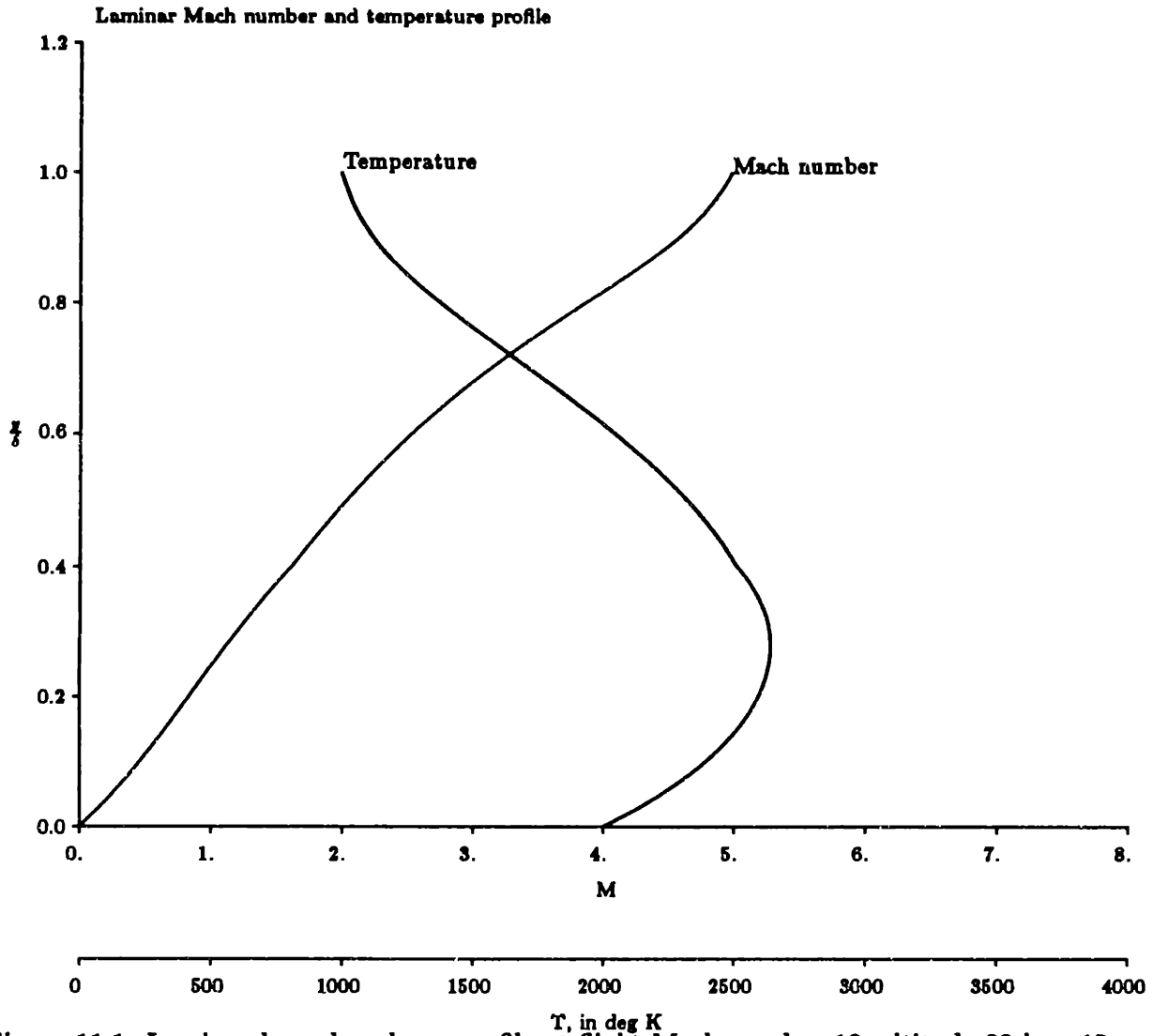

Figure 11.1: Laminar boundary layer profile at flight Mach number 16, altitude 30 km, 12 degree forebody wedge angle

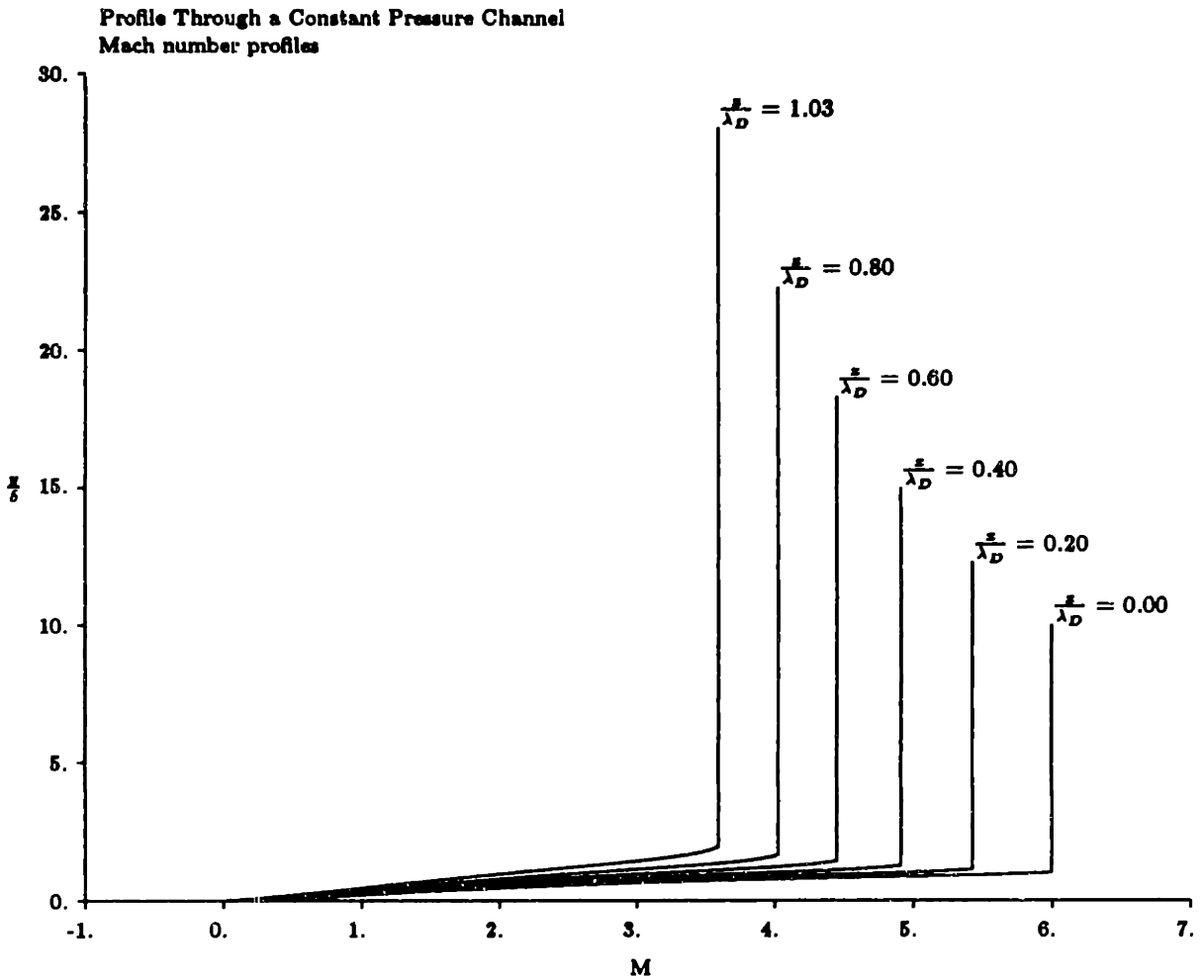

Figure 11.2: Mach number profiles at various stations through a constant pressure combustor

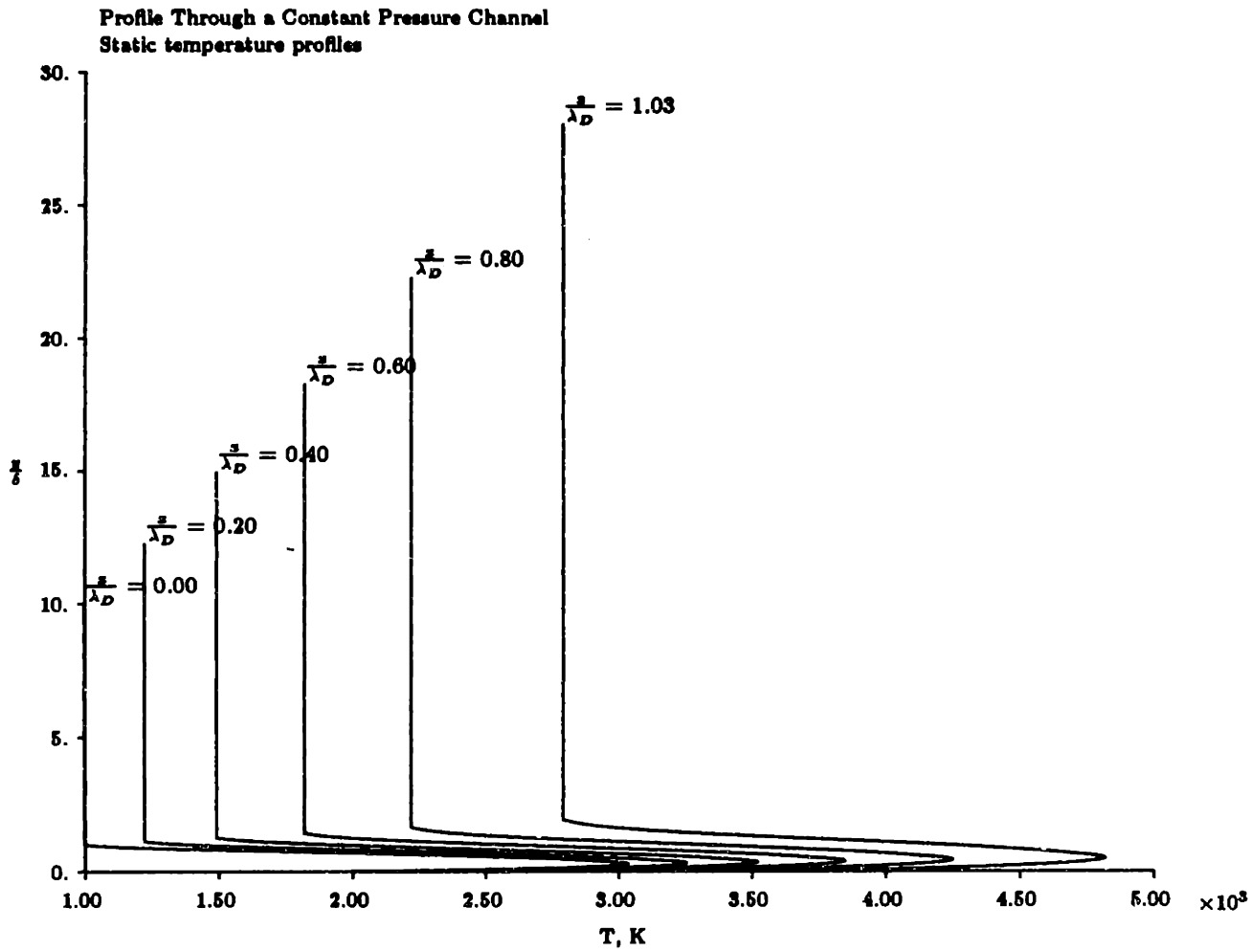

Figure 11.3: Static temperature profiles at various stations through a constant pressure combustor

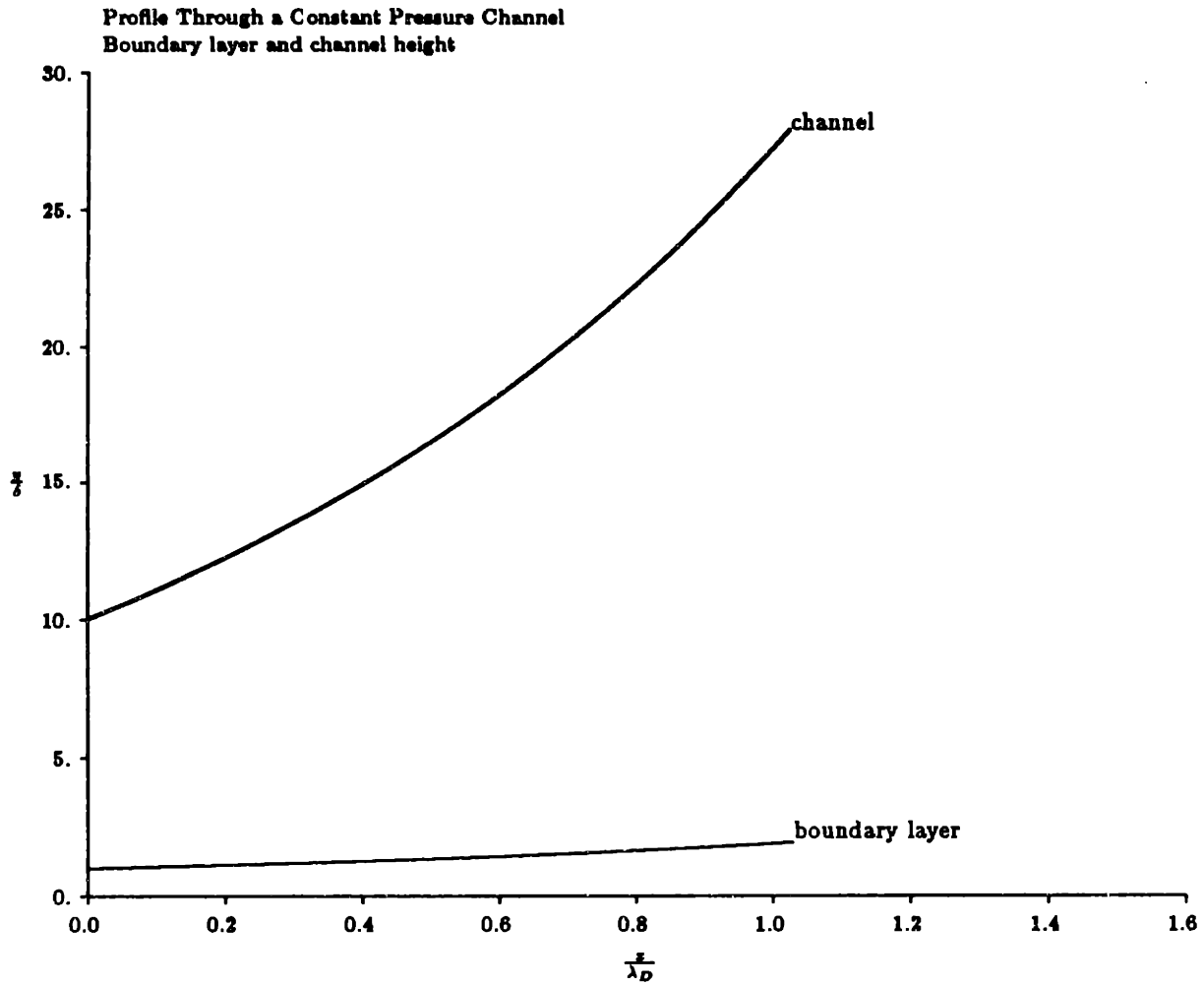

Figure 11.4: Channel height and boundary layer height in a constant pressure combustor

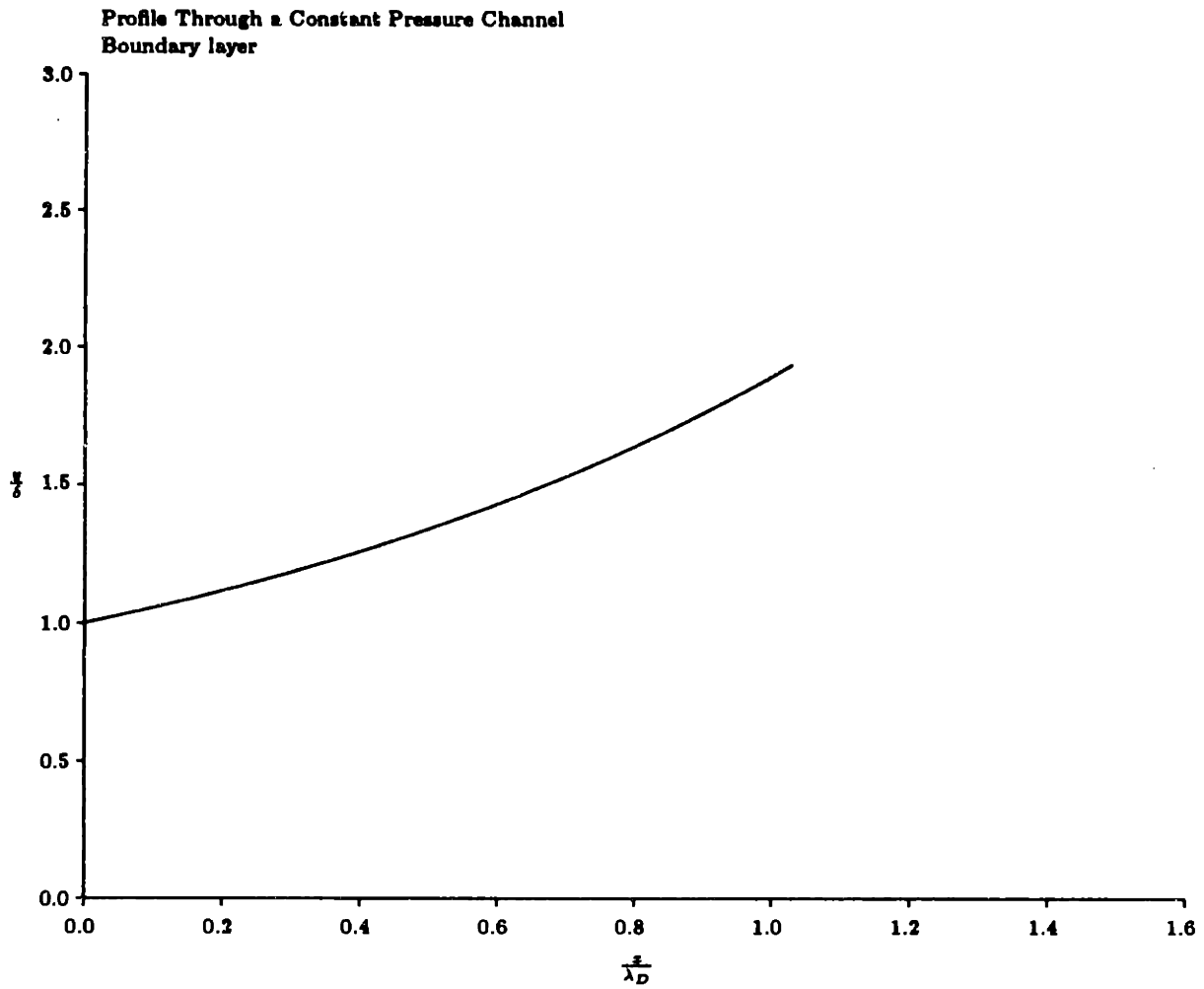

Figure 11.5: Magnified view of boundary layer height in a constant pressure combustor

Although the Mach number does not seem to change much from the values for expected with a uniform inlet, as shown on the comparison in Figure 11.6, the effect of the profile on this channel flow is apparent in Figure 11.7, which presents the static pressure along the channel, compared to the expected uniform pressure profile. The presence of the profile has dropped the static pressure by about 4% at the end of the channel, which is not very significant. Along with this drop in static pressure is a decrease in static temperature, but one that is just barely perceptible, as seen in Figure 11.3.

Because this solution has not included any changes in the heating rate, the total temperature is unchanged throughout the combustor, and the total pressure is imperceptibly altered from the values calculated for a uniform one-dimensional flow. Figures 11.9 and 11.10 present the static temperature and static pressure profiles at the same stations as the profiles presented above. The total temperature in the free-stream has been raised from an incoming 6600 K to 8400 K, and the total pressure is 104 atm. Note that these values are shifted slightly from the analytical example given above, because the incoming free-stream conditions of Mach 6.044 at 1021 K did not precisely match the analytical example at Mach 6, 1000 K. However, the amount of added heat is identical.

It is easy to see why the profile has little influence on the behavior of the constant pressure combustor. This combustor has been designed so that the pressure-raising effect of heat addition exactly counters the pressure-reducing effect of area increase. Once this is done, there is no change in momentum, which is why the formulation for this combustor design is so simple.

If the heating rate is not changed, and the logarithmic derivative of channel area is the same, the profile can have no effect on the combustor behavior. In fact, the area derivative is balanced by the heating rate referenced to the local static temperature:

$$\frac{dA}{A} = \frac{dT_o}{T} \tag{11.1}$$

so there is some effect from the profile, but it is a minor one for the particular profile properties selected here.

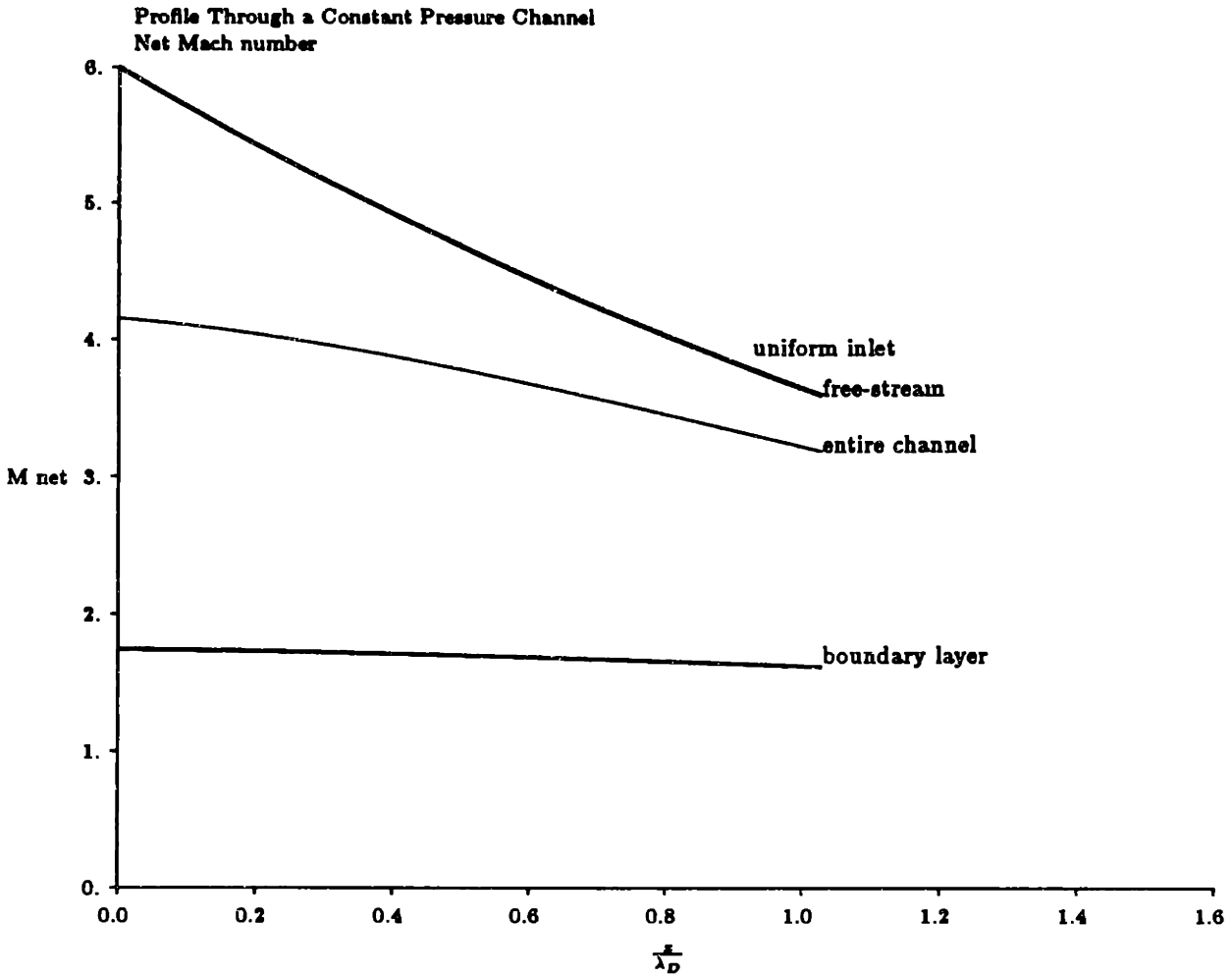

Figure 11.6: Effective uniform Mach numbers in a constant pressure combustor. Free-stream is nearly indistinguishable from uniform solution

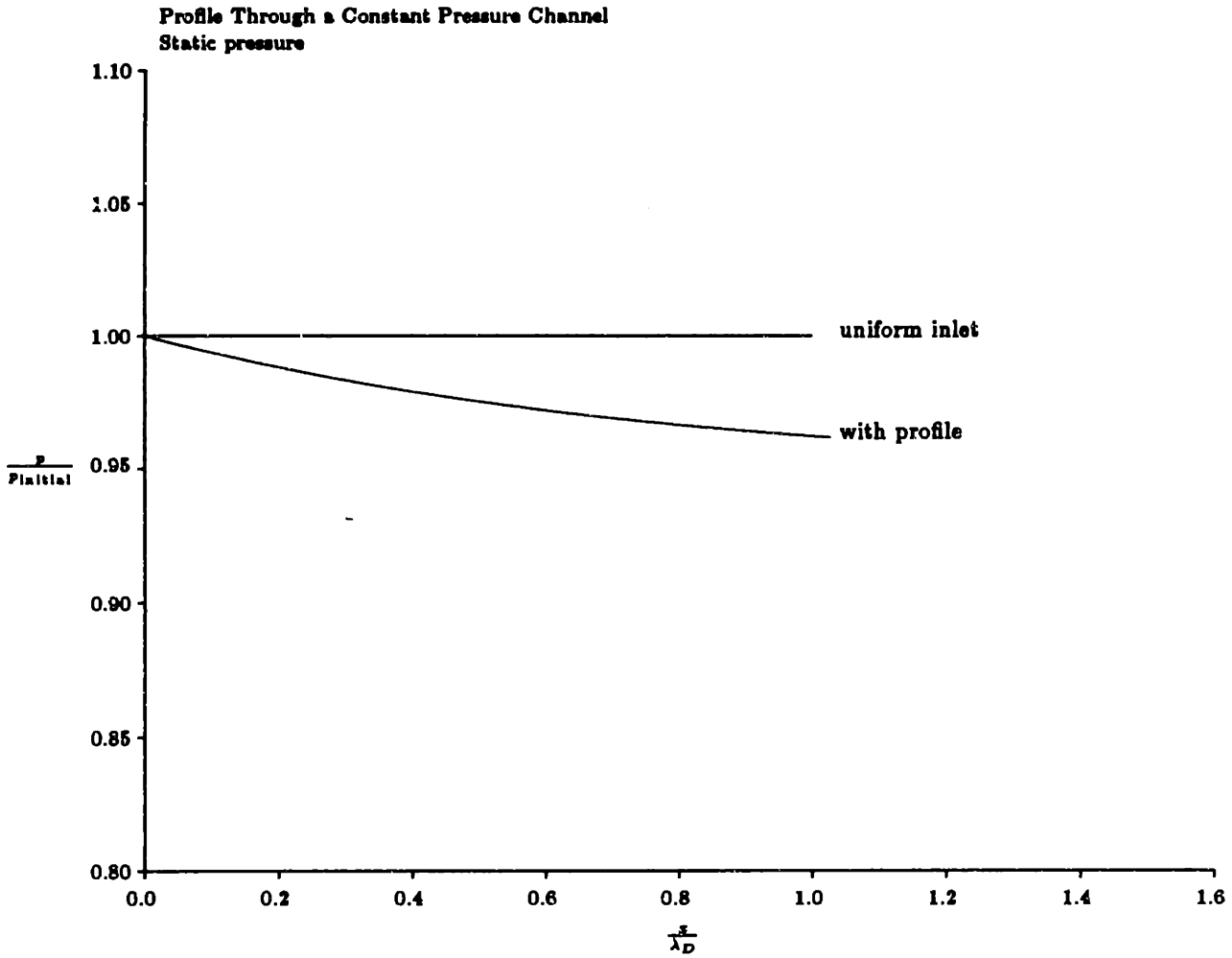

Figure 11.7: Free-stream static pressure along a constant pressure combustor

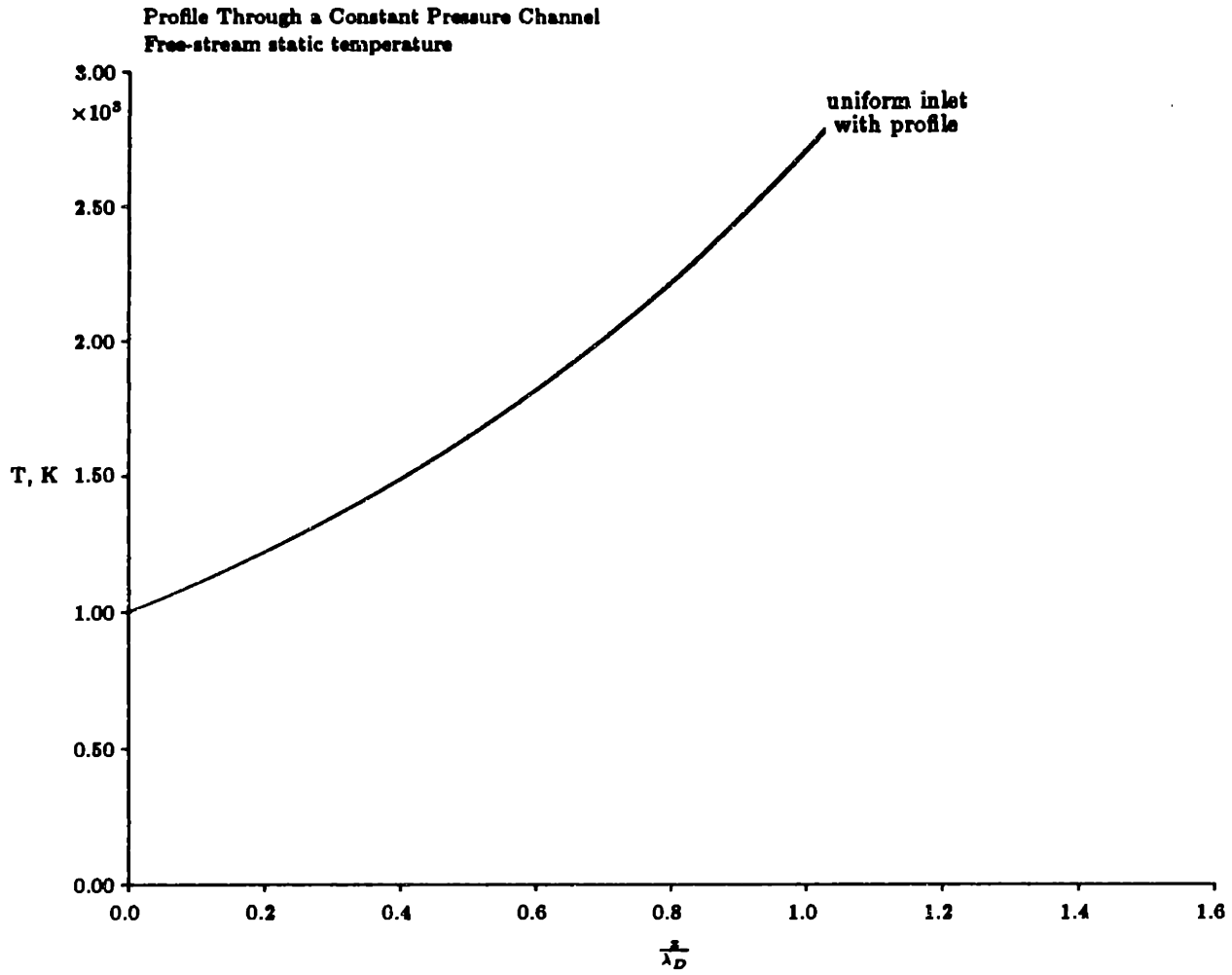

Figure 11.8: Free-stream static temperature along a constant pressure combustor. Free-stream is nearly indistinguishable from uniform solution

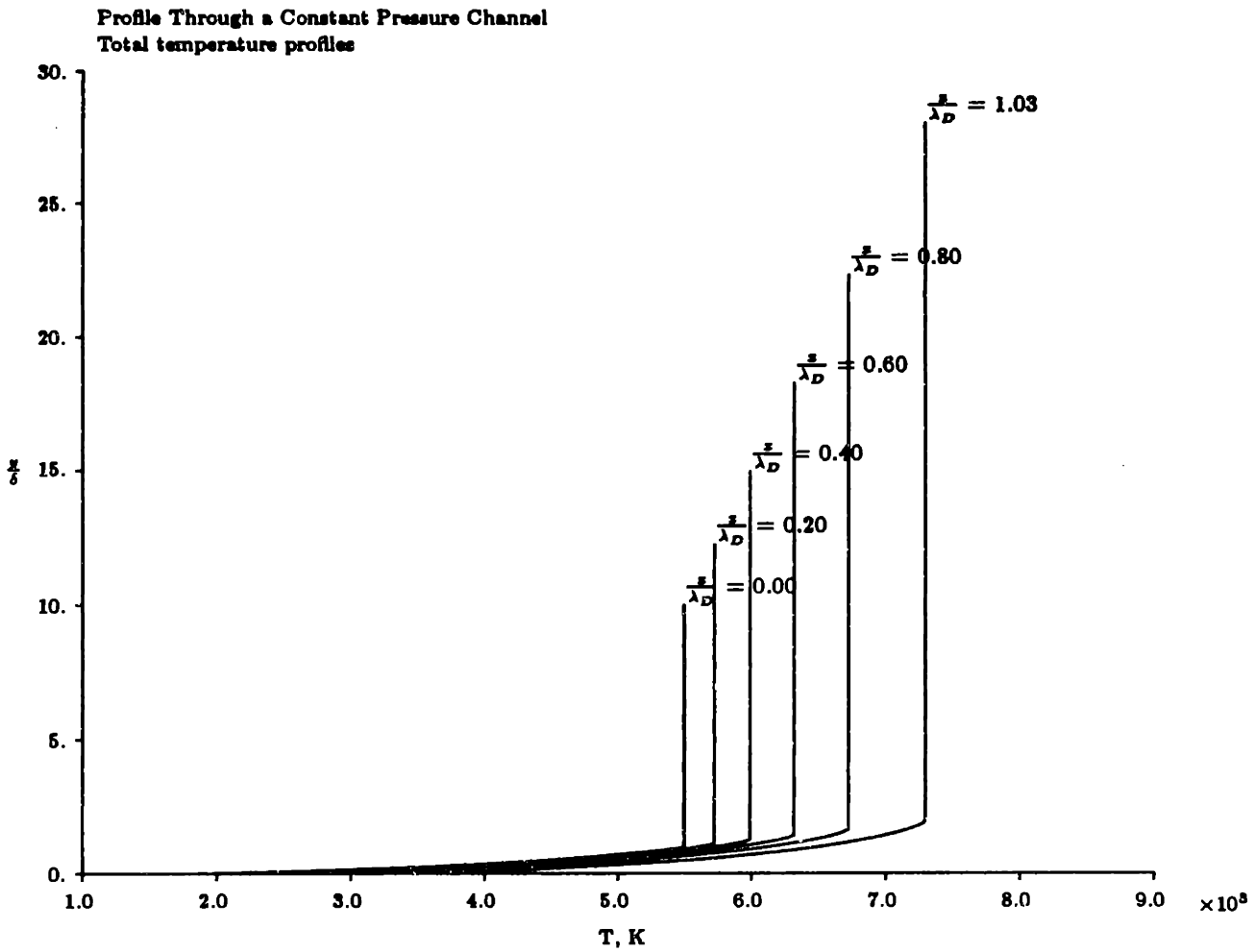

Figure 11.9: Free-stream total temperature along a constant pressure combustor

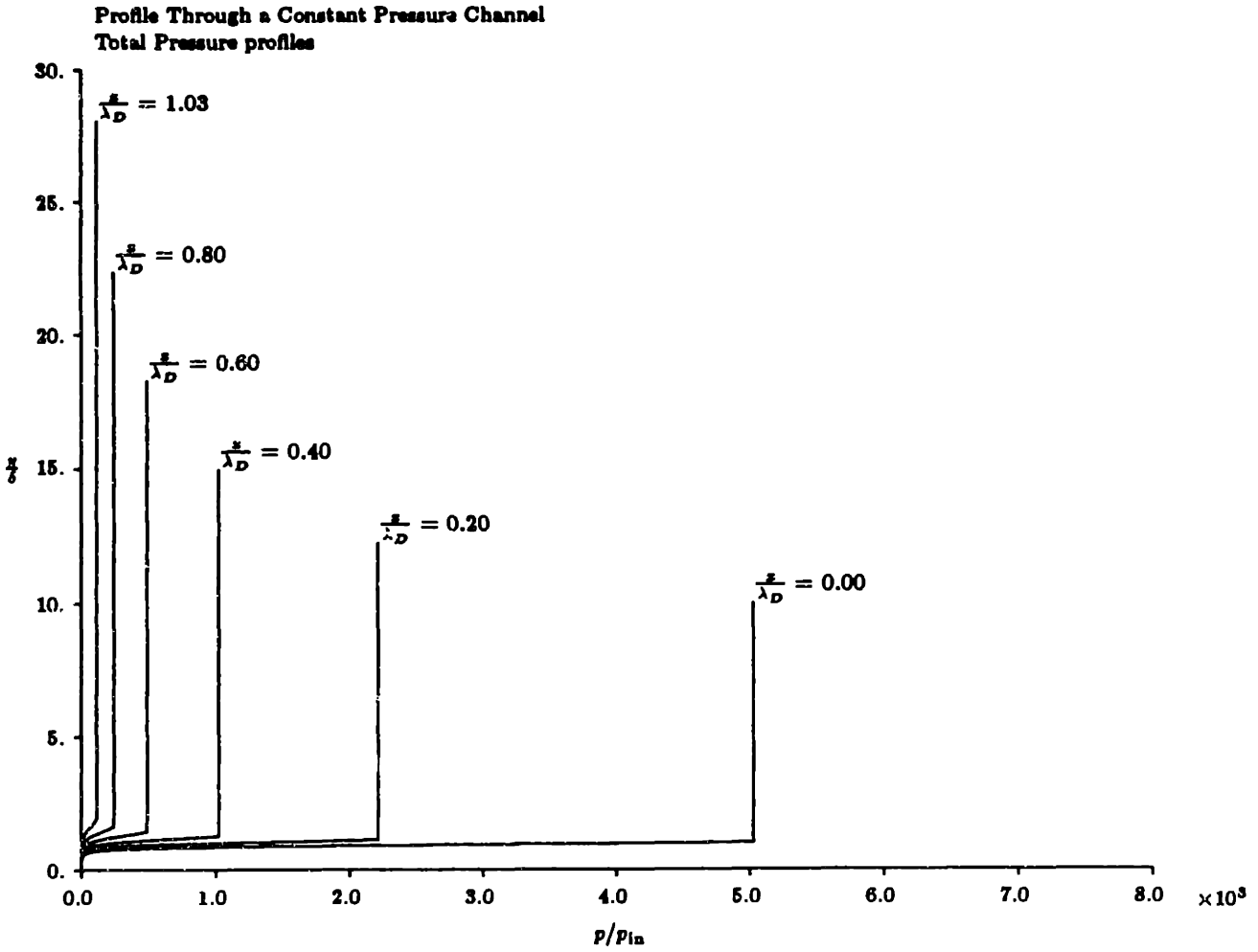

Figure 11.10: Free-stream total pressure along a constant pressure combustor

11.1.2 With Local Heating Rate Correction

A more interesting solution to the constant pressure combustor performance results from the inclusion of local thermodynamic effects on the rate of heat addition. Because the channel behavior is so dependent on matching area changes with heat addition, alterations in the heat addition rate can produce large scale changes in local thermodynamic properties, which in turn produce larger changes in heat addition, and there is thus a multiplying effect.

In chapter 1, a curve fit was presented for the time for the hydrogen-air reaction to reach 95% completion. The simplest model of local thermodynamic effects on heat addition is to assume that the local rate of heat addition is proportional to the equilibrium temperature rise divided by the reaction time. Thus, at each point in the flow, the temperature rise and reaction time can be calculated and compared to the uniform flow values at the same location. The rate at which heat is added is then taken to be equal to the expected rate for uniform flow, multiplied by the ratio of actual reaction rate to uniform flow reaction rate. The heating rate is converted to a streamwise derivative of heat addition by dividing by the local velocity. The streamwise derivative of heat addition is then:

$$\frac{dT_o}{dx}(p,T) = \frac{dT_o}{dx}_{\text{uniform}} \left(\frac{t_{\text{reaction, uniform}}}{t_{\text{reaction}}(p,T)}\right) \left(\frac{\Delta T(p,T)}{\Delta T_{\text{uniform}}}\right) \left(\frac{U}{U_{\text{uniform}}}\right) \qquad (11.2)$$

When reaction time is increased, the rate of heat addition has decreased; similarly, when the flow velocity has increased, the streamwise derivative of heat addition has decreased.

Several limits must be placed on the reaction time calculation. If the local pressure has risen above the cutoff pressure at a given temperature, combustion will cease and the reaction will stop. Similarly, above 3200 K, hydrogen addition results in dissociation, not heat release, so the amount of heat released must drop to zero at that point, and become negative at higher temperature. This is actually accounted for automatically by the temperature rise estimate, since ΔT becomes negative above 3200 K. Also, in the calculation, it is important to check that the total heat release does not exceed the heat available from the fuel. Because the channel flow solution simply models heat addition at each point, it is necessary to check the total heat added to each streamtube, and cut off heat addition if the available energy has been reached.

It must be emphasized that this model is just a simple approximation to the actual changes in finite rate chemistry that would occur under varying thermodynamic conditions, and the resulting conclusions should be treated as qualitative indications of trends, rather than design results. Dynamic effects have been left out of the modelling. In general, the combustion behavior will also be strongly dependent on the fuel injection profile. These important effects have not been considered in this model. However, the assumptions of constant pressure and constant temperature combustion are themselves idealizations, the practicality of which is questionable.

The behavior of flow in a constant pressure combustor has been solved with the inclusion of approximate reaction rate effects described above, for the same flight conditions as before. The resulting Mach number profiles at the same stations are presented in Figure 11.11.

Note that these profiles are quite similar to those presented without a heating correction, once again indicating that thermodynamic conditions are much more sensitive than Mach number. The temperature profiles do show a noticeable change in the boundary layer, because combustion is inhibited at high temperatures. Indeed, above 3200 K, there is no increase in the boundary layer temperature, as expected, since heat release has stopped there. The final free-stream temperature is also lower, indicating less overall heat release in the combustor, as we shall find in succeeding figures.

Figures 11.13 and 11.14 present the boundary layer thickness through this heat-corrected combustor. The boundary layer experiences rapid growth at the entrance to the combustor, then decreases in *relative* thickness farther along the channel. This is an indication that there is rapid combustion in the boundary layer initially, and reduced combustion downstream. This is because the elevated temperatures through most of the boundary layer result in more rapid combustion, provided the temperature is below the combustion limit. In addition, the relatively low speed of the boundary layer means that a given heat release rate results in a higher streamwise gradient of heat addition.

The corresponding uniform Mach numbers of the boundary layer and the entire channel show these same trends, as seen in Figure 11.15. As the boundary layer is experiencing

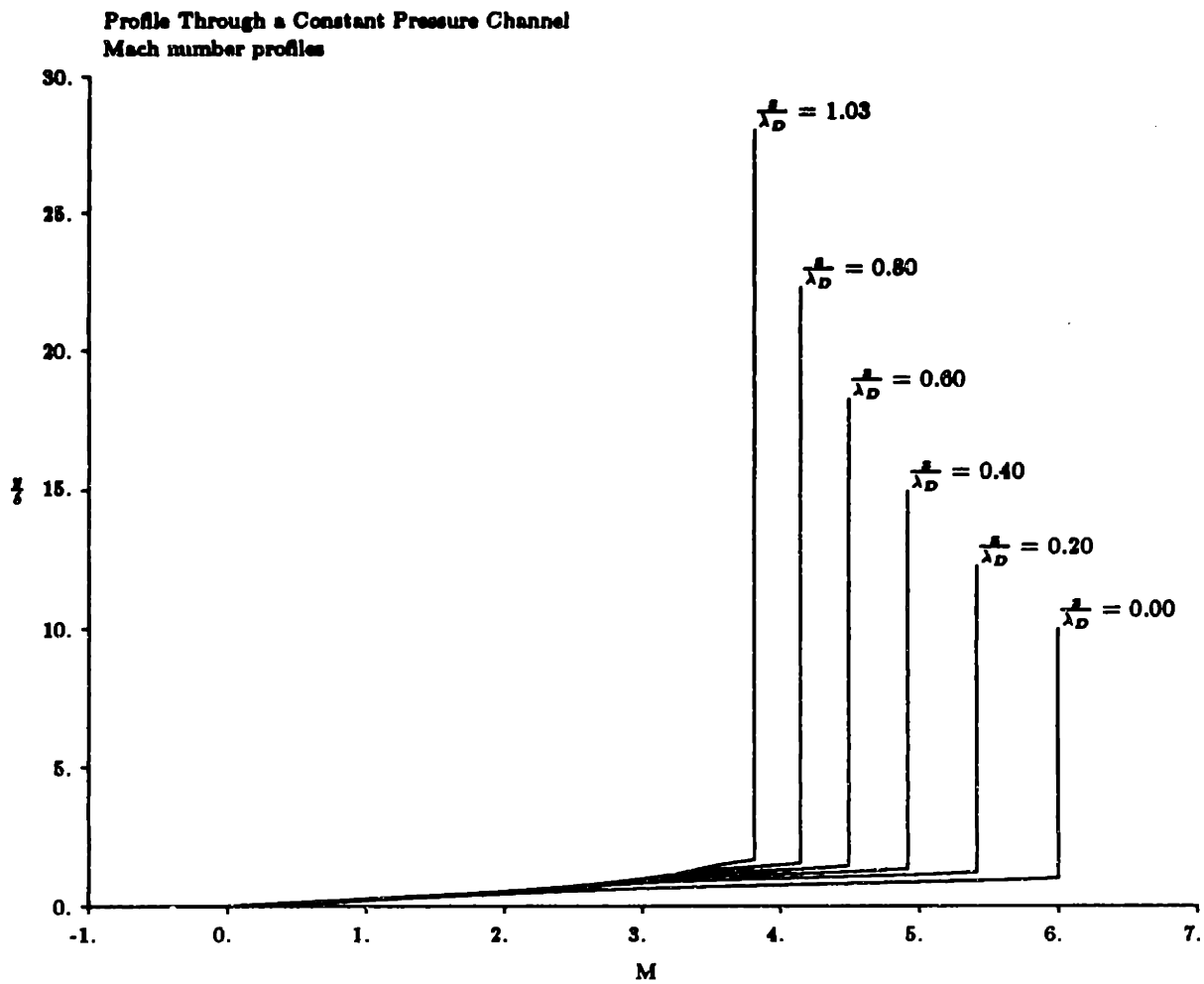

Figure 11.11: Mach number profiles at various stations through a constant pressure combustor with heating correction

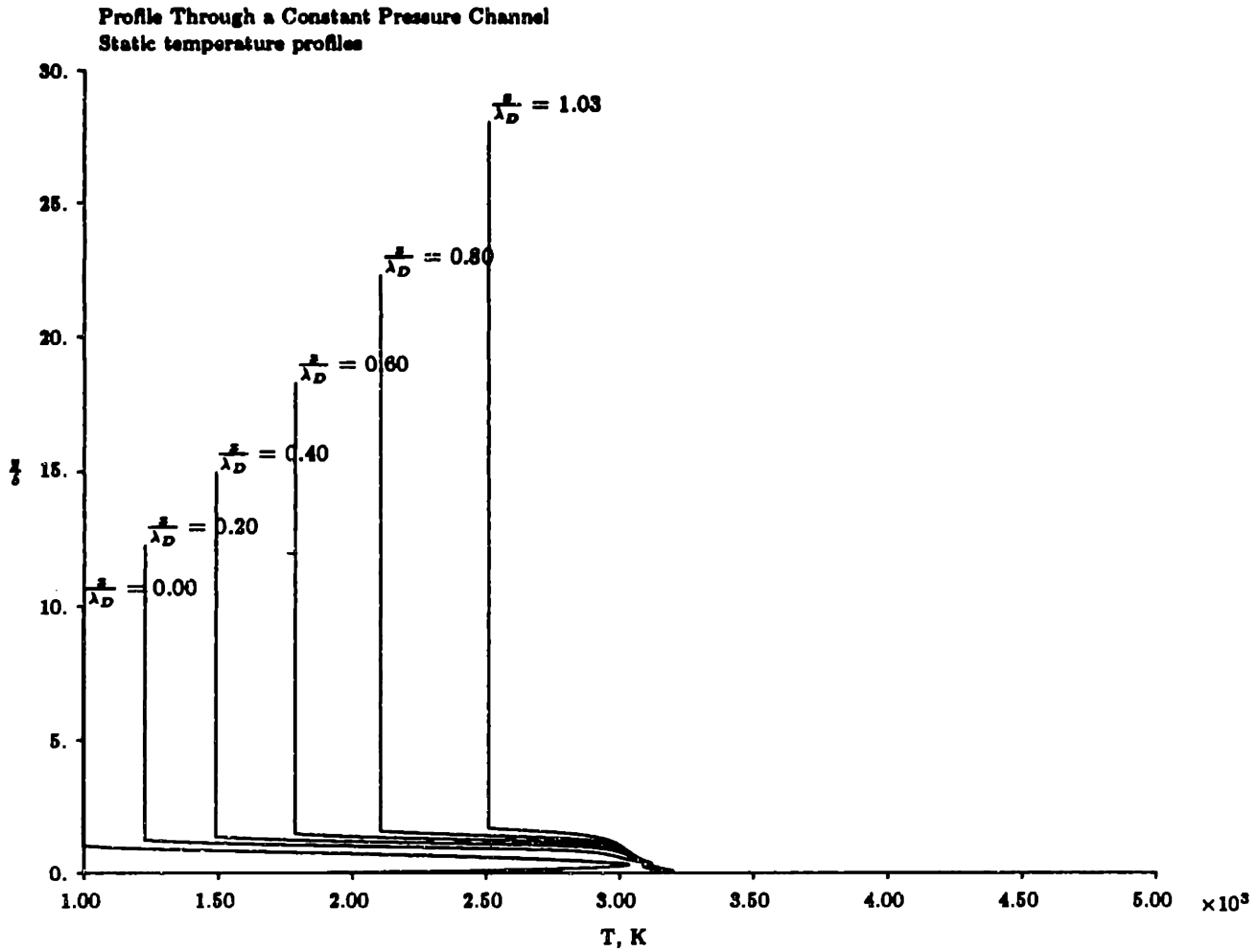

Figure 11.12: Static temperature profiles at various stations through a constant pressure combustor with heating correction

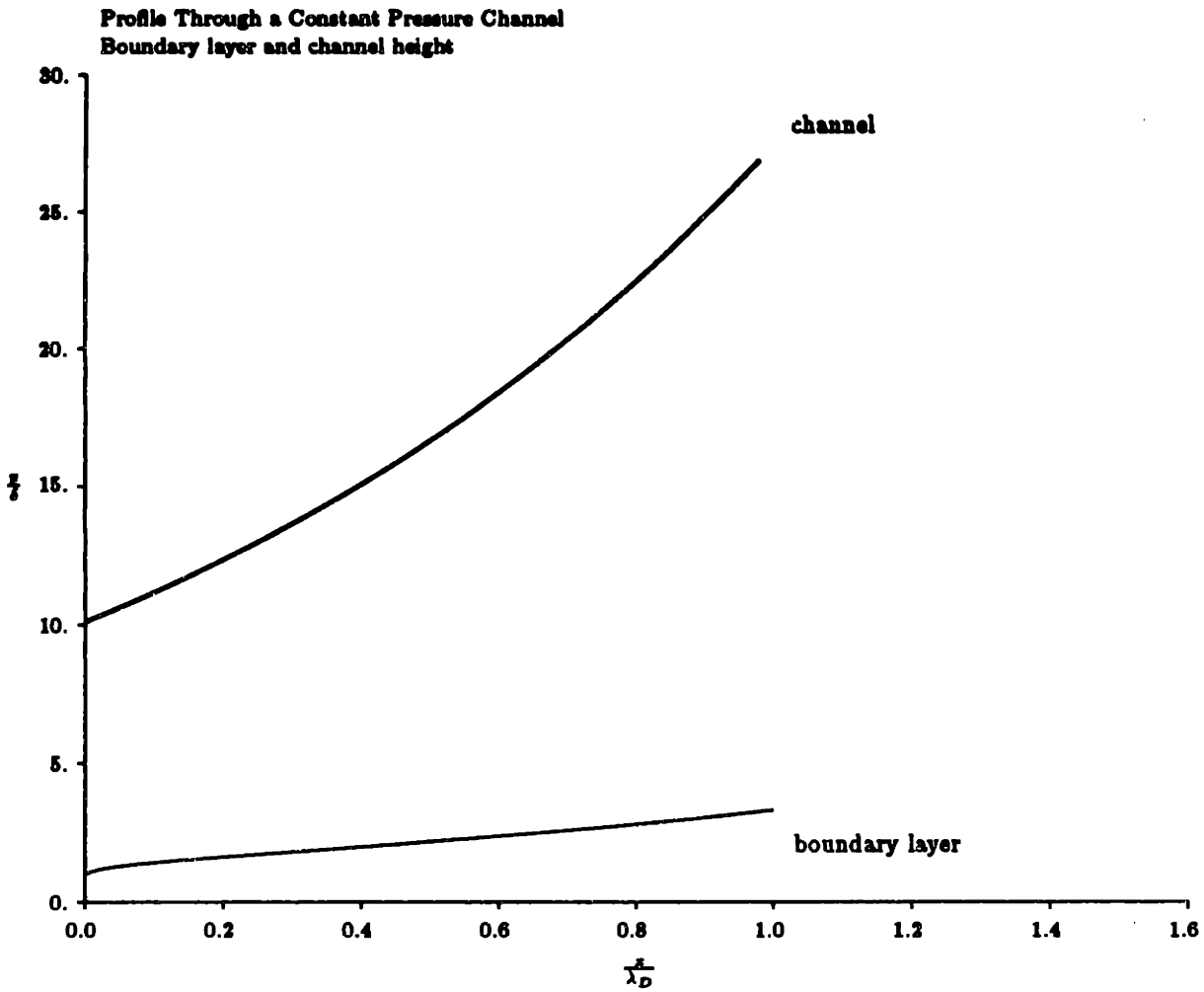

Figure 11.13: Channel height and boundary layer height in a constant pressure combustor with heating correction

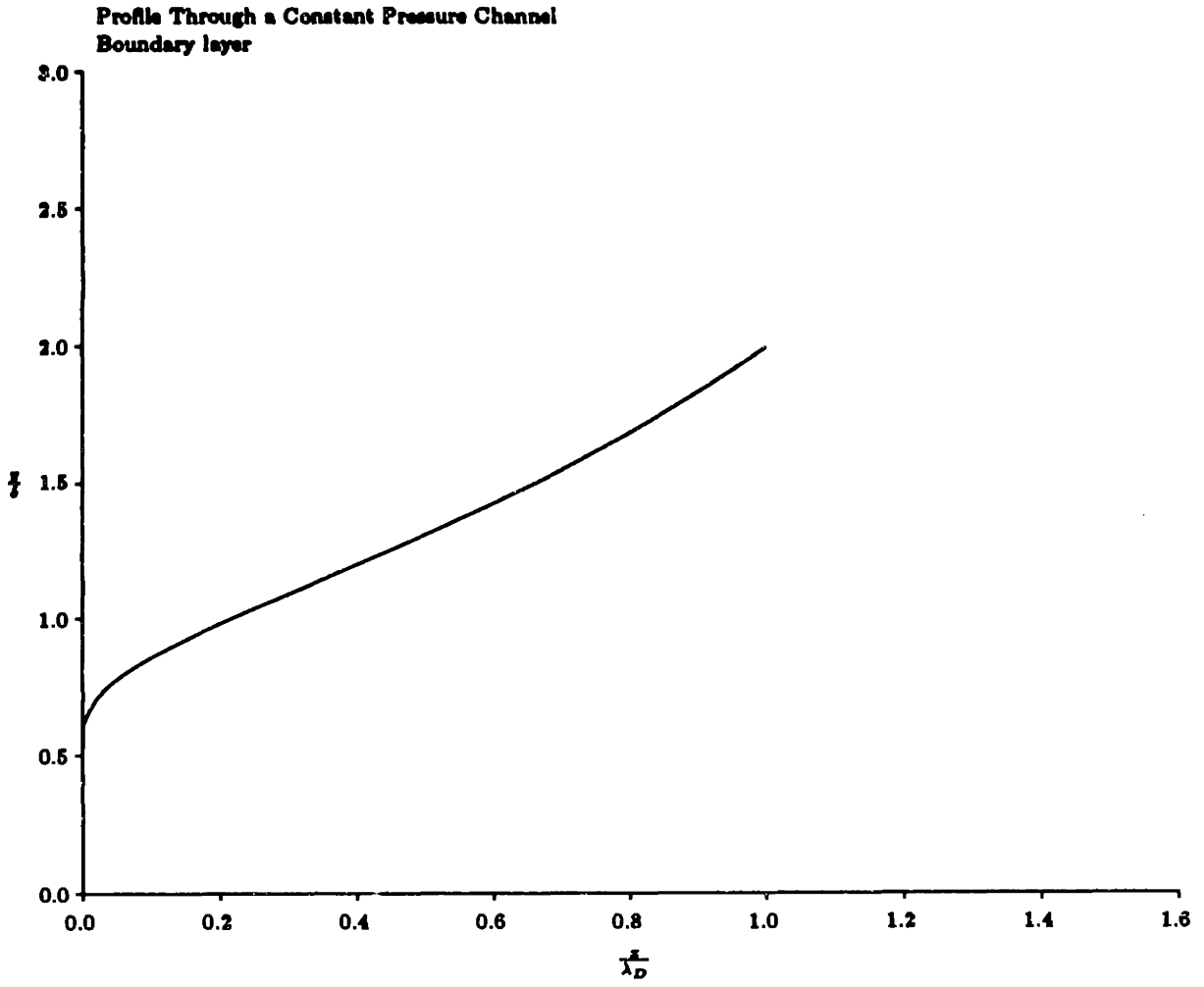

Figure 11.14: Magnified view of boundary layer height in a constant pressure combustor with heating correction

rapid heat addition, the Mach number throughout moves towards unity, a trend which is reflected in the value of the representative uniform Mach number.

Heat release in the constant pressure combustor is tailored to offset the effects of area increase on pressure. In the period of rapid heat release inside the boundary layer, at the channel entrance, there is a net rise in static pressure, as the heat addition exceeds the pressure- reducing effects of area change. As the boundary layer heat addition ceases, the net heat addition in the channel drops below the point where it can compensate for area change, and there is a drop in pressure as the flow expands. These trends are seen in the static pressure plot of Figure 11.16, which shows a rapid rise and overshoot of the initial pressure in the first 10% of the channel, followed by a gradual decrease to about 90% of the initial value. The corresponding static temperature changes are plotted in Figure 11.12, which also shows a decrease from the expected uniform flow values. The rapid increase in boundary layer heating at the channel inlet has little effect on the temperature because temperature is less sensitive to such changes than pressure.

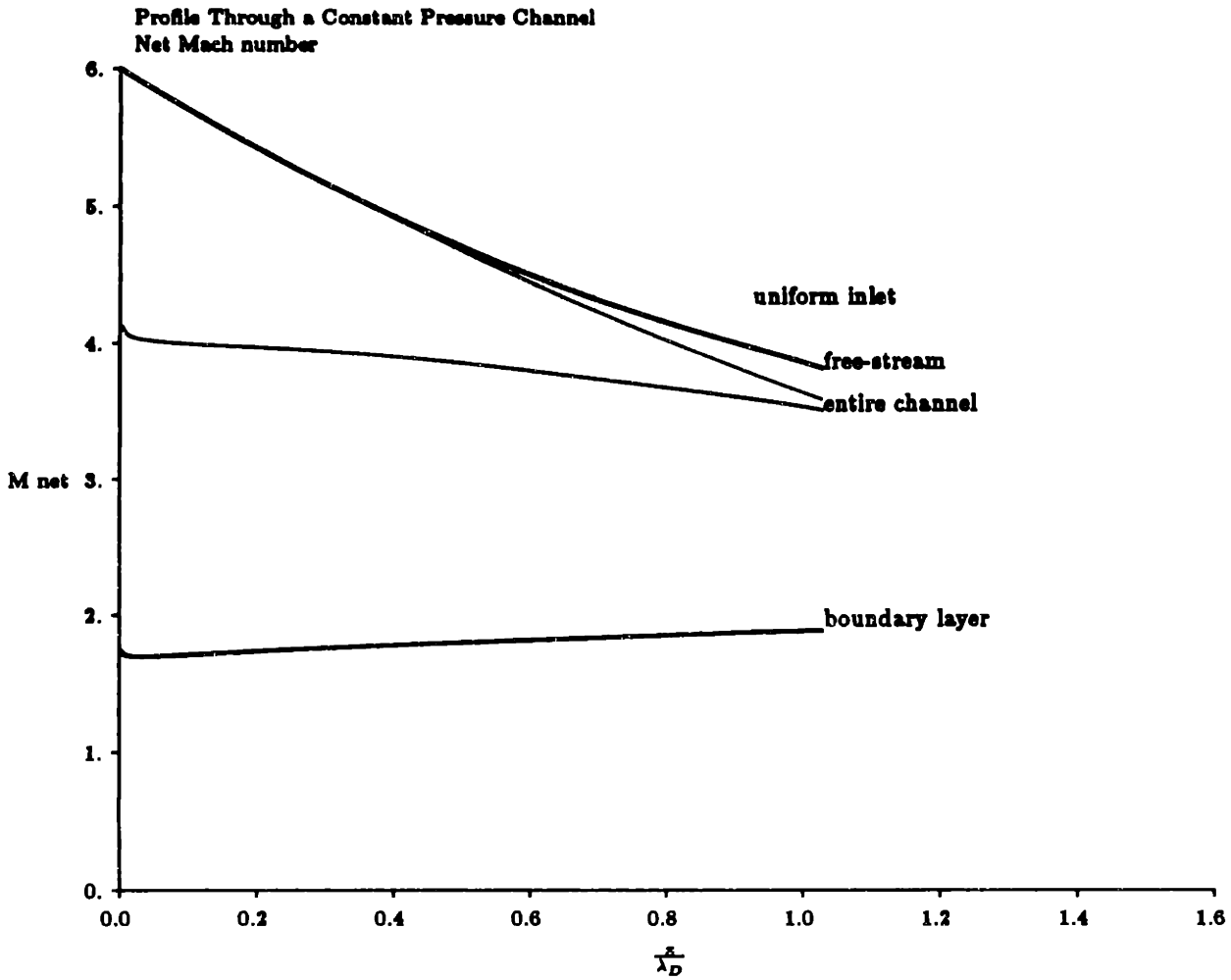

Figure 11.15: Effective uniform Mach numbers in a constant pressure combustor with heating correction

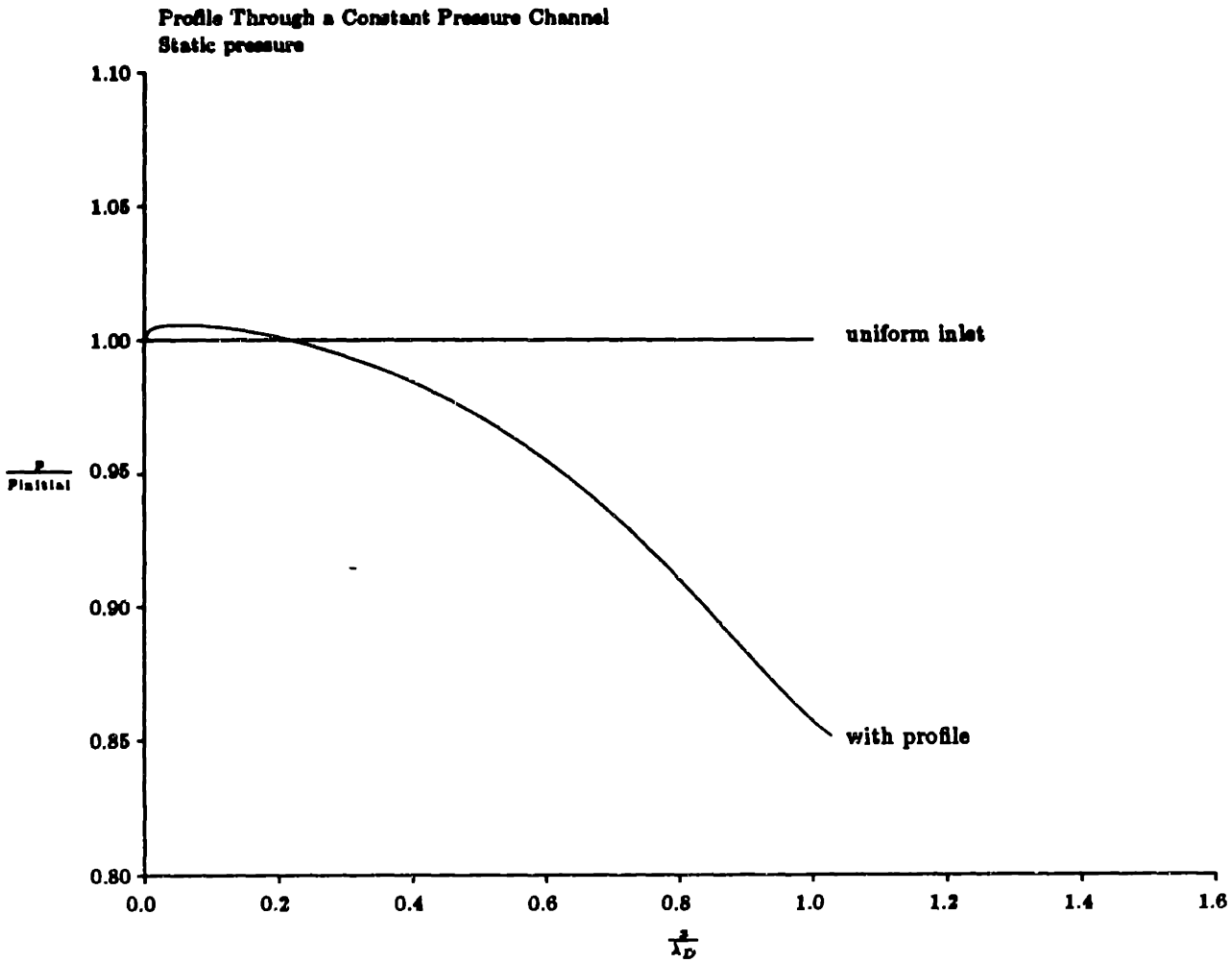

Figure 11.16: Free-stream static pressure along a constant pressure combustor with heating correction

With the heating rate correction, the boundary layer heat addition is greatly reduced because of the high initial temperature. This will subtract from the total energy addition in the combustor. Also important are the effects that the deviating thermodynamic conditions will have on heat addition in the free-stream. With lower free-stream pressure and temperature, heating rates will be lower than those expected in the uniform flow solution. The total temperature profiles are shown in Figure 11.18, where it can be seen that free-stream total temperature has risen only 1684 K of the original 1800 K available from the combustion reaction, to 8094 K, a loss of nearly $6\frac{1}{2}\%$. The corresponding total pressure performance is pictured in Figure 11.19. The final total pressure is 126 atmospheres, 20% higher than expected for uniform flow. This is not surprising because the heat addition has been lower.

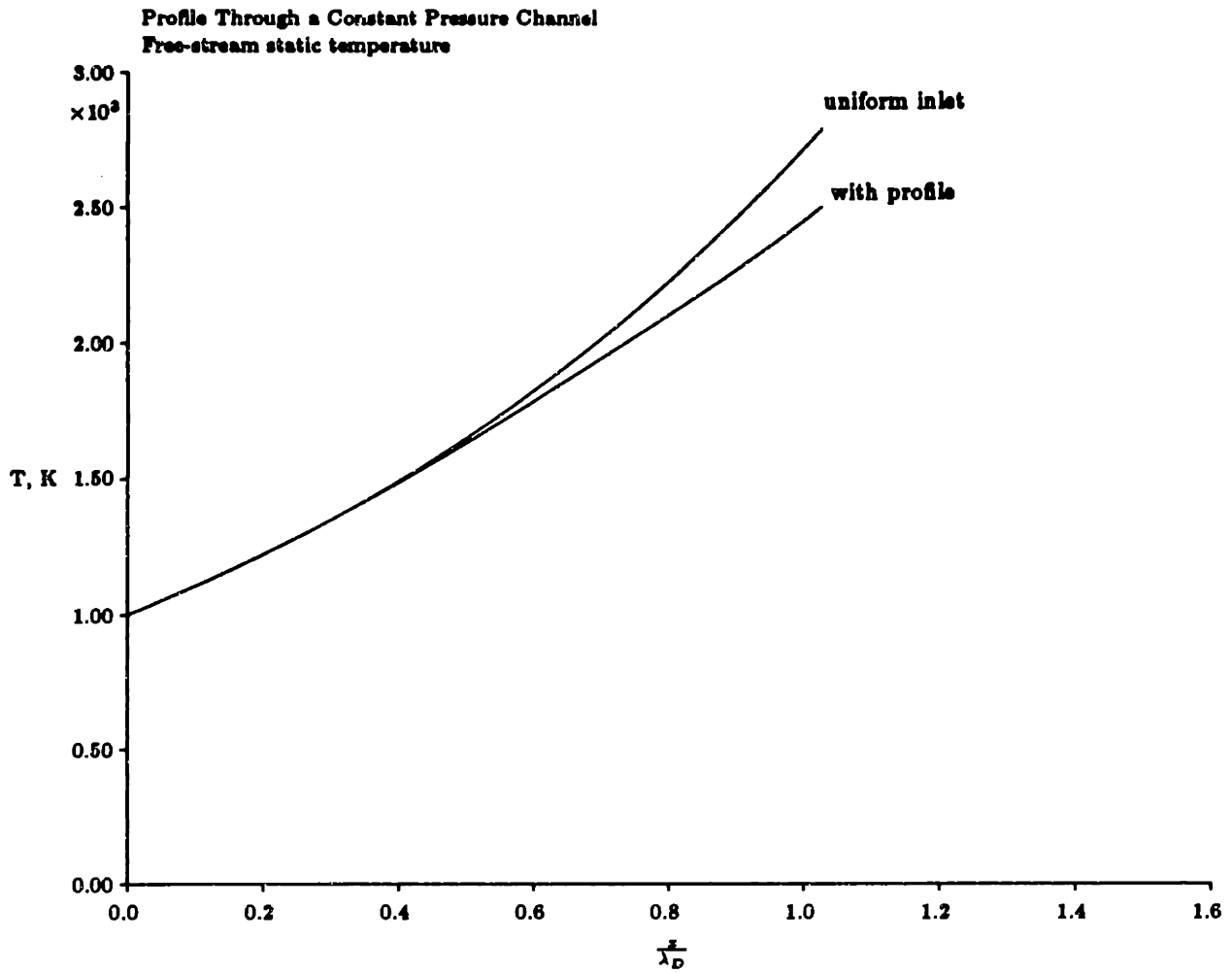

Figure 11.17: Free-stream static temperature along a constant pressure combustor with heating correction

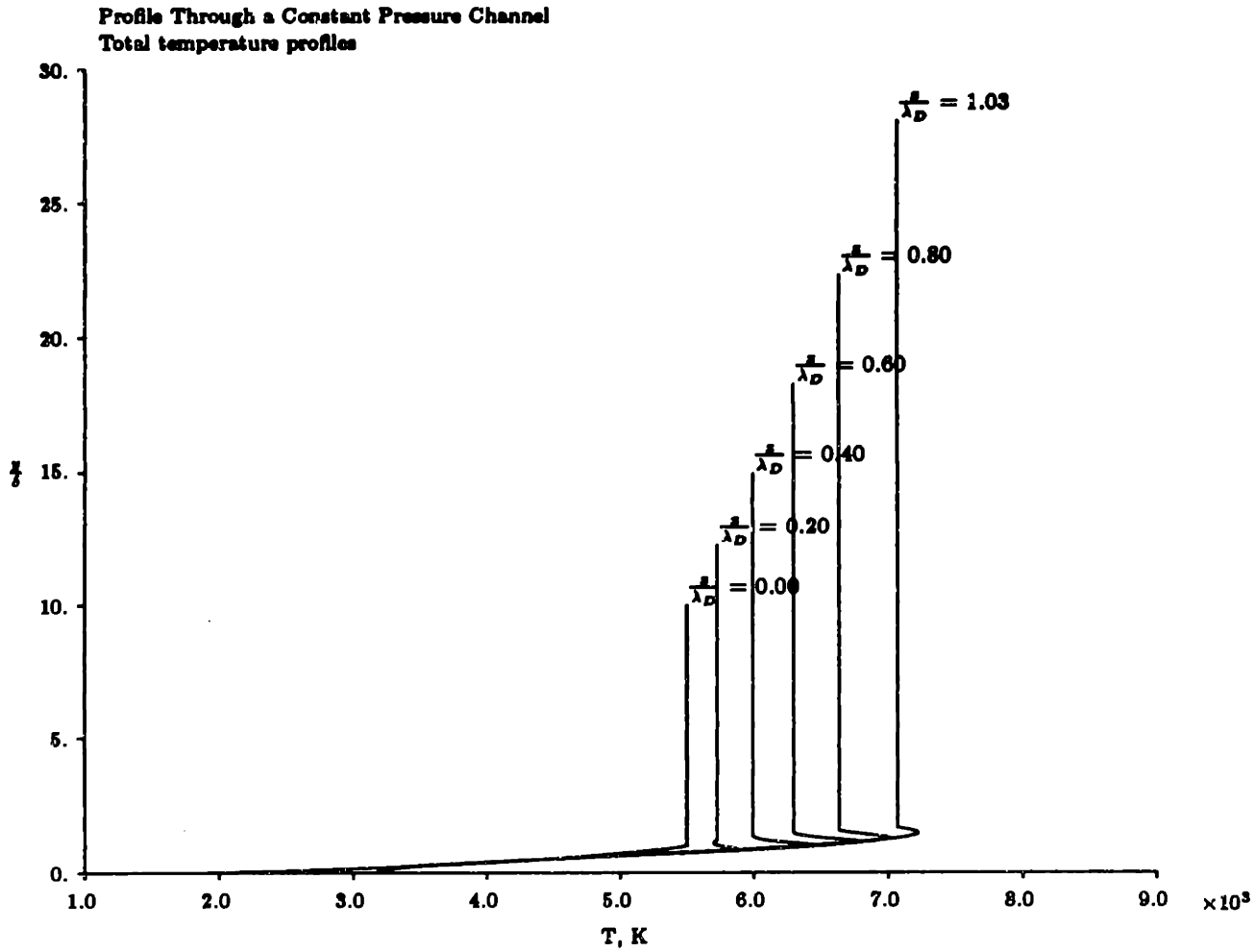

Figure 11.18: Free-stream total temperature along a constant pressure combustor with heating correction

If combustion does not continue in the nozzle, either because the nozzle is frozen or too short, the profile has resulted in a loss in total temperature in the free-stream. In addition, fuel added to the boundary layer has been lost, since the boundary layer temperature is limited, and there is little mass in the boundary layer. With the above final conditions coming out of the combustor, and adding in the energy from incoming fuel enthalpy and kinetic energy, the exhaust velocity after a perfectly expanded nozzle would be 4624 m/sec. The specific impulse of this engine would be 1570 secs, correcting for the fuel which is wasted in the boundary layer. This is a drop of 12% in specific impulse. Note that thrust will be reduced in approximate proportion to the thickness of the boundary layer, since the mass flux and heat addition there are much smaller than in the free-stream.

If the same boundary layer profile shape enters a constant pressure channel filling 25% of the inlet area, the resulting loss in heat addition is even more pronounced. In this case the thermodynamic changes are qualitatively similar to the above example, but the final total temperature drops to 7950 K, and the total pressure is 132 atm. The exhaust velocity without nozzle combustion would be 4595 m/sec, and the specific impulse, again correcting for lost fuel in the boundary layer, would be 1220 seconds, a dramatic loss. Even without correcting for lost fuel (i.e. if boundary layer fuel injection could be eliminated) specific impulse would drop to 1625 seconds with this 25% boundary layer. Figure 11.20 presents the specific impulse for the constant pressure combustor at Mach 6, 1000 K inlet temperature, at several more values of boundary layer fraction. Values are also shown for the "corrected" specific impulse, where realizable heat addition in the boundary layer is essentially lost. Note that the heating losses in the free-stream represent about 1/3 of the losses due to failed combustion in the boundary layer, so this is a noticeable effect. This boundary layer loss is a frozen loss, *independent of whether the heat addition process is mixing limited or reaction rate limited*, and so has more general applicability.

Of course, the static pressure and temperature drop translates into a reduction of the rate at which heat is added. This can be countered by making the combustor longer, with the penalty of a heavier engine. With a boundary layer of 10% initial thickness, 89 % of the available combustion enthalpy was released in the constant pressure combustor sized for uniform operation. However, the pressure was dropping monotonically, so the the

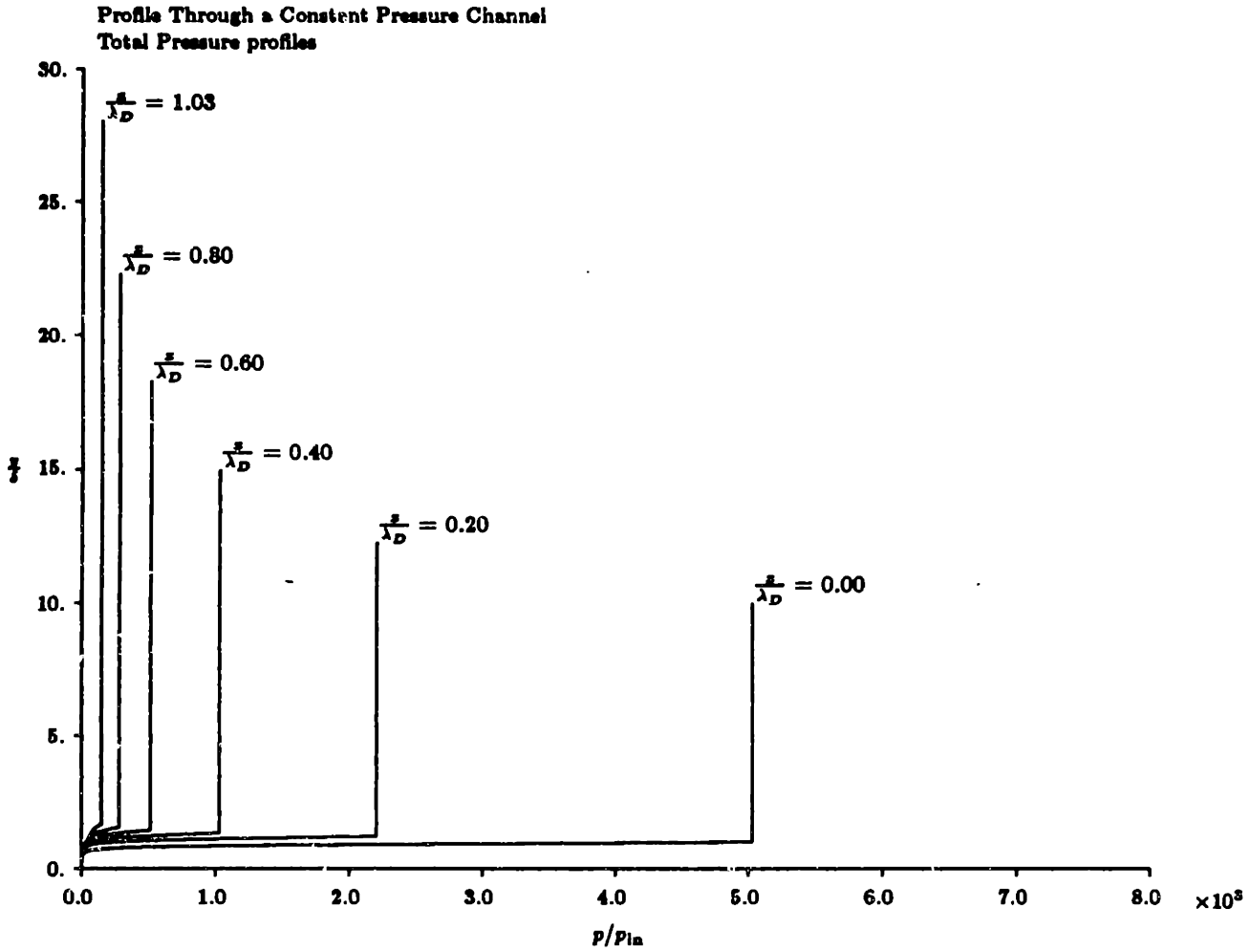

Figure 11.19: Free-stream total pressure along a constant pressure combustor with heating correction

combustion rate at the exit is only about 50% of the uniform flow design value. In order to release all combustion energy, the combustor with 10% boundary layer would have to be about 20% longer than the uniform inlet design. With a 25% boundary layer thickness at the inlet, the combustor would have to be 50% longer.

11.2 Constant Area/Constant Temperature Combustor

The constant area combustor with rapid heat addition was identified above as presenting a reasonable design, both in terms of providing efficient performance with limited adverse pressure gradient. This engine is also subject to the adverse effects of the boundary layer on free-stream combustion.

11.2.1 Without Changes to the Heating Rate

Figures 11.21 and 11.22 present the Mach number and temperature profiles through a constant area/constant temperature combustor without correcting heat addition for local thermodynamic conditions. These results are presented for the same inlet profile as was input to the constant pressure combustor, at 10% of the inlet area. As with the constant pressure combustor, the profiles do not deviate much from the expected values when local thermodynamic effects on the heating rate are not included. Mach number at the exit of the constant area region is about 3.6, and it remains fairly constant throughout the constant temperature region. Figure 11.23 shows that the static pressure also follows the predicted analytical behavior, rising by a factor of 2.9 when rapidly heated, then dropping back to about 1.5 times the inlet pressure. Temperature also follows the predicted analytical uniform solution closely, rising to the expected 2800 K, and falling only slightly in the constant temperature region, as shown in Figure 11.24.

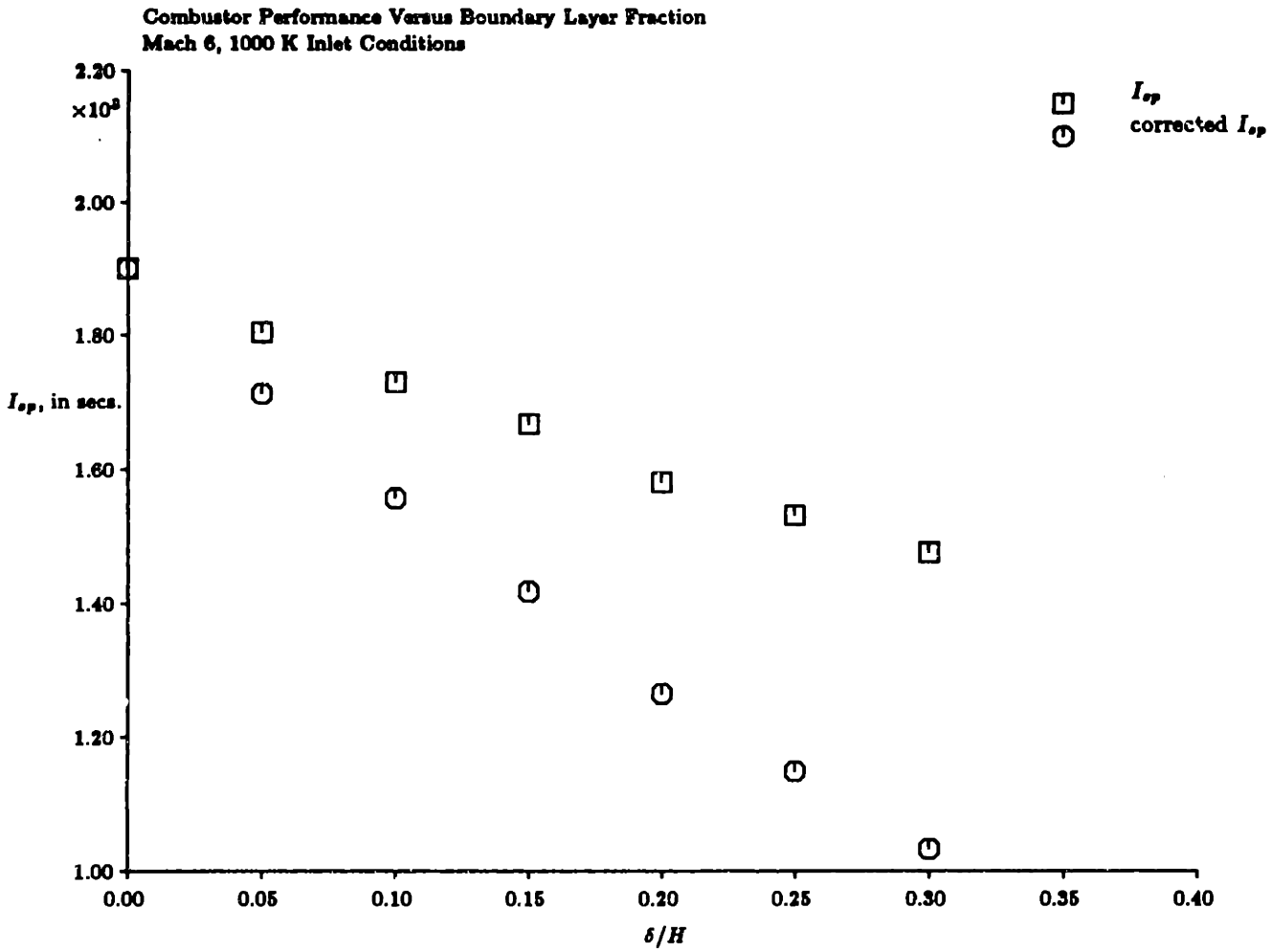

Figure 11.20: Specific impulse in a constant pressure combustor with heating correction

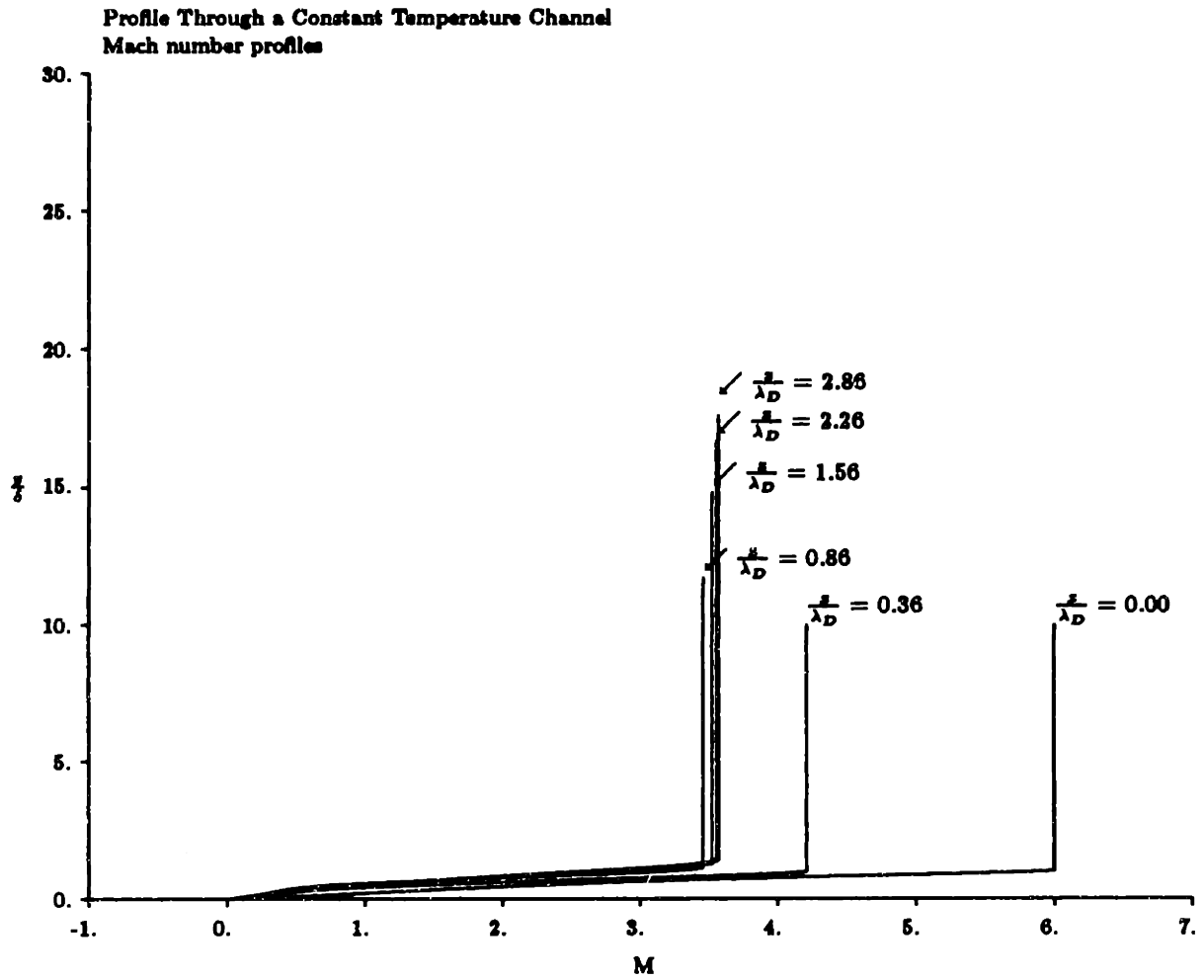

Figure 11.21: Mach number profiles at various stations through a constant temperature combustor

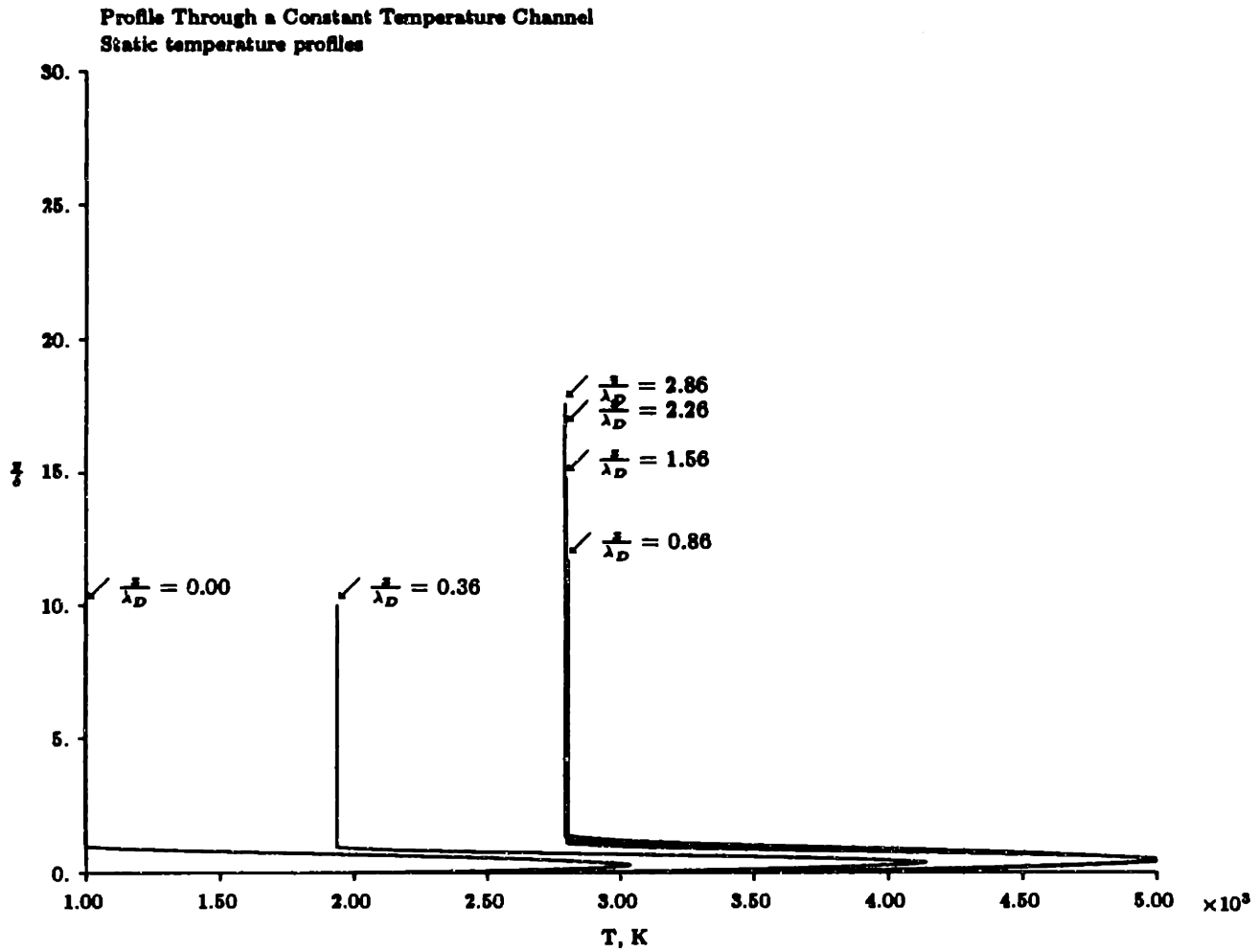

Figure 11.22: Static temperature profiles at various stations through a constant temperature combustor

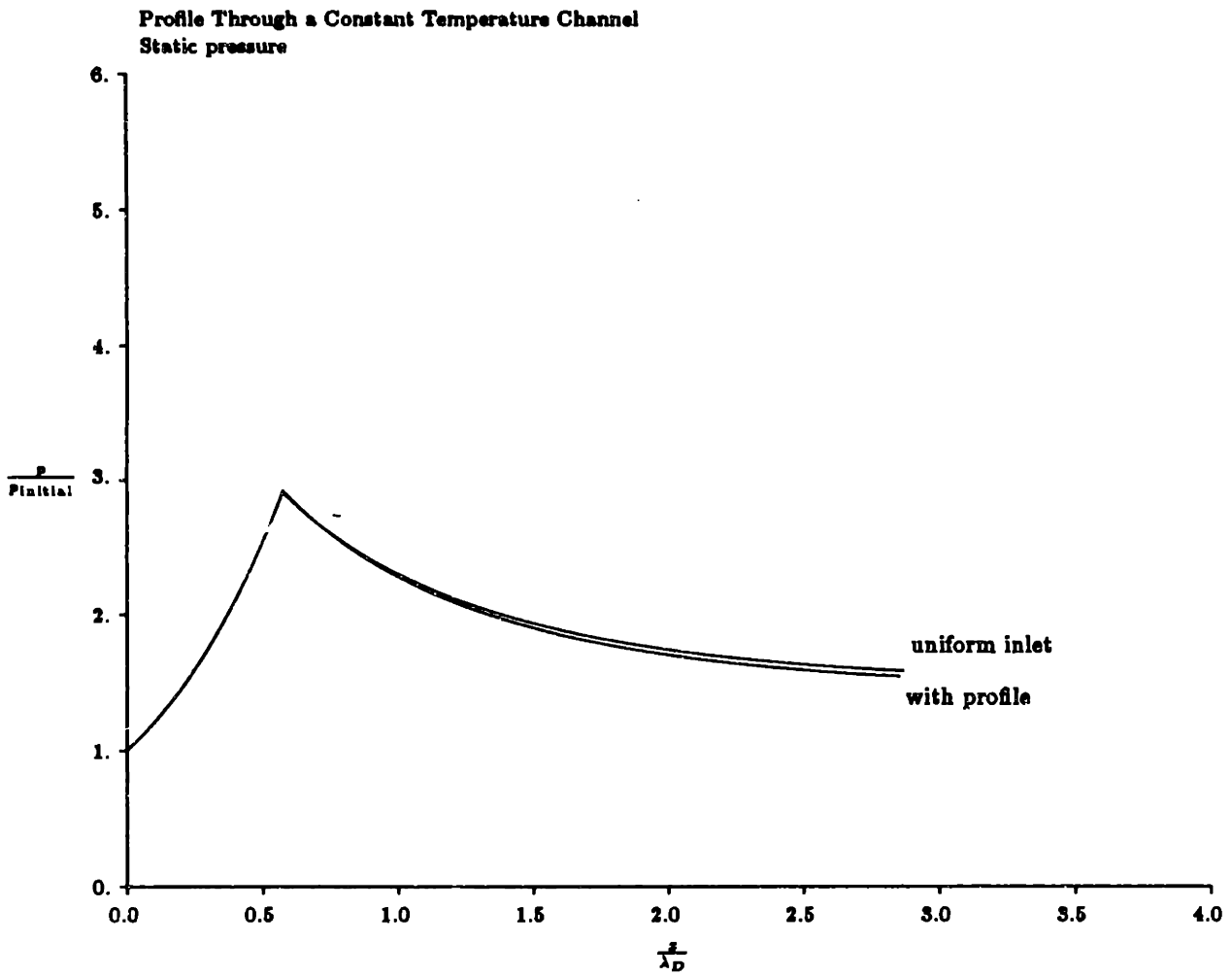

Figure 11.23: Free-stream static pressure along a constant temperature combustor

The free-stream Mach number falls very close to the analytical expectations, as shown in Figure 11.25, and the characteristic uniform boundary layer Mach number ranges from between 1.8 to 1.5, with a minimum at the end of the rapid heating. In Figures 11.26 and 11.27 it is once again clear that the boundary layer has nearly constant area. In the constant area duct, where $dA/A = 0$, the boundary layer will therefore have no effect on the free-stream. In the constant temperature region, the boundary layer will raise the magnitude of dA/A because the free-stream area is smaller than for the entire channel, but the change in area is the same. This is why there is a slight drop in temperature and pressure in the constant temperature region. However, since so little heat is actually added in this region, the boundary layer effect is minimal.

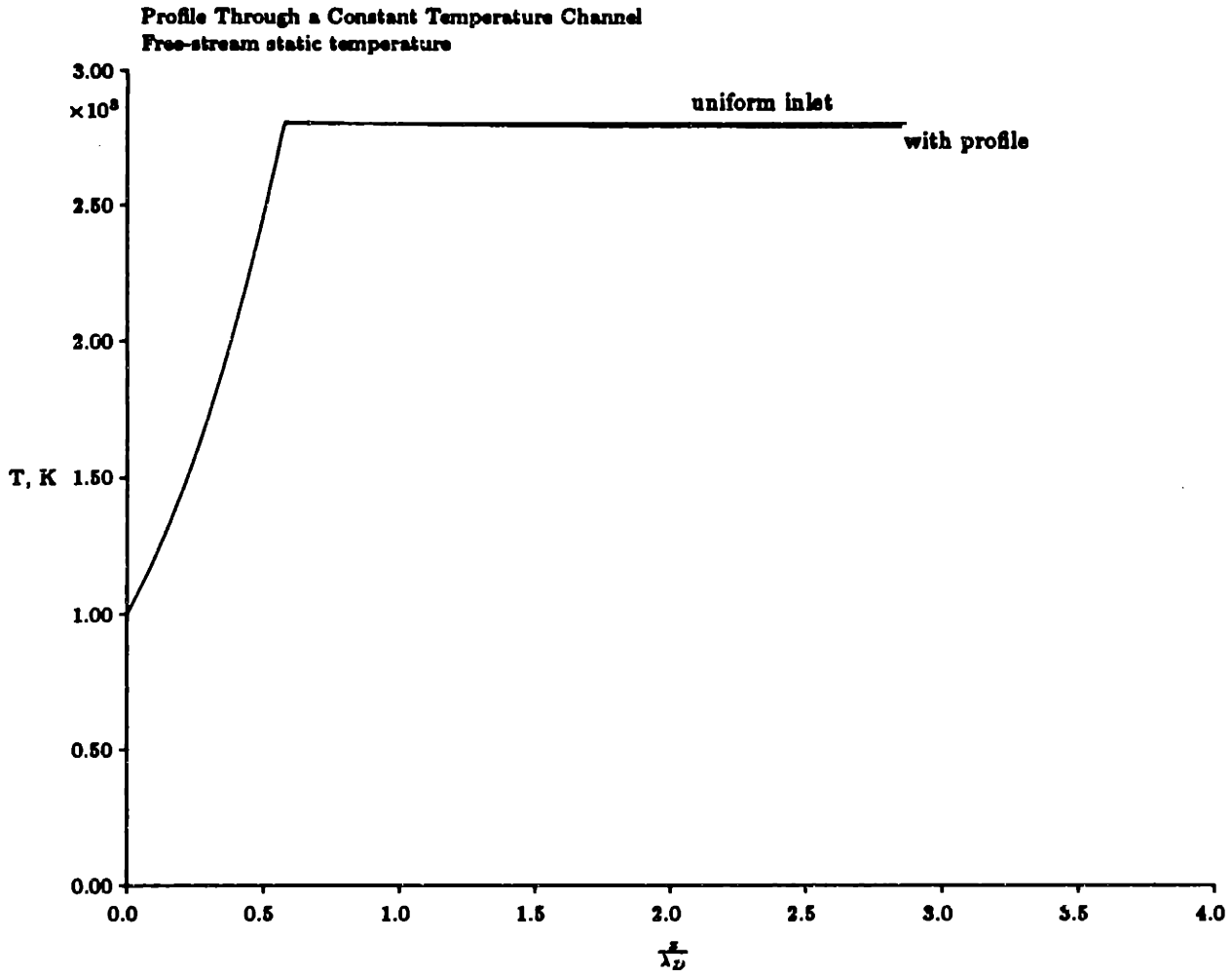

Figure 11.24: Free-stream static temperature along a constant temperature combustor

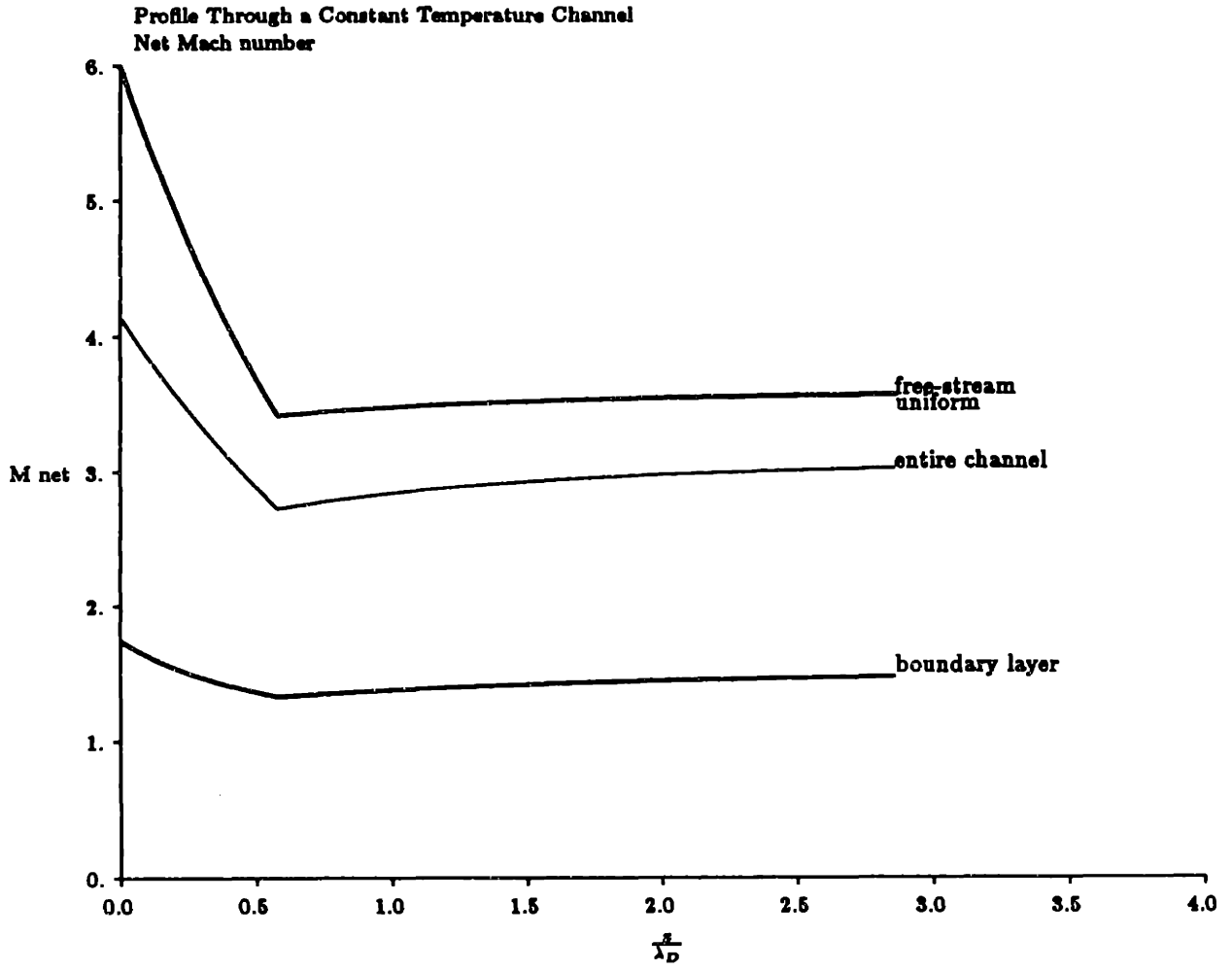

Figure 11.25: Effective uniform Mach numbers in a constant temperature combustor

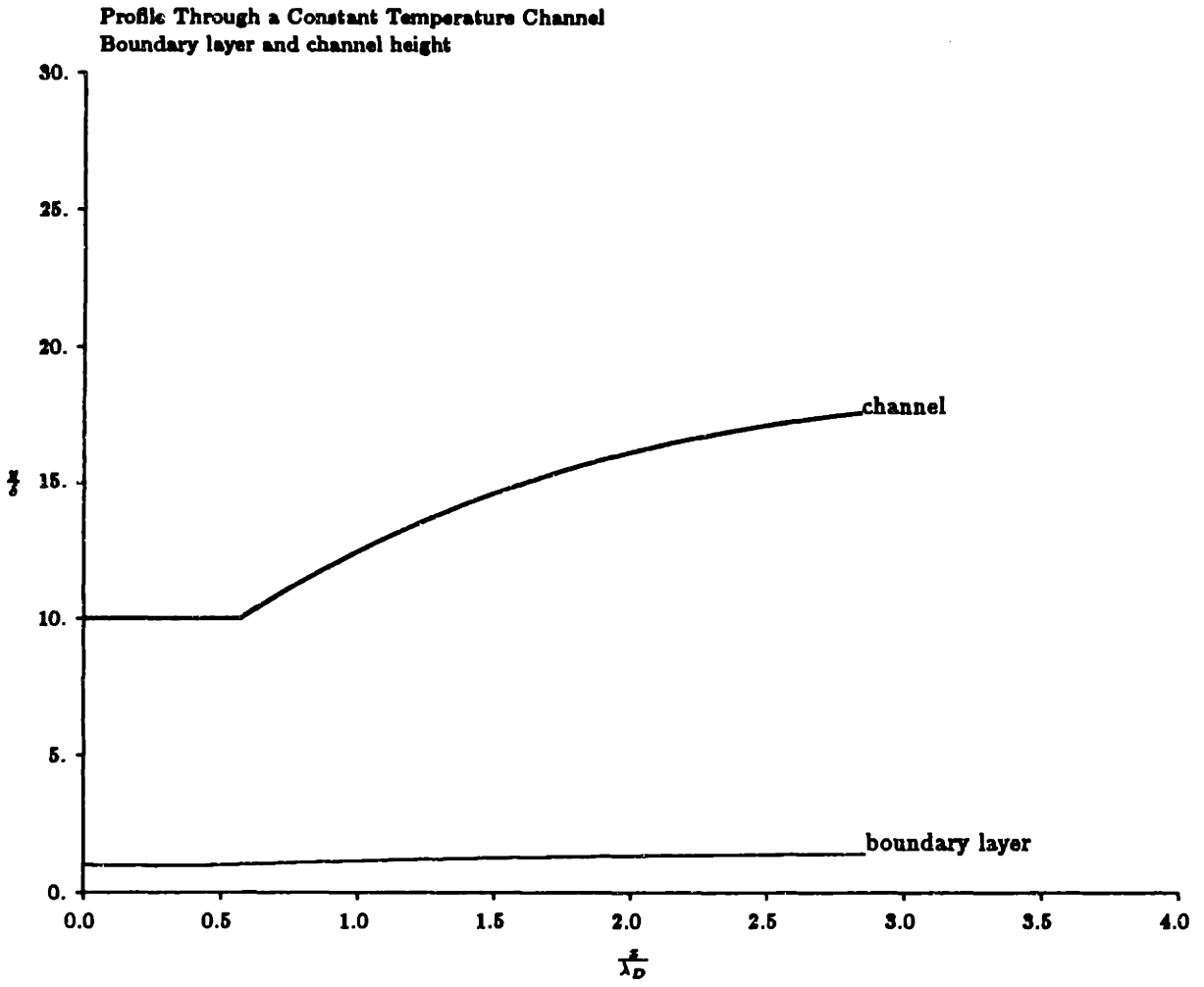

Figure 11.26: Channel height and boundary layer height in a constant temperature combustor

Finally, the total temperature and pressure profiles are presented in Figures 11.28 and 11.29. The free-stream values are identical to those expected from the analytical solution, because no change has been incorporated in the heat addition.

11.2.2 With Local Heating Rate Correction

When corrections are made for the rate of heat addition, the constant temperature combustor shows noticeable changes in operation, as did the constant pressure combustor. The above example was recalculated with the same approximation for local thermodynamic effects on heating rate that was used with the constant pressure case. The resulting Mach number profiles and temperature profiles are presented in Figures 11.30 and 11.31. Comparing these to Figures 11.21 and Figure 11.22, the Mach number at the exit of the constant area region is higher with heating correction, which indicates less heat has been added. The temperature coming out of the constant area region is also substantially lower than before. Note that the maximum boundary layer temperature has been limited.

With less heat addition, static pressure and temperature are noticeably lower than expected coming out of the region of rapid heating, as demonstrated in Figures 11.32 and 11.33. This corresponds to higher exit Mach number, and once again suggests less heat has been added. The free-stream Mach number remains above the expected uniform flow value through the entire engine (Figure 11.34).

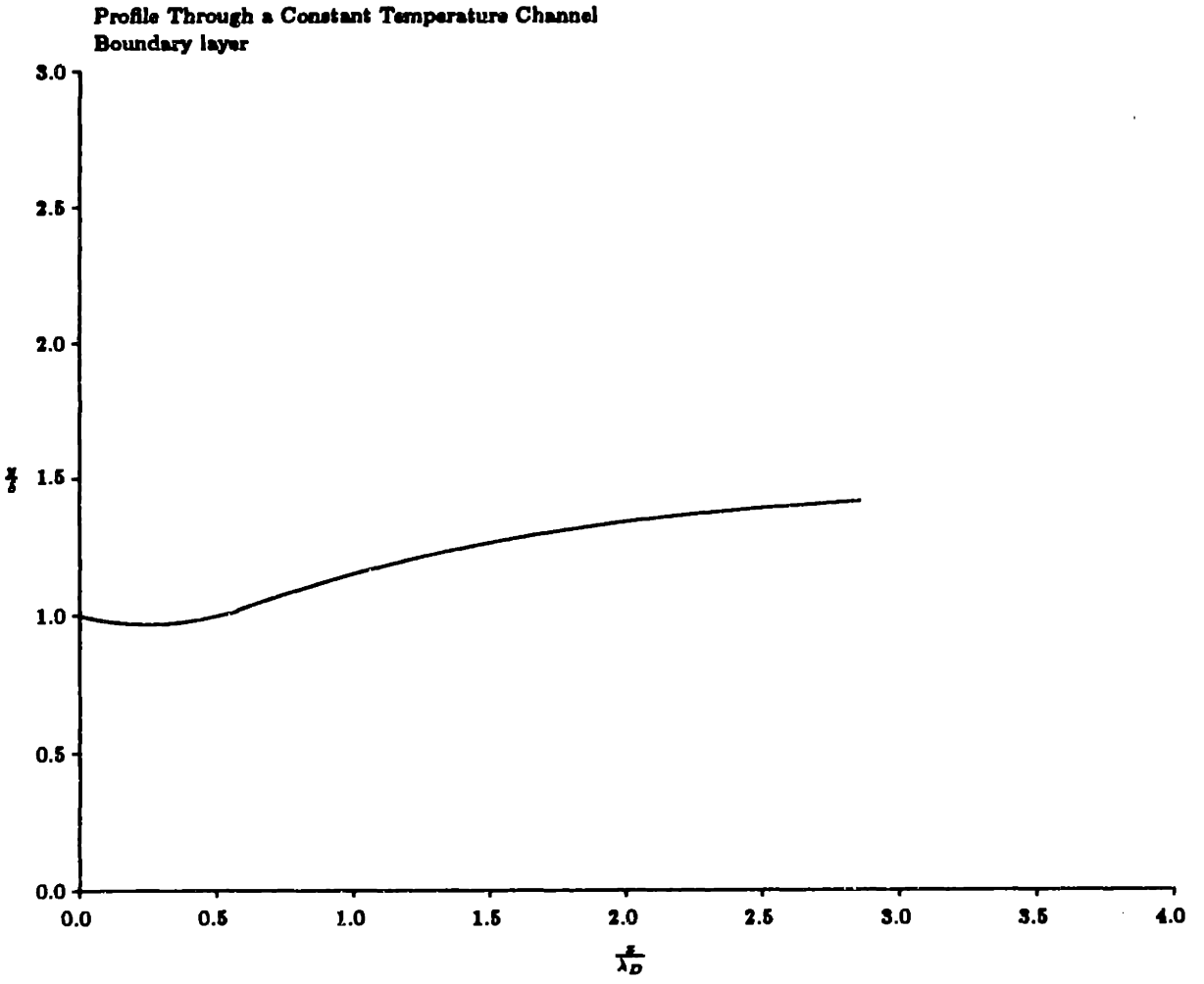

Figure 11.27: Magnified view of boundary layer height in a constant temperature combustor

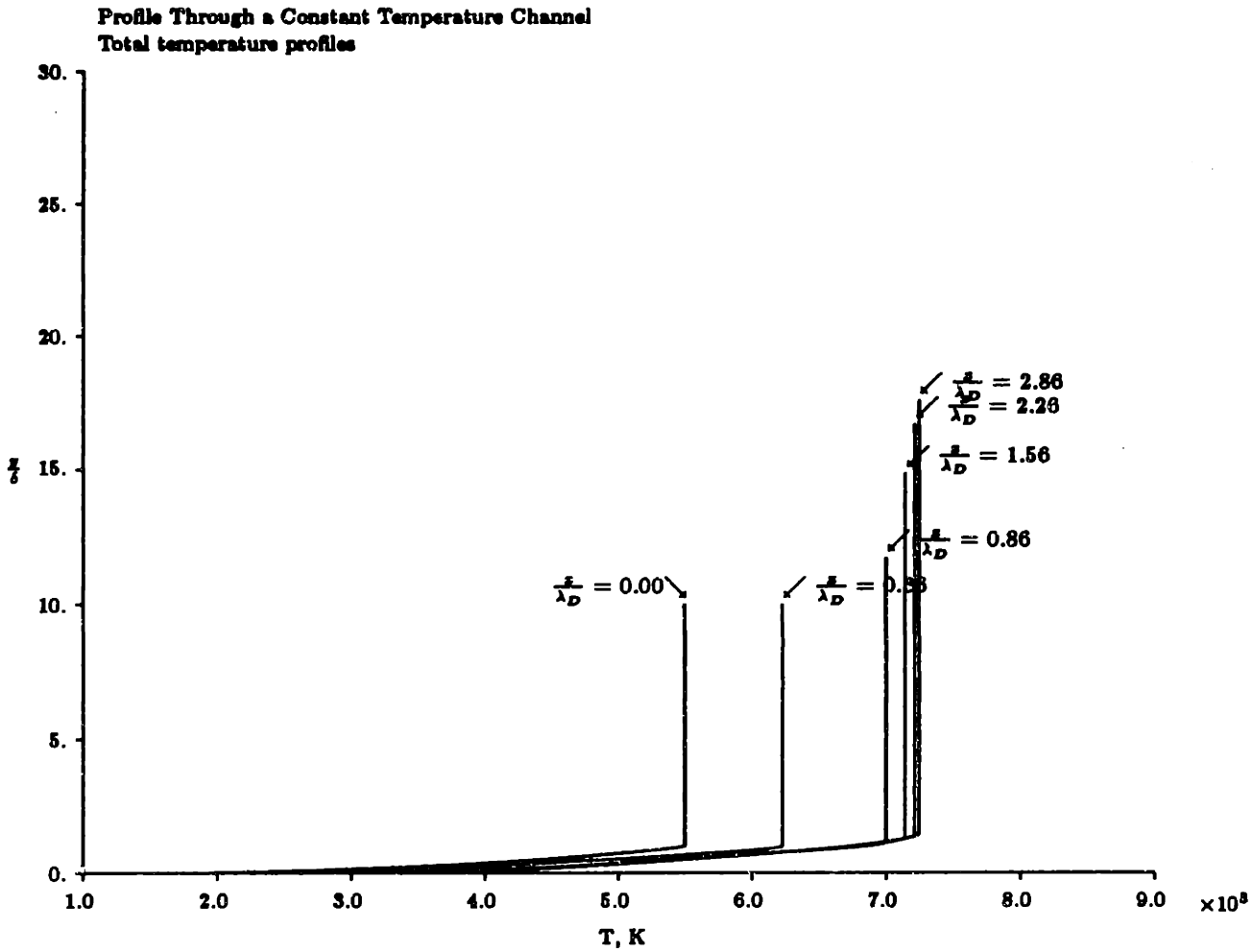

Figure 11.28: Free-stream total temperature along a constant temperature combustor

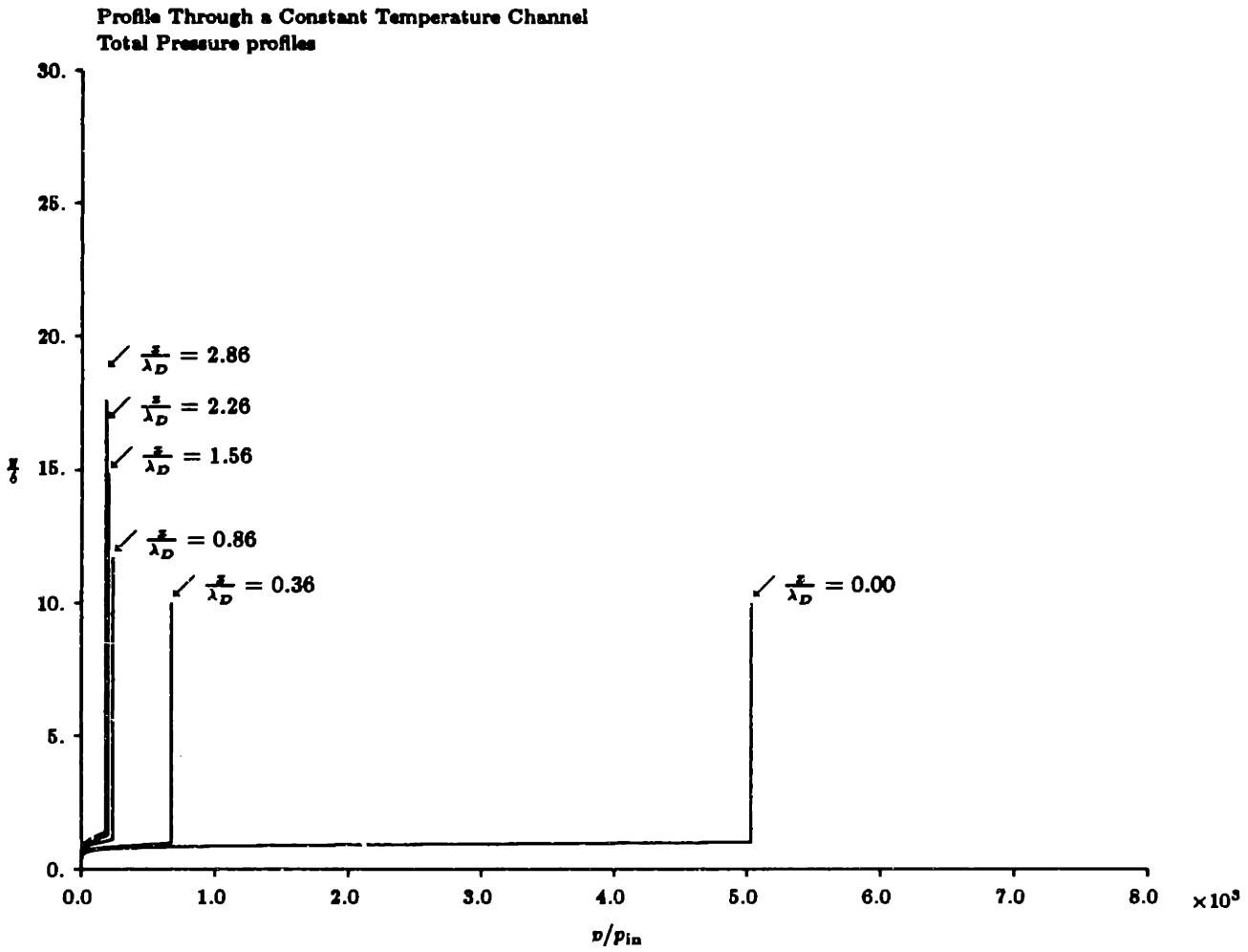

Figure 11.29: Free-stream total pressure along a constant temperature combustor

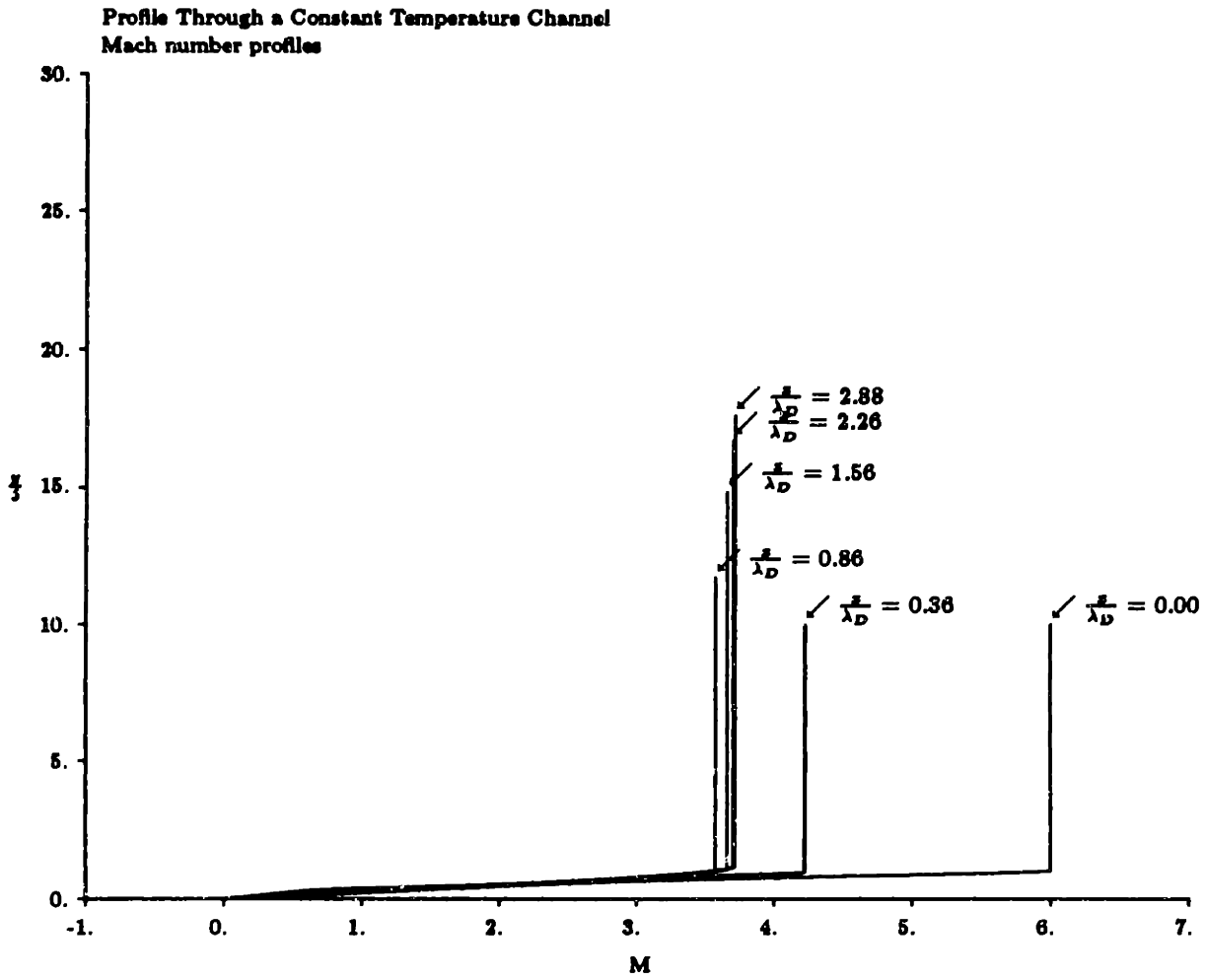

Figure 11.30: Mach number profiles at various stations through a constant temperature combustor with heating correction

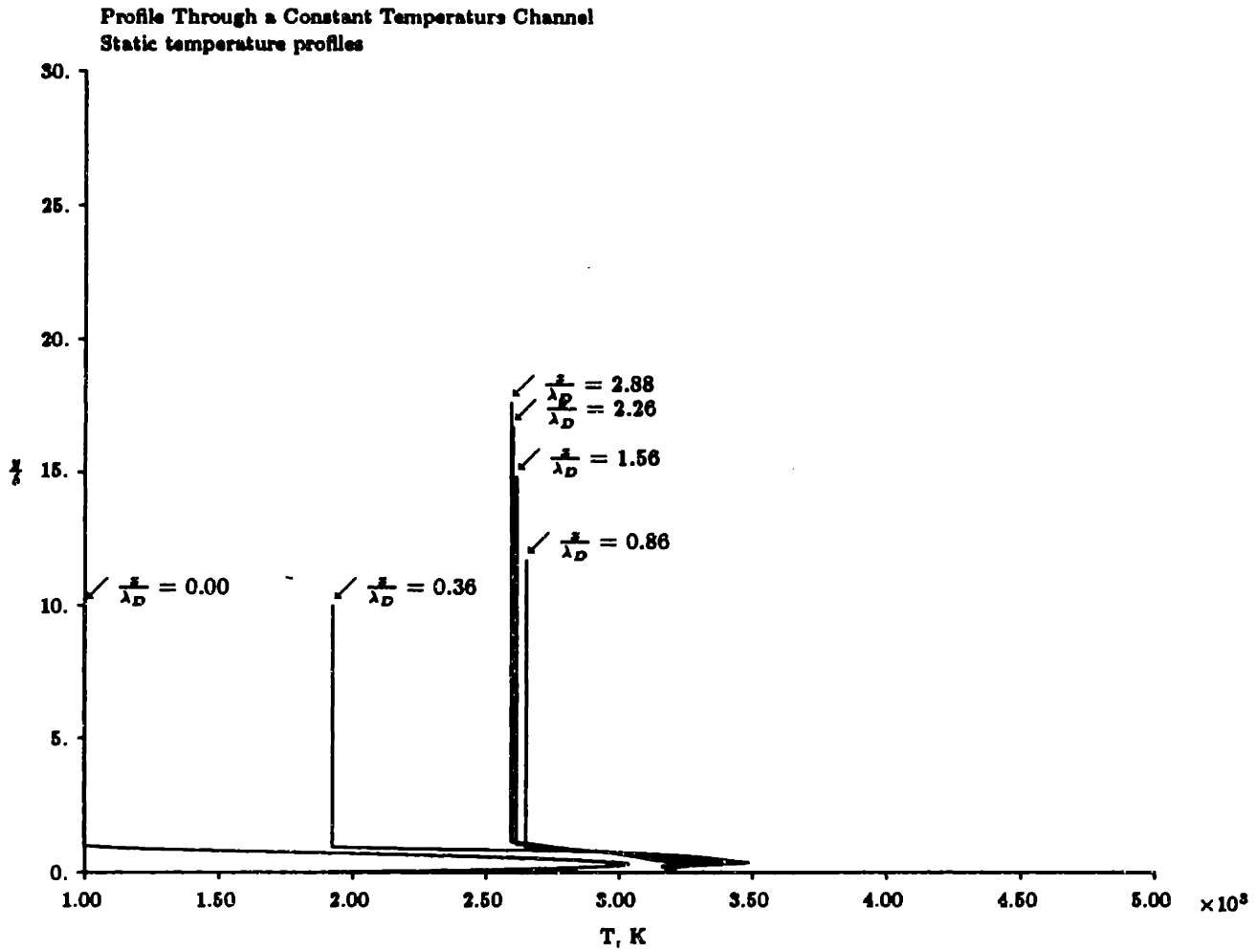

Figure 11 31: Static temperature profiles at various stations through a constant temperature combustor with heating correction

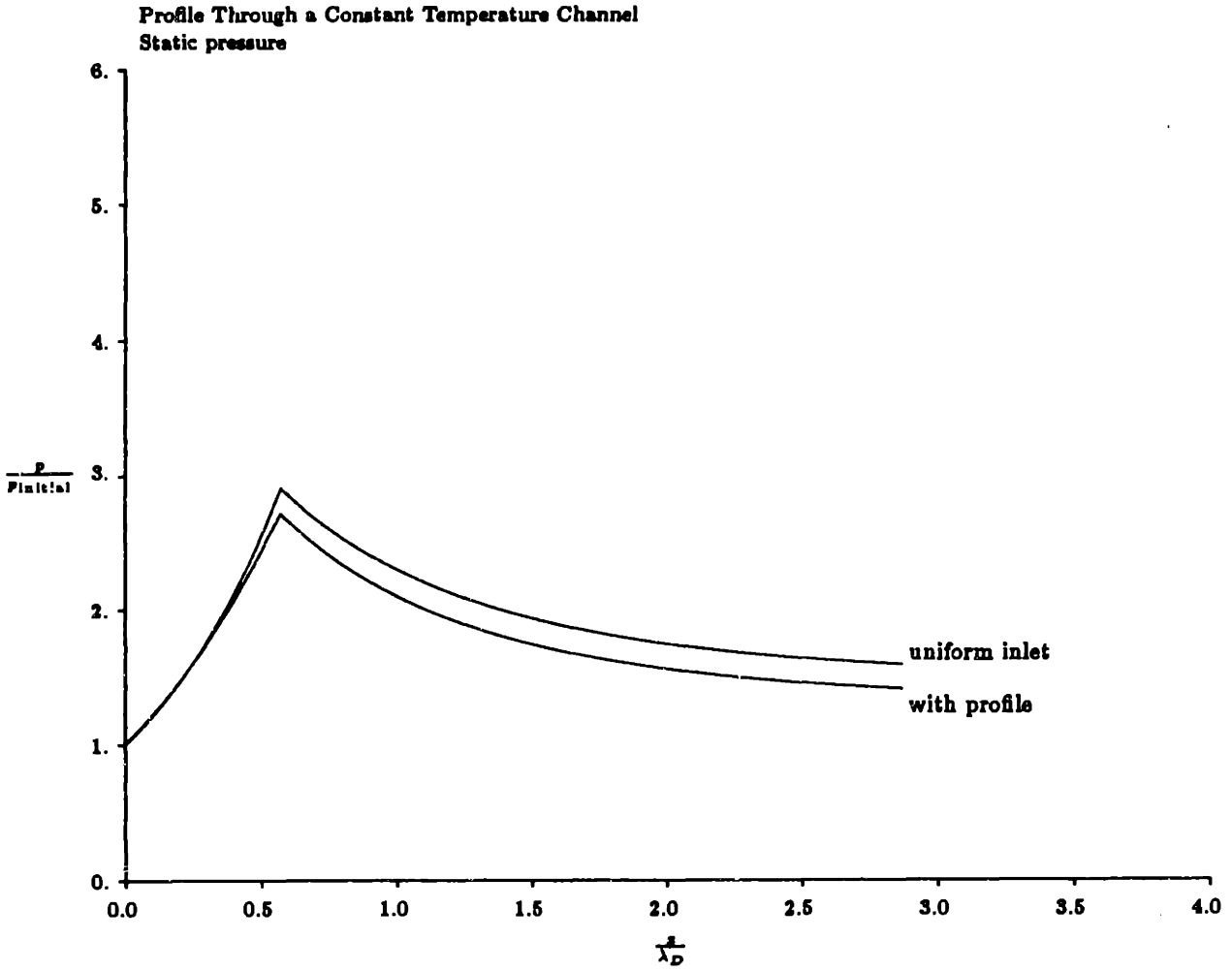

Figure 11.32: Free-stream static pressure along a constant temperature combustor with heating correction

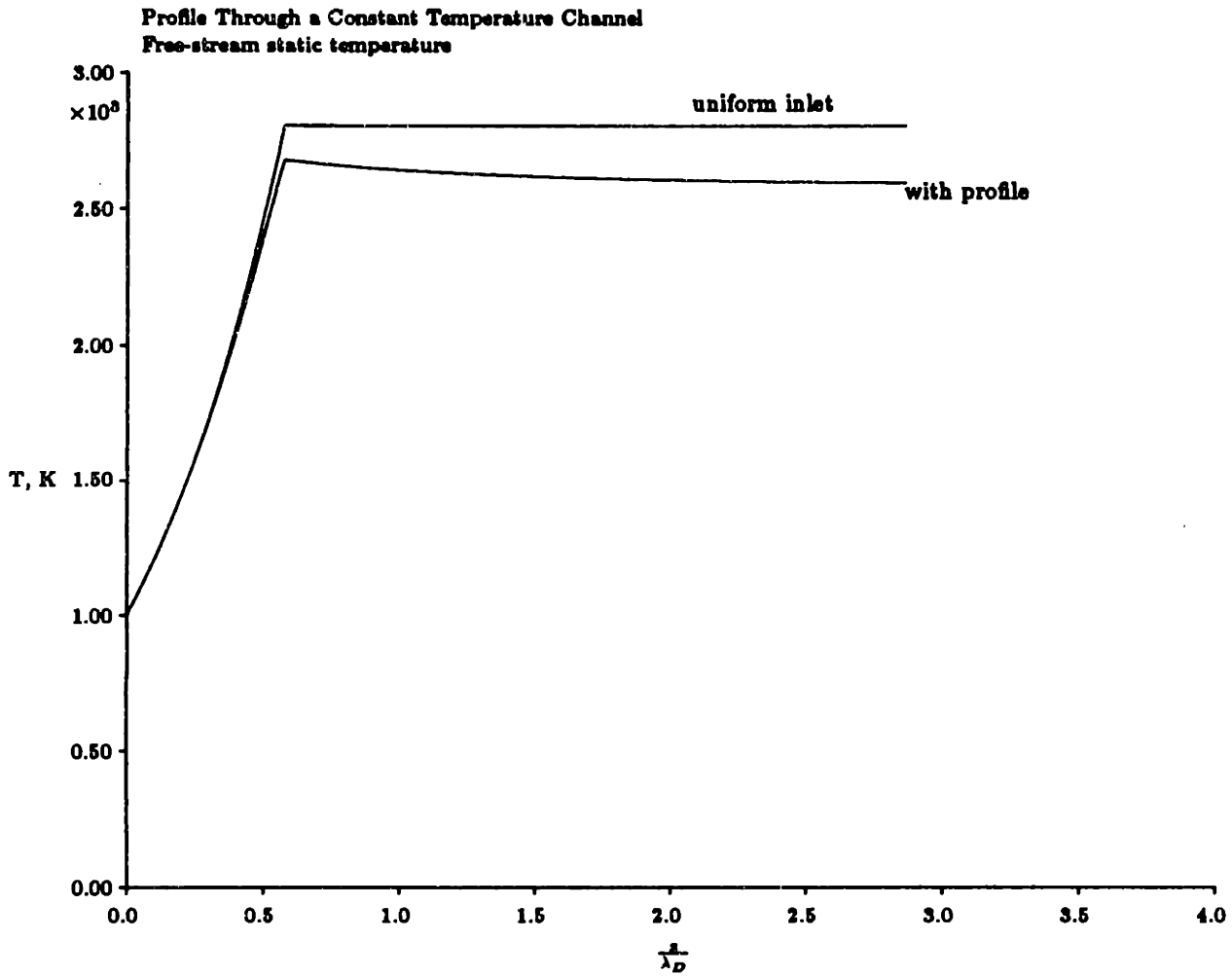

Figure 11.33: Free-stream static temperature along a constant temperature combustor with heating correction

The mechanism for these changes has been discussed in reference to the constant pressure combustor. Initially, there is rapid combustion throughout most of the boundary layer, resulting in a more rapid pressure rise, a thickening of the boundary layer (as seen in Figures 11.35 and 11.36) and a sudden drop in the characteristic uniform boundary layer Mach number. After this rapid combustion, the boundary layer is too hot to support further combustion. Heat addition in the free-stream increases pressure, which compresses the boundary layer, so the static pressure in the constant area region is lowered, along with the heating rate. The resulting total temperature and pressure profiles are pictured in Figures 11.37 and 11.38.

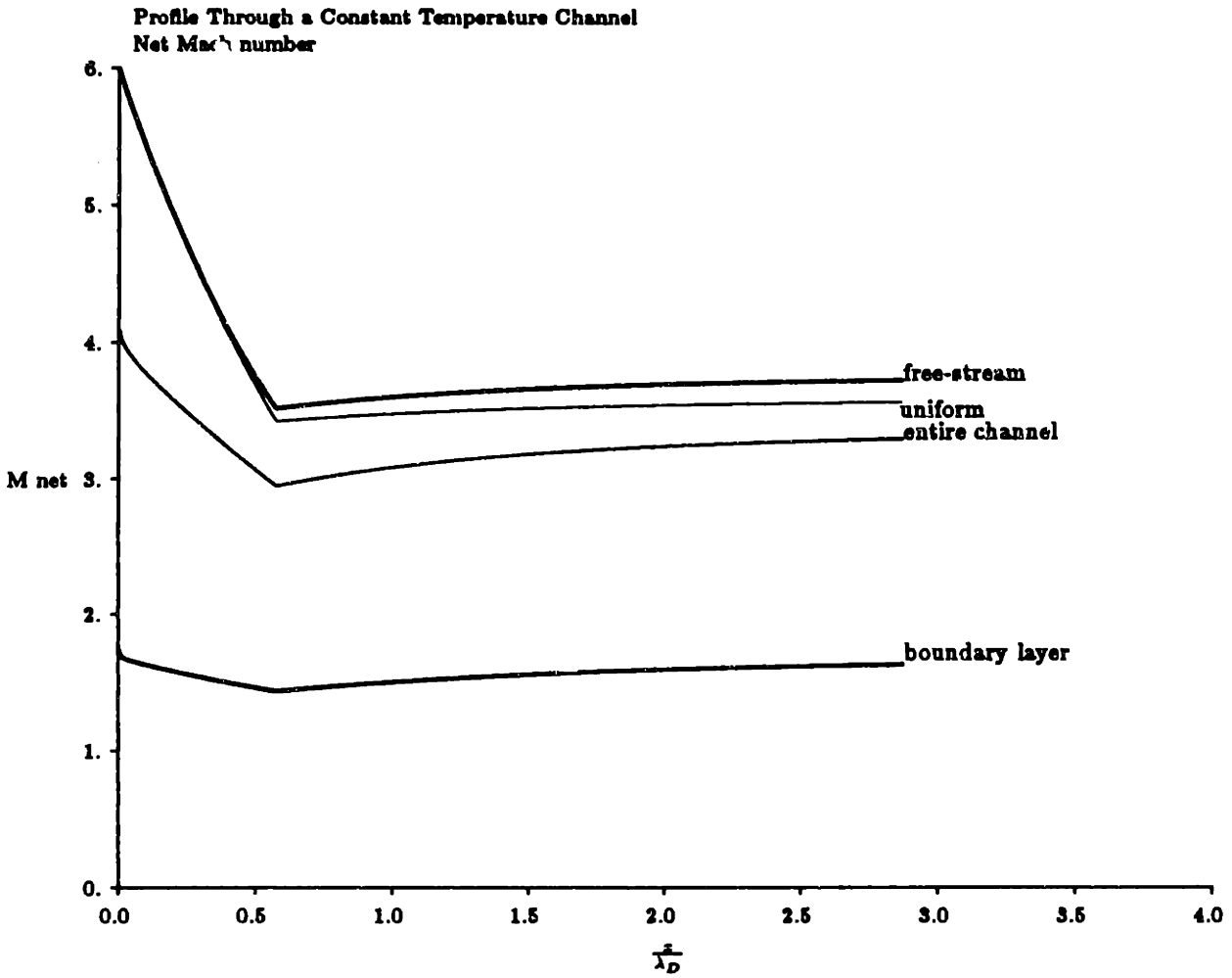

Figure 11.34: Effective uniform Mach numbers in a constant temperature combustor with heating correction

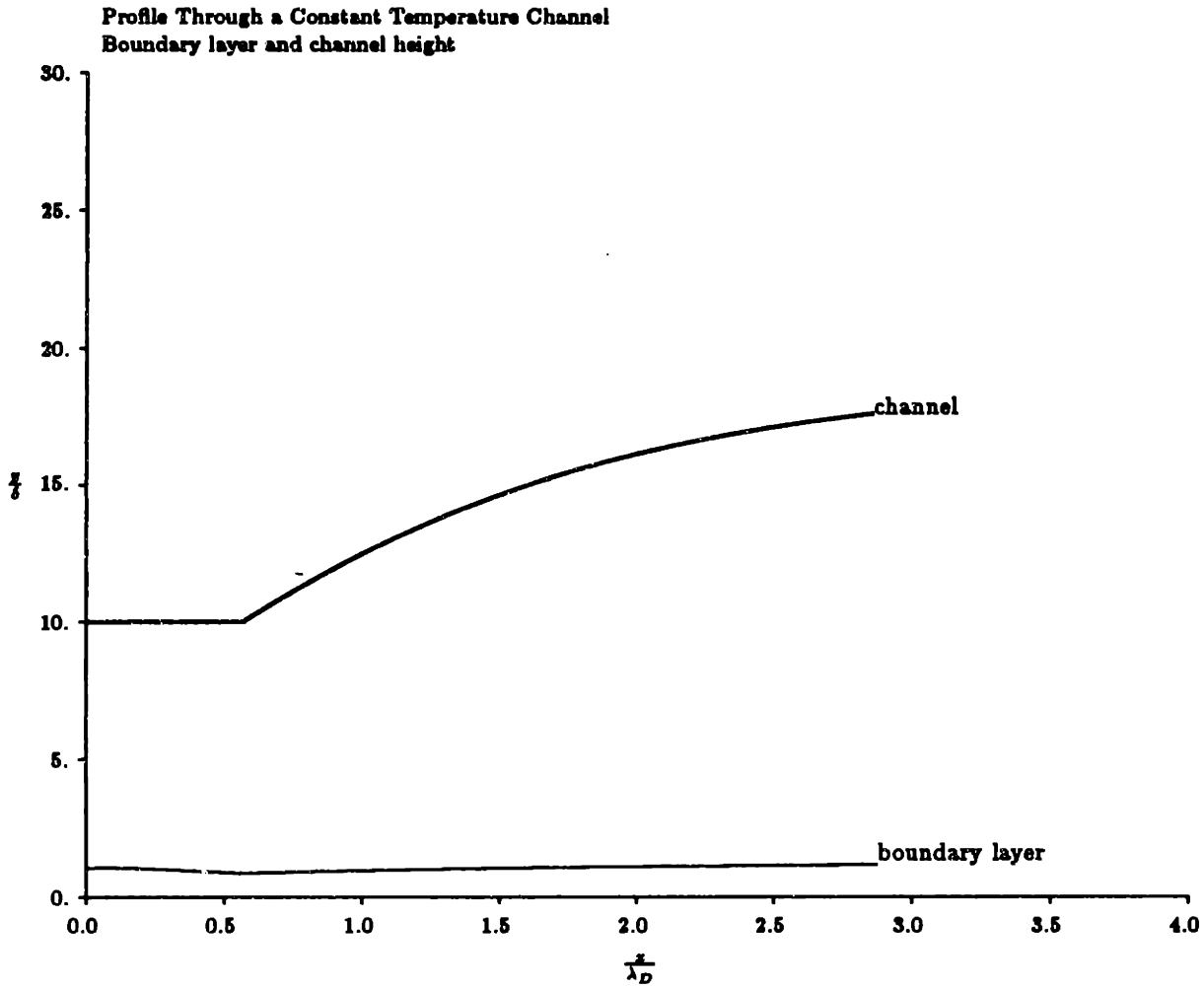

Figure 11.35: Channel height and boundary layer height in a constant temperature combustor with heating correction

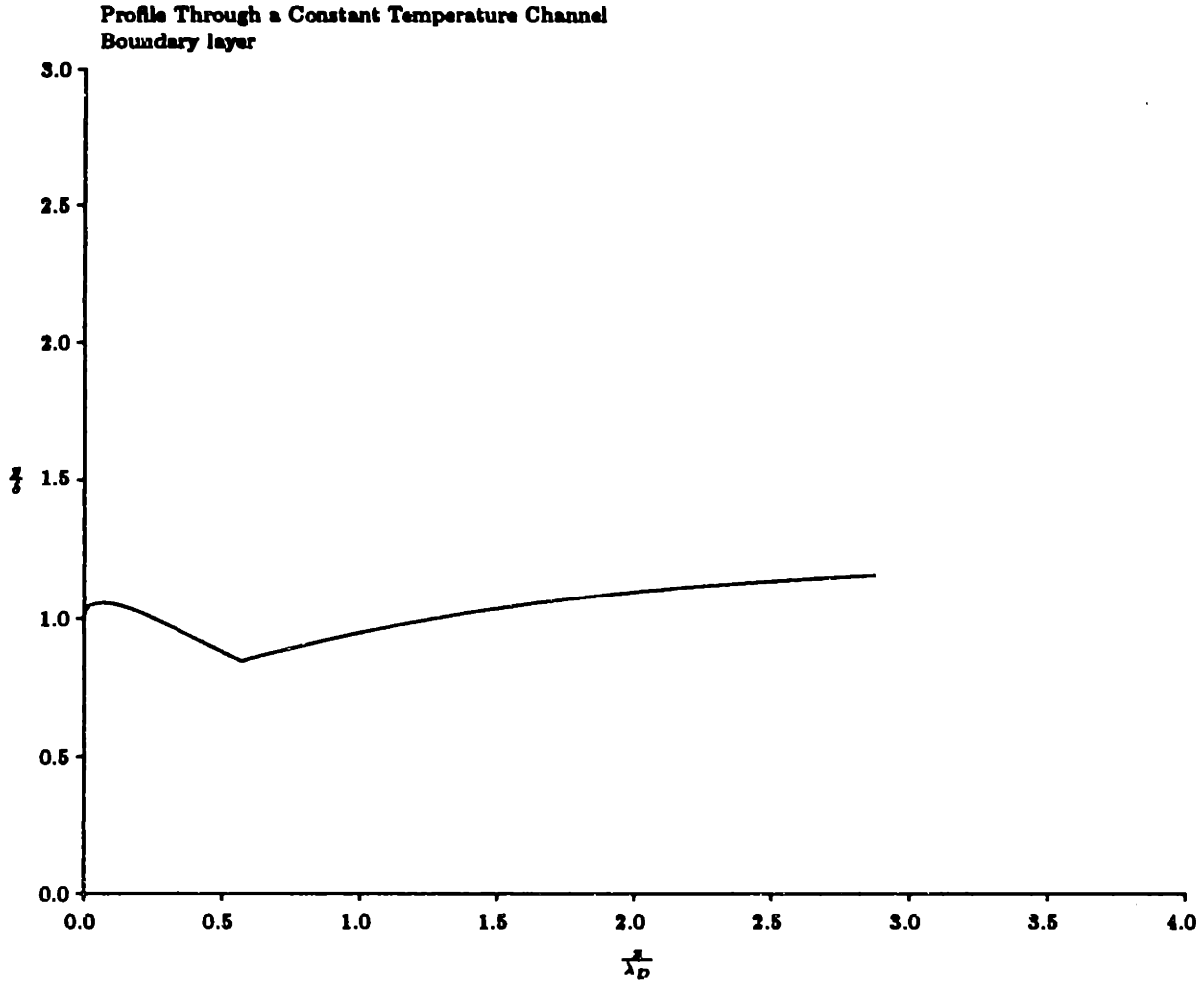

Figure 11.36: Magnified view of boundary layer height in a constant temperature combustor with heating correction

With the heating correction, the constant temperature combustor total temperature has risen to 7,868 K from the initial 6400 K, with a total pressure of 219 atm. This will produce an exhaust velocity of 4603 m/sec, and a specific impulse of 1654 seconds. Correcting for lost fuel in the boundary layer, the specific impulse would be 1490 secs. The uniform flow constant temperature combustor produced an exhaust velocity of 4673 m/sec, and a specific impulse of 1900 seconds, so it is immediately apparent that the detrimental effects of the boundary layer have been larger in the constant temperature combustor than in the constant pressure solution.

Figure 11.39 presents the specific impulse for this combustor as a function of boundary layer area fraction at the inlet. In general, the constant temperature combustor suffers substantially lower loss in specific impulse than the constant pressure channel. Beyond a relative boundary layer thickness of 15%, the uncorrected specific impulse is nearly independent of boundary layer height in this design.

11.3 Incorporating Combustor Losses in Inlet Efficiency

Evaluating the ultimate impact of the boundary layer on combustor performance will depend on the details of the individual combustor design. For instance, the loss of heat addition in the boundary layer delays the reaction rate in the free-stream if it is reaction rate-limited. If the combustor has been sized for ideal uniform conditions, this delayed reaction time will result in reduced enthalpy. On the other hand, the combustor could be designed with sufficient channel length that the combustion reaction will run to completion, so there will be no net loss in heat addition. This combustor would be longer, and therefore heavier, than the uniform inlet design. The loss introduced by the boundary layer would therefore be increased engine weight, not reduced specific impulse.

Regardless of the loss mechanism, the boundary layer, in changing the performance of an engine that has not been properly designed to account for an inlet profile, has introduced inefficiencies. The boundary layer profile is a direct consequence of the forebody shape. Thus, the inlet design has had a direct impact on the performance of the combustor. To

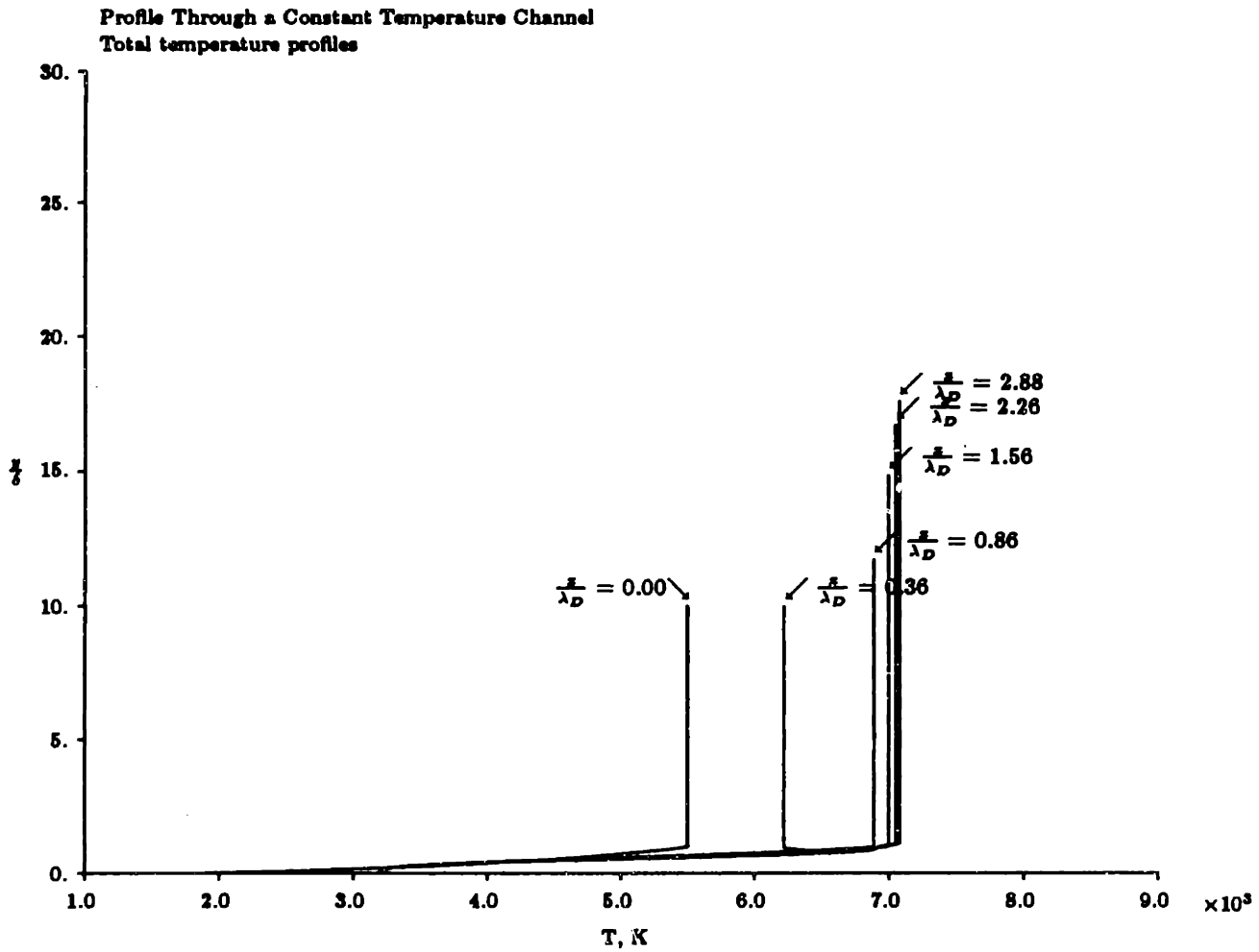

Figure 11.37: Free-stream total temperature along a constant temperature combustor with heating correction

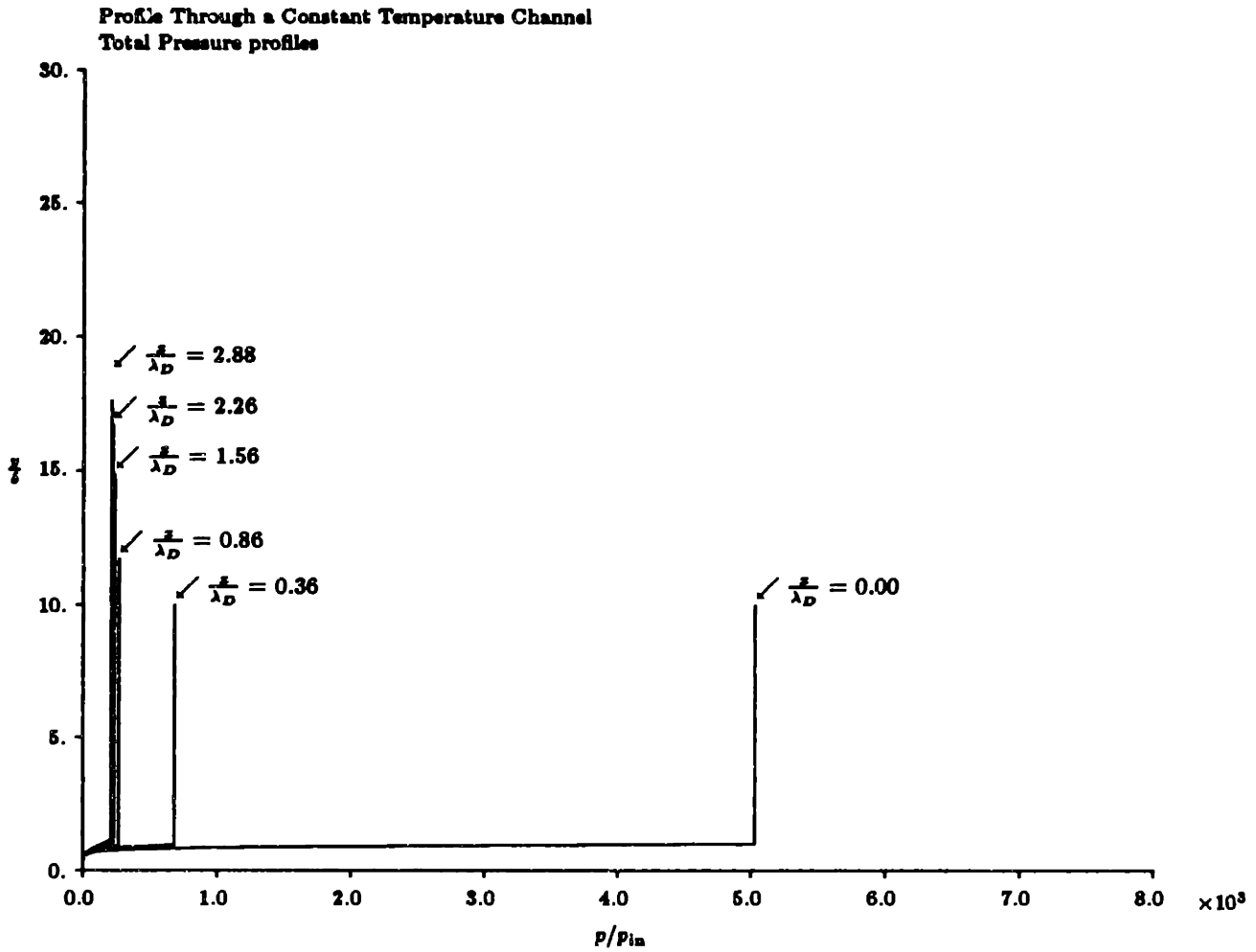

Figure 11.38: Free-stream total pressure along a constant temperature combustor with heating correction

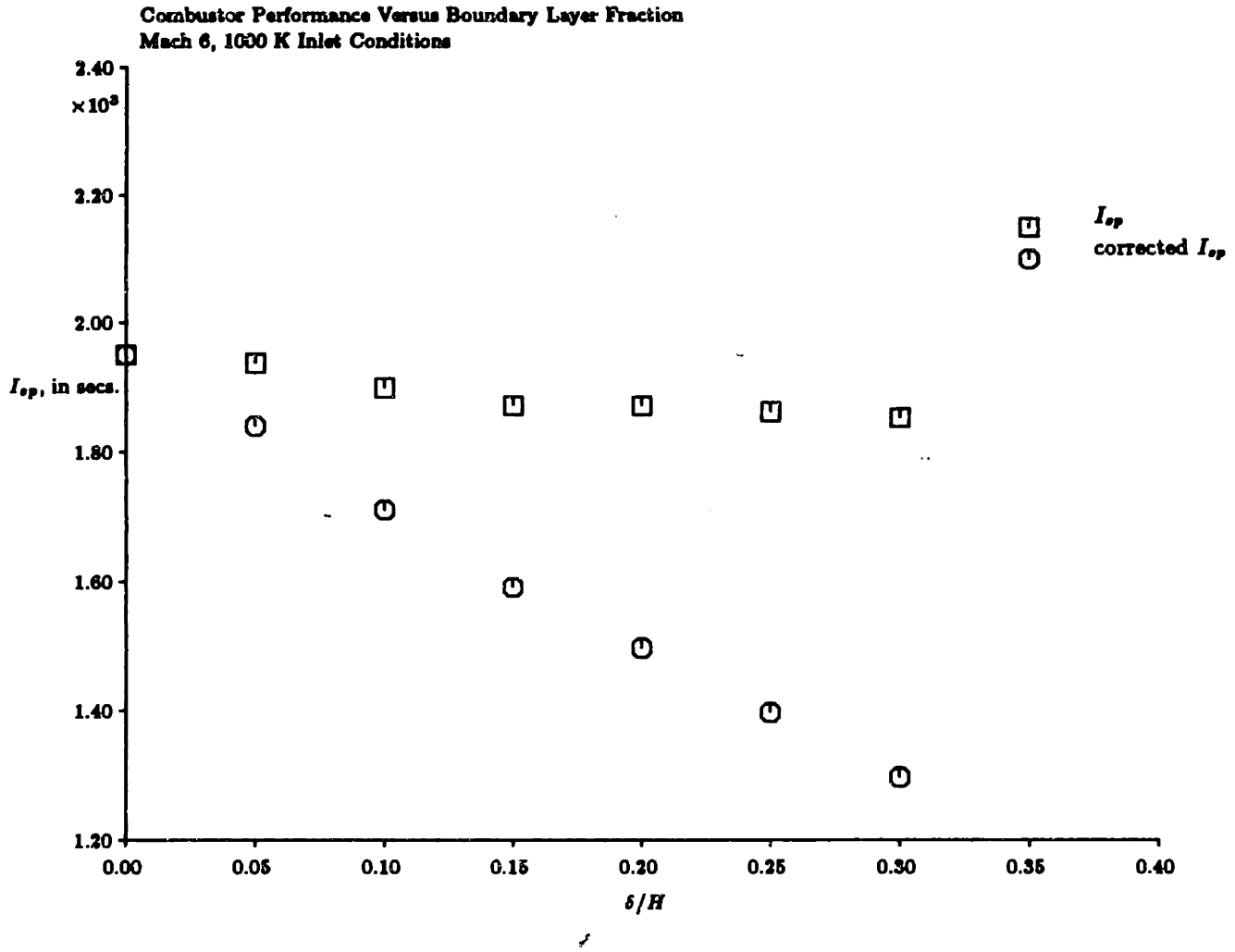

Figure 11.39: Specific impulse in a constant temperature combustor with heating correction

correctly evaluate the efficiency of a forebody inlet design, particularly for purposes of comparison with competing designs, it is appropriate to consider the adverse effects on combustor performance caused by the inlet profile.

The most common measure of hypersonic inlet performance is the kinetic energy efficiency, η_d, defined as the ratio of the available kinetic energy after diffusion to the available kinetic energy before diffusion when the flow is expanded to ambient pressure [2]. Thus, we can write:

$$\eta_d = \frac{h_o - h'}{h_o - h} \tag{11.3}$$

where h_o is the ambient stagnation enthalpy, h is the ambient static enthalpy, and h' is the hypothetical enthalpy obtained by isentropic expansion at the end of the inlet to ambient conditions. This parameter has the desirable properties of being insensitive to flight Mach number, and being very convenient for use with Mollier data.

The question arises as to how best to incorporate viscous effects into an efficiency parameter such as the kinetic energy efficiency. It is natural to suggest that some average kinetic energy efficiency should be defined which includes the boundary layer profile, and the resulting deficit of kinetic energy. This approach is questionable, because it isn't clear that there is an appropriate means of averaging, or weighting an integration. More importantly, it is contradictory to the notion of unmixing streamtubes. If the inlet profile is not mixed out (which has been the assumption throughout this work) the deficit in the boundary layer will have no direct bearing on the free-stream.

Attempting to include boundary layer effects in some generalized efficiency parameter is another means of treating the inlet as a one-dimensional flow, which ignores the fact that the profile is fundamentally multi-dimensional. In this work, some means of simplifying the influence of the boundary layer have been presented, but this has always been in the guise of a modified two- dimensional structure. For instance, the simplest model of the inlet profile presented above was the notion of the uniform Mach number, in which the profile for the entire channel was replaced by a uniform streamtube of some appropriate Mach number. This was seen to be useful in characterizing properties at one given station only, and not to be a good prediction of property changes downstream. To predict engine properties, the

profile had to the followed down the channel.

It is not obviously justified to talk about an average kinetic energy efficiency in an attempt to blend the boundary layer and the free-stream properties when these streamtubes will not mix, and so will have separate properties. The kinetic energy efficiency of the free-stream will therefore not be changed by the presence of the boundary layer, except in variations induced in the strength of the bow shock, and these will be negligible in the weak interaction region.

Viscosity will introduce wall shear, and this will affect momentum. Swithenbank [37] has attempted to correct the kinetic energy efficiency for viscous effects by calculating the coefficient of friction based on inlet capture area and using it to define an effective inlet velocity. Once again, it is questionable whether this approach is meaningful above the boundary layer, where the wall shear has not penetrated. The very notion of the boundary layer approximation allows us to neglect wall shear in the free- stream. If the free-stream flow does not mix with the boundary layer profile, we must again dismiss the notion of boundary layer affecting the value of "recoverable" kinetic energy in the free-stream. It is possible to correlate the calculated viscous effects with kinetic energy efficiency. This provides some means of comparing inlets.

The kinetic energy efficiency can be related to the forebody wedge angle because it is a function of the shock strength. Following Kerrebrock [2], the total pressure ratio across the bow shock π_d on the inlet diffuser can be written in terms of the kinetic energy efficiency and the flight Mach number:

$$\pi_d = \left[1 + (1 - \eta_d)\frac{\gamma - 1}{2} M_o^2\right]^{-\gamma/(\gamma-1)} \tag{11.4}$$

The kinetic energy efficiency can therefore be solved in terms of the shock strength:

$$\eta_d = 1 \; - \; 2\frac{\pi_d^{-(\gamma-1)/\gamma} - 1}{(\gamma - 1)M_o^2} \tag{11.5}$$

where the total pressure ratio across the shock is a function of flight Mach number and wedge angle.

The boundary layer thickness is also related to the flight Mach number and wedge angle,

so the demonstrated changes in combustor performance can be related to the kinetic energy efficiency. The added losses in exhaust velocity can be converted to losses in total kinetic energy. Although this loss is occurring in the combustor, it can be thought of as originating from the inlet, because the boundary layer structure is determined by the inlet. If this loss is then included in the kinetic energy loss of the inlet, a new kinetic energy efficiency can be derived *for the free-stream* based on the total exhaust velocity deficit. Use of this viscous-corrected parameter is inconvenient, for it assigns combustor losses to the inlet, and therefore does not permit the ready calculation of inlet properties. However, it does provide an indication of the impact of viscous inlet effects on the entire engine system.

The exhaust velocity-corrected kinetic energy efficiency is plotted in Figure 11.41. This viscous-modified efficiency is not averaged, but rather based on the gross properties of the free-stream. The area- averaged kinetic energy efficiency is also plotted in Figure 11.41 Note that the specific impulse correction is strongly dependent on the choice of combustor. Here, values have been calculated for the Mach 6, 1000 K inlet temperature constant pressure design.

The exhaust velocity-corrected kinetic energy efficiency is higher than area-averaged kinetic energy efficiency. This is because the exhaust velocity approach applies only to the free-stream, and does not consider the changes in thrust and specific impulse that result from mass flux and combustion losses in the boundary layer. In general, for moderate wedge angles, the area-average efficiency has viscous losses that are approximately equal to the shock losses. If the inviscid inlet has $\eta_d = .95$, the viscous inlet will have $\eta_d \simeq .90$. The exhaust velocity-corrected efficiency is generally about 1% lower than the inviscid value, and is therefore much less sensitive to changes in the boundary layer structure of the inlet. At very low and very high Mach numbers, the corrected kinetic energy efficiency will approach the inviscid value. At these points, viscous losses will have minimal effect on the free-stream, since combustion is most sensitive at the middle of the transatmospheric trajectory.

It is possible to include the lost thrust due to the presence of the boundary layer in another modified kinetic energy efficiency. Once again, averaging across the inlet profile is an incorrect approach to including these effects. What matters most is final effect on

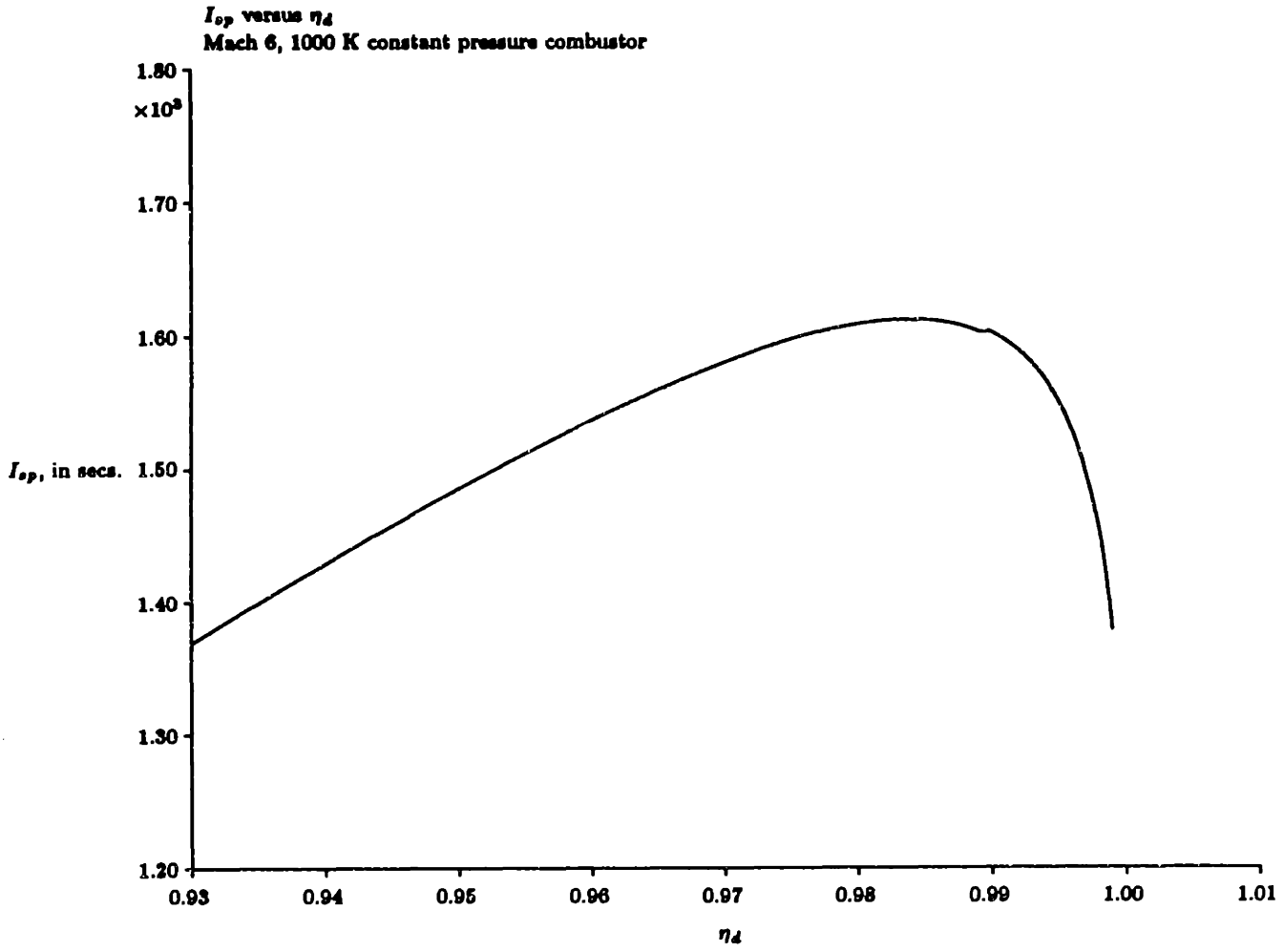

Figure 11.40: Correlation of specific impulse versus inlet kinetic energy efficiency

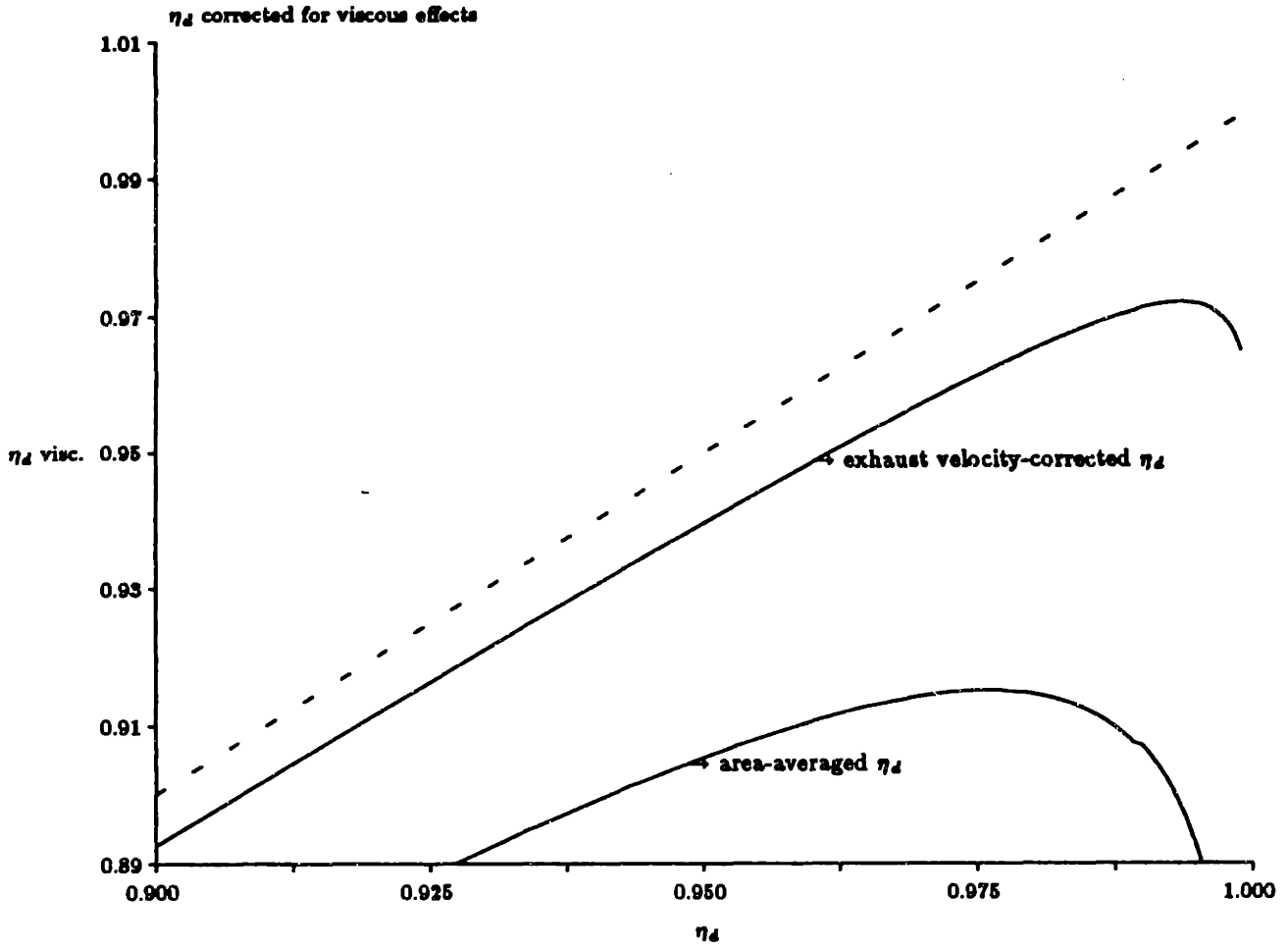

Figure 11.41: Exhaust velocity-corrected kinetic energy efficiency

engine performance. To include thrust losses in the kinetic energy efficiency, the total exhaust kinetic energy can be compared to the total inlet kinetic energy in the forebody capture area. Such an efficiency is presented in Figure 11.42 for the same inlet design, where it is assumed that there is no increase in capture area to accommodate mass flux losses due to boundary layer.

This thrust-corrected value is qualitatively similar to the result of assuming that the boundary layer provides no contribution to the thrust. This is because the boundary layer has very little mass flux, and there is little heat addition because of the high temperatures, assuming the nozzle is frozen. Losses in this efficiency parameter are much greater than those of the area-averaged value.

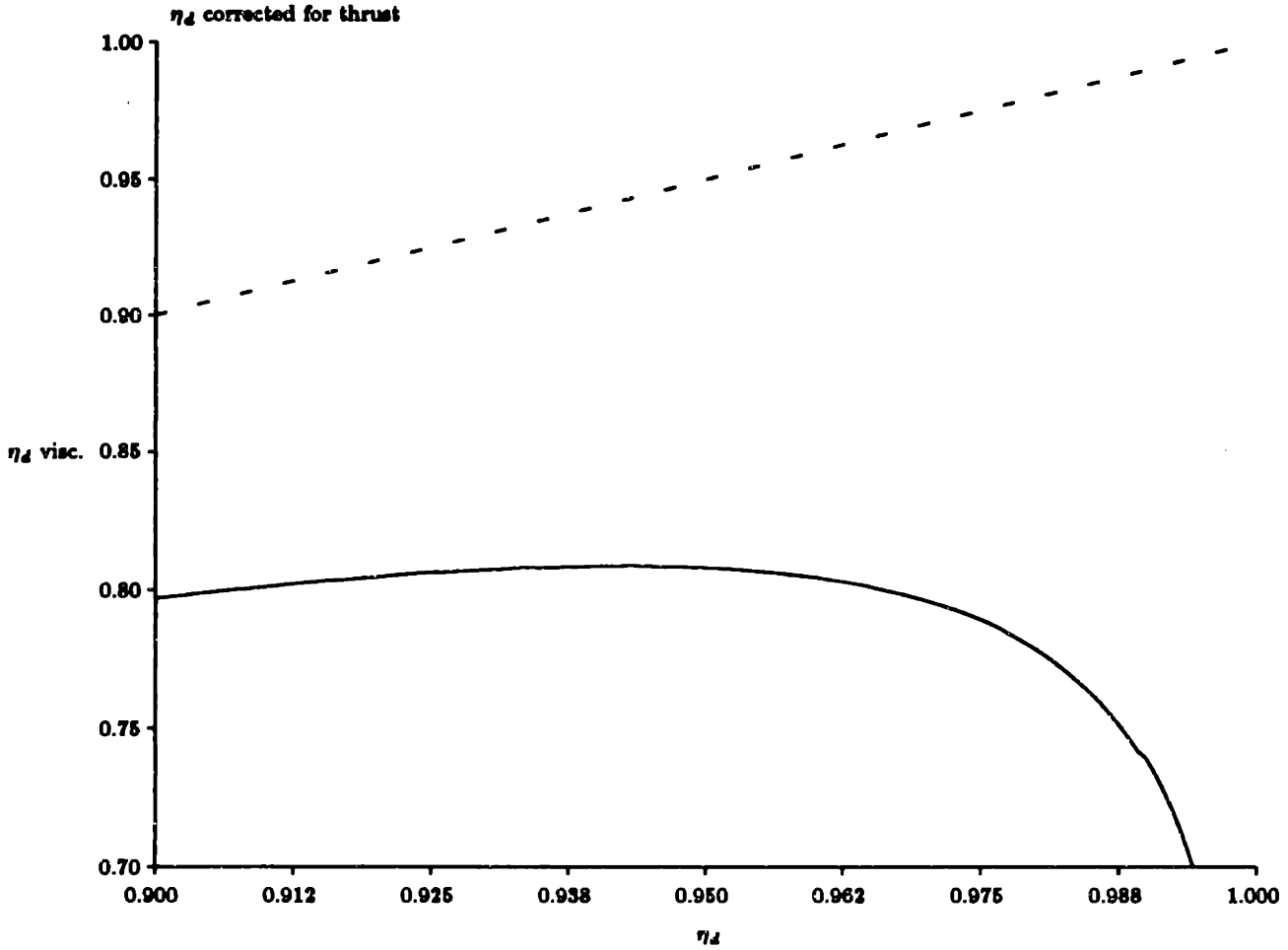

Figure 11.42: Thrust-corrected kinetic energy efficiency

Chapter 12
Conclusions

12.1 Review of Findings

The results of laminar boundary layer calculations at hypersonic velocities characteristic of the maximum Mach numbers and ultimate altitudes of a transatmospheric vehicle demonstrate that, at small angle of attack, the boundary layer can represent a substantial portion of the engine inlet flow. On a 1 atm. dynamic pressure trajectory, the laminar boundary layer will represent a maximum of 5% of the shock layer on a 10 meter long surface at Mach 12, rising to 25% at orbital velocities. On higher trajectories, the relative boundary layer thickness will be even larger; 10% of the inlet at Mach 10 and 50% at mach 25 for 1/10 atm. dynamic pressure. Because the shock layer grows linearly with distance, while the boundary layer grows with the square root of distance, the relative boundary layer thickness decreases with distance. It was shown that, if the boundary layer occupies 20% of the shock layer on a 10 meter plate, it will represent only $12\frac{1}{2}\%$ of the area at 30 meters.

It has been recalled from classical hypersonic boundary layer theory that such boundary layers are very sensitive to angle of attack. In general, above 5 degrees wedge angle, the boundary layer thickness is approximately inversely proportional to angle of attack. This effect is also apparent on forebody wedges; a boundary layer that forms on a 5 degree wedge will be reduced to half its original thickness by a 5 degree ramp. As a result, the actual boundary layer thickness will be a sensitive function of the size and geometry of the inlet.

It was demonstrated that the forebody boundary layer complicates the condition of matching the bow shock to the engine cowl. For inviscid flow, it was shown that there is an unique wedge angle for each Mach number at which the bow shock is fixed against small changes in wedge angle. This wedge angle generally provides acceptable thermodynamic

conditions at the inlet. It was determined that for boundary layers in excess of 2% relative thickness, this fixed condition cannot be realized because the boundary layer thickness changes with angle of attack.

The continuous profile generated by a laminar boundary layer was compared to a two-streamtube compound model, which is the simplest one-dimensional flow model. It was shown that the continuous profile can be compared to a uniform streamtube at a unique equivalent Mach number which is typically between 1 and 2. This characteristic Mach number was shown to be insensitive to the free-stream Mach number at hypersonic conditions.

It was found that the profile results in a drop in free-stream pressure after passage through a shock. The shock induces a normal pressure gradient, which is equilibrated by compressing the boundary layer and expanding the free-stream. At Mach 20, a 25% relative boundary layer resulted in a 10% drop in static pressure after passage through a shock on a 5 degree wedge. This effect will be multiplied if there are more shocks down the channel.

Inside the engine, it was shown that the laminar boundary layer will alter the *free-stream* properties. For instance, a Mach $13\frac{1}{2}$ flow in a convergent channel was found to have the thermodynamic properties of a Mach 4 flow with 10% relative boundary layer thickness, as measured by its response to changes in channel area. Turbulent boundary layers were found to have little effect on the free-stream flow properties. In general, the forebody profile behaves as a compound *supersonic* flow, and the boundary layer was found to be more resistant to changes in thickness than the free-stream. For instance, in a constant pressure combustor which experiences a three-fold increase in total channel area, a 10% relative thickness laminar boundary layer grows by only 90%.

It was seen that the presence of a thick laminar forebody boundary layer in the combustor of a supersonic combustion ramjet can result in changes in local thermodynamic properties that reduce the heating rate, and in turn, the net engine performance. Primarily as a result of static pressure losses, a drop in the rate of combustion was observed in reaction-rate limited combustors in the free-stream, and in the boundary layer in general. This can translate into a net loss of available enthalpy if combustion does not continue,

either in an expanded combustor channel, or in the nozzle. In the constant pressure combustor designed for Mach 14 flight, a 15% loss of static pressure was observed with a 10% relative thickness boundary layer. Because the dropping static pressure further reduces the heating rate in the free- stream, which drops the static pressure even more, this effect grows very quickly. For the above case, specific impulse was observed to drop 16% because of the presence of the profile; alternately, the engine would have to be lengthened another 20% to realize the full combustion release.

Although this work has concentrated on changes induced in the combustion process, the results can be generalized for any heat addition process. At near-orbital Mach numbers, it has been suggested that the heat added in the combustor will be derived exclusively from the incoming fuel enthalpy and relative kinetic energy, not by combustion, because of the difficulty of high Mach number combustion. It was found that the boundary layer tends to increase the free-stream Mach number in a combustor channel. This means that the Mach number with heat addition will generally be higher with a boundary layer, regardless of whether the heat addition process is due to combustion or fuel addition. Heat addition at higher Mach number incurs higher losses, and so the boundary layer will reduce combustor performance in this case as well.

The ultimate impact of the boundary layer on combustor performance will be evaluated based on the details of the individual combustor design. If the combustor has been sized for ideal uniform conditions, the profile-induced reaction time delay will result in reduced enthalpy for reaction rate-limited combustors. On the other hand, the combustor could be designed with sufficient channel length that the combustion reaction will run to completion, so there will be no net loss in heat addition. This combustor would be longer, and therefore heavier, than the uniform inlet design. The loss introduced by the boundary layer would therefore be increased engine weight, not reduced specific impulse.

Regardless of the loss mechanism, it is clear that the boundary layer, in changing the performance of an engine that has not been properly designed to account for an inlet profile, has introduced inefficiencies. The boundary layer profile is a direct consequence of the forebody shape. Thus, the inlet design has had a direct impact on the performance of

the combustor. To correctly evaluate the efficiency of a forebody inlet design, particularly for purposes of comparison with competing designs, it is appropriate to consider the adverse effects on combustor performance caused by the inlet profile.

The kinetic energy efficiency was modified to include profile effects. It was argued that:

- Viscous corrections for the kinetic energy efficiency should not be calculated with profile averages because there is minimal downstream mixing.
- Inlets are properly evaluated and compared based on the losses they induce in the combustor and the total engine performance, not just on the losses at the combustor inlet station. A complete analysis must also include a consideration of external aerodynamics, which has not been covered in this work.
- The net effect of viscous losses depends on the specific combustor and nozzle design, and inlets must be evaluated with this in mind.
- The *free-stream* kinetic energy efficiency can be corrected for the drop in exhaust velocity or thrust due to the inlet boundary layer as a basis of design comparison.

12.2 Hypersonic Vehicle Design Recomendations

The one-dimensional approach suggested in this work should not be viewed as a design tool, so much as an indication of important effects that must be accounted for in more detailed evaluations. The general conclusions that are drawn suggest some guidelines for hypersonic vehicle design.

If the effects of laminar boundary layers are to be avoided, it is suggested that some active control of forebody shape or inlet lip will be necessary. It was shown that a compression ramp can be used to reduce the boundary layer thickness, as do increased angle of attack and body thickness, but the resulting losses associated with the corresponding strong shocks may not be tolerable. It is also suggested that the trajectory and angle of attack may be chosen to minimize the boundary layer thickness, or at least consider the performance

tradeoffs associated with the losses from thick boundary layers. For instance, since it was found that the boundary layer thickness grows quickly with altitude, complications due to the boundary layer profile will be less significant on a lower-altitude trajectory. Boundary layer control may also put restrictions on the range of vehicle attitude; since the boundary layer grows with decreasing angle of attack, a hypersonic vehicle may have to maintain some minimum angle of attack.

The presence of a thick boundary layer on the forebody of a hypersonic vehicle must be accounted for in assessing the performance of an air-breathing engine. In addition to changing the bow shock location and mass ingestion with varying angle of attack, the boundary layer will introduce a low-speed region that will change the flow Mach number through the scramjet. Associated with this will be changes in the expected thermodynamic conditions inside the combustor. The boundary layer may also choke a channel that would not have choked with uniform flow. Designing an engine for the boundary layer will be difficult given the changing thickness with altitude and angle of attack. A vehicle which will maneuver must be able to accept boundary layers of varying dimensions, with resulting changes in combustion length and total thrust, unless some active boundary layer control is employed.

The impact of inlet gradients suggests that computational solutions, and experimental studies, cannot accurately assess the performance of air-breathing hypersonic propulsion without fully considering the viscous external flowfield of the vehicle, throughout the ranges of vehicle attitude and trajectory. An actual scramjet design must take full account of the inlet flow profiles throughout the likely range of attitude and altitude. Active control of the forebody boundary layer, bow shock position, scramjet geometry, and fuel addition pattern may be required if a transatmospheric vehicle is to have flexibility in attitude and trajectory.

While the laminar boundary layer profile had significant effects on the free-stream, the fuller turbulent profile had relatively small impact. This suggests that it may be desirable to force the boundary layer to become turbulent, if such is possible. Since the turbulent boundary layer will introduce higher losses on the forebody, selecting the transition point may be an important step in engine-airframe integration.

12.3 Directions for Future Research

A list of important topics for future research can be drawn from the assumptions and simplifications that were avoided in this work:

- Vehicle Shape: Because the engine flow depends directly on the external flow field, particularly over the forebody, a better definition of candidate vehicle geometries must be defined for proper engine analysis, especially if three-dimensional effects are to be included. This is particularly true to resolve issues of static stability of hypersonic aircraft.
- Trajectory selection: Because the combustor conditions are set directly by the external flow field, more exact trajectory specifications and vehicle control parameters must be determined. The engine design and trajectory analysis are closely coupled.
- Atmosphere modelling: Steady-state atmosphere models were used in this work, but gusting and unsteady phenomena must be defined to determine whether they must be incorporated in inlet flowfield studies. In particular, large-scale atmospheric density variations may impact engine inlet conditions.
- Transition to turbulence: The simple data correlations available currently must be refined, particularly to resolve the conflict between ground test data and flight vehicles, and to include more complicated shapes and leading edge bluntness effects. Means of inducing transition at hypersonic speeds will be of interest.
- Separation: The conditions leading to separation and its effect on the boundary layer profile and heating loads is of utmost importance, especially if the forebody will have ramps and there are adverse pressure gradients in the combustor.
- Finite-rate chemistry: Chemical models in this work were the simplest correlations of finite-rate calculations. A more complete treatment would include finite-rate considerations directly.
- Inlet design penalties: The losses incurred by bow shock mismatch, as well as the tradeoffs between various inlet designs (i.e. number of ramps, three-dimensionality, cowl orientation) must be resolved for inclusion in a more complete analysis.

- Channel pressure gradients: The streamtube model can be modified to include shocks and channel curvature. Future work should explore the effect of these phenomena on the profile structure and the resulting free-stream variations in combustors of known geometry.

- Supersonic mixing: It has been assumed that fuel mixes as desired in the combustor. In reality, this will be very difficult to accomplish, if it is even possible, and the practicality of hypersonic engine design depends on the resolution of this issue. In this work, the profile effects have been evaluated in terms off induced changes in the free-stream. If the heat release is mixing-limited, profile-induced combustion delays will be less important.

Bibliography

[1] Roger E. Bilstein. *Stages to Saturn*, page 405. National Aeronautics and Space Administration, Washington, D.C., 1981. NASA SP-4206.

[2] J.L. Kerrebrock. *Aircraft Engines and Gas Turbines*, chapter 10. MIT Press, Cambridge, Mass., 1984.

[3] R.J. Weber and J.S. MacKay. *An Analysis of Ramjet Engines Using Supersonic Combustion*. Technical Report 4386, NACA, 1958.

[4] D. Papamoshou and A. Roshko. *Observations of Supersonic Shear Layers*. AIAA paper 86-0162, 1986. 24th Aerospace Sciences Meeting.

[5] J.D. Anderson. *Modern Compressible Flow With Historical Perspective*, chapter 4. McGraw-Hill Inc., New York, 1982.

[6] Rodger Biasca. *Chemical Kinetics of SCRAMJET Propulsion*. Master's thesis, MIT Department of Aeronautics and Astronautics, September 1988. in preparation.

[7] Antonio Ferri. Review of problems in application of supersonic combustion. *J. Roy. Aero. Soc.*, 68(645):575–597, 1964. Seventh Lancaster Memorial Lecture.

[8] Clayton R. Rogers and Charles J. Schexnayder. *Chemical Kinetic Analysis of Hydrogen-Air Ignition and Reaction Times*. Technical Report TP-1856, NASA, 1981.

[9] observation by Prof. M. Martinez-Sanchez, Department of Aeronautics and Astronautics, MIT.

[10] personal communication with Prof. E. Ressler, Sibley School of Mechanical and Aerospace Engineering, Cornell University.

[11] P. Waltrup. Liquid-fueled supersonic combustion ramjets: a research perspective. *J. Propulsion*, 3(6):515–525, 1987.

[12] *U.S. Standard Atmospheres 1976*. NOAA,NASA,and USAF, Washington, D.C., October 1976.

[13] Stefan Schreier. *Compressible Flow*, pages 426–432. John Wiley and Sons, New York, 1982.

[14] P.H. Rose and W.I. Stark. Stagnation point heat transfer measurements in dissociated air. *J. Aero. Sci.*, 25:86–97, 1958.

[15] Sabri Sansoy. *Design Optimization of a Transatmospheric Launch Vehicle*. Master's thesis, MIT Department of Aeronautics and Astronautics, September 1987.

[16] M.S. Holden, A.R. Wieting, J.R. Moselle, and C. Glass. *Studies of Aerothermal Loads Generated in Regions of Shock/Shock Interaction in Hypersonic Flow*. AIAA paper 88-0477, 1988.

[17] C.F. Newberry, H.S. Dresser, J.W. Byerly, and W.T. Riba. *Evaluation of Forebody Compression at Hypersonic Mach Numbers.* AIAA paper 88-0479, 1988.

[18] L. M. Mack. Linear Stability Theory and the Problem of Supersonic Boundary-Layer Transition. *AIAA Journal*, 13:278–289, 1975.

[19] K.F. Stetson. *Nosetip Bluntness Effects on Cone Frustum Boundary-Layer Transition in Hypersonic Flow.* AIAA paper 83-1763, 1983.

[20] N.W. Sheetz. Ballistics range boundary-layer transition measurements on cones at hypersonic speeds. In C.S. Wells, editor, *Viscous Drag Reduction*, pages 53–84, Plenum Press, New York, 1980.

[21] J.V. Rackich and M.J. Lanfranco. Numerical Computation of Space Shuttle Laminar Heating and Surface Streamlines. *J. Spacecraft*, 14:265–272, 1977.

[22] L. Trilling and R.J. Hakkinen. *The Interaction of an Oblique Shock with a Laminar Boundary Layer.* Technical Report 57-1, MIT Fluid Dynamics Research Group, 1957.

[23] M. Drela, M. Giles, and W.T. Thompkins. *Conservative Streamtube Solution of Steady-State Euler Equations.* AIAA paper 84-1643, 1984.

[24] personal communication with Prof. M. Drela, Department of Aeronautics and Astronautics, MIT.

[25] C.B. Cohen and E. Reshotko. *Similar Solutions for the Compressible Laminar Boundary Layer with Heat Transfer and Pressure Gradient.* Technical Report 1293, Lewis Flight Propulsion Laboratory, 1957.

[26] L. Lees. Laminar heat transfer over blunt nosed bodies at hypersonic flight speeds. *Jet Propul.*, 26:259–274, 1956.

[27] A.H. Shapiro. *Dynamics and Thermodynamics of Compressible Fluid Flow.* Volume 1, Ronald Press, New York, 1954. Art. 8.3.

[28] A. Bernstein, W.H. Heiser, and C. Hevenor. Compound-compressible nozzle flow. *Journal of Applied Mechanics*, 34:548–554, 1967.

[29] J.H. Perry and R.A. East. Experimental measurements of cold wall turbulent boundary layers. In *Hypersonic Boundary Layers and Flow Fields*, AGARD, NATO, May 1968.

[30] M.H. Bertram, A.M. Jr. Carey, and A.H. Jr. Whitehead. Experiments with hypersonic turbulent boundary layers on flat plates and delta wings. In *Hypersonic Boundary Layers and Flow Fields*, AGARD, NATO, May 1968.

[31] M.H. Bertram and T.A. Blackstock. *Some Simple Solutions to the Problem of Predicting Boundary-layer Self-Induced Pressures.* Technical Report TN D-798, NASA, 1961.

[32] F. M. White. Hypersonic Laminar Viscous Interactions on Inclined Flat Plates. *ARS Journal*, 32:780–781, 1962.

[33] J. Deleny and J.G. Marvin. *Shock-Wave Boundary Layer Interactions.* Technical Report AGARDograph 280, North Atlantic Treaty Organization, 1986.

[34] P.G. Hill and C.R. Peterson. *Mechanics and Thermodynamics of Propulsion*, page 49. Addison-Wesley Co., Reading, Mass., 1970.

[35] N. Curle. The effects of heat transfer on laminar-boundary-layer separation in supersonic flow. *Aeronautical Quarterly*, 12:309–336, November 1961.

[36] observation by Prof. M. Martinez-Sanchez, Department of Aeronautics and Astronautics, MIT.

[37] J. Swithenbank. Hypersonic air-breathing propulsion. *Progress in the Aeronautical Sciences*, 229–294, 1966.

[38] T.Y. Li and H.T. Nagamatsu. Shock Wave Effects on the Laminar Skin Friction of an Insulated Plate at Hypersonic Speeds. *J. Aero. Sci.*, 20:345–355, 1953.

[39] K. Stewartson. *The Theory of Laminar Boundary Layers in Compressible Fluids*. Oxford Mathematical Monographs, 1958.

[40] W.H. Dorrance. *Viscous Hypersonic Flow*. McGraw-Hill, New York, 1962.

[41] W.D. Hayes and R. Probstein. *Hypersonic Flow Theory*. Academic, New York, 1st edition, 1959. Only 1st edition covers viscous flow.

[42] A.H. Shapiro. *Dynamics and Thermodynamics of Compressible Fluid Flow*. Volume 2, Ronald Press, New York, 1954. Art. 19.3.

[43] Wing-fai Ng. *Time Resolved Measurements in a Transonic Compressor Stage*. PhD thesis, MIT Department of Mechanical Engineering, 1983.

[44] R. Courant and K.O. Friedrichs. *Supersonic Flow and Shock Waves*. Interscience Publishers, Inc., New York, 1948.

[45] G.M. Elfstrom. Turbulent hypersonic flow at a wedge-compression corner. *J. Fluid Mech.*, 53(1):113–127, 1972.

[46] R. Descher. Nonuniform flow through nozzles. *J. Aircraft*, 15(7):416–421, 1987.

[47] F. Wazelt. *Suitable Averaging techniques in Non-Uniform Internal Flows*. Technical Report AGARD advisory report 182, North Atlantic Treaty Organization, June 1983.

[48] H.W. Liepmann and A. Roshko. *Elements of Gasdynamics*. John Wiley and Sons, Inc, New York, 1957.

Appendix A

Laminar Hypersonic Boundary Layer Model

A.1 Three-layered model

The viscous hypersonic flow is divided into three regions:

1. The undisturbed free stream above the shock.
2. An inviscid shock layer below and adjacent to the shock.
3. A hypersonic boundary layer between the inviscid shock layer and the plate.

Li and Nagamatsu [38] originally argued that the shock layer is fully viscous, and solved for the boundary layer structure with the shock as the upper edge of the boundary layer, without an inviscid region. Stewartson [39] pointed out that this is an incorrect model; his argument is based on the fact that the hypersonic boundary layer is very hot, and thus has low density, and almost no mass flow. In the hypersonic limit, the upper edge of the boundary layer approaches a streamline, (i.e. almost no mass is entrained into the flow after the initial growth region) but a shock cannot correspond to a streamline, so the shock must be above the boundary layer edge.

Dorrance [40] used vorticity considerations to show that a fluid element can be traced by comparing its position of entry into the boundary layer with its passage through the shock, and found that a given particle enters the boundary layer far downstream of where it crossed the shock (i.e. the boundary layer and the shock are distinct).

Hayes and Probstein [41] have shown that the viscous boundary layer thickness δ can be related to the density ratio across the bow shock,$\epsilon = \rho_2/\rho_1$, the mean free path at the

shock, λ_s, and the shock layer thickness Δ as

$$\lambda_s \Delta \simeq \sqrt{\epsilon}\, \delta^2 \tag{A.1}$$

For a highly oblique shock, $\epsilon \simeq O(1)$, so if $\lambda_s < \Delta$, the boundary layer will be smaller than the entire shock layer. Recall that the mean free path in atmosphere varies from 6.6×10^{-8} m at sea level to 7.9×10^{-5} m at 50 km altitude [12]. Thus, for shock layers of about a meter thickness, the boundary layer/inviscid shock region model will be valid up to and beyond 50 km altitude, which encompasses the likely range of operation for an aerospace plane. At higher altitudes, the mean free path becomes so large that the applicability of this model would be questionable. For instance, at 100 km, $\lambda_s = 1.42 \times 10^{-1}$ m. Hayes and Probstein have also demonstrated that the assumption of a fully viscous shock layer would violate the boundary layer conditions.

There is strong coupling between the boundary layer and the bow shock. The shock angle will determine the pressure ratio across the shock, which in turn sets the boundary layer thickness. The boundary layer thickness in turn sets the effective displacement which determines the shock angle.

Classically, shock-boundary layer interactions of this type are categorized as *weak* or *strong*. Strong interactions refer to those in which the boundary layer drastically modifies the shape of the shock, and in which the induced pressure ratios across the shock are large. The simplest example of a strong interaction is the case of an infinitely thin flat plate parallel to a supersonic flow. In the inviscid case, there will be no shock because the plate corresponds to a streamline; in the viscous solution, a boundary layer forms on the plate, and this appears as a normal flow displacement, which in turn produces a shock. Thus, a shock is generated solely by the presence of a boundary layer.

Strong interactions generally occur at the leading edge of the boundary layer, while the boundary layer growth is greatest and thus the boundary layer slope is steepest. Weak interactions, in which the boundary layer simply adds to the body dimension, are typically encountered when the slope of the boundary layer is small. Bertram and Blackstock [31] have combined these regimes into a single similarity solution, which was expanded by White [32]

to include flow over an inclined plane.

Results of detailed analyses of the strong interaction zone have shown that the boundary layer thickness scales with the three-fourths power of the streamwise coordinate, and that the inviscid layer is proportional in thickness to the boundary layer [40]. The boundary layer carries almost none of the mass in the shock layer, because of its low density, so the shock layer is highly stratified. Also, because very little fluid is entrained into the boundary layer, the stratification is preserved far downstream, presumably into the engine inlet.

Note that if the leading edge of the body is blunt, its shape may dominate over the boundary layer in configuring the shock over the strong interaction zone. Directly ahead of a blunt body, the bow shock will be normal, and therefore experience a much larger pressure rise than farther downstream. This favorable pressure gradient can overwhelm the effect of the apparent bluntness of the upstream portion of the boundary layer. Throughout this work, it will be assumed that leading edges are sharp enough that the strong interaction solution is applicable to the forebody leading edge

A.2 Laminar Boundary Layer Solution

The boundary layer thickness of the forebody flow has been modelled using the classical flat plate interaction theory, which will be reviewed briefly.

White [32], following Bertram and Blackstock [31], showed from hypersonic similarity theory that the hypersonic boundary layer displacement thickness could be represented as

$$\frac{\delta^*}{x} = \frac{1}{M_\infty} \frac{2\Lambda}{\sqrt{P}} \tag{A.2}$$

where $P \equiv \frac{p}{p_\infty}$, the pressure ratio across the shock.

The pressure gradient due to shock curvature is assumed negligible, as Bertram and Blackstock demonstrated. Note that in the hypersonic limit, the mass flux in the boundary layer is so low that displacement thickness is approximately equal to the actual boundary layer thickness, and the two concepts can be merged.

The A function characterizes the gas/wall heat transfer, and is here written for general Prandtl number, Pr, fitting the results for $Pr = 1.$ and $Pr = .73$ to a power law form;

$$\Lambda = \{.4302\, Pr^{.1344}\left(\frac{T_w}{T_r}\right) + .1660\, Pr^{.2854}\}(\gamma - 1)\overline{\chi} \tag{A.3}$$

where $\overline{\chi}$ is the Lees interaction parameter, defined as

$$\overline{\chi} \equiv \frac{M_\infty^3\sqrt{C}}{\sqrt{Re_{x,\infty}}} \tag{A.4}$$

in which

$$C = (\frac{\mu_w}{\mu_\infty})(\frac{T_\infty}{T_w}) \tag{A.5}$$

We use the Sutherland model to calculate μ:

$$\frac{\mu}{\mu_o} = \left(\frac{T}{T_o}\right)^{3/2} \frac{T_o + 110°K}{T + 110°K} \tag{A.6}$$

From classical hypersonic similarity theory, we know that the Lees parameter characterizes the strength of the boundary layer/ shock interaction [40]. The strong interaction limit occurs at $\overline{\chi} \gg 1$ and the weak interaction range is at $\overline{\chi} = O(1)$. At $\overline{\chi} \ll 1$ interactions are negligible.

In general, there is no closed form solution for the shock pressure ratio. At small angles, the pressure ratio approaches unity, so that $\sqrt{P} \simeq 1$ far along the plate, in the so-called weak interaction region. Thus, for large values of x, corresponding to small values of $\overline{\chi}$,

$$\frac{\delta^*}{x} \simeq \frac{2\Lambda}{M_\infty} \tag{A.7}$$

with a slope that approaches zero as $x \to \infty$.

At any angle, Shapiro [42] has shown that

$$P = 1 + \frac{\gamma M^2}{2} C_P \tag{A.8}$$

where the pressure coefficient C_P is given by

$$\frac{C_P}{\left[1 - \frac{1}{2}C_P\right]} = \frac{4M^2\sin^2\beta - 1}{M^2(\gamma + \cos\beta) + 2} \tag{A.9}$$

A closed-form solution for shock pressure ratio can be found at large Mach numbers and small wedge angles such that $\tan\Theta_{wedge} \simeq \Theta_{wedge}$ and $\cos\beta_{shock} \simeq 1$, $C_P \ll 1$:

$$P = 1 + \frac{\gamma(\gamma+1)}{4}K^2 + \gamma K\sqrt{1+\left[\frac{\gamma+1}{4}K\right]^2} \tag{A.10}$$

where

$$K = M_\infty\left(\Theta_{wedge} + \frac{d\delta^*_{b.l.}}{dx}\right) \tag{A.11}$$

is the hypersonic similarity parameter.

It is assumed that the total wedge angle is positive, or else the forebody flow would have to be treated as an expansion flow. The second angle term, due to boundary layer slope, is transformed into a function of the Lees parameter:

$$\frac{d\delta^*_{b.l.}}{dx} = \frac{\Lambda}{M_\infty}\left(\frac{1}{\sqrt{P}} + \frac{\overline{\chi}}{2P^{3/2}}\frac{dP}{d\overline{\chi}}\right) \tag{A.12}$$

Note that as $\overline{\chi} \to 0$, the hypersonic similarity parameter K approaches $M_\infty\,\Theta_{wedge}$ as should be the case in the weak interaction zone.

For large values of K and small values of $\Lambda(\overline{\chi})$, the pressure parameter P in equation (A.10) scales with $(M_\infty\,\Theta_{wedge})^2$. Thus, the wedge angle is dominant in setting the shock pressure ratio. This is not surprising, since the hypersonic shock position relative to the wedge is insensitive to wedge angle, but the pressure ratio is not. In this case, the boundary layer thickness is essentially independent of Mach number directly, as the M_∞ terms in Λ and P approximately cancel, leaving $\overline{\delta^*} \propto (\Theta_{wedge}\sqrt{x})^{-1}$ in equation (A.2).

The effective wedge angle, due to the plate angle of attack and the boundary layer displacement, is

$$\Theta_{effective} = \Theta_{wedge} + \frac{d\delta^*_{b.l.}}{dx} \tag{A.13}$$

from which the local shock angle β can be calculated, assuming a closely- wrapped shock (where characteristics intersect a region of the shock directly above the surface from which they emanate)

$$\tan\Theta_{effective} = 2\cot\beta\left[\frac{M_\infty^2\sin^2\beta - 1}{M_\infty^2(\gamma+\cos 2\beta)+2}\right] \tag{A.14}$$

The inviscid shock layer thickness is estimated from the local shock angle by integrating along the top surface of the boundary layer, the path of which we denote as η,

$$\Delta_s = \int_0^\eta \tan\beta(\eta')d\eta' \tag{A.15}$$

The shock is fit subject to the condition that, in the weak interaction region, its slope and strength are identical to the inviscid solution, but it is displaced by the boundary layer.

Because leading edge bluntness may dominate the strong interaction region, we assume a shock stand-off distance as given by Hayes and Probstein [41]

$$\frac{\Delta_{\text{stand-off}}}{R_{\text{nose}}} = \frac{\epsilon}{1+\sqrt{\frac{g_\xi}{3}}} \tag{A.16}$$

which displaces the start of the boundary layer forward, and thus essentially adds to the boundary layer thickness down the plate. The resulting strong pressure gradient from the blunt-edged shock is not included in the model, but it may be assumed that the leading edge surfaces of an actual hypersonic vehicle would be sharp enough to avoid serious effects of that sort.

The above model is iterated in $\overline{\chi}$, which is an inverted spatial coordinate:

$$\lim_{\overline{\chi}\to 0} x = \infty \tag{A.17}$$

$$\lim_{\overline{\chi}\to \infty} x = 0 \tag{A.18}$$

Thus, the solution begins at the weak interaction limit and proceeds to the strong limit. In the present implementation, a simple Euler forward iteration scheme is used. The derivative in equation (A.12) is calculated with a finite difference method between two closely spaced values of $P(\overline{\chi})$. Care must be taken in incrementing $\overline{\chi}$ because the resulting spatial coordinate, and therefore the Reynolds number, is inversely proportional to $\overline{\chi}^2$. Smaller increment steps are required at large $\overline{\chi}$ to adequately resolve the strong interaction zone.

Thus far, the presented model has ignored real gas effects that might be expected in a hypersonic flow, such as dissociation and ionization. Dorrance has argued that dissociation

actually has little effect on transport properties, since it changes the viscosity of air by at most 5%, so we ignore chemical dissociation effects [40]. Ionization would have an enormous impact on the flow, particularly since the Prandtl number would fall as free electrons became the dominant energy transporters. In fact, the flow kinetic energy will be below the level required to reach ionization temperatures, so for a practical hypersonic vehicle, ionization can be ignored. This is fortunate, because material considerations limit the surface temperatures to levels far below ionization temperatures. The model does not consider effects at the leading edge, where dissociation and ionization temperatures may be encountered, and the flow may behave as a rarefied gas. Also, the distinction between equilibrium and frozen speed of sound is ignored.

Some real gas effects can be included in the above model by varying the value of the ratio of specific heats, γ. At high temperatures, γ will be reduced as higher-order vibrational energy modes are excited in the gas molecules. Thus, the value of γ will relax as the flow proceeds from the shock along the plate.

Ideally, the relaxation of γ would be modelled by considering time-dependent reaction rates. Unfortunately, the boundary layer model is iterated in the Lees interaction parameter, $\overline{\chi}$, which is an inverse space coordinate. Thus, for simplicity, the value of γ is allowed to decay exponentially in space, with a characteristic decay length calculated from the ideal mean free path. This is a reasonable approximation to the actual change in γ, which is a fundamentally exponential process due to collisional equilibration. Special care must be taken in selecting the $\overline{\chi}$ increment to avoid instabilities in the solution with a variable γ, as drastic increases in γ between iteration points can produce unacceptable oscillations in the inverse transformation to spatial coordinates.

Appendix B

Shock Position and Surface Oscillations

B.1 Inviscid Dynamic Shock Motion

At high Mach number, if surface motion is approximately normal to the surface, the unsteady oblique bow shock flow field in the weak interaction zone can be assumed to have an unsteady normal component, and a steady tangential component, fixed in the frame of the shock. Thus, the unsteady oblique bow shock behavior can be discerned from a simpler unsteady normal shock model, just as the classical steady oblique shock properties are determined entirely from the normal velocity components.

It is useful to recall that the steady solution for the shock ahead of a 1-d piston moving at constant velocity U_{piston}, plotted with distance from the origin versus time, resembles that for a 2-d oblique wedge shock with incident velocity U_{wedge} plotted with shock y distance versus x,if the wedge has angle $\theta_{\text{wedge}} = U_{\text{piston}}/U_{\text{wedge}}$ and the piston time axis has units such that $t = x_{\text{wedge}}/U_{\text{wedge}}$. The unsteady solution for the oscillating wedge will resemble that for a 1-d piston which moves at some steady-state, constant velocity, plus the oscillatory component.

In the classical normal shock solution, an upstream normal Mach number is specified, and from this, a downstream Mach number is calculated. In the unsteady problem at hand, both an upstream Mach number and a downstream Mach number are specified, the downstream value being set by the equilibrium, classical fixed shock solution plus a perturbation introduced by surface oscillations. In order to satisfy continuity, momentum and energy conservation with arbitrary upstream and downstream Mach numbers, the shock must move so as to change the apparent shock-relative Mach number of both upstream and downstream.

Because the pressure ratio across the shock changes as the shock-relative upstream Mach number changes, the shock layer and boundary layer motion cannot be treated with simple linear oscillator theory. The behavior of the flow on either side of a low frequency oscillating shock is developed following the quasisteady approach of Ng and Kerrebrock [43]. First, the unsteady continuity equation in integral form

$$-\iint_S \rho\vec{V}\cdot\vec{n}dS = \frac{\partial}{\partial t}\iiint_\mathcal{V} \rho d\mathcal{V} \tag{B.1}$$

is evaluated for a control volume around the shock, as so:

$$\rho_2 u_2 - \rho_1 u_1 = (\rho_2 - \rho_1)W \tag{B.2}$$

where region 1 is upstream of the shock, region 2 is downstream, and W represents the speed of the shock itself. The time derivatives of density have been neglected in the unsteady term of this equation, as so:

$$\frac{\partial}{\partial t}(\rho\mathcal{V}) \simeq \rho\frac{\partial\mathcal{V}}{\partial t} \tag{B.3}$$

which results in the right hand side of equation (B.1). This quasi-steady assumption thereby treats the moving shock as if it were a steady-state solution with constant velocity at each point in time. As will be shown, this assumption restricts the following development to low frequency surface motions, since at higher frequencies, the time derivative of thermodynamic properties will become large. Note that with $W = 0$ the continuity equation reduces to the relation for normal, fixed shocks, as expected.

Similarly, the unsteady momentum equation

$$-\iint_S (\rho\vec{V}\cdot\vec{n}\,\vec{V} + p\vec{n})\,dS = \frac{\partial}{\partial t}\iiint_\mathcal{V} \rho\vec{V}\,d\mathcal{V} \tag{B.4}$$

becomes

$$(\rho_2 u_2^2 - \rho_1 u_1^2) + (p_2 - p_1) = (\rho_2 u_2 - \rho_1 u_1)W \tag{B.5}$$

and the unsteady energy equation in the absence of heat addition or work

$$-\iint_S \rho\left(h + \frac{V^2}{2}\right)\vec{V}\cdot\vec{n}\,dS = \frac{\partial}{\partial t}\iiint_\mathcal{V} \rho\left(e + \frac{V^2}{2}\right)d\mathcal{V} \tag{B.6}$$

becomes

$$(\rho_2 u_2 T_{t\,2} - \rho_1 u_1 T_{t\,1}) = (\rho_2 T_{t\,2} - \rho_1 T_{t\,1}) W - \frac{\gamma - 1}{\gamma} (\rho_2 T_2 - \rho_1 T_1) W \tag{B.7}$$

where we have used $h = C_p T$, $h = e + RT$, and $R/C_p = \frac{\gamma - 1}{\gamma}$ and assumed constant specific heat at constant pressure C_p.

Combining equations (B.2) and (B.5) results in:

$$\frac{p_2}{p_1} = 1 + \frac{\rho_1 (u_1 - W)}{p_1} (u_1 - u_2) \tag{B.8}$$

or, in terms of Mach numbers,

$$\frac{p_2}{p_1} = 1 + \gamma (M_1 - M_w) \left(M_1 - \frac{u_2}{a_1} \right) \tag{B.9}$$

where $M_w = W/a_1$, the absolute shock Mach number relative to the upstream region.

Defining $M_2' \equiv u_2/a_1$ and $P \equiv p_2/p_1$, we can rewrite the momentum expression more simply as

$$P = 1 + \gamma (M_1 - M_w) (M_1 - M_2') \tag{B.10}$$

where the pressure ratio across the shock is $P = p_2/p_1$, as before. It is most convenient to define all Mach numbers in terms of the upstream speed of sound because it is independent of the downstream perturbation conditions.

The energy equation (B.7) can similarly be written in terms of Mach numbers by substituting for the total temperature from the isentropic flow relation, which is still valid upstream and downstream of the shock under the quasisteady assumption:

$$\frac{T_t}{T} = \left(1 + \frac{\gamma - 1}{2} M^2 \right) \tag{B.11}$$

so that

$$\rho_2 T_2 \left[(u_2 - W) \left(1 + \frac{\gamma - 1}{2} M_2^2 \right) + \frac{\gamma - 1}{\gamma} M_w \right] = \tag{B.12}$$
$$\rho_1 T_1 \left[(u_1 - W) \left(1 + \frac{\gamma - 1}{2} M_1^2 \right) + \frac{\gamma - 1}{\gamma} M_w \right]$$

or

$$p = \frac{\left[(M_1 - M_w)\left(1 + \frac{\gamma-1}{2}M_1^2\right) + \frac{\gamma-1}{\gamma}M_w\right]}{\left[(M_2' - M_w)\left(1 + \frac{\gamma-1}{2}M_2^2\right) + \frac{\gamma-1}{\gamma}M_w\right]} \tag{B.13}$$

Although it is ultimately of interest to solve for the moving shock velocity, and hence its position relative to the surface, the moving shock Mach number can be removed explicitly from equation (B.13) by rearranging equation (B.10) as

$$M_w = M_1 + \frac{(1-p)}{\gamma(M_1 - M_2')} \tag{B.14}$$

Equation (B.13) depends on both $M_2 = u_2/a_2$ and $M_2' = u_2/a_1$. These can be related with the continuity and momentum equations:

$$\begin{aligned} M_2'^2 &= M_2^2 \left(\frac{a_2}{a_1}\right)^2 \\ &= M_2^2 \frac{p_2}{p_1}\frac{\rho_1}{\rho_2} \end{aligned} \tag{B.15}$$

into which p_2/p_1 can be substituted from equation (B.10). From continuity, the density ratio is:

$$\begin{aligned} \frac{\rho_1}{\rho_2} &= \frac{u_2 - w}{u_1 - w} \\ &= \frac{M_2' - M_w}{M_1 - M_w} \end{aligned} \tag{B.16}$$

which we can use to solve for M_2, using equation (B.14) to substitute for M_w:

$$M_2^2 = M_2'^2\, p \left(1 - \frac{\gamma(M_2' - M_1)^2}{p - 1}\right) \tag{B.17}$$

Equations (B.13), (B.17),and (B.14) cannot be solved in closed form, but they provide a unique solution for the shock pressure ratio, and hence the shock velocity, as a function of upstream conditions and the downstream velocity perturbation. In general, the downstream velocity perturbation is the sum of the effects of relative wall velocity and the rate of change of boundary layer thickness, primarily due to shock-induced pressure variations. Thus, with a boundary layer, the downstream Mach number is dependent on the shock velocity, so the entire field is strongly coupled.

It is important to note that the downstream Mach number is the total Mach number, the sum of the equilibrium (steady, fixed shock) and oscillatory Mach numbers. Since it is ultimately of interest to observe the shock motion relative to the equilibrium state, the downstream Mach number can be separated into its components. From steady oblique shock theory, the downstream Mach number in terms of upstream Mach number is:

$$M_2^2 = \frac{1 + \frac{\gamma-1}{2} M_1^2}{\gamma M_1^2 - \frac{\gamma-1}{2}} \tag{B.18}$$

It is convenient to transform this into an expression for the equilibrium value of M_2', the downstream Mach number in terms of the unchanging upstream speed of sound, with the oblique shock temperature ratio:

$$\frac{T_2}{T_1} = \left[1 + \frac{2\gamma}{\gamma+1}(M_1^2 - 1)\right]\left[\frac{2 + (\gamma-1)M_1^2}{(\gamma+1)M_1^2}\right] \tag{B.19}$$

such that

$$M'_{2,\,\text{equilibrium}} = \frac{(\gamma-1)M_1^2 + 2}{(\gamma+1)M_1} \tag{B.20}$$

This in turn can be substituted into the above formulations for continuity, momentum, and energy, with

$$M_2' = M'_{2,\,\text{oscillatory}} + \frac{(\gamma-1)M_1^2 + 2}{(\gamma+1)M_1} \tag{B.21}$$

so that M_w can be solved directly in terms of the surface motion.

The quasi-steady shock motion for various incident normal shocks, M_w, normalized to the surface Mach number M_2, is shown in Figure B.1, plotted at various incident normal Mach numbers. Several interesting features are apparent in this plot. Observe that, at each incident Mach number, there is a minimum surface Mach number at which the quasisteady flow equations can be solved. Recalling the comparison between the 1-d piston and an oblique wedge shock, this limit is analogous to the maximum wedge angle criterion for steady, oblique wedge shocks. For the Mach numbers shown, the shock velocity is generally close to that of the surface. For instance, at incident Mach number 1.5, the shock Mach number is typically about 80% of the surface Mach number. As incident Mach number increases, the shock velocity approaches, then exceeds the surface velocity. Note also that, at each incident Mach number, the shock velocity becomes a smaller fraction of the surface velocity as the surface velocity increases.

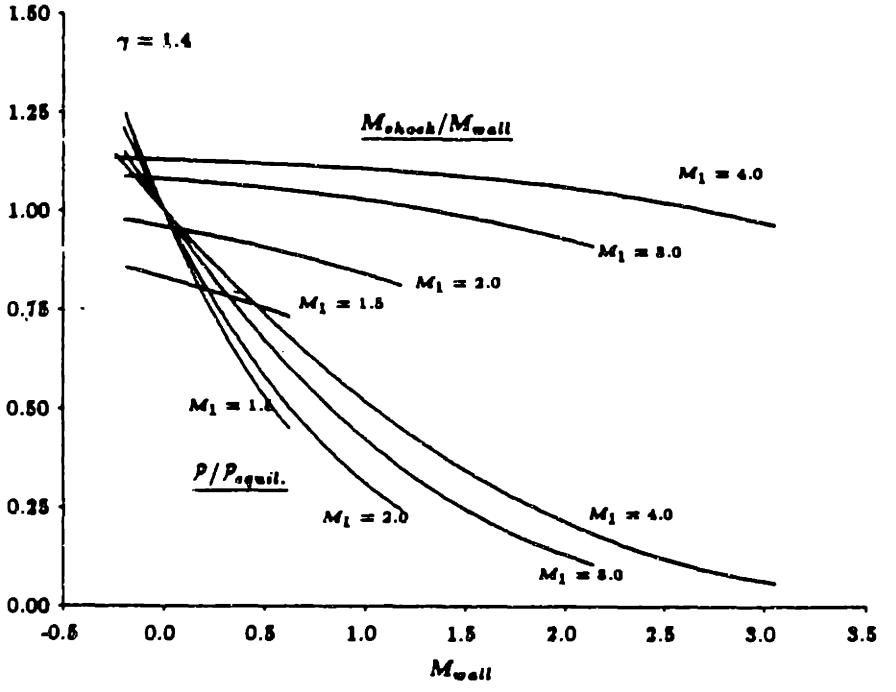

Figure B.1: Relative shock motion and pressure ratio versus surface motion. Top set of lines represents M_w/M_2, while lower set is the oscillation pressure ratio divided by the equilibrium value

When the surface velocity is zero, the shock velocity will also be zero, so it might be expected that the ratio of shock velocity to surface velocity would approach unity at that point. In fact, this is not the case. Indeed, the ratio of shock velocity to surface velocity decreases monotonically with increasing surface velocity. This result is consistent with the findings of the previous section, in which it was shown that there is only one specific wedge angle at which a shock will remain statically fixed, relative to the surface, at a given incident Mach number. Similarly, there is only one incident Mach number in the quasisteady model at which the shock velocity matches the surface velocity exactly in the limit of small surface velocities. For $\gamma = 1.4$, that incident Mach number is 2.2, which is approximately equal to the normal Mach number at each of the fixed-shock wedge angles presented in Table 4.1.

The quasisteady solution is converted to a plot of relative shock motion as a function of surface oscillation frequency, for fixed values of oscillation amplitude. Figure B.2 is a typical representation of the extremes of shock motion relative to the surface motion, at conditions corresponding to a wedge of 5 degrees flying at Mach 20, 50 km, with a 1 cm oscillation amplitude. In the limit of zero oscillating frequency, the relative shock motion approaches the oscillation amplitude. This occurs because, at low frequency, the downstream oscillation velocity approaches zero, and thus the moving surface can have no effect on the shock, so the relative motion is just the surface motion. Observe that the shock motion matches the surface motion even at relatively low frequencies, implying that throughout most of the frequency range, the shock is approximately fixed relative to the surface.

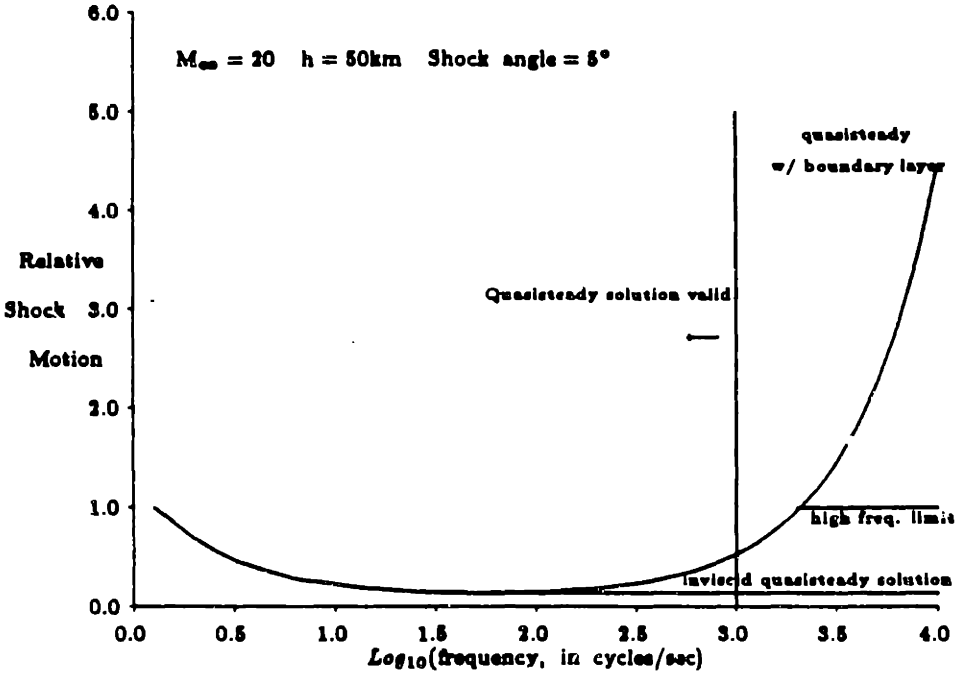

Figure B.2: Relative shock motion versus oscillation frequency. Quasisteady soltuion limit is calculated for a 1 meter thick downstream region between the shock and the surface

Recall that the quasisteady assumption is only valid at low frequencies. At higher frequencies, the time derivatives of thermodynamic properties will become important. The quasisteady model can be checked for self-consistency by examining the magnitude of $\mathcal{V}\partial\rho/\partial t$ versus $\rho\partial\mathcal{V}/\partial t$ by inverting equation (B.16) and differentiating with respect to time, holding the upstream density constant and assuming some reasonable value for the control volume height (say, a few meters, corresponding to the width of the shock layer.) Doing this, we find a cutoff in the applicability of the quasisteady model, in the neighborhood of 1 kHz for the solution presented above.

Although the frequency range above the quasisteady regime must be handled with the complete unsteady equations, some simplifications can be drawn for extremely high frequencies. In the quasisteady range, continuity is satisfied in the presence of surface motion by moving the shock, while the instantaneous values of density remain unchanged. The quasisteady assumption fails when the downstream region experiences large order density changes to satisfy continuity requirements. In the limit of high frequency, this density change will accommodate all of the plate motion, and the shock will remain stationary.

This regime can best be understood with the 1-d piston analogy. An oscillating piston that generates a finite compression wave as it moves into the gas generates a finite expansion, or rarefaction wave, as it withdraws. The expansion wave will catch up with the compression wave and weaken it, eventually cancelling it if the piston motion is symmetrical [44]. The highest frequency surface motion that can drive the shock corresponds to the point where compression waves generated by the oscillating surface are cancelled by subsequent rarefaction waves before they reach the shock, so the shock is not affected by the surface motion. For the conditions of Figure B.2, cancellation occurs beneath the shock at a minimum frequency of about 100 kHz, above which the shock will presumably remain fixed even in the presence of surface motions. Between 1 kHz and 100 kHz, the motion will be something between these two limits.

B.2 Dynamic Motion With a Hypersonic Boundary Layer

The above solution has made no consideration of the effect of the thick hypersonic boundary layer on the surface. The boundary layer will in fact alter the downstream velocity, and so change the downstream perturbation conditions as perceived by the shock. The boundary layer is affected by the shock motion because the pressure ratio across the moving shock can differ substantially from the pressure ratio across the equilibrium shock. As the surface Mach number increases (moving away from the shock), the pressure ratio decreases. The converse happens when the wall moves towards the shock. The variation in shock pressure ratio with surface Mach number is also shown in Figure B.1.

The downstream thermodynamic properties do not vary symmetrically with surface velocity, as pointed out by Ng [43]. For instance, with upstream normal Mach number 1.5, the static pressure ratio increases 25% over the steady value when the surface moves at Mach -.19, referenced to the upstream speed of sound, but decreases only 22% at a surface Mach number of +.19. Thus, the time- averaged shock pressure ratio over one complete cycle of pure sinusoidal surface motion will be slightly greater than the steady-state value for the same upstream Mach number, so the average boundary layer thickness should be correspondingly smaller. In actuality, this effect is very small over the range of conditions that would be encountered in the sorts of vehicles being considered herein.

As was shown earlier, the laminar boundary layer thickness is inversely proportional to the square root of the pressure ratio across the shock in the steady state. It is therefore reasonable to assume that the shock motion, driven by surface motion, will in turn change the size of the boundary layer, and thus the effective flow displacement surface. The effect of this boundary layer motion, when added to that of the actual surface motion, may either amplify or diminish the total net downstream oscillation velocity in the quasi-steady model.

The time rate of change of the boundary layer thickness is expressed in terms of the time rate of change of the pressure ratio. It is assumed that the boundary layer thickness will scale with some power of the shock pressure ratio. If the boundary layer expands and compresses isentropically, its thickness will scale with $P^{-1/\gamma}$; in the equilibrium boundary

layer limit, as shown by the work of Bertram and Blackstock [31], it will scale with $P^{-1/2}$. If δ_o^* and P_o are the equilibrium values of boundary layer displacement thickness and shock pressure ratio (assumed constant in the weak interaction region), the time varying boundary layer thickness can be represented as

$$\delta^*(t) = \delta_o^* \left(\frac{P_o}{P(t)}\right)^{\frac{1}{n}} \tag{B.22}$$

with $\gamma < n < 2$. The time derivative of boundary layer thickness, and thus, the perceived velocity of the displacement surface relative to the plate surface, is:

$$\frac{\partial \delta^*}{\partial t} = -\frac{1}{n}\,\delta_o^*\,\frac{P_o^{1/n}}{P(t)^{(n+1)/n}}\frac{\partial P}{\partial t} \tag{B.23}$$

The pressure term exponent $(n+1)/n$ typically ranges in value from 1.5 with boundary layer equilibrium to 1.8 for isentropic compression at high temperature, so the difference between the isentropic compression assumption and equilibrium boundary layer motion is relatively insignificant. These assumptions have neglected dynamical changes in the boundary layer flow due to changing free-stream pressure, which will tend to reduce the variation in boundary layer thickness.

Thus, with the equilibrium boundary layer-shock pressure ratio, and assuming the surface moves only in the normal direction, we can write the total downstream Mach number in terms of the equilibrium value, the wall oscillation velocity u_{wall}, the shock angle β and the surface angle θ, and the boundary layer thickness:

$$M_2'(t) = M_{2\,\text{equil.}}' + \frac{1}{a_1}\left(u_{\text{wall}}(t')\,\cos(\beta-\theta) + \frac{1}{2}\,\delta_o^*\,\frac{\sqrt{P_o}}{P(t'')^{3/2}}\frac{\partial P}{\partial t}(x'',t'')\right) \tag{B.24}$$

Observe that in equation (B.24) the Mach number at time t has been expressed in terms of the wall velocity at time t' and the shock pressure ratio and its derivative at position x'' and time t'' because disturbances propagate at a finite velocity. Depending on the propagation length, this may introduce a phase shift between the peak pressure ratio, leading to smallest boundary layer, and maximum outward surface velocity. Thus, wall motion and pressure ratio may either reinforce or counteract each other, depending on the

propagation path, so the shock motion must be considered in terms of the size of the shock layer and the local Mach number.

The finite propagation speed of wall and shock disturbances actually simplifies the analysis of shock motion with the boundary layer. It is reasonable to model the shock motion by assuming the wall velocity affects the downstream conditions on some portion of the shock farther along the surface, along a characteristic, causing that region of the shock to move, changing its pressure ratio, which affects the boundary layer thickness even farther down the surface. This boundary layer motion, added to the surface oscillation, is the total displacement seen by some portion of the shock even farther along the surface. We have found that the moving shock has a speed and amplitude comparable to that of the moving wall for most frequencies, so the solutions with the boundary layer that are of the most interest will be those in which the boundary layer thickness variations overwhelm the actual plate motion.

The small angle of the characteristics at the Mach numbers of interest here implies that the boundary layer contribution to shock motion will only be important for large forebodies, and thus, large vehicles. For instance, for a section of the shock being driven by boundary layer oscillations 30 meters from the leading edge of a 5 degree wedge travelling at Mach 20, the initial driving wall disturbance originated only 6 meters along the wedge surface. The same wedge at Mach 10 would experience boundary layer motion effects on the shock 30 meters down the surface from wall motions that occur only 2 meters from the leading edge.

Figure B.2 also shows the quasisteady solution for shock motion with a 2 meter thick boundary layer being driven initially by a 1 cm amplitude wall motion. The presence of the boundary layer greatly increases the amplitude of shock motion at high frequencies, where shock pressure ratio changes become important. In this case, the shock is still following the apparent change in downstream velocity, but that downstream perturbation has been greatly amplified by the thickness variations fo the boundary layer. In other words, the boundary layer has amplified the apparent motion of the surface, as perceived by the shock.

At first, this might suggest that the boundary layer will substantially increase the amplitude of shock motion. However, for the specific conditions depicted in this figure, the boundary layer amplification is only significant in the region of frequencies *above* which the quasisteady solution is self-consistent. As indicated above, at moderately high frequencies, the effect of downstream displacements on shock position is diminished, and at very high frequencies, eliminated, by the time variation of thermodynamic properties. Therefore, we may conclude that, for most reasonable transatmospheric flight conditions, the forebody bow shock will remain fixed relative to a moving surface even in the presence of a thick boundary layer. The influence of the boundary layer on shock-inlet matching need be taken into account only for steady-state changes in angle of attack.

Appendix C
Incorrect Attempts at Avoiding Singular Behavior at the Wall

C.1 Viscous Height and Slip Velocity Solutions

It is first worth investigating whether the wall problem can be avoided while retaining the inviscid assumption. Two approximations present themselves. One approach might be to select some effective viscous displacement height ϵ above the wall, from which the integration can begin, to avoid the singularity. Another solution would be to determine a slip velocity at the wall, thereby avoiding the zero velocity condition. Both of these approaches, though seemingly simple, are fundamentally flawed, and it will be seen later that the complete inviscid assumption must be relaxed to permit the inclusion of some viscous effects at the wall.

There are two problems with the viscous displacement height approach. First, no obvious criteria exist for accurately determining that displacement height. It might be argued that this length scale could be selected on the basis of some fundamental physical argument. For instance, it might be set to some multiple of the mean free path, or to some assumed viscous penetration height, based on an assumed viscous diffusion rate from the wall. However, because of the strength of the singularity in the integral, the final solution will be extremely dependent on the value of ϵ chosen. In effect, selecting ϵ will determine the final value of β, which will in turn determine the entire compound nature of the channel flow.

With a lower integration limit, the integral solution for β in a power-law Mach number profile becomes:

$$\beta = \frac{H - H^{2n}\epsilon^{(1-2n)}}{\gamma(1-2n)M_e^2} - \frac{H-\epsilon}{\gamma} \tag{C.1}$$

In the vicinity of $n \simeq 1$:

$$\beta \simeq \frac{H}{\gamma}\left(\frac{H}{\epsilon}-1\right)\frac{1}{M_e^2}-\frac{H-\epsilon}{\gamma} \tag{C.2}$$

For $\epsilon \ll H$, this becomes

$$\beta \simeq \frac{H}{\gamma}\left(\frac{H}{\epsilon M_e^2}-1\right) \tag{C.3}$$

If $H/\epsilon \gg M_e^2$ the compound flow parameter is inversely proportional to ϵ. Order-of-magnitude arguments are inappropriate for such a sensitive parameter. Furthermore, the typical hypersonic flow profiles are sonic very close to the wall. Selecting even a moderate value for ϵ may well eliminate the entire low-speed portion of the flow.

Another difficulty with this approach is that the introduction of an external length scale will prevent the application of similarity solutions for the laminar boundary layer to this channel flow. As will be shown later, the retention of the similarity form greatly simplifies the flow profile solutions in the channel. Indeed, the assignment of some ϵ is essentially an ad hoc means of including viscosity in this solution. By setting a lower limit on the integration, it is assumed that pressure gradient effects at the wall are exactly cancelled out by the normal gradient in shear, thus satisfying the no-slip criterion.

The other means of avoiding the wall singularity mentioned above is to assign a slip velocity at the wall, so that $1/M^2 \neq \infty$ when $y = 0$. This approach is similar to that taken by Elfstrom [45] in studying the separation of a compressible turbulent boundary layer subject to a ramp-induced shock-generated pressure-rise. Indeed, for the case of a *turbulent* boundary layer profile, such an approach may be acceptable because of the velocity slope near the wall. For the turbulent case, selection of a slip velocity would essential skip over the laminar sub- layer, where it is assumed that viscous effects exactly cancel pressure gradients. Elfstrom chose a slip velocity by linearly extrapolating the velocity above the laminar sub-layer to the wall. However, because the so-called wake region above the wall is not itself linear, such an extrapolation is often difficult.

The slip velocity approach is inadequate for the laminar boundary layer. In the laminar boundary layer profile, velocity increases almost linearly with height above the wall (especially when considered in the transformed incompressible plane.) Thus, there is no simple way to extrapolate the profile to a finite value at the wall. In fact, there will be a

slip velocity at the wall which scales in proportion to the mean-free-path, so it is tempting to select a non-zero wall velocity based on some mean-free-path assumption. This solution is very similar to the viscous displacement height approach, and is invalid for the same reasons, namely the difficulty of accurately selecting the wall value, and the sensitivity of the β parameter to this choice.

In addition to the difficulties involved, the introduction of a slip velocity or displacement height is objectionable because it would entail bringing rarefied gas assumptions into a continuous fluid model. One of the principle goals of a continuous fluid model is the elimination of the need to consider individual molecular processes. Once the continuous flow assumption is made, the fluid should be describable entirely in terms of the bulk transport properties, without recourse to include molecular-scale properties.

The problems encountered at the wall might be eliminated if the entire boundary layer were averaged in some sense before the net effect on the channel flow is evaluated. Descher [46] solved for the behavior of continuous profiles by taking an "equivalent" area average of stagnation properties across the channel, and then observing their evolution. However, he used area-averaging because it is the most common average used for experimentally determining engine thrust; there is no obvious physical justification for doing so. Indeed, the form of the β parameter suggests that both Mach number and area would have to be considered for averaging. Descher's results are somewhat difficult to apply to general profiles, and their simplest application is to so-called "nearly uniform" profiles in which the area averaging approach would be most valid.

In experimental evaluation, mass averaging or momentum averaging are often favored, because they conserve the properties being averaged over [47]. The particular merits of each averaging scheme is a matter of some debate, especially in the experimental community. Both mass averaging and momentum averaging are inappropriate for application to the hypersonic boundary layer profile, since the mass flux in the boundary layer is very small (and equal to 0 in the limit of $M_{\text{free stream}} \rightarrow \infty$.) As such, a mass-averaged or momentum- averaged quantity will tend to lose boundary layer influences. Further, there is no justification for averaging the flow properties in a profile that is not mixing out.

C.2 The Failure of Weighting Function Methods

It has been argued that viscosity must be added to the integral formulation in order to extend the streamtube model to the no-slip condition at the wall. However, in the course of this investigation, it was originally suggested that the wall boundary condition might be eliminated while retaining the purely inviscid, pressure-matched model, by suitably weighting the integral representation of the profile. Because this idea seems promising, it is worth exploring the reasons for its failure.

In solving for the continuous profile, especially when the streamtube summation is converted to an integral representation, it is tacitly assumed that all streamtubes are of equal area. In fact, there is no physical reason to make this assumption, and it is done merely as a mathematical convenience. Indeed, since the notion of the streamtube is an abstraction used to approximate the non-mixing nature of the flow, it would be equally permissible to decompose the flow into streamtubes of different areas.

The streamtube nearest the wall is the one that introduces a singularity in the summation solution. That is because it is the streamtube that satisfies no-slip, and thus has zero velocity. The notion of a zero- velocity streamtube is incompatible with the one-dimensional flow equation development. For instance, in the derivation of the 1-d flow equations, equation (6.24) was divided by u^2 to obtain equation (6.25). This is mathematically invalid when $u = 0$. The mathematical difficulties introduced by the zero wall velocity cannot be avoided by solving in terms of Mach number. In general, a zero Mach number flow is a valid condition because it can represent a flow with finite velocity, but infinite speed of sound, as would be the case in an incompressible flow. However, in the profile of interest here, the $M = 0$ constraint at the wall corresponds directly to $u = 0$, so the singular behavior cannot be avoided by solving for the limit of wall Mach number.

A weighting function might be selected so that the area of the troublesome wall streamtube approaches zero and does not drive the β integral to divergence. The one-dimensional

flow equation for streamtube area is weighted on both sides by a function, $w(y)$, as follows

$$w(y)\frac{dA}{dx} = \frac{w(y)A}{\gamma}\left[\frac{1}{M^2} - 1\right]\frac{d\ln P}{dx} \tag{C.4}$$

Where $w(y) = 0$ at $y = 0$, and $w(y) \rightarrow 0$ as fast as $M^2 \rightarrow 0$. Then, $w(y)A$ is the streamtube area, with A some constant parameter. Several obvious choices are available for selecting $w(y)$; for instance, $w(y) = y^2$, since velocity scales linearly with y at the wall, or $w(y) = M^2$, which would cancel the Mach number singularity anywhere in the flow.

The right side of equation (C.4) can be integrated simply, by changing $dA \rightarrow dy$. However, the left side is difficult to handle, and its meaning is unclear, since it can no longer be incorporated directly into a proper integral. If both sides of equation (C.4) are integrated over the entire channel height, H, for a 2-d channel:

$$\int_0^H w(y)\frac{dy}{dx} = \int_0^H \left[\frac{1}{M^2} - 1\right]\left(\frac{d\ln P}{dx}\right)\frac{w(y)dy}{\gamma} \tag{C.5}$$

where the left side is not a proper integral statement. In the original treatment, the integral over the streamtube areas was identically equal to the streamwise derivative of the total channel area:

$$\int_0^H \frac{dy}{dx} = \frac{d}{dx}\int_0^H dy = \frac{dH}{dx} \tag{C.6}$$

made possible because the integral of the derivative equals the derivative of the integral. This is convenient because dH/dx is a known quantity, specified by the particular geometry selected for the channel walls. With the weighting function, the left-hand side of equation (C.4) cannot be related to a simple known quantity.

The integration is accomplished with Leibnitz's rule:

$$\frac{d}{dx}\int_0^{H(x)} w(x,y)dy = \int_0^{H(x)} \frac{\partial w(x,y)}{\partial x}dy + w(x,H)\frac{dH}{dx} \tag{C.7}$$

Rearranging equation (C.7), the streamwise change in channel area is:

$$w(x,H)\frac{dH}{dx} = \frac{d}{dx}\int_0^{H(x)} w(x,y)dy - \int_0^{H(x)} \frac{\partial w(x,y)}{\partial x}dy \tag{C.8}$$

The first term on the right-hand side of equation (C.8) is solved from the weighted expression for one- dimensional area change, equation (C.4):

$$\int w(y)\frac{dy}{dx} = \int \left[\frac{1}{M^2} - 1\right] d\ln P\frac{w(y)dy}{\gamma} \tag{C.9}$$

Assuming $w(y)$ has been selected correctly, this integral will not diverge, and so can be solved with an assumption of completely inviscid flow. The second term, cannot be handled because

$$\frac{\partial w}{\partial x} = \frac{\partial w}{\partial y}\frac{\partial y}{\partial x} \tag{C.10}$$

At first glance, it might be assumed that $\partial y/\partial x = 0$, because the coordinate frame is fixed. But, the coordinate y used above is the *streamtube* coordinate; thus, $\partial y/\partial x$ is not zero, but rather is defined as the change in vertical position of the streamtube as it proceeds through the channel. This is evaluated for an arbitrary streamtube by summing the change in height of all the streamtubes above or below:

$$\frac{dy}{dx} = \frac{d}{dx}\int_0^Y dy \tag{C.11}$$

where the normal coordinate Y must be an absolute position, independent of the streamtube position $y(Y)$. The right-hand side of equation (C.11) is evaluated with the one-dimensional area change relationship:

$$\frac{dy}{dx}(Y) = \int_0^Y \left[\frac{1}{M^2} - 1\right]\frac{d\ln P}{dx}\frac{dy}{\gamma} \tag{C.12}$$

But this is once again singular at the wall, so the method has failed.

Appendix D

Estimating the Normal Pressure Gradient Through a Shock at Small Wedge Angles

The strength of the shock-imposed pressure gradient can be estimated from the equation for downstream pressure and the shock angle relationship. Since the wedge angle is constant over the profile, it is most desirable to express the shock angle in terms of the wedge angle, with a close form expression that can be used in the pressure equation. As stated above, however, such is not possible because the usual small shock angle assumption cannot be made in the lower regions of the boundary layer. Because the free-stream is hypersonic, we can safely assume small wedge angle, which simplifies the problem considerably, following the development of Liepmann and Roshko [48].

In the limit of small wedge angle, the shock angle approaches the Mach angle, given by

$$\lim_{\beta_{\text{shock}} \to 0} \beta_{\text{shock}} = \sin^{-1}\left(\frac{1}{M}\right) \tag{D.1}$$

From the familiar shock angle /wedge angle plots (often called β-θ-M diagrams) [5], the shock angle increases fairly linearly with wedge angle for small wedge angles (say, less than 5°).

In the limit of small wedge angle,

$$\beta_{\text{shock}} \simeq \sin^{-1}\left(\frac{1}{M_1}\right) \tag{D.2}$$

where M_1 is the upstream Mach number, as before. For convenience, define

$$z \equiv (M_1^2 \sin^2 \beta_{\text{shock}} - 1) \tag{D.3}$$

The small wedge angle assumption means that $z \simeq 0$. Equation (7.1) can be written in terms of z:

$$\tan\theta = \frac{2\cot\beta_{\text{shock}} z}{M_1^2(\gamma + \cos\beta_{\text{shock}}) + 2} \tag{D.4}$$

Eliminating β_{shock} from the definition of z:

$$\sin^2 \beta_{\text{shock}} = \left(\frac{z+1}{M_1^2}\right) \tag{D.5}$$

or,

$$\beta_{\text{shock}} = \sin^{-1}\left(\frac{\sqrt{z+1}}{M}\right) \tag{D.6}$$

the value of $\cot \beta_{\text{shock}}$ is then represented by

$$\cot \beta_{\text{shock}} = \sqrt{\frac{M_1^2 - z - 1}{z+1}} \tag{D.7}$$

so that

$$\cos 2\beta_{\text{shock}} = 1 - 2\left(\frac{z+1}{M_1^2}\right) \tag{D.8}$$

The shock angle is now expressed in terms of z only by substituting for the β_{shock} terms:

$$\tan\theta = \frac{2\sqrt{\frac{M_1^2-1-z}{z+1}}z}{M_1^2\left(\gamma+1-\frac{2(z+1)}{M_1^2}\right)+2} \tag{D.9}$$

$$= \frac{2\sqrt{\frac{M_1^2-1-z}{z+1}}z}{(\gamma+1)M_1^2 - 2z} \tag{D.10}$$

Again, the limit of small wedge angle, $\theta \to 0$ is also the limit of $z \to 0$;

$$\lim_{z\to 0} \simeq \frac{2z\sqrt{M_1^2 - 1 - z}}{(\gamma+1)M_1^2} \tag{D.11}$$

Care must be taken with the term under the square root, $(M_1^2 - 1 - z)$. The small z limit is not always $\lim_{z\to 0}(M_1^2 - 1 - z) \simeq (M_1^2 - 1)$, because when $M_1 \simeq 1$, $(M_1^2 - 1 - z) \simeq z$.

Under the assumption that $M_1^2 - 1 - z \simeq M_1^2 - 1$,

$$\tan\theta = \frac{2\sqrt{M_1^2 - 1}}{(\gamma+1)M_1^2}z \tag{D.12}$$

This same result is found more rigorously with a binomial expansion of the numerator term,

$$\sqrt{M_1^2 - 1 - z} = \sqrt{M_1^2 - 1}\left(1 - \frac{z}{M_1^2 - 1}\right)^{1/2} \tag{D.13}$$

$$= \sqrt{M_1^2 - 1}\left(1 - \frac{z}{2(M_1^2 - 1)}\right) \tag{D.14}$$

The binomial expansion is only valid when $M_1^2 \gg 1$. Under these conditions,

$$\tan\theta = \left[\frac{2\sqrt{M_1^2-1}}{(\gamma+1)M_1^2}\right] z - \left[\frac{1}{(\gamma+1)M_1^2\sqrt{M_1^2-1}}\right] z^2 \tag{D.15}$$

As long as $M_1^2 \gg 1$, the z^2 term can be dropped for small z, which is accomplished by simply setting $M_1^2 - 1 - z = M_1^2 - 1$ for small z.

In the limit of $M_1 \simeq 1$, we can write $M_1^2 - 1 - z \simeq z$ and thus

$$\tan\theta = \frac{2z^{3/2}}{(\gamma+1)M_1^2} \tag{D.16}$$

Both of these limits can be solved for z as a function of the wedge angle. For $M_1 \gg 1$,

$$z = \frac{(\gamma+1)M_1^2}{2\sqrt{M_1^2-1}}\tan\theta \tag{D.17}$$

and for $M_1 \simeq 1$,

$$z = \left(\frac{\gamma+1}{2}M_1^2\tan\theta\right)^{2/3} \tag{D.18}$$

Once z is known, the pressure ratio across the shock is uniquely determined. Equation (7.4) can be written as

$$\frac{p_2}{p_1} = 1 + \frac{2\gamma}{\gamma+1}z \tag{D.19}$$

Substituting for the two limits of z, and noting that $\tan\theta \simeq \theta$ if $\theta \simeq 0$,

- $M \gg 1$:

  The shock pressure ratio is:

$$\frac{p_2}{p_1} = 1 + \frac{\gamma M_1^2}{\sqrt{M_1^2-1}}\theta \tag{D.20}$$

  The pressure gradient generated by the shock is:

$$\frac{\partial p_2}{\partial y} = p_1\gamma\theta\frac{\partial}{\partial y}\left(\frac{M_1^2}{\sqrt{M_1^2-1}}\right) \tag{D.21}$$

$$= p_1\gamma\theta\left(\frac{M_1(M_1^2-2)}{(M_1^2-1)^{3/2}}\right)\frac{\partial M}{\partial y} \tag{D.22}$$

$$\simeq p_1\gamma\theta\frac{\partial M}{\partial y} \tag{D.23}$$

where changes in γ across the profile have been neglected.

- $M \simeq 1$:

The shock pressure ratio is:

$$\frac{p_2}{p_1} = 1 + \left(\frac{2}{\gamma+1}\right)^{1/3} \left(\gamma M_1^2 \theta\right)^{2/3} \tag{D.24}$$

The pressure ratio generated by the shock is

$$\frac{\partial p_2}{\partial y} = p_1 \left(\frac{2}{\gamma+1}\right)^{1/3} (\gamma\theta)^{2/3} \frac{\partial}{\partial y}\left(M_1^{4/3}\right) \tag{D.25}$$

$$= p_1 \frac{4}{3} \left(\frac{2}{\gamma+1}\right)^{1/3} (\gamma\theta)^{2/3} \left(M_1^{1/3}\right) \frac{\partial M_1}{\partial y} \tag{D.26}$$

$$\simeq p_1 \frac{4}{3} \left(\frac{2\gamma^2}{\gamma+1}\right)^{1/3} (\theta)^{2/3} \frac{\partial M_1}{\partial y} \tag{D.27}$$

With these two limits, the magnitude of the imposed pressure gradient can be estimated. For $\gamma \simeq 1.3$,

$$\frac{\partial p_2}{\partial y} = 1.3\, p_1\, \theta\, \frac{\partial M}{\partial y} \qquad M_1 \gg 1 \tag{D.28}$$

$$\frac{\partial p_2}{\partial y} = 1.7\, p_1\, \theta^{2/3}\, \frac{\partial M}{\partial y} \qquad M_1 \simeq 1 \tag{D.29}$$

(D.30)

In the laminar case, for $\theta \simeq 5°$, and a Mach number gradient $\partial M/\partial y \simeq M_o/\delta$, with $M_o = 10$

$$\frac{\partial p_2}{\partial y} = 1.13 \left(\frac{p_1}{\delta}\right) \qquad M_1 \gg 1 \tag{D.31}$$

$$\frac{\partial p_2}{\partial y} = 3.15 \left(\frac{p_1}{\delta}\right) \qquad M_1 \simeq 1 \tag{D.32}$$

(D.33)

This is a substantial gradient, especially near the wall,and cannot be ignored in the calculations. Note also that, although the pressure gradient is much greater in the low-speed regions, the exact details of this portion of the flow are questionable because separation of the boundary layer due to the shock may affect this region drastically. In the turbulent profile, the same magnitude of pressure changes across the profile, but in a much smaller distance, on the order of 10% of the boundary layer height.

Appendix E

One-dimensional Combustor Designs

E.1 Analytical Model of the Constant Pressure Combustor

In chapter 5, a simple combustor profile was presented for a two- stream analysis. This combustor was designed for constant pressure operation, which was achieved by setting both area and temperature to exponential functions of the streamwise coordinate. As a result, Mach number and static temperature were exponential as well. Though perhaps overly-idealized, the constant pressure assumption makes for some very simple analysis, from which much physical insight can be drawn.

In this chapter the constant pressure combustor will be used as one example to demonstrate the compound-compressible flow characteristics of an inlet flow with profile. Recall that such a combustor is designed for one-dimensional flow by setting the logarithmic derivative of pressure equal to zero in the pressure influence coefficient expression:

$$\frac{dP}{P} = 0$$

$$\Longrightarrow \left[\frac{\gamma M^2}{1-M^2}\right]\frac{dA}{A} = \left[\frac{\gamma M^2}{1-M^2}\right]\frac{dT}{T} \tag{E.1}$$

$$\text{or } \frac{dA}{A} = \frac{dT}{T} \tag{E.2}$$

This is satisfied by exponential functions of the streamwise coordinate, as we found in chapter 5.

The concept of total temperature is only meaningful in a calorically perfect gas, with constant specific heat. Although enthalpy is conserved, total temperature can change if C_p changes. Throughout this chapter, heat addition will be referred to in terms of total

temperature rise rather than enthalpy rise, to be compatible with the results of compressible fluid mechanics for calorically perfect gases. This requires that the flow total temperature be corrected as C_p changes, so enthalpy is conserved. One means of simplifying this is to define some average C_p which is representative of the entire channel. This introduces inaccuracies, but permits ready solution of the analytical problem. The inlet total temperature can be defined by dividing total enthalpy by this C_p. Combustor heat addition is then handled in terms of total temperature addition, which must be consistent with this value of C_p so that the final enthalpy is correct.

The constant pressure combustor has the desirable characteristic that it is resistant to separation, because there is no adverse pressure gradient. For this reason, Swithenbank has favored it as the design of choice [37]. The total temperature profile also has reasonable behavior, because we would expect the heating to trail off exponentially, since it is the product of a collisional process.

Because pressure is constant, and the flow is assumed inviscid, the velocity cannot change in a constant pressure combustor. Thus, all heat addition appears as thermal energy, with the flow kinetic energy remaining constant. As a result, we can write $dT_{\text{total}} = dT_{\text{static}}$ in such a combustor. An increase in total temperature results directly in an increase in static temperature.

For purposes of analyzing the channel flow, the area profile, $A(x)$, or rather, the streamwise derivative of area, dA/dx, and the heat addition, dT_{total}/dx must be specified. These values come directly out of the constant pressure assumption.

The constant pressure channel area is exponentially increasing, along with the static temperature:

$$A = A_{\text{initial}}\ e^{x/\lambda_D} \tag{E.3}$$

$$T = T_{\text{initial}}\ e^{x/\lambda_D} \tag{E.4}$$

As heat is added, the flow is expanded just enough to keep the kinetic energy constant. The Mach number is decreasing because the velocity is constant, and temperature is rising. This effect can be seen from the influence coefficient expression for the square of the Mach

number:

$$\frac{dM^2}{M^2} = \left[\frac{-2\left(1+\frac{\gamma-1}{2}M^2\right)}{1-M^2}\right]\frac{dA}{A} + \left[\frac{1+\gamma M^2}{1-M^2}\right]\frac{dT}{T} \tag{E.5}$$

where we have used the fact that $dT_{\text{total}} = dT_{\text{static}}$ if velocity is constant. With $dA/A = dT/T$, we can see that

$$\frac{dM^2}{M^2} = -\frac{dT}{T} \tag{E.6}$$

a result which was stated without proof in chapter 5.

The heating profile along the engine channel is specified directly because any change in total temperature goes directly to static temperature. This is the basis for setting

$$\frac{dT_{\text{total}}}{dx} = \frac{\overline{T}_{\text{total}}}{\lambda_D}\left(1+\frac{\gamma-1}{2}\overline{M}^2\right)^{-1} e^{x/\lambda_D} \tag{E.7}$$

as was done in chapter 5. The term $\overline{T}_{\text{total}}$ is then simply the initial value of total temperature entering the engine. Knowing this and an initial Mach number $\overline{M}$, the heating profile is fully determined.

One aspect of this combustor is that, with an exponential temperature profile, the flow will simply get hotter and hotter, unless we limit the amount of heat that is input through the channel. There is no built-in limit to the heat addition in this channel. Indeed, the only scale that exists is the length parameter, λ_D. To size the engine, the final value of x must be bounded. This is done by putting a limit on the total heat addition available, ultimately set the available chemical energy of the reacting system.

The static temperature equation is used to calculate the heat input with the isentropic relation:

$$T_{\text{total}}(x) = \overline{T}(1+\frac{\gamma-1}{2}M(x)^2)e^{x/\lambda_D} \tag{E.8}$$

Writing the initial static temperature in terms of the initial total temperature and Mach number, and noting that the Mach number decreases exponentially down the channel:

$$T_{\text{total}}(x) = \overline{T}_{\text{total}}\frac{e^{x/\lambda_D}+\frac{\gamma-1}{2}\overline{M}^2}{1+\frac{\gamma-1}{2}\overline{M}^2} \tag{E.9}$$

If the final total temperature is known, the above expression can be inverted to solve

for the heat addition length:

$$x_{\text{final}} = \lambda_D \ln \left\{ \frac{T_{\text{total,final}}}{T_{\text{total,initial}}} \left(1 + \frac{\gamma - 1}{2} \overline{M}^2\right) - \frac{\gamma - 1}{2} \overline{M}^2 \right\} \tag{E.10}$$

This provides the limit to combustor length.

In reality, it can be assumed that accomplishing constant pressure combustion would be a difficult task in a supersonic combustion engine. The vagaries of the high-speed combustion process, especially since they are so dependent on the mixing process at high Mach number, introduce uncertainties that make realization of such behavior impractical.

The constant pressure assumption is certainly not the only simple one that can be made. For instance, the combustor could be designed to operate at a specific, constant temperature. The specification of this is somewhat more difficult than for the constant pressure case.

E.2 Analytical Model of the Constant Temperature Combustor

The constant temperature combustor may be thought of as the opposite operating limit to the constant pressure design. Recall that all the heat energy of the constant pressure scheme went into thermal energy. In the constant temperature design, all heat energy goes into kinetic energy of the flow. While this may seem desirable from an energetics standpoint, there may be large increases in pressure associated with the combustion process, and this may induce separation. The constant pressure assumption derives its simplicity from the fact that, without a pressure gradient, momentum remains constant in the channel.

Just as the constant pressure combustor was derived from the influence coefficient expression for pressure, so the shape of the constant temperature combustor can be solved from the corresponding influence coefficient expression for temperature:

$$\frac{dT}{T} = 0 \tag{E.11}$$

$$\Longrightarrow \left[\frac{(\gamma-1)M^2}{1-M^2}\right]\frac{dA}{A} = -\left[\frac{1-\gamma M^2}{1-M^2}\right]\frac{dT_o}{T}$$

$$\frac{dA}{A} = -\left[\frac{1-\gamma M^2}{(\gamma-1)M^2}\right]\frac{dT_{\text{total}}}{T} \tag{E.12}$$

The total temperature can be written in terms of the constant static temperature and Mach number. Starting with the isentropic flow equation relating total and static temperature,

$$T_o = T(1+\frac{\gamma-1}{2}M^2) \tag{E.13}$$

written in logarithmic form:

$$\frac{dT_o}{T_o} = \frac{dT}{T} + \frac{\frac{\gamma-1}{2}M^2}{1+\frac{\gamma-1}{2}M^2}\frac{dM^2}{M^2} \tag{E.14}$$

and noting once again that $2d\ln M = d\ln M^2$, the area relationship becomes:

$$\frac{dA}{A} = (\gamma M^2 - 1)\frac{dM}{M} \tag{E.15}$$

This is readily integrated, so that between station 1 and station 2,

$$\frac{A_2}{A_1} = \frac{M_1}{M_2}\exp\left\{\frac{\gamma}{2}(M_2^2 - M_1^2)\right\} \tag{E.16}$$

At any position x, the area can be defined in terms of the initial Mach number and area, M_1 and A_1:

$$A(x) = A_1\frac{M_1}{M(x)}\exp\left\{\frac{\gamma M_1^2}{2}\left(\frac{M(x)^2}{M_1^2} - 1\right)\right\} \tag{E.17}$$

It is inconvenient to carry the Mach number around, since the Mach number profile is not specified directly. Instead, the varying Mach number $M(x)$ can be written in terms of the total temperature, because the static temperature is constant. From equation(E.14):

$$\frac{dT_o}{T} = (\gamma-1)M\,dM \tag{E.18}$$

Integrating both sides between stations 1 and 2:

$$T_{\text{total 2}} - T_{\text{total 1}} = T\frac{\gamma-1}{2}(M_2^2 - M_1^2) \tag{E.19}$$

Thus, the Mach number at station 2 can be defined by the heat addition and the initial Mach number:

$$M_2 = \sqrt{\frac{T_{\text{total 2}} - T_{\text{total 1}}}{T}\frac{2}{\gamma-1} + M_1^2} \tag{E.20}$$

Removing the Mach number from under the square root sign,

$$M_2 = M_1\sqrt{\frac{T_{\text{total 2}} - T_{\text{total 1}}}{T_{\text{total 1}} - T_1} + 1} \tag{E.21}$$

If M_1 is hypersonic, the total temperature will be much greater than the static temperature, and the Mach number relationship is greatly simplified:

$$M_2 = M_1\sqrt{\frac{T_{\text{total 2}}}{T_{\text{total 1}}}} \tag{E.22}$$

The area then follows the form:

$$A(x) = A_1\sqrt{\frac{T_{\text{total 1}}}{T_{\text{total}}}}\exp\left\{\frac{\gamma M_1^2}{2}\left(\frac{T_{\text{total}}}{T_{\text{total 1}}} - 1\right)\right\} \tag{E.23}$$

A heating profile can be specified, and plugged into the above equation to solve for area at any location. A reasonable assumption is an exponential heating process, of the form:

$$T_{\text{total}} = T_{\text{total 1}} + T_{\text{total 1}}\,\Delta(1 - \mathrm{e}^{-x/\lambda_D}) \tag{E.24}$$

where λ_D is the design characteristic heating length, similar (though not equal) to the length scale defined for the constant pressure scheme, and Δ is defined as the fractional increase in total temperature, referenced to the initial total temperature. The ratio of total temperature at any x to that at station 1 is therefore

$$\frac{T_{\text{total}}}{T_{\text{total 1}}} = 1 + \Delta(1 - e^{-x/\lambda_D}) \tag{E.25}$$

so that the streamwise derivative of total temperature is

$$\frac{dT_{\text{total}}}{dx} = \frac{T_{\text{total 1}}\,\Delta}{\lambda_D}\mathrm{e}^{-x/\lambda D} \tag{E.26}$$

Once again, it should be pointed out that total temperature is not a conserved property if C_p is changing, and care must be taken to keep total temperature consistent with C_p so that the correct enthalpy change is realized. In talking about total temperature rise here, we are actually referring to a rise in enthalpy at some assumed average C_p.

Plugging this profile into the area equation, the area at any x position in terms of the initial conditions is:

$$A(x) = \frac{A_1}{\sqrt{1+\Delta(1-e^{-x/\lambda_D})}} \exp\left\{\frac{\gamma M_1^2 \Delta}{2}\left(1-e^{-x/\lambda_D}\right)\right\} \tag{E.27}$$

The streamwise derivative of area is found by differentiating equation(E.27) with the assumed heating profile:

$$\frac{dA}{dx}(x) = \frac{A(x)}{2\lambda_D}\left[\frac{\gamma M_1^2 \Delta\left(1+\Delta(1-e^{-x/\lambda_D})\right)-\Delta}{(\Delta+1)e^{x/\lambda_D}-\Delta}\right] \tag{E.28}$$

Once M_1 and Δ are specified, the combustor area profile is determined. The constant pressure combustor required only the specification of a characteristic combustion length scale, and a total heating limit; the form of the heating profile was determined by the pressure condition. For constant temperature operation, an assumption must be made about the heating profile.

For purposes of calculation, the constant temperature combustor has a major practical advantage. The combustion process is temperature limited, and the engine wall cooling may be limited as well. By fixing the temperature in the channel, it will never rise above the combustion limit or exceed the capabilities of the cooling system. This is not the case with the constant pressure device, where the temperature rises exponentially. Since there is no explicit check on temperature, it may well rise to unreasonable values.

The constant temperature combustor will also be more efficient, presumably, because the heat addition process will be occurring throughout at a very high temperature. The smaller the difference in heat reservoir temperature to working fluid temperature, the smaller the entropy rise. Note however that Mach number is increasing in the constant temperature combustor, because all energy goes into kinetic, and the speed of sound is constant. As the Mach number increase, the losses associated with heat addition become greater, as was pointed out in chapter 1, when the comparison between supersonic and subsonic combustion was made. On the other hand, the constant pressure combustor has exponentially decreasing Mach number, and thus the losses are decreasing as well. Since heat addition in the constant pressure assumption is increasing exponentially with streamwise distance, a greater portion

is added to the flow at lower Mach number. It is therefore unclear which will deliver lower overall losses. The decision must be based on inlet conditions and the heat addition profile.

The pressure field is easily determined. The temperature is constant, so the Mach number is proportional to velocity. Similarly, the pressure is proportional to density. From equation (E.16) above, and using the one-dimensional steady-flow continuity equation:

$$\rho_1 U_1 A_1 = \rho_2 U_2 A_2 \tag{E.29}$$

an expression for the density can be written directly:

$$\frac{\rho_2}{\rho_1} = \exp\left\{\frac{-\gamma}{2}(M_2^2 - M_1^2)\right\} \tag{E.30}$$

The pressure ratio across two stations in the channel is then:

$$\frac{p_2}{p_1} = \exp\left\{\frac{-\gamma}{2}(M_2^2 - M_1^2)\right\} \tag{E.31}$$